



HAL
open science

Mechanistic study of the multivalent effect on glycosidase inhibition : design, synthesis and biological evaluation of multimeric iminosugars

Yan Liang

► **To cite this version:**

Yan Liang. Mechanistic study of the multivalent effect on glycosidase inhibition : design, synthesis and biological evaluation of multimeric iminosugars. Other. Université de Strasbourg, 2021. English. NNT : 2021STRAF039 . tel-04416212

HAL Id: tel-04416212

<https://theses.hal.science/tel-04416212v1>

Submitted on 25 Jan 2024

HAL is a multi-disciplinary open access archive for the deposit and dissemination of scientific research documents, whether they are published or not. The documents may come from teaching and research institutions in France or abroad, or from public or private research centers.

L'archive ouverte pluridisciplinaire **HAL**, est destinée au dépôt et à la diffusion de documents scientifiques de niveau recherche, publiés ou non, émanant des établissements d'enseignement et de recherche français ou étrangers, des laboratoires publics ou privés.

ÉCOLE DOCTORALE DES SCIENCES CHIMIQUES
UMR 7042

THÈSE

présentée par :

Yan LIANG

soutenue le : **26 October 2021**

pour obtenir le grade de :

Docteur de l'université de Strasbourg

Discipline/ Spécialité : Chimie

**Etude Mécanistique de l'Effet
Multivalent sur l'Inhibition des
Glycosidases :**
**Conception, Synthèse et Evaluation Biologique
d'Iminosucres Multimériques**

THÈSE dirigée par :

M. COMPAIN Philippe

Professeur, Université de Strasbourg

THÈSE encadrée par :

Mme. BODLENNER Anne

Maîtresse de Conférences, Université de Strasbourg

RAPPORTEURS :

Mme. PELLEGRINI-MOÏSE Nadia

Maîtresse de Conférences, Université de Lorraine

Mme. XIE Joanne

Professeure, ENS Paris-Saclay

AUTRES MEMBRES DU JURY :

Mme. SEEMANN Myriam

Directrice de Recherches, CNRS

M. ALIX Aurélien

Maître de Conférences, Université Paris-Saclay

Mme. BODLENNER Anne

Maîtresse de Conférences, Université de Strasbourg

Acknowledgements

First of all, I am particularly grateful to Dr. Nadia PELLEGRINI-MOÏSE, Prof. Joanne XIE, Dr. Myriam SEEMANN, and Dr. Aurélien ALIX for agreeing to read and review this thesis.

Special thanks to the State Scholarship Fund (managed by China Scholarship Council) for the scholarship that allowed me to pursue my study in France as a PhD.

Sincere thanks to Prof. Philippe COMPAIN for initially accepting my application to join his team. Philippe was very friendly and showed great patience in teaching me and correcting my mistakes in my work. He always said “petit à petit, on devient moins petit” to motivate me to move forward. His rigorous approach to science is an example that I will always follow.

From the day I arrived in Strasbourg, Dr. Anne BODLENNER started to offer me all sorts of help, both in life and at work, which also caused a lot of pressure on her. I sincerely thank Anne for the time she gave me throughout these years. I could not have finished my thesis without her tremendous help.

Thanks to Dr. Damien HAZELARD for teaching me how to use some of the instruments in the laboratory, and for taking the time to help me whenever I had questions.

Dr. Nicolas KERN is a young and knowledgeable researcher. Much thanks to him for his comments and suggestions on my work at the group meetings. I sincerely wish him many more achievements.

I also address my thanks to my former colleagues Maëva PICHON and Damien TARDIEU. Maëva taught me some rules for the lab, which allowed me to integrate more quickly. And, she is a good friend with whom I often shared happy or troubling things. Damien left late in the afternoon so that I was not working alone in the lab.

Special thanks to my colleague Marine DESNOYERS, one of my best friends, and also my baby's aunt. She was a great comfort during my pregnancy. Her concern helped me to get through the most challenging year. I sincerely invite her to come to China as a guest.

Likewise, much thanks to Haijuan LIU and Adrien LAPORTE. Haijuan often shared her bench with me, which gave me more space to do reactions. Adrien is the funniest boy I have ever met. He is very friendly and basically never turns down a request. I wish both of them good luck for the future.

Thanks to Emeric WASIELWSKI for helping me to analyze complex NMR spectra. Thanks also to Mathieu CHESSE for teaching me to use some of the analytical instruments as well as the microwaves.

A big thank you to Grace, without whom I would not have been able to complete the synthesis work involved in the second objective of the thesis in almost five months and the limited space available.

Thanks to ALL my friends in Strasbourg and in France for their help over these years, especially in 2020.

At last, a big thank you to my family for their understanding and support. My family will always be my source of strength to overcome difficulties.

Table of Contents

Introduction	1
Chapter I : GLYCOSIDASES AND THEIR INHIBITION	5
I Glycosidases : role and classification	6
I.1 Glycosidases among Carbohydrate-processing enzymes.....	6
I.2 Catalytic machinery of glycosidases.....	7
II Development of reversible glycosidase inhibitors	11
II .1 The interest of glycosidase inhibitors.....	11
II .2 Iminosugars	12
II .2.1 Monocyclic iminosugars.....	13
II .2.2 Bicyclic iminosugars	14
II .3 Thiosugars.....	16
II .4 Carbasugars.....	17
II .5 Disaccharide inhibitors.....	19
II .6 Non-glycosidic derivatives	20
III Multivalency as a chemical organization and cooperation principle for glycosidase inhibition	21
III.1 Examples of multivalency as a key principle in Nature.....	21
III.2 Techniques for quantification of multivalent interactions	23
III.3 Multivalent glycosidase inhibitors	25
III.3.1 Definition of the multivalent effect	25
III.3.2 Quantification of multivalent interactions with enzymes and inhibitors	26
III.3.3 State of the art of multivalent glycosidase inhibitors in 2020	26
III.3.3.1 The seminal sparks	26
III.3.3.2 Exploration of clusters based on different scaffolds.....	29
III.3.3.2.1 Clusters based on fullerene scaffold.....	29
III.3.3.2.2 Clusters based on β -cyclodextrin scaffold.....	36
III.3.3.2.3 Clusters based on porphyrin scaffold.....	41
III.3.3.2.4 Clusters based on cyclopeptoid scaffold	42

III.3.3.2.5 Clusters based on calix[4]arene and calix[8]arene scaffolds.....	47
III.3.3.2.6 Others	51
III.3.3.3 The more the better? Plateau effect displayed by cyclopeptoid based clusters and comparison with giant fullerenes.....	52
III.3.4 Mechanisms accounting for inhibitory multivalent effect	53
IV Objectives of this PhD.....	54
IV.1 Questions related to the chelate and the sliding effects.....	54
IV.2 Detailed objectives and strategy	54
Chapter II : PREPARATION OF THE MAIN COMPONENTS	
COMPOSING THE TARGETED CLUSTERS.....	58
I Cu(I)-catalyzed azide-alkyne cycloaddition.....	59
II Synthesis of three types of clickable ligands.....	62
II.1 Preparation of a monovalent-ligand related to the clickable tripod.....	62
II.2 Preparation of the clickable tripod.....	64
II.3 Preparation of the “hindered” monovalent-ligand related to the clickable tripod	65
II.3.1 Synthetic strategy.....	65
II.3.2 Synthesis of 2-{2-[2-(2-azidoethoxy)ethoxy]ethoxy}ethan-1-ol	67
II.3.3 Synthesis of the “hindered” monovalent-ligand 183	67
II.4 Characterization of the “hindered” monovalent-ligand dendron 183	71
II.4.1 ¹ H NMR spectra	71
II.4.2 Infra-Red spectrum	72
II.4.3 Mass spectra	73
Chapter III : CLUSTERS SYNTHESIS AND STRUCTURE-ACTIVITY	
RELATIONSHIPS STUDY OF MULTIVALENT EFFECT WITH JACK	
BEAN α -MANNOSIDASE.....	75
I. Synthesis of multivalent cyclopeptoid-based clusters.....	76
I.1 Click coupling between the prepared ligands and various cyclopeptoid scaffolds	76
I.1.1 Synthesis of the <i>O</i> -acetylated 2×1-valent glycomimetic	76
I.1.2 Synthesis of the <i>O</i> -acetylated 4×1 and 4×3-valent clusters.....	78

I.1.3 Synthesis of the <i>O</i> -acetylated 12×1-valent cluster	81
I.1.4 Synthesis of the <i>O</i> -acetylated “hindered” 12×1-valent cluster	83
I.2 Deprotection of acetyl groups on the clusters	88
II. Biological evaluation	91
II.1 Basics of enzyme kinetics	92
II.1.1 Michaelis-Menten equation	92
II.1.2 The different inhibition modes and their kinetics	94
II.2 Enzymatic assay results	105
II.3 Mechanistic studies based on analytical ultracentrifugation	114
Chapter IV : SYNTHESIS OF GLYCOSYL CYANIDES BY RING- OPENING OF 1,6-ANHYDRO SUGARS WITH TMSCN	117
I Introduction	118
I.1 Synthetic strategies to access glycosyl cyanides	118
I.2 Recent developments in the ring-opening of 1,6-anhydro sugars	122
II Stereoselective ring-opening of 1,6-anhydro sugars for the synthesis of glycosyl cyanides	125
II.1 Principal methods for the synthesis of 1,6-anhydro sugars	125
II.2 Exploring cyanide ring-opening of 1,6-anhydrosugars and identification of optimized reaction conditions	128
III Scope investigation of the ring-opening reaction	130
III.1 Synthesis of 1,6-anhydrosugar substrates	130
III.2 Substrate scope studies	131
IV Conclusion	134
General Conclusion	136
Résumé de la thèse	142
Bibliography	159
Experiment part	170

Abbreviations & acronyms

AFM	Atomic force microscopy
AUC-SV	Analytical ultracentrifugation sedimentation velocity
CAZymes	Carbohydrate-active enzymes
CDs	Cyclodextrins
CEs	Carbohydrate Esterases
CuAAC	Cu(I)-catalyzed azide-alkyne cycloaddition
DFT	Density functional theory
DGJ	Deoxygalactonojirimycin
DLS	Dynamic light scattering
DMDP	(2 <i>R</i> ,5 <i>R</i>)-dihydroxymethyl-(3 <i>R</i> ,4 <i>R</i>)-dihydroxypyrrolidine
DMJ	Deoxymannojirimycin
DNJ	Deoxynojirimycin
ESI-MS	Native electrospray mass spectrometry
GH	Glycoside Hydrolases
GM	Golgi α -mannosidase
GTs	Glycosyl Transferases
H	Heavy chain
HA	Haemagglutinin
HBV	Hepatitis B virus
HCV	Hepatitis C virus
HNJ	α -homonojirimycin
IC₅₀	half maximal inhibitory concentration
IR	Infra-Red
ITC	Isothermal titration calorimetry
JBα-man	Jack bean α -mannosidase
K_i	Inhibition constant
L	Light chain
LAH	Lithium aluminium hydride
(LH)₂	JB α -man is composed by two LH heterodimers
LM	Lysosomal α -mannosidase
MALDI	Matrix-Assisted Laser Desorption Ionization
NAD⁺	Nicotinamide Adenine Dinucleotide
Neu5Ac	N-acetylneuraminic acid
NJ	Nojirimycin
NMR	Nuclear Magnetic Resonance
1<i>N</i>-OMJ	1-amino-5 <i>N</i> ,6 <i>O</i> -oxomethylenemannnojirimycin
1<i>N</i>-ONJ	1-amino-5 <i>N</i> ,6 <i>O</i> -oxomethylenenojirimycin
NPs	Nanoparticles
PLs	Polysaccharide Lyases
QCM	Quartz crystal microbalance
RP	Relative potency
RP/<i>N</i>	Relative potency per inhibitor head
SA	Sialic acid
SARs	Structure-activity relationships
SARS-CoV-2	Severe Acute Respiratory Syndrome Coronavirus-2
SGLT2	Sodium-dependent glucose cotransporter 2
SMFS	Single molecule force spectroscopy
SPR	Surface plasmon resonance

Su
 α -Glc

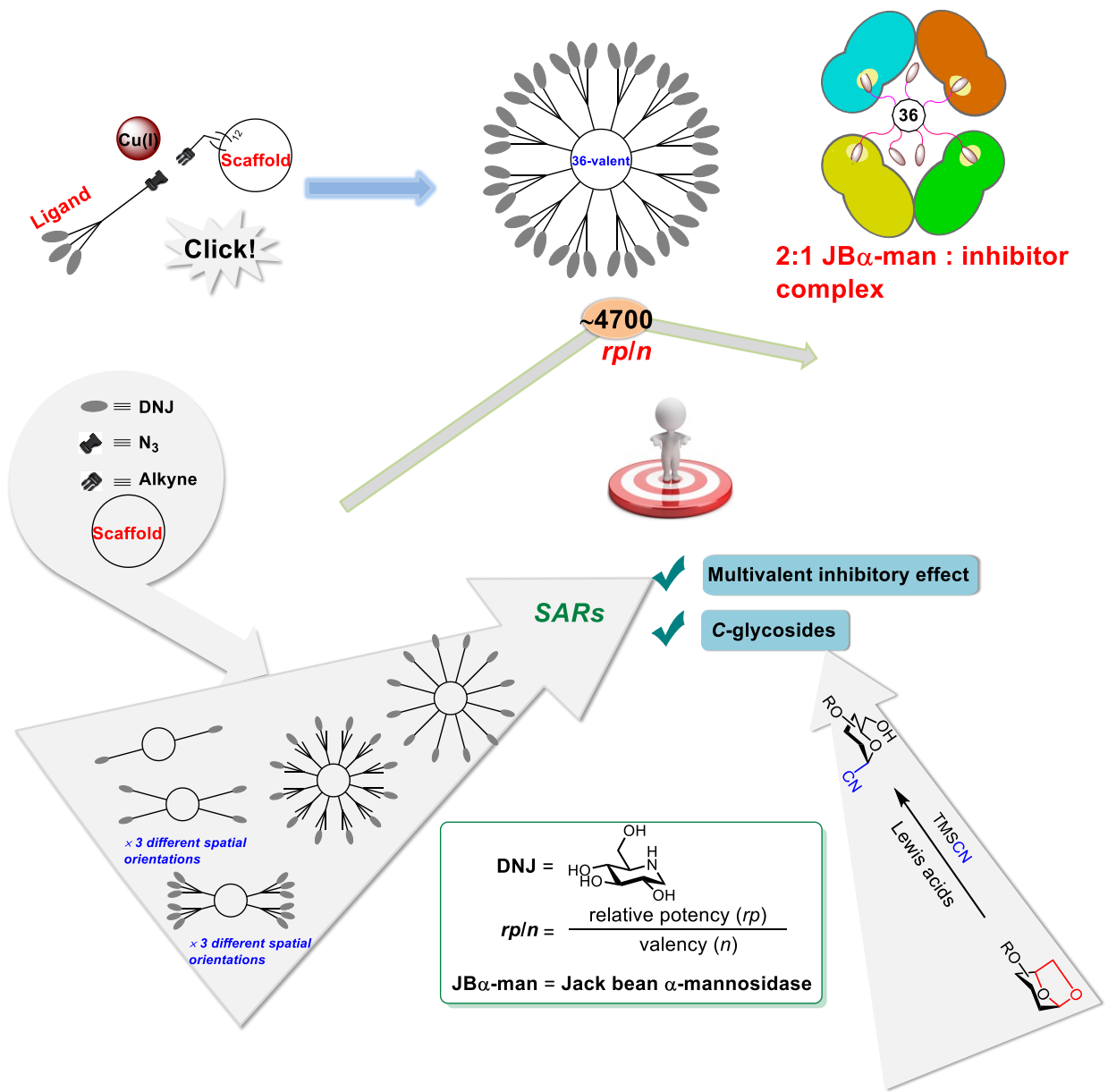
Succinimidyl
 α -D-glucopyranoside

Introduction

Iminosugars (also incorrectly referred to as aza-sugars) are sugar analogues in which the endocyclic oxygen atom of the natural sugar is replaced by a nitrogen atom. The initial interest in iminosugars as therapeutics focused on their inhibitory properties against glycosidase.^[1] In 1999, Bols *et al.* used multimeric iminosugar-like compounds arguing that it could be :“interesting to investigate the effect of multivalency on glycosidase inhibition.”^[2] This was the first attempt to perform such a study. Ten years later, the group of Gouin and Kovensky reported the first example of a small, but quantifiable effect in glycosidase inhibition.^[3] One year later, in 2010, the first observation of a strong multivalent effect for glycosidase inhibition was reported.^[4] Then, explosive investigations and outstanding achievements about the multivalent inhibitory effect were published. In particular, in 2016, a 36-valent cyclopeptoid-based DNJ cluster that displayed the best multivalent effect on glycosidase inhibition reported so far was disclosed.^[5] The formation of a strong chelate sandwich-type complex between two enzymes and one multimeric inhibitor explained, in part, the outstanding affinity enhancement observed.

C-glycosides represent an essential group of hydrolytically stable glycomimetics showing valuable biological activities, such as antibacterial, antitumor, antiviral properties.^[6-8] Our laboratory has recently prepared the first examples of multivalent C-glycosides based on C₆₀-fullerene or β -cyclodextrin cores as molecular probes to study the mechanisms underlying the multivalent effects in glycosidase inhibition.^[9]

In this context, the main objective of this thesis was to push the understanding of the multivalent inhibitory effect based on a structure-activity relationships study (SAR), to probe the minimum amount of ligands needed to reach a high effect, and explore a new synthetic strategy to access C-glycosides. To achieve these goals, a novel library of cyclopeptoid-based DNJ clusters with defined valences and spatial orientations were prepared thanks to click chemistry, and a new method for the stereoselective synthesis of glycosyl cyanides as C-glycoside precursors was developed.



Chapter 1 :

GLYCOSIDASES AND THEIR INHIBITION

I Glycosidases : role and classification

I.1 Glycosidases among Carbohydrate-processing enzymes

Carbohydrates, the most abundant class of organic compounds on earth, are involved in many biological processes. They are constituents of all living organisms in Nature and play a great variety of biological functions like providing metabolic energy, protecting life from environment as constituents of cell walls and extracellular matrix, and being the complex code for recognition on cell surfaces.^[10] Although the carbohydrates are mainly composed of three elements: carbon, hydrogen, and oxygen, the diverse spatial structures of hydroxyl groups on their skeletons, the linkage between single units in polysaccharides in a linear or branched way, and the conjugation with noncarbohydrate portions brings an enormous complexity among carbohydrates and glycoconjugates. Carbohydrate-active enzymes (CAZymes) control the high level of complexity of carbohydrates *via* the processes of carbohydrates assembling (glycosyltransferases) and breakdown (glycoside hydrolases, polysaccharide lyases, carbohydrate esterases) (Figure 1).^[11,12] EC numbers, i. e., Enzyme Commission numbers, are codes associated with enzyme-catalyzed reactions. They do not specify enzymes, which means enzymes catalyzing more than one class of reactions would bear multiple EC numbers. The continuously updated website <http://www.cazy.org> provides a comprehensive classification for CAZymes.

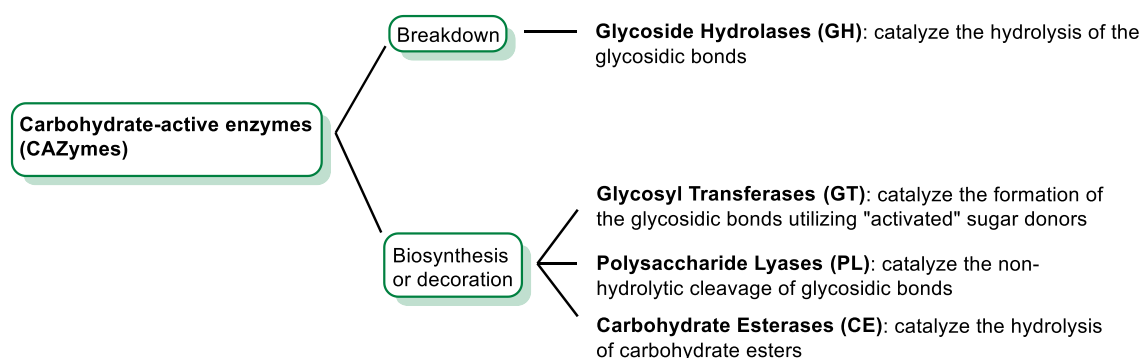


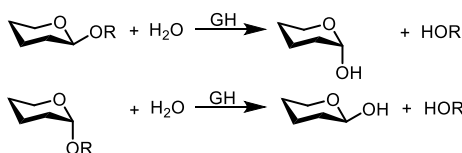
Figure 1 : Synthesis and degradation of complex carbohydrates catalyzed by carbohydrate-active enzymes.

For most organisms, around 1-3% of the genes in the genome are dedicated to encoding carbohydrate-active enzymes.^[12] Among these enzymes, glycoside hydrolases (GH) (EC 3.2.1.-), which are commonly referred to as glycosidases, occupy a large proportion and are responsible for catalyzing glycosidic bonds' hydrolysis. The acceleration of the hydrolysis by glycosidases can reach as much as 10^{17} -fold compared to the spontaneous case.^[13] Sequence-based classification of glycoside hydrolases is a rather different method from the EC classification. It is based on the similarities of GH's amino acid sequence and also correlates with catalytic machinery.^[12,14,15] According to this method, the abundant GH have been categorized into more than 100 families, which are available through the CAZypedia.^[16] Thanks to the conserved nature of GH, many valuable predictions (e. g., mechanistic information and the geometry of the catalytic residues) could be made for newly discovered glycosidases.^[12,14,15]

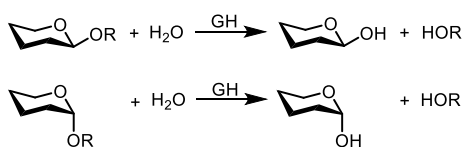
I.2 Catalytic machinery of glycosidases

Glycosidases significantly promote the hydrolysis of extremely stable glycosidic linkage in glycosides,^[13] resulting in the formation of the corresponding sugar moiety and the free aglycon. Since the 1950s, biologists have been interested in studying the reaction mechanism. In 1953, two catalytic mechanisms, i. e., inverting and retaining glycoside hydrolases, were first outlined by D. E. Koshland (as shown in Scheme 1).^[17]

Glycoside hydrolases (GH) with inverting configuration:



Glycoside hydrolases with retaining configuration:



Scheme 1 : Inverting and retaining glycoside hydrolases.^[17]

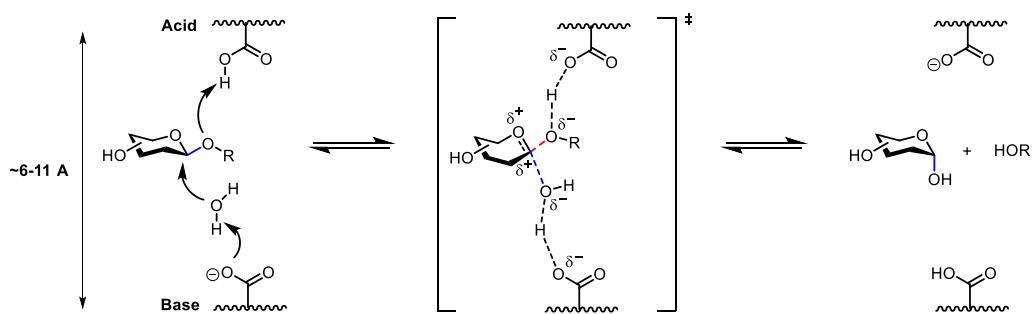
As the research continues, several variant mechanisms are gradually being elucidated to complement these two classical and most commonly employed mechanisms. The different mechanisms are described below.

● Glycoside hydrolases with inverting configuration

Inverting glycoside hydrolase mechanism displays some noteworthy features,^[18,19] including :

- relying on two carboxylic acid residues from two amino acid – commonly Glutamic or Aspartic acids – chains flanked by the substrate glycoside
- typically with 6-11 Å space apart from those two residues, which allows the entrance of both the water molecule and the substrate
- including a single oxocarbenium ion-like transition state
- via* single displacement.

The process is exhibited in Scheme 2. During the hydrolysis reaction, one of the carboxylic acids protonates the departing aglycone's oxygen atom, promoting the cleavage of the glycosidic bond. Correspondingly, the other carboxylic acid positioned on the opposite side acts as a general base, abstracting a proton from the incoming water. The deprotonation of water yields the nucleophilic hydroxide that attacks at the anomeric carbon. The bond-forming and bond-breaking proceed through the single oxocarbenium ion-like transition state. At this stage, the ring oxygen's electron-donating effect is conducive to stabilize the developing positive charge of the anomeric carbon. Additionally, in some inverting cases (e. g., β -glucosidases), the C-2 hydroxyl group OH could steady the transition state by its hydrogen bonding with the deprotonated form of carboxylic acid (i. e., the carboxylate base). The deprotonated water attacks the anomeric carbon from the opposite direction to that of the departing aglycone, leading thereby to the formation of a hemiacetal with inverted configuration.



Scheme 2 : Mechanism of inverting glycoside hydrolases.

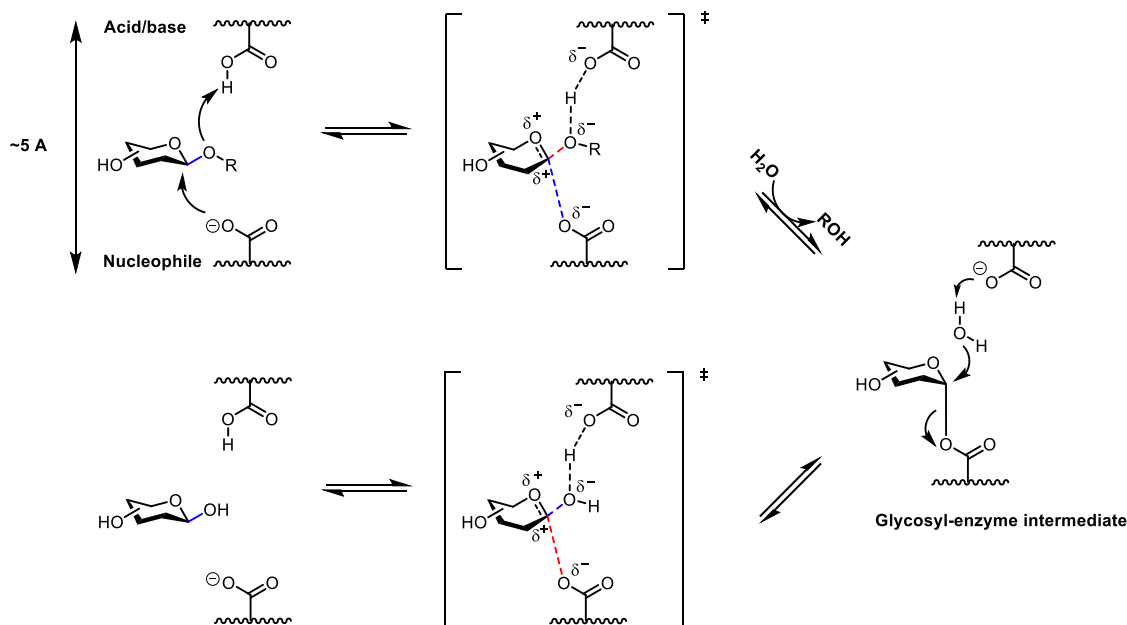
● Glycoside hydrolases with retaining configuration

A. Classic Koshland type retaining mechanism

Similar to the classical inverting mechanism, Koshland's classic retention mechanism also possesses several key characteristics,^[18] represented as follows :

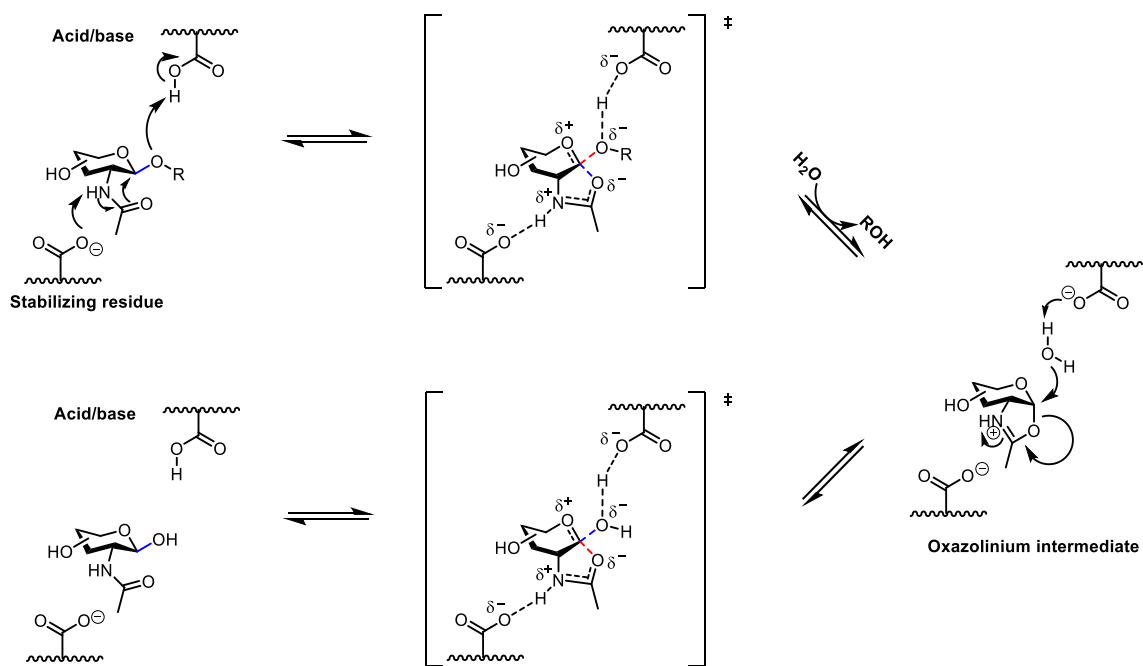
- i. relying on two carboxylic acids (typically glutamate or aspartate), one acting as an acid/base and the other as a nucleophile
- ii. the distance between the two residues is 5 Å apart
- iii. proceeding through a double-displacement or glycosylation-deglycosylation (two-step) route
- iv. involving a formation of glycosyl-enzyme intermediate, which is flanked by two oxocarbenium transition states.

The reaction starts with the attack of the nucleophile (i. e., deprotonated carboxylate) at the anomeric carbon atom. Concomitantly, the other residue plays the role of a general acid by donating a proton to the departing aglycone oxygen atom. Thereby a glycosyl-enzyme intermediate with inverted configuration formed after the oxocarbenium ion-like transition state. This step, leading to the formation of the covalent intermediate, is often referred to as the glycosylation step. It is followed by the hydrolytic cleavage of C-O bond between the substrate and the enzyme, which is known as the deglycosylation step. The deprotonated general acid/base residue who acted as an acid in the glycosylation step now plays the role of a base abstracting a proton from the incoming water molecule. Then the nucleophilic OH group attacks the anomeric carbon of the intermediate adduct, through a second oxocarbenium ion-like transition state, leading to the second inversion of the anomeric configuration, forming an hemiacetal with retaining configuration (Scheme 3).^[20,21]



B. Neighboring-group participation mechanism

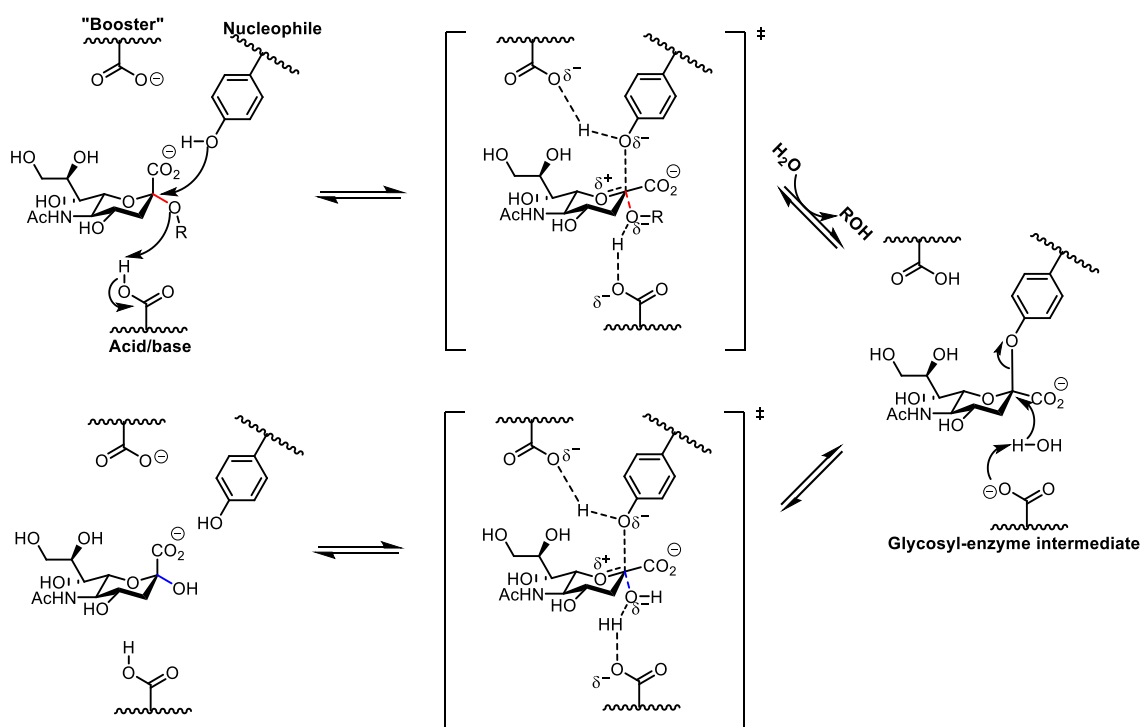
In most cases, the glutamate and aspartic acid residues of the enzyme catalyze the cleavage of glycosidic bonds: one is general acid, and the other acts as nucleophile or base. In particular, glycosidases of GH families 18, 20, 25, 56, 84, and 85 could hydrolyze the substrates possessing an *N*-acetyl (acetamido) or *N*-glycolyl moiety at the C-2 position, which acts through a neighboring-group participation mechanism and leads to a retaining configuration at the anomeric center (Scheme 4).^[20,22–24]



In contrast to the classical Koshland's mechanisms, the amino acid residue of the enzyme no longer plays as a nucleophile; instead, the intramolecular acetamido group at C-2 of the substrate attacks at the anomeric carbon atom, leading to formation of an oxazolinium intermediate. Typically, the carboxylate group on the enzyme's active site contributes to stabilizing the charge development in the transition state. There is one point to note : glycosidases do not always catalyze the hydrolysis of substrates containing a 2-acetamido group with this neighboring-group participation mechanism. For instance, enzymes categorized in the families 3 and 22 catalyze the hydrolysis through the classical retaining Koshland-type mechanism and the other hexosaminidases *via* the inverting mechanism.^[21]

C. Atypical nucleophiles

The sialidases and trans-sialidases that belong to GH families 33 and 34 utilize tyrosine as an alternative nucleophile to the traditional carboxylate moiety, leading to retaining configuration (depicted in Scheme 5). The neutral tyrosine is favored with those negatively charged substrates as it can avoid the charge repulsion between the negatively charged substrate and the carboxylate residue. To enable the nucleophilic attack at the C-2 carbon position of the substrate, the tyrosine is deprotonated by an adjacent carboxylate residue, thereby forming an inverted glycosyl-enzyme intermediate. Afterwards, the covalent bond between the sialic acid and the glycoside is truncated with the assistance of incoming water to generate the product with retention of configuration.^[20]



Scheme 5 : Retaining mechanism using atypical nucleophiles.^[20]

Some other unusual reaction mechanisms were discovered, such as a) the GH family 4 and 109 through nicotinamide adenine dinucleotide (NAD⁺) cofactor hydrolysis;^[25] b) the retaining mechanism of α -glucan lyases belonging to GH 31 *via* the elimination of glycosyl-enzyme intermediate, followed by the enol product tautomerization to final sugar;^[22,25] c) the myrosinases in GH family 1 bearing an excellent leaving group enables the first glycosylation

without the assistance of an acid residue, but with the recruitment of an exogenous base for the deglycosylation of the glycosyl-enzyme adduct.^[22,25]

II Development of reversible glycosidase inhibitors

As described above, glycosidases which are ubiquitous enzymes in Nature, play a fundamental role in diverse biological processes, such as energy uptake, the catabolism of carbohydrates in the intestines, and metastasis development, viral or bacterial infection, among others. The dysfunction or deficiency of a given glycosidase has been implicated in a plethora of diseases. Therefore, the design and synthesis of glycosidase inhibitors not only possessing high potency but also displaying specificity over other enzymes have earned high interest, and is an important field of research both in academia and the pharmaceutical industry. Broadly, the abundant glycosidase inhibitors can be divided into two categories : reversible and irreversible inhibitors (or referred to as noncovalent and covalent inhibitors). The following account will focus on the quest for reversible inhibitors and their applications.

II .1 The interest of glycosidase inhibitors

Glycosidase inhibitors display enormous therapeutic potential in many chronic or pandemic diseases, for instance lactose intolerance,^[26] lysosomal storage disorders,^[27-29] diabetes,^[30] and viral infections,^[31] resulting in more and more inhibitors that are being discovered from naturally occurring sources or human-made structures. However, native carbohydrates display many drawbacks when being considered as therapeutic agents, such as very weak binding affinities and poor pharmacokinetic properties.^[32] Glycomimetics are therefore developed as more drug-like candidates, which imitate the structure and function of native glycans, but show enhanced enzymatic stability and can offer improved binding affinity (e. g., enhanced metal chelation) by ways such as deoxygenation, pre-organization, and better pharmacokinetic features (e. g., increased oral bioavailability) *via* improving permeability, limiting metabolic degradation, *etc.*^[32,33] In this thesis, inhibition properties of representative sugar mimics devised by replacement of endocyclic oxygen atom with another atom would be described.^[34] For example, using a nitrogen atom in place of the endocyclic hemiacetal oxygen of a natural sugar gives iminosugars, a sulfur atom forms thiosugars, and a carbon atom produces carbasugars (Figure 2).^[35] Besides, other potent structures could be categorized as disaccharides and non-glycosidic inhibitors.^[26] The next sections will describe the five types of inhibitors mentioned above in detail.

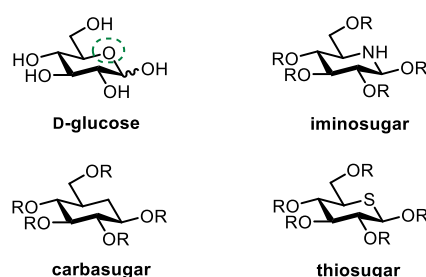


Figure 2 : Examples of glycomimetics generated by the replacement of the endocyclic oxygen atom of a natural sugar by a nitrogen, a sulfur, or a carbon atom.

II.2 Iminosugars

Iminosugars are polyhydroxylated low-weight molecules resembling monosaccharide sugars, in which the endocyclic oxygen of the natural sugar is replaced by a nitrogen atom. Iminosugars of natural origin are widely distributed in plants and microorganisms.^[1] As they have a high water solubility, they were typically disregarded and discarded with the water phase, until the 1980s when the Pharma extracted new ingredients from plant materials with organic solvents. Iminosugars attracted early attention as pharmaceutical compounds. The initial interest in iminosugars as therapeutics focused on their inhibitory properties.^[1] Their inhibition power benefits from : a) the electronic (when protonated) and shape resemblance with the oxocarbenium transition states structure formed in the process of hydrolysis or glycosylation of a natural substrate,^[36] which increases their competitiveness against the natural substrate; b) the interactions of the hydroxyl groups in iminosugar with enzyme's active site that is suggested to influence the binding affinity between the inhibitor and the enzyme.

With the developments in the field of iminosugars, it became clear that these sugar analogs possess considerable biological effects or therapeutic potency. For example, several α -glucosidase inhibitors are used in the treatment of type II diabetes (see II.2.1). The α -glucosidases and α -amylases are membrane-bound and located in the epithelium of the small intestine. They are responsible for the hydrolysis of ingested carbohydrates into absorbable monosaccharides, thereby raising the blood glucose level after meals. The therapeutic approach is that the inhibitors delay the carbohydrates digestion, as a result, the blood glucose concentration is decreased. Another striking employment of iminosugars as marketed drugs is to alleviate the symptoms of lysosomal storage disorders (as the most representative one being Gaucher's disease). The dysfunctional β -glucocerebrosidase in Gaucher's patients leads to the accumulation of the glucosylceramide causing enlargement of liver and spleen.^[37] Inhibitors of the glucosylceramide synthase lowers the biosynthesis of glucosylceramide, a substrate reduction process having an indirect effect on this substrate accumulation.

Furthermore, iminosugars also awake a bumper attention in the pharmaceutical industry that is directed towards wider biological effects, encompassing acting as immune modulators, agonists for carbohydrate sensor, or chaperones of misfolded proteins.^[1] Current efforts also open broader opportunities to treat HIV, HBV (hepatitis B virus), HCV (hepatitis C virus), and other virus infections such as SARS-CoV-2 (severe acute respiratory syndrome coronavirus-2).^[38,39]

In the following text, description of iminosugars will be concentrated on two main categories: the monocyclic and the bicyclic ones. Figure 3 illustrates the general scaffolds of a) the monocyclic iminosugars that comprise the five-membered rings of pyrrolidines, six-membered rings of piperidines, and seven-membered rings of azepanes; b) the bicyclic iminosugars including pyrrolizidines, indolizidines and nortropanes.

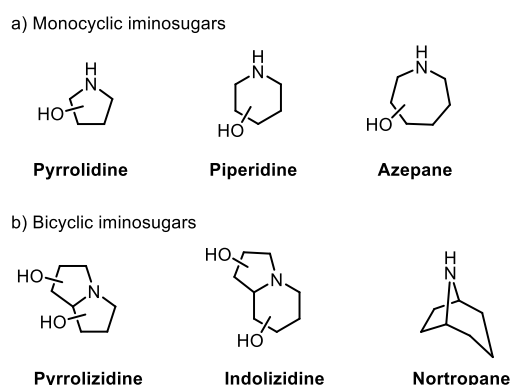


Figure 3 : Generic structures of monocyclic and bicyclic iminosugars.

II.2.1 Monocyclic iminosugars

In 1966, nojirimycin (NJ, **1**) (Figure 4) was discovered as the first natural piperidine glucose mimic setting off the development of the field of iminosugars. It was isolated from a *Streptomyces* strain and originally demonstrated to possess antibiotic properties. Moreover, it showed inhibitory ability against both α - and β -glucosidase.^[40] The NJ's hydroxyl group at C-1 position is fairly unstable; hence, the iminosugar deoxynojirimycin (DNJ, **2**) lacking this OH group was synthesized by Paulsen *et al.* in the following year.^[41] Around ten years after the initial preparation of DNJ by artificial synthesis, it was also proven to be present in Nature, when extracted from the mulberry trees' roots and named moranoline,^[42] and, alternatively, isolated from the genera *Bacillus* and *Streptomyces* culture.^[43–45] Finally, DNJ was tested to be a good inhibitor against α -glucosidases, while 1,2-dideoxynojirimycin, separated from buckwheat seeds and referred to as fagomine (**3**),^[46] showed weaker inhibiting activities over α -glucosidases.^[47] Deoxymannojirimycin (DMJ, **4**) and deoxygalactonojirimycin (DGJ, **5**), are epimers of DNJ. DMJ that could be isolated from the leaves of *Derris malaccensis* acts as an inhibitor of Golgi α -mannosidase I of rat liver.^[47] DGJ exhibits more potent inhibitory activity for α -galactosidase than β -galactosidase. Further decorations based on DNJ template, occurring naturally or human prepared, produced diverse glycoside analogues with different inhibition potency and specificity for glycosidases. For example, the α -homonojirimycin (HNJ, **6**), possessing an identical inhibitory activity against α -glucosidase to that of DNJ, sets the first case of naturally existing DNJ derivative. It is a structure with a carbon decoration at DNJ C-1 position. Nitrogen-modification of DNJ also results in the formation of many potent inhibitors. For example, Miglitol (**7**), a DNJ derivative with a hydroxyethyl substitution at the nitrogen-position, and Miglustat (**8**) are the first two marketed iminosugar drugs. Miglitol^[48], also under the brand name Glyset[®], was designed to treat type II diabetes by preventing the breakdown of the ingested carbohydrates, which therefore suppresses a booming rise of glucose concentration in blood following the meals. Miglitol has an engaging feature that it is almost fully absorbed from the gut. The Miglustat (also referred to as Zavesca[®]) is licensed for the treatment of type I Gaucher disease^[49] and Niemann-Pick type C disease.^[37]

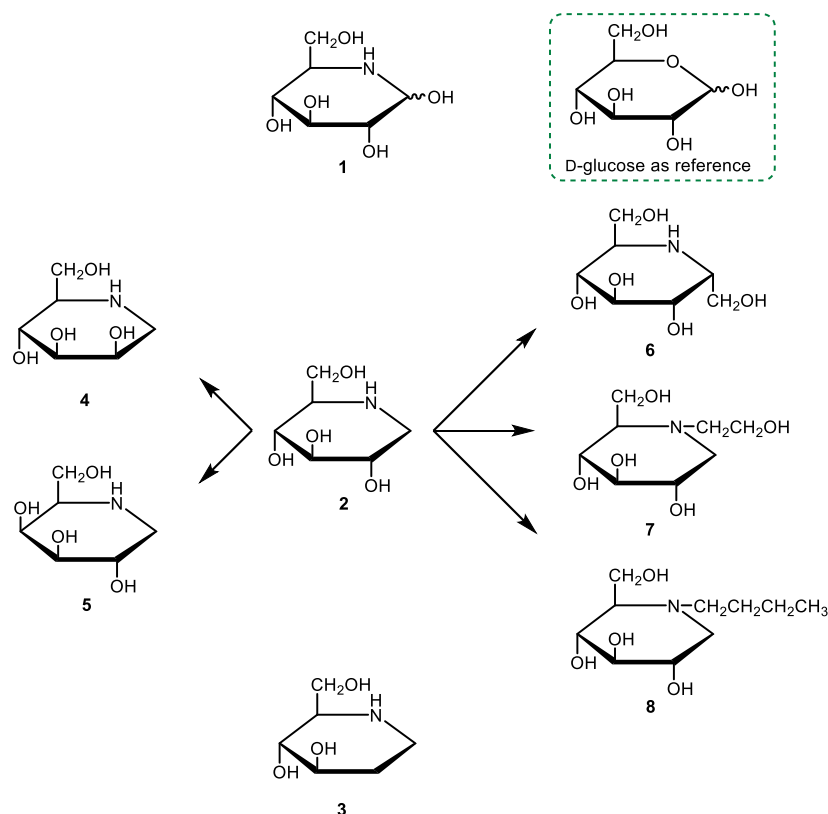


Figure 4 : Structures of nojirimycin (1), deoxynojirimycin (2), fagomine (3), deoxymannojirimycin (4), deoxygalactonojirimycin (5), α -homonojirimycin (6), miglitol (7), *N*-butyl deoxynojirimycin (8).

II.2.2 Bicyclic iminosugars

As the bicyclic iminosugars also show potent and specific inhibitory activities against glycosidases, these compounds have attracted a lot of attention. The most generic scaffolds of this class are pyrrolizidines and indolizidines.

Alexine (9) (Figure 5) was the first example of the bicyclic pyrrolizidine iminosugar (also an alkaloid), isolated from *Alexa leiopetala*, with carbon decoration at the C-3 position rather than the typical C-1 position.^[50] It resembles the structure of 2*R*,5*R*-dihydroxymethyl-3*R*,4*R*-dihydropyrrolidine (DMDP) (10) that is an inhibitor of glucosidase,^[51] which therefore suggested alexine may possess inhibitory properties against glycosidases. R. J. Nash and co-workers did some biological evaluations for alexine, showing that alexine had weaker enzymatic inhibition than DMDP against β -glucosidase and β -galactosidase.^[50] Australine (11) also possesses the particular substitution pattern as Alexine (9), bearing a carbon substituent at the C-3 position. It is a tetrahydroxy pyrrolizidine iminosugar isolated from the seeds of *Castanospermum australe* and identified as a potent inhibitor of amyloglucosidase.^[52]

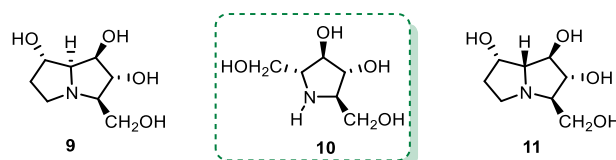


Figure 5 : Structures of Alexine (9), DMDP (10), Australine (11).

Swainsonine (12) (Figure 6), the first known iminosugar possessing an indolizidine scaffold,

could be isolated not only from plants such as locoweed but also from microorganisms.^[53] In fact, its toxicity to livestock, with clinical symptoms of nervousness, depression, emaciation, tremors, reproductive alterations, and so forth, led to its isolation.^[53] Despite the poisoning of animals, it displays several significant pharmacological effects in human beings. For example, it is a powerful inhibitor of Golgi α -mannosidase II that is involved in the *N*-linked glycosylation of proteins,^[54] which thereby blocks the biosynthesis of sophisticated oligosaccharides. Furthermore, it also has anti-tumor activity, works as an immunomodulator, and is a potential chemotherapeutic drug,^[37] which motivated the development of more Swainsonine analogs. However, it has some side effects, e. g., severe hepatotoxicity, which is related to non-specific mannosidase inhibition. Castanospermine (**13**), isolated from the seeds of *Castanospermum australe*, is another naturally occurring bicyclic iminosugar that belongs to the indolizidine class. It has similar structure as Swainsonine (**12**) and could also be regarded as a DNJ's bicyclic derivative. A number of α -glucosidases (such as maltase, Glucosidase I and II, amyloglucosidase, etc.) and β -glucosidases (like lactase) were found to be inhibited by this tetrahydroxylated iminosugar.^[53] A. A. Watson *et al.* presented its wide therapeutic applications in an excellent review.^[53] Celgosivir (**14**) is a synthetic ester pro-drug of the natural castanospermine that inhibits α -glucosidase I.^[55] It exerts its antiviral activity *via* blocking the maturation of *N*-glycans, which results in reduced virus production.^[56] It was designed initially for HIV treatment up to Phase I-II clinical trials.^[57,58] Phase II clinical trials have also been conducted with treatment-naïve HCV patients, showing a modest antiviral effect as monotherapy.^[58,59] In addition, Celgosivir has shown potent activity towards SARS-CoV-2, which provides a possible pathway for treating COVID-19.^[58] (-)-Steviamine (**15**), possessing structural similarity to Swainsonine (**12**), is an indolizidine iminosugar with an alkyl substituent on the piperidine ring, isolated from *Stevia rebaudiana* leaves.^[60] It is the first naturally existing product showing the inhibitory activity of α -galactosaminidases, which sheds light on the design of chaperones for treating Schindler-Kanzaki disease and strategy for cancer therapy.^[61]

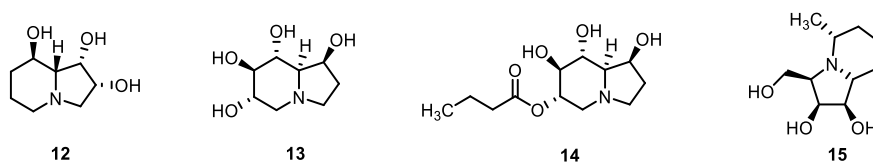


Figure 6 : Structures of D-Swainsonine (**12**), Castanospermine (**13**), Celgosivir (**14**), (-)-Steviamine (**15**).

Nortropane is a new class of bicyclic iminosugar, which contains polyhydroxylated Calystegines. Calystegines are the secondary metabolites of plants displaying special structural features : a) a nortropane ring system; b) a high degree of hydroxylation differing in the hydroxyl groups' number, position, and stereochemistry on the nortropane scaffold; c) an aminoketal functionality at a position that is common to the two rings.^[62] Figure 7 presents three Calystegines, Calystegine A₃ (**16**), Calystegine B₁ (**17**), and Calystegine C₁ (**18**). A. A. Watson *et al.* listed the sources of some naturally occurring nortropane iminosugars and further summarized the glycosidases inhibited respectively.^[53]

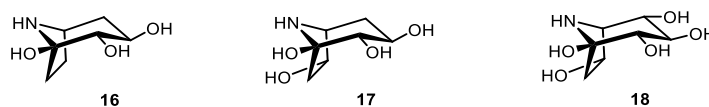


Figure 7 : Structures of Calystegine A₃ (**16**), Calystegine B₁ (**17**), and Calystegine C₁ (**18**).

II.3 Thiosugars

Thiosugars are also a class of very promising sugar mimics, in which a sulfur atom is replacing the endocyclic oxygen of the natural sugar or the oxygen of the glycosidic bond of disaccharides. The presence of sulfur atoms gains unique physicochemical properties for this type of compounds. Compared with oxygen, sulfur is owning more disperse electron density (or being more polarizable, less electronegative), the C-S bond is longer and less stable and less polar than the carbon oxygen bond. The anomeric effect and global flexibility are also different.^[33] Since sulfur electronegativity is close to the carbon's one, thiosugars benefit from enhanced lipophilicity, which can improve hydrophobic interactions with the protein and also reduces desolvation requirements. Thiosugars with S-glycosidic linkage are more stable to chemical and enzymatical hydrolysis because of lower basicity and thus less formation of the conjugate acid intermediate involved in glucoside hydrolysis.^[63] However, they also have enhanced flexibility. Thiosugars with endocyclic S atom are also more stable, have a reduced polar surface area and a modified pyranoside conformation.^[33] Altogether, with their different polarity, enhanced lipophilicity geometric and flexibility changes, thiosugars benefit from improved biological activities and better oral bioavailability than the other carbohydrates analogs.^[26,33]

The functionalized thiosugars are potential targets that enrich the carbohydrate-based therapeutics. However, naturally occurring thiosugars are not abundant in Nature. 5-Thio-D-mannose (**19**) (Figure 8), isolated from the marine sponge *Clathria pyramida* in 1987, is the first natural occurrence of a free 5-thiosugar. Correspondingly, before the isolation of **19** from Nature, the synthetic 5-thio-D-glucose (**20**) was provided in 1962 as the first example of this class.^[64] Salacinol (**21**) and Kotalanol (**22**) are two popular natural 1,4-thioanhydrosugars, which possess skeletons of sulfonium salt-containing heterocycles. They were isolated from the antidiabetic herb used in Indian Ayurvedic traditional medicine and exhibited potent inhibitory activity of intestinal α -glucosidases (e. g., sucrase, maltase, and isomaltase).^[65,66] Besides, interestingly, they were found to display more potent inhibitory effects on sucrase than the commercial α -glucosidase inhibitor acarbose which will be introduced in the following section.

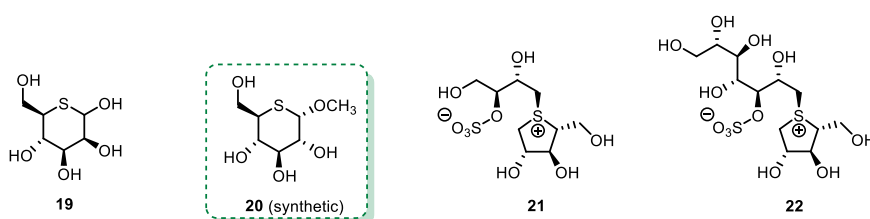


Figure 8 : Structures of 5-thio-D-mannose (**19**), 5-thio-D-glucose (**20**), Salacinol (**21**), and Kotalanol (**22**).

Synthetic thiosugars supply the quantity and variety of compounds of such kind. 1-Deoxy-3-S-(1-thio- α -D-glucopyranosyl)-mannojirimycin (**23**) and 1-deoxy-3-O-(5-thio- α -D-glycopyranosyl)-mannojirimycin (**24**) are thio analogs of 1-deoxy-3-O-(α -D-glucopyranosyl)-mannojirimycin (**25**) (a potent inhibitor of *endo*- α -D-mannosidase) by replacement of the glucosyl unit with 1-thioglucose or 5-thioglucose in the disaccharide **25**.^[67] Since the thioglycosides, with a glycosidic sulfur atom, have better stability against either enzymatic cleavage or chemical degradation, **23** and **24** may therefore be more stable inhibitors against *endo*- α -D-mannosidase than their oxygen counterpart **25**. In 2018, our lab reported an expeditious synthesis of 1-thiotrehalose (**26**) and its derivatives **27** and **28** based on the

original use of commercially available tri-*O*-benzyl-1,6-anhydro-D-glucose.^[68]

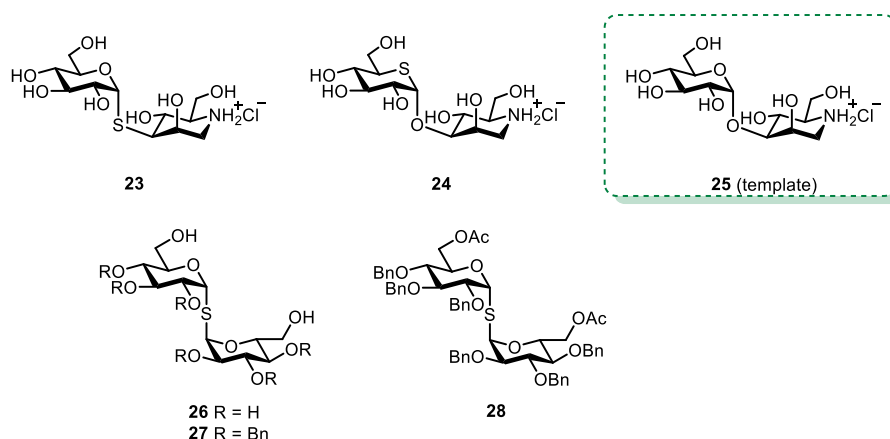


Figure 9 : Structures of 1-deoxy-3-S-(1-thio- α -D-glucopyranosyl)-mannojirimycin (**23**), 1-deoxy-3-O-(5-thio- α -D-ghicopyranosyl)-mannojirimycin (**24**), 1-deoxy-3-O-(α -D-glucopyranosyl)-mannojirimycin (**25**), 1-thiotrehalose (**26**) its derivatives **27** and **28**.

II.4 Carbasugars

Carbasugars are a class of alicyclic analogs of a cyclic monosaccharide obtained by replacing the endocyclic oxygen atom with a methylene group. In 1966, McCasland *et al.* first described this glycomimetic, which is also expressed as “pseudo-sugar”, by synthesizing the first carbasugar 5a-carba- α -D-galactopyranose (**29**) (Figure 10),^[69] which was, five years later, isolated from the fermentation broth of several *Streptomyces* species.^[26] Carbasugars closely resemble the structures of carbohydrates. On the other hand, the substitution of the acetal linkage in natural sugar with a non-hydrolysable ether and loss of the anomeric effect (Figure 2) leads to a significant distinction. Therefore, they are supposed to possess original biological properties and enhanced stabilities compared to their carbohydrate precursors. The achievements in medicine stimulating the research in this field and more and more attention is therefore being paid to the synthesis and identification of novel carbasugars.^[26,70,71] Figure 10 reveals some examples of carbasugars that could be found in Nature, of which, Conduritols and cyclophellitols play as glycosidase inhibitors.^[26,72]

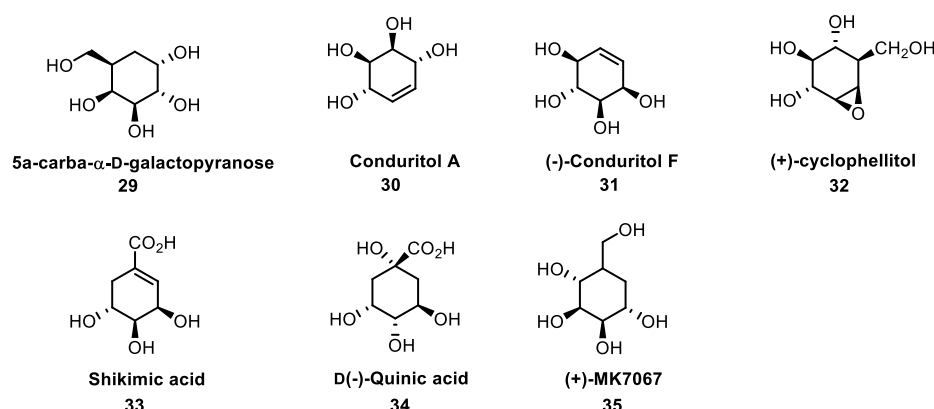


Figure 10 : Examples of naturally occurring carbasugars.^[26,72]

Amino carbasugars are carbasugars derivatives in which the *O*-glycosidic bond is replaced by

a C-N bond. Figure 11 presents some instances of amino carbasugars, namely validamine (5a-carba- α -D-glucopyranosylamine, **36**), valienamine (5, 5a-unsaturated, **37**), hydroxyvalidamine (**38**), and valioline (39). They are of natural occurrences, which were first obtained from the fermentation broth of the antibiotic validamycin A (**41**) (Figure 12, see below).^[73] Carboglycosylamines showed in Figure 11 display more or less inhibitory activity against α -glucosidases.^[73]

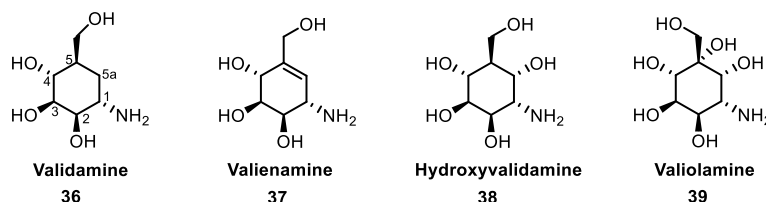


Figure 11 : Examples of amino carbasugars.

Carbasugars have acquired successful applications in medicine and clinical treatment. Acarbose (**40**) (Figure 12) isolated from *Actinoplanes sp.*, containing the active pharmacophore of valienamine N-linked to OH-4 of a 6-deoxy-D-glucose residue, is a marketed carbapentasaccharide α -glucosidase inhibitor for the treatment of type II diabetes mellitus under the brand names Glucobay[®] and Precose[®].^[74] The valienamine (**37**) also participates in constructing another commercially crucial family of compounds possessing disparate biological activity, that is, the validamycins.^[74] These compounds were separated from *Streptomyces hygroscopicus var. limoneus*, and perform remarkable activity against pathogenic fungi.^[75] Validamycin A (**41**) is the most abundant representative whose structure comprises a valienamine (**37**) component attached through a nitrogen bridge to a second cyclitol, i. e., validamine (**36**), in which the double bond has been reduced. Besides, in validamycin A (**41**), the double bond reduced validamine **36** is linked *via* a β -glycosidic linkage to the OH-4 of a D-glucose moiety. An essential aspect of validamycin A is that it sets the starting point for developing the semisynthetic compound voglibose (**42**), an α -amylase inhibitor of the second generation. Voglibose (**42**) is another commercialized antidiabetic agent being 20 times more potent than acarbose (**40**).^[74] In 2018, Shing and co-workers investigated novel small molecules **43-46** as potential antidiabetic agents exerting potent and selective inhibition of the sodium-dependent glucose cotransporter 2 (SGLT2), which can help reducing the blood glucose concentration by promoting urinary glucose excretion.^[76]

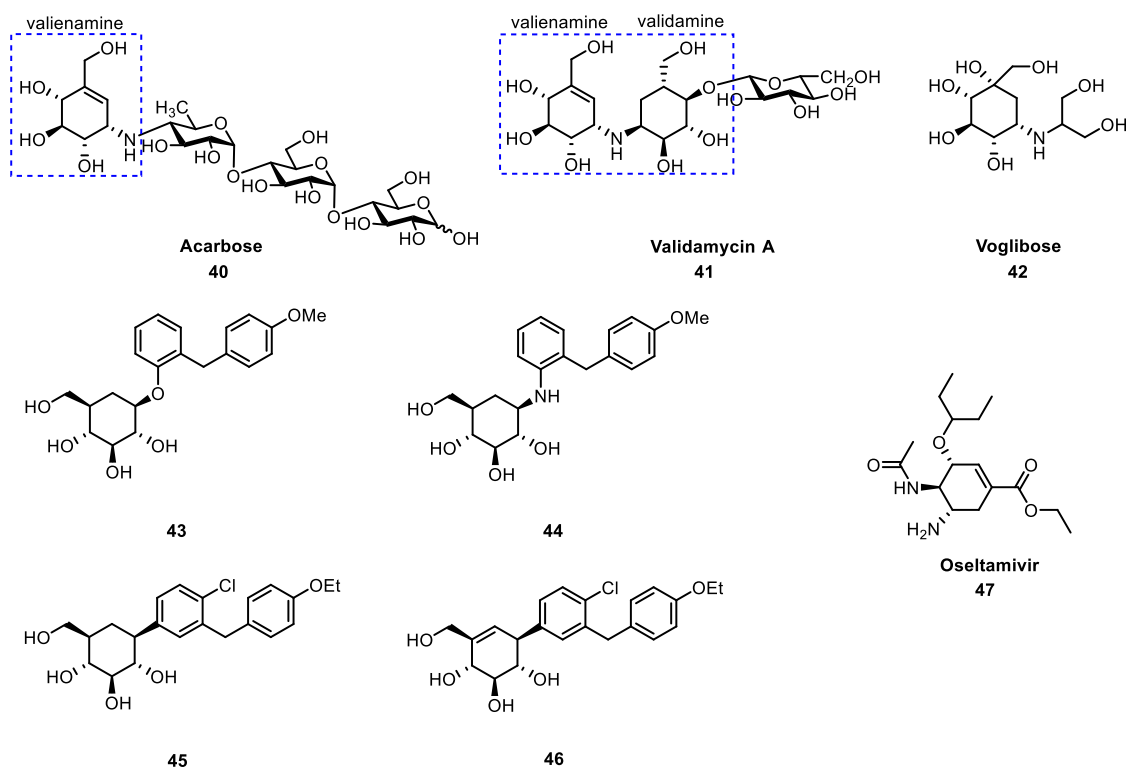


Figure 12 : Structures of Acarbose (40), Validamycin A (41), Voglibose (42), carbasugar SGLT2 inhibitors (43-46), Oseltamivir (47).

Oseltamivir (47) (Figure 12) is another popular amino pseudosugar which is sold as an anti-influenza drug under the well-known trade name Tamiflu®. Oseltamivir exhibits inhibitory activity towards the enzyme neuraminidase responsible for disseminating the virus and is widely utilized to treat influenza A viruses.^[77]

II.5 Disaccharide inhibitors

Kojibiose (2-*O*- α -D-glucopyranosyl-D-glucose) and Nigerose (3-*O*- α -D-glucopyranosyl-D-glucose) are two important natural examples of disaccharides inhibitors (shown in Figure 13). Kojibiose (α 1-2 linkage), isolated from saké and koji extracts in 1957, inhibits the α -glucosidase acting on (Glc)₃(Man)₉(GlcNAc)₂, while Nigerose, produced from degradation of amylopectin, inhibits the α -glucosidase active on (Glc)₁₋₂(Man)₉(GlcNAc)₂.^[78-80] The discovery of these two compounds lays the essential foundations for developing novel disaccharide analogs that could help to treat HIV infections.

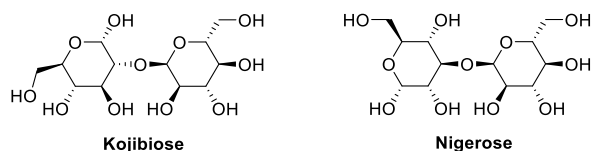


Figure 13 : Structures of Kojibiose and Nigerose.

By definition, C-disaccharides are disaccharide analogs in which a carbon atom replaces the interglycosidic oxygen bond resulting in the formation of a fairly stable glycoside mimic that is not prone to hydrolysis.^[81] Figure 14 exhibits simple structures of β -*O*-disaccharides *versus*

β -C-disaccharides.^[81] Given their main scaffold is similar to the parent sugar, it stands to reason that these derivatives could also elicit glycosidase inhibition. Postema *et al.* prepared an array of β -C-disaccharides *via* a radical allylation-RCM strategy that showed modest inhibition against β -glucosidase.^[81]

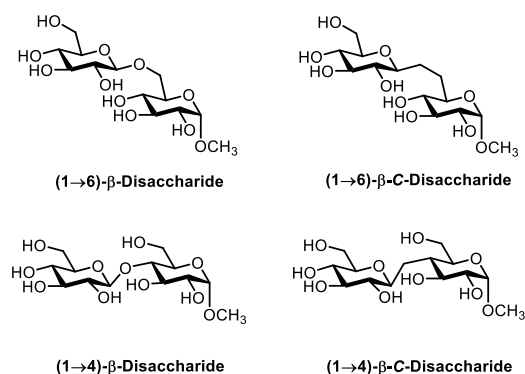
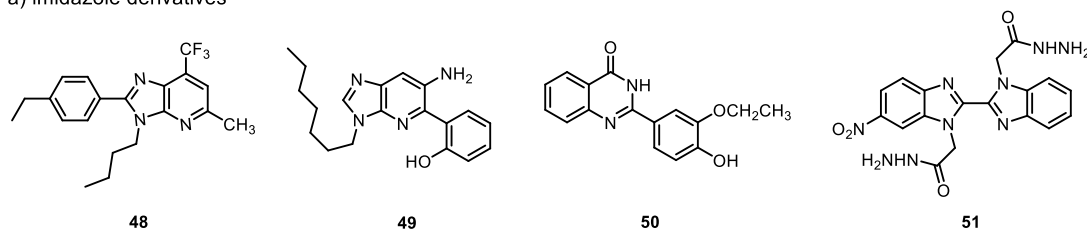


Figure 14 : β -O-disaccharides versus β -C-disaccharides.^[81]

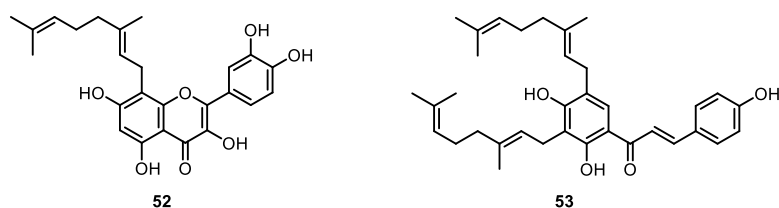
II.6 Non-glycosidic derivatives

There are also many non-glycosidic compounds showing moderate to excellent glycosidase inhibitory activity. Z. Y. Liu *et al.* summarized a panel of newly synthesized α -glucosidase inhibitors that are not based on a sugar scaffold and investigated their structure-activity relationships (SARs) in antidiabetic studies. In their review, the α -glucosidase inhibitors of such kind were classified into three categories, that is, imidazoles and pyrazoles, chromones and macrocyclic compounds.^[82] Structures of some relevant examples are shown in Figure 15.

a) imidazole derivatives



b) chromone derivatives



c) macrocyclic compounds

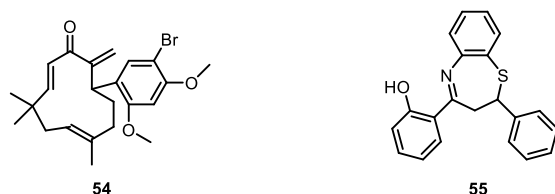


Figure 15 : Examples of synthetic non-glycosidic α -glucosidase inhibitors.^[82]

Several non-glycosidic α -glucosidase inhibitors are naturally occurring and were isolated from marine sources. The tetrahydroisoquinoline alkaloids (Figure 16) named schulzeines A-C (**56-58**) were obtained from the hydrophilic extract of the marine sponge *Penares schulzei* possessing potent inhibitory activity towards α -glucosidase.^[83] Baicalein (**59**) was isolated from a very different source, marjoram leaves of *Origanum majorana*, plants. It is a 5,6,7-trihydroxyflavone elucidated as a potent α -glucosidase inhibitor.^[84]

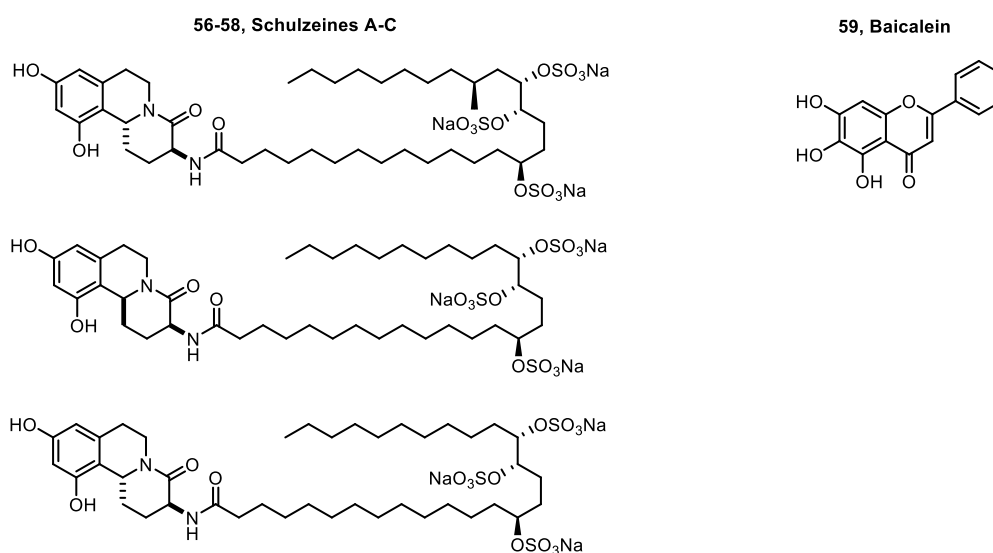


Figure 16 : Examples of non-glycosidic α -glucosidase inhibitors in Nature.

It is well known that α -glucosidases are involved not only in the glycogenolysis, but also in the glycan trimming of glycoproteins, which is an extensive biological process, comprising the facilitating of protein folding in the endoplasmic reticulum, the stabilization of cell-surface glycoproteins and information and addressing coding. Therefore, the inhibitors of α -glucosidases are clinically important for treating diseases such as cancer, diabetes, and viral infections.^[31,85,86] The biological activities of non-glycosidic compounds against α -glucosidase highlights a novel option to design and achieve more α -glucosidase inhibitors without mimicking the natural substrate of the enzymes. And more importantly, this new class of inhibitors, the non-glycosidic ones, may be helpful for eliminating certain physicochemical drawbacks that carbohydrates analogues present.

III Multivalency as a chemical organization and cooperation principle for glycosidase inhibition

Multivalent interactions can be widely used to achieve a targeted reinforcement of interaction between different molecules. They exert a crucial factor in biological activities, including adhesion, recognition, and signal processes. An overview of multivalency utilization as a chemical organization and cooperation principle for glycosidase inhibitors will be presented before introducing the objectives of this thesis research work.

III.1 Examples of multivalency as a key principle in Nature

Multivalency plays as a key principle in Nature to achieve strengthened but reversible interactions. An obvious and easy to understand example of this concept is the design of

velcro (Figure 17, right), which imitates the principle behind the burr (Figure 17, left). The force of individual hooks entangling with loops is weak, and they are easy to be separated. However, when multiple hooks on one side of velcro connect with loops on the other side simultaneously, the two surfaces can firmly adhere to each other to resist external forces, such as sliding. As it is well-known, the more hooks and loops are interacting per unit area at the same time, the stronger the binding of the two surfaces. Moreover, the multiple interactions are reversible by sequentially separating every single hooks and loops.



Figure 17 : The principle behind the burr (left) in Nature and the artificial imitation material, Velcro (right).^[87]

The multiple interactions of a multivalent system display a dramatic enhancement of binding affinity on a molecular scale compared to its monovalent reference that interacts in a one-to-one interaction. The adhesion of a virus to the target host cell's surface is a typical instance of multivalent interactions (Figure 18). Haemagglutinin (HA) and sialidase are surface glycoproteins of the influenza virus that are carbohydrate-recognizing proteins, able to recognize the sialic acid (SA) also called *N*-acetylneuraminic acid (Neu5Ac) (Figure 18, **60**) of humans cells. HA comprises three identical subunits, and is densely anchored to the lipid membrane of the virus (about 2-4 per 100 nm² or 600-1200 per virus particle).^[77,88] The terminal α -ketosidically linked Neu5Ac residues, capping the ends of many glycoconjugates, are also distributed densely on the host cell-surface (50-200 per 100 nm² roughly).^[88] The multiple simultaneous interactions, the recognition process, between the virus HA and the target host cell-surface SA lead to a stable attachment, which triggers the first step of infection. The virus is subsequently endocytosed, then occurs fusion, preparation of the virion progeny, and budding to exit the target host cell. The newly synthesized virion progeny is ultimately released by sialidase cleaving the α -ketosidically linked Neu5Ac residues from both virus and the host-cell surface.

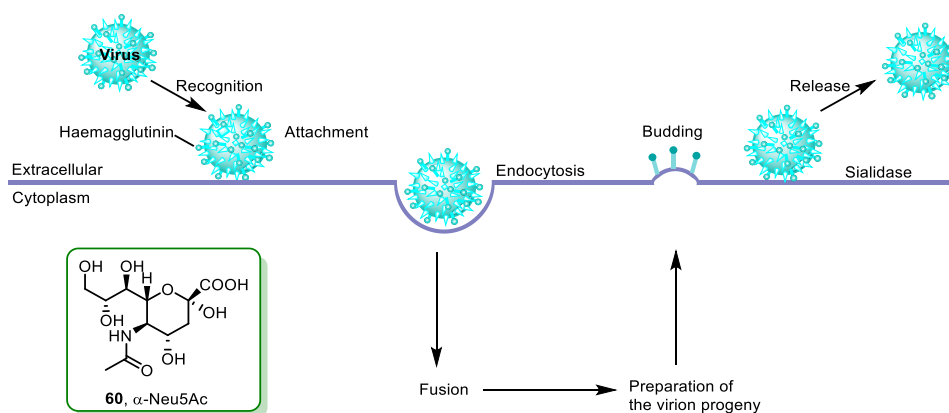


Figure 18 : Life cycle of the influenza virus and the structure of α -Neu5Ac **60**.^[77]

The principle that many particles or biological systems interact *via* simultaneous multiple molecular contacts is of therapeutic interest, since it provides interesting strategies for designing drugs.

III.2 Techniques for quantification of multivalent interactions

Quantification of the binding parameters is essential for multivalent interactions, not only the fundamental studies but also the applications. Several techniques have already been developed to quantify multivalent interactions. The following text demonstrates some of the most important techniques.^[87,89,90]

➤ Fluorescence

1. Solution-based fluorescence competition assay

Lectins, one of major groups of carbohydrate-binding proteins, are abundant in all species and play important roles in infection and disease.^[33] The solution-based fluorescence competition assay allows to derive the binding affinity of glyconanomaterials with lectins through the construction of a dose response curve of fluorescence vs. concentration of glyconanomaterials. The lectins or nanomaterials must be measurably fluorescent, no matter inherently or tagged with a fluorescent dye. In the experiment, varying concentrations of glyconanomaterial and a competing ligand, i. e., a free carbohydrate, with fixed concentration are incubated coupled with the lectin. Therefore, lectin will form two equilibria, one with glyconanomaterial and another one with the free carbohydrate. The interactions between glyconanomaterial and lectin result in the formation of agglomerates of glyconanomaterial-lectin, which can be precipitated by centrifugation, leaving the unbound glyconanomaterial in the supernatant. Further, the supernatant's fluorescence intensity is measured, and therefore, a dose-response curve can be constructed. S. H. Liyanage and co-workers employed this method to determine the apparent dissociation constant between the tetrameric plant lectin concanavalin A and carbohydrate-functionalized gold nanoparticles.^[89]

2. Fluorescence competition assay on microarray

Microarrays allow the reactions or assays to be carried out on a wafer or a glass, which are referred to as "lab-on-a-chip" devices. The spots, printed by a robotic printer, containing the reagents form the arrays, which provide the sites and conditions for conducting hundreds and thousands of assays at the same time. The microarrays devices combined with fluorescence can be applied to determine the binding affinity of glyconanomaterials and lectins interactions. In an array, the ligand is fixed on the solid substrate, while the analyte molecule is in solution.^[91] The fluorescence intensity of the product obtained by treating the ligand with the analyte molecule is related to both the analyte concentration and the binding kinetics. S. H. Liyanage and co-workers also developed a super-microarray for detecting the binding affinity of various carbohydrates with lectins on one single microarray concurrently.^[92]

➤ QCM

Quartz crystal microbalance (QCM) provides an indirect method to report the binding events, i.e., the association/dissociation rates and association/dissociation constants. The detection relies on a sensor chip, a piezoelectric crystal, whose resonant frequency can respond rather sensitively to its surface's mass change. Therefore, QCM is able to detect monolayer surface coverage as low as one $\text{ng cm}^{-2} \text{ Hz}^{-1}$,^[93] which makes it possible to monitor interactions at the

molecular level. In the assay, a gold film immobilized with ligands overlays the piezoelectric crystal, and the analyte molecules are prepared in solutions with varying concentrations. The sensor chip treating with the solution results in mass changes on the sensor surface, which is reflected as a variation of frequency (ΔF). Eventually, the association/dissociation constants are obtained by monitoring ΔF vs. time with different concentrations of analyte. QCM is a label-free technique without utilization of additional tags, which makes it versatile and possible to monitor real-time events with a liquid cell allowing the studies of different conditions.

➤ **SPR**

Surface plasmon resonance (SPR) is an optical sensor based on the excitation of surface plasmon, belonging to the refractometric sensing devices. In principle, resonance occurs when the incident photons frequency matches the natural oscillation frequency of the surface plasmon, leading to an absorption and the peak position is sensitive to the refractive index changes at or near the metal surface.^[94] It offers an indirect and a label-free technique to measure the multivalent interactions of the samples in the solution in contact with the ligands immobilized on a thin film, such as a gold film or a metal film covered with a carboxymethylated dextran layer.^[95] The parameters of binding affinity and kinetic, for example, association/dissociation constant and association/dissociation rates, can be obtained by monitoring the signals resonance/response units vs. time. As the incident light does not perforate through the analyte solution, SPR, therefore, possesses another attractive virtue that it is suitable for measuring samples in colored or turbid solutions.

➤ **ITC**

Isothermal titration calorimetry (ITC) is a non-destructive and label free (i. e., ligands or substrates with no need for immobilization on a solid film or modification of a fluorescent tag) technique to obtain the complete thermodynamic and kinetic parameters including binding enthalpy, binding entropy, free binding enthalpy, association constant, and stoichiometry by measuring the evolution of heat during biomolecular interactions.^[96] In the assay, aliquots of the binding ligand are titrated into the sample cell that contains the binding substrate at a constant temperature. With the advancement of technology, the heat released or absorbed in molecular interactions of nanomole (μg) levels can be detected by the state-of-art ITC instruments.^[97] Nevertheless, the formation of aggregates, especially in the case of multivalent ligands, would lead to misleading data in the measurement of thermodynamic parameters.

➤ **DLS**

Dynamic light scattering (DLS) has been utilized to determine the binding affinity between glyco-NPs (nanoparticles) and lectins. The quantitative analysis is based on the hypothesis that there are no interactions between particles in the dilute suspensions either by collisions or electrostatic forces, and the particle size decides the speed of particle movement. DLS allows calculation of the particles' hydrodynamic volume depending on the diffusion rate of particles. The multivalent interactions of glyco-NPs with lectins change the particle size in a concentration dependent manner as the formation of cross-linked aggregations, whereas the particle size remains unchanged if glyco-NPs do not interact with lectins.^[98-101] By varying the lectin concentration, the size of agglomerates is measured, followed by the fitting of the computed hydrodynamic diameter (of agglomerates) to a proper binding isotherm to give the dissociation constant. DLS is also a label-free and non-destructive method.

There are also other techniques quantifying multivalent interactions. Single molecule force spectroscopy (SMFS) complementing atomic force microscopy (AFM) technique measures the binding strength between bacteriophage P22 tailspike proteins and O-antigenic lipopolysaccharides of Gram-negative Salmonella typhimurium S. enteritidis, S. typhi253Ty (S. typhimurium) directly.^[102] Nuclear Magnetic Resonance (NMR) spectroscopy provides structural aspects of multivalent-induced complexes.^[103] X-ray crystallography helps the understanding of binding modes.^[104] UV/Vis spectroscopy allows the determination of association constants.^[87]

Among all the techniques mentioned above, ITC,^[105] DLS,^[106] AFM,^[106] X-ray crystallography^[104], and UV/Vis spectroscopy^[5] have already been employed to study the mechanisms behind the multivalent inhibitory effect in glycosidase. (see paragraph III.3)

III.3 Multivalent glycosidase inhibitors

III.3.1 Definition of the multivalent effect

Multivalent interactions are ubiquitously involved in numerous biological recognition processes.^[87,88] They are defined as the interactions between a multivalent ligand and a multivalent receptor and are compared to the interaction monovalent ligands with the same multivalent receptor. The compound bearing multiple copies of bioactive unit or ligand (by connection to a scaffold) shows better biological response, such as the overall binding affinity and selectivity, with respect to the response given by the sum of the individual bioactive units (Figure 19a). For lectins, the “bioactive unit” is a ligand. Since enzymes are catalyzing a reaction, the “bioactive unit” can’t be the substrate which would be cleaved but should be something recognized but not transformed, thus a reversible inhibitor ! For lectin/ligands interactions, the multivalent effects were quantified thanks to the determination of association constants. For enzyme/inhibitors multivalent interactions, the inhibition constants are determined. The relative potency (*rp*) is related to affinity enhancement over the monovalent reference or relative to the monovalent reference (Figure 19b). Correspondingly, *rp/n* is relative affinity enhancement per inhibitor head. The multivalent effect generally refers to as a *rp/n* being over 1, meaning over the statistical effect.^[107] On basis of this concept, a great deal of multivalent systems have been synthesized. For instance, in the last decade, carbohydrate chemists have extensively prepared plenty of glycoclusters to study the multivalent effect in glycosidase inhibition.^[108]

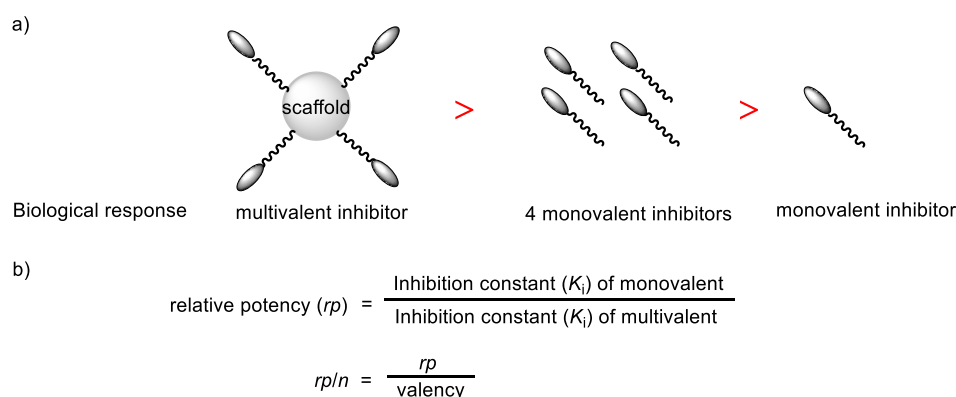


Figure 19 : a) Cartoon representation of the multivalent effect; b) Definition of *rp* and *rp/n*.

From theoretical point of view, the concept of multivalent effect suits better to lectin-carbohydrate interactions. Typically, lectins only show low affinities to their native ligands due to ligands engaging lectins through weak interactions, such as H-bonding.^[33] However, as lectins possess multiple and easily accessible binding sites, the binding affinity could be spectacularly enhanced by using multivalent glycoclusters who are able to bridge multiple binding sites on lectins simultaneously.^[109,110] An enzyme usually has one active site and it was counter intuitive to expect a multivalent effect with them. The fact is, however, that impressive results have been obtained in the field of multivalent glycosidase inhibitors, especially the 36-valent cluster **135d** (Figure 32) showing the largest binding enhancement (4700-fold on a valency-corrected basis) reported on a glycosidase so far.^[5,108]

III.3.2 Quantification of multivalent interactions with enzymes and inhibitors

UV/Vis or fluorimetric spectroscopy allows the measurement of the kinetics of enzymatic reactions thanks to chromogenic or fluorogenic substrates. Michaelis-Menten equations are used to determine the dissociation constant from the initial velocities of the inhibited reaction (at different inhibitor and substrate concentrations) compared to the non inhibited one. For example, the measurement of inhibitor's K_i against Jack bean α -mannosidase (the enzyme used for this thesis), 4-nitrophenyl- α -D-mannopyranoside can act as the substrate in the inhibition test.^[111] The enzymatic hydrolysis of this substrate will release 4-nitrophenol, which is weakly colored at the pH of inhibition test but turns yellow at pH>10. Sodium carbonate solution is used to quench the hydrolysis and favours the formation of colored 4-nitrophenolate. The produced 4-nitrophenolate is measured continuously at 405 nm. The optical density measured for the blank group is subtracted from the optical density of the corresponding experimental group (containing the inhibitor, substrate, and enzyme), then divided by the reaction time, giving access to the initial velocity. Fitting the inverse of the initial velocity to either Dixon plot, the double-reciprocal Lineweaver Burk plot, or the Morrison equation gives the dissociation constant.

III.3.3 State of the art of multivalent glycosidase inhibitors in 2020

III.3.3.1 The seminal sparks

The first examples of multivalent inhibitors of glycosidases were the five synthetic tethered divalent iminosugars reported by Johns and Johnson in 1998.^[112] In that period, it was observed that tethered dimeric substrates often displayed dramatic differences in the physical and biological properties when compared to their parent monomeric counterparts.^[113,114] Inspired by those precedents in literature, Johns and Johnson rationally designed iminosugar glycosidase inhibitors in the D-manno series with different conformational rigidity and stereochemistry in the scaffolds to investigate their contributions to the biological activity (Figure 20). The target compounds were prepared by *de novo* synthetic methodology.^[112]

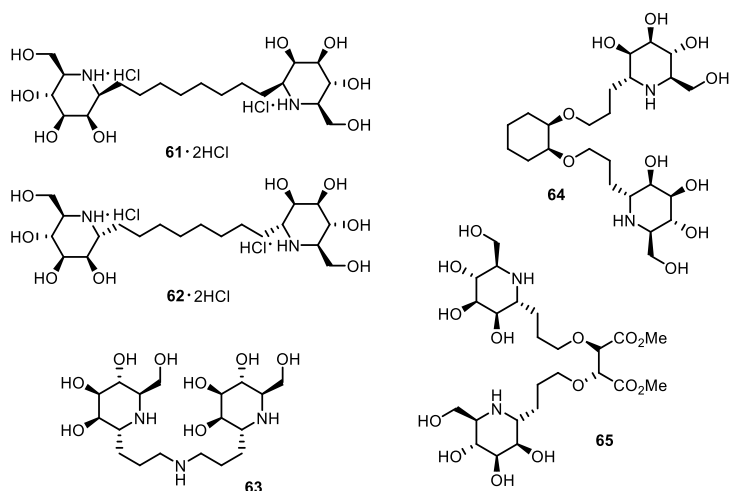


Figure 20 : Structures of divalent iminosugars 61-65.

Out of the five scaffolded divalent DMJ analogues **61-65**, only structure **61** was evaluated against seven common glycosidases, i. e., α -glucosidase (yeast), β -glucosidase, α -galactosidase, β -galactosidase, α -mannosidase, β -mannosidase, and amyloglucosidase. Iminosugar **61** was found to show inhibitory activity towards amyloglucosidase and α -mannosidase displaying IC_{50} values of 20 μ M and 49 μ M, respectively.^[112] However, the authors did not try to assess any possible multivalent effect.

In 1997, Bols and co-workers completed the synthesis of the racemic (\pm) 1-azafagomine (\pm)-**66** (Figure 21), an iminosugar analogue close to fagomine **3** (Figure 4) with a second nitrogen atom in place of the anomeric carbon atom. This is a potent glycosidase inhibitor which inhibits α -glucosidase (yeast) and β -glucosidase (almond) with K_i values of 3.9 μ M and 0.65 μ M, respectively.^[115,116] The basis of this excellent inhibitory activity is closely related to its ability to electronically and sterically resemble the transition state of glycoside hydrolysis when protonated. In 1999, the solid-phase synthesis of a tetravalent iminosugar **67** bearing 1-azafagomine units was carried out thanks to their interest about investigating the effect of multivalency on glycosidase inhibition.^[2] The tetravalent azafagomine **67** was found to show a good inhibition potency against β -glucosidase (almond) with a K_i value of 70 μ M. However the multivalent effect could not be quantified as the monovalent model was a weak inhibitor, the K_i of which was not determined.^[117]

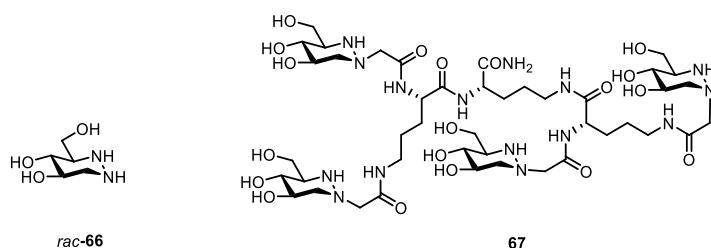


Figure 21 : Structure of racemic (\pm) 1-azafagomine (\pm)-66 and tetravalent iminosugar 67.

Four years later, in 2003, Y. Le Merrer and co-workers synthesized stable inhibitors with increased selectivity by modulating the aglycon part of 1,6-dideoxy-1,6-imino-D-mannitol **68** and 1,5-dideoxy-1,5-imino-L-gulitol **69** with non-hydrolyzable bond thanks to *N*-linkage.^[118] They prepared two divalent iminosugars, **70** and **71** (Figure 22), and evaluated their inhibitory activity over four common glycosidases (β -D-glucosidase, α -D-glucosidase, α -D-mannosidase,

and α -L-fucosidase), among which compound **70** showed competitive and selective inhibition towards α -L-fucosidase with a K_i value of 15 μ M.^[118]

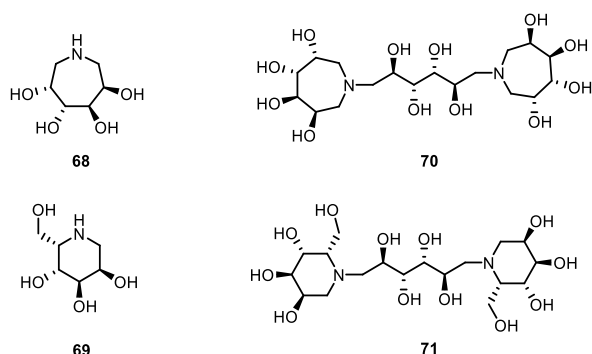


Figure 22 : Structures of divalent iminosugars **70**, **71**, and their parent iminosugars **68**, **69**.

However, maybe because the di- and tetra-valent iminosugars reported above did not display a dramatical improvement of inhibition potency, no new achievement was reported before the year 2009. That means, before 2009, few glycosidase inhibitors of low valency were prepared; and it was not possible to quantify their multivalent effects.

It was not until 2009 that the first systematic evaluation of multivalent iminosugars modulating the affinity and selectivity of glycosidase inhibition was described by S. G. Gouin, J. Kovensky *et al.*^[3] Their work was based on significant affinity enhancements observed for systems of glycoclusters and lectins possessing a single binding site.^[107] In this study, they provided a series of mono-, di-, and tri-valent 1-deoxynojirimycin-based glycosidase inhibitors **72-76** (Figure 23) by “click chemistry”. Their design was ingenious and had the following three main advantages : i) the monovalent references **72**, **73** with ethylene glycol (EG) linkers of different lengths allowed the quantification of a possible multivalent effect; ii) the use of the alkynyl-(ethyleneglycol) derivatives as scaffolds improved water solubility thanks to the hydrophilic property of EG, and avoided interferences caused by scaffold-glycosidase interactions as EGs can prevent non-specific protein adsorption;^[119] iii) the study of the structure-activity relationship achieved by using clusters featured with different valencies or different linkers between the active moieties to inhibit a panel of glycosidases (β -galactosidase (Bovine liver), α -galactosidase (Green coffee beans), β -glucosidase (almonds, pH 7.3), α -glucosidase (Bakers’ yeast), β -mannosidase (*Helix pomatia*), α -mannosidase (Jack bean), isomaltase (Bakers’ yeast), naringinase (*Penicillium decumbens*), amyloglucosidase (*Aspergillus niger*)). The trivalent iminosugar **76** showed a multivalent effect with Jack bean α -mannosidase (JB α -man) (7.6-fold more potent than the monovalent **73**).^[3] Their work not only provided the first example of a quantifiable multivalent effect, but also revealed that valency modulates the inhibitory selectivity against glycosidase.

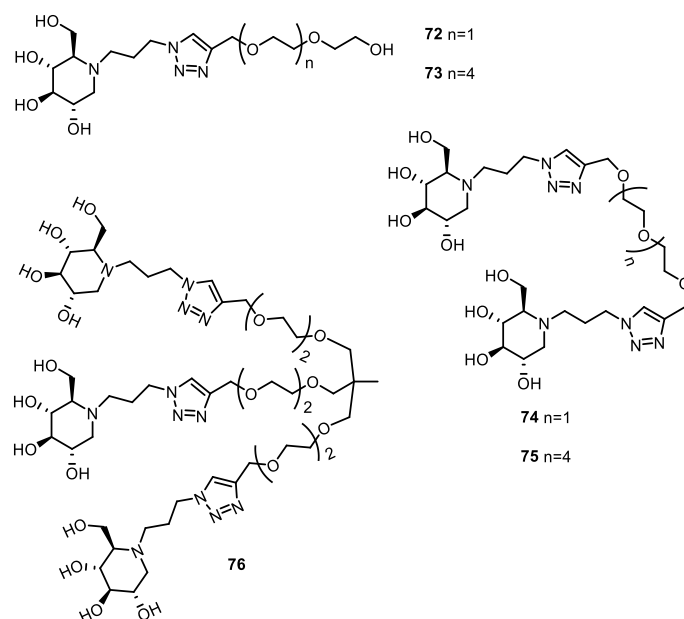


Figure 23 : Structures of the mono-, di-, and tri-valent iminosugars 72-76.

III.3.3.2 Exploration of clusters based on different scaffolds

III.3.3.2.1 Clusters based on fullerene scaffold

Fullerenes, along with graphite and diamond, are the third allotropic form of carbon. They are composed exclusively of carbon atoms. Their intrinsic structural features combining three-dimensionality, hydrophobicity and unique electronic properties have made them outstanding scaffolds for the construction of promising nanostructures that are useful for various scientific disciplines, including materials science, biological and medicinal chemistry.^[120–122] Among the fullerenes, C_{60} , also referred to as buckminsterfullerene, is the most representative example that has attracted extensive attention for the exploration of its chemical and physical properties. Hexa-adducts, with a T_h -symmetrical octahedral addition pattern, represent an interesting class of C_{60} buckminsterfullerenes. They can be obtained by means of cycloadditions, solid state reactions and nucleophilic cyclopropanations and serve as a compact rigid spherical scaffold for the construction of dendrimers.^[123]

In 2010, Compain *et al.*, taking advantage of Nierengarten group's strategy for the synthesis C_{60} building blocks with polyalkyne decorations,^[124] prepared a symmetrical and globular dodecavalent "DNJ ball" **77** (Figure 24) based on fullerene hexakis adduct bearing 12 alkynes.^[4] The synthetic strategy is a general method to build large clusters, which involves the Cu^I -catalyzed azide-alkyne cycloaddition (CuAAC) between polypropargylated scaffold and ready to click head with azide.^[4] The inhibitory activity of cluster **77** and its parent monovalent analog **78** were evaluated towards a panel of commercially available glycosidases (Table 1). Table 1 displayed three types of multivalent inhibition profiles, that is, affinity increase, unaffected affinity, and affinity decrease. By inhibiting $JB\alpha$ -man, DNJ cluster **77** showed the best affinity enhancement, of up to three orders of magnitude, in comparison with the counterpart **78**. This was the first example of a large multivalent effect in glycosidase inhibition. For isomaltase (Baker's yeast) and naringinase (*Penicillium decumbens*), a moderate binding enhancement - two orders of magnitude higher than the monomer - was observed. It showed similar inhibition constant K_i values to the corresponding monovalent when inhibiting

amyloglucosidases (*Asp. Niger*) and bovine liver β -glucosidase. Regarding β -glucosidase from sweet almond, cluster **77** is less efficient than the monovalent **78**, displaying an affinity decrease of ninefold compared to the parent monovalent iminosugar. The best multivalent effect for the dodecavalent **77** in relation to monovalent **78** ($rp/n = 179$) against J β -man highlighted the high potential of multivalent design within the context of glycosidase inhibition.

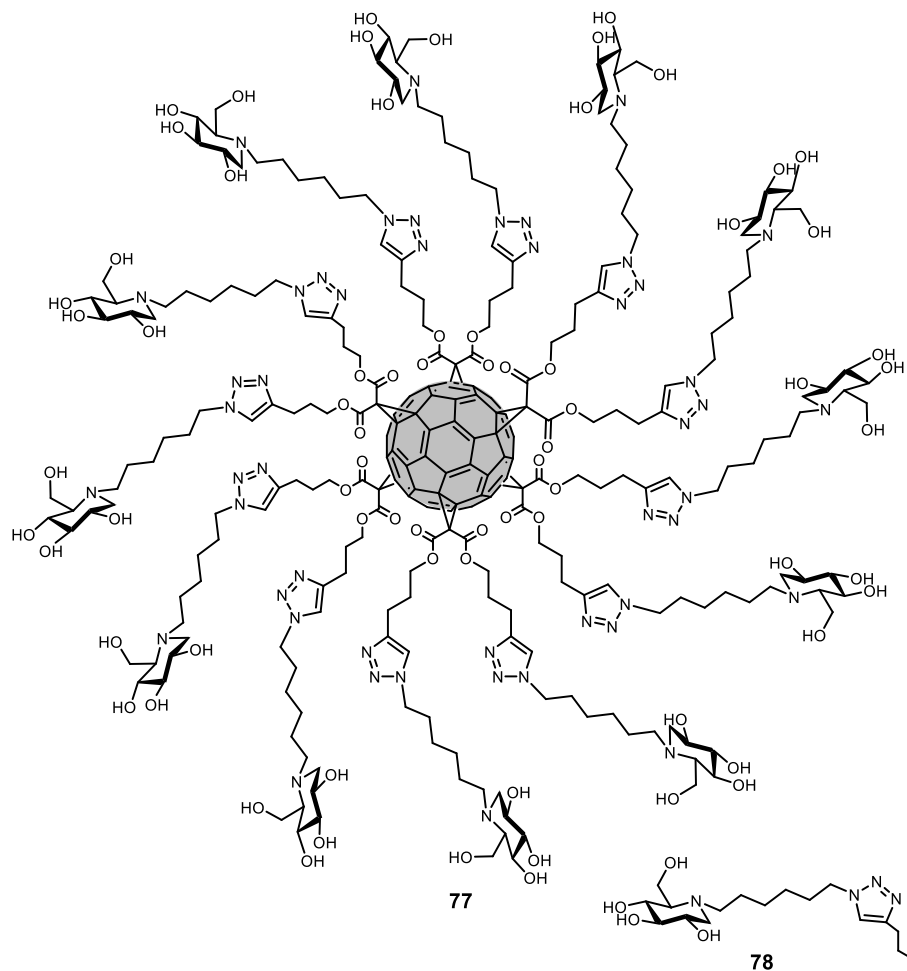


Figure 24 : Structures of dodecavalent “DNJ balls” **77** and its monovalent counterpart **78**.

Enzyme	Monovalent control 78 K_i [μM]	Dodecaivalent cluster 77 K_i [μM]	$rp^{[a]}$	$rp/n^{[b]}$
β -galactosidase (Bovine liver)	262	34	7.7	0.64
α -galactosidase (<i>Aspergillus niger</i>)	NI ^[c]	NI ^[c]	-	-
α -galactosidase (Green coffee beans)	NI ^[c]	84	-	-
β -glucosidase (Almonds pH 7.3)	11	95	0.1	0.01
β -glucosidase (Bovine liver)	482	247	1.9	0.16
Amyloglucosidase (<i>Asp. Niger</i>)	0.71	0.69	1.0	0.08
α -glucosidase (Baker's yeast)	152	18	8.7	0.72
Isomaltase (Baker's yeast)	943	10.5	89.8	7.48
naringinase (<i>Penicillium decumbens</i>)	9.1	0.41	22.2	1.84
β -mannosidase (<i>Helix pomatia</i>)	NI ^[c]	NI ^[c]	-	-
α -mannosidase (Jack bean)	322	0.15	2147	179

[a] Relative inhibition potency (rp) = K_i (monovalent reference)/ K_i (cluster). [b] rp/n = rp /number of DNJ units (n). [c] NI : no inhibition detected at 2 mM.

Table 1 : Glycosidase inhibitory activities K_i [μM] of monovalent **78 and dodecaivalent DNJ cluster **77**.**^[4]

Subsequently, in 2013, to study the mechanisms behind the inhibitory multivalent effect in glycosidase inhibition, Ortiz Mellet and co-workers prepared four isotropic dodecaivalent C_{60} -fullerene- sp^2 -iminosugar balls with the decoration of matching or mismatching inhibitory motifs, 1-amino-5*N*,6*O*-oxomethylidenennojirimycin (1*N*-ONJ) and its C-2 epimer 1-amino-5*N*,6*O*-oxomethylidenemannojirimycin (1*N*-OMJ), towards a set of glycosidases (Figure 25).^[125] The option for those two peripheral motifs 1*N*-ONJ and 1*N*-OMJ was motivated by the features that 1*N*-ONJ (in monovalent form) has selective inhibitory properties against α -glucosidase,^[126–128] whereas 1*N*-OMJ intensively promotes α -mannosidase inhibition.^[126] Besides, due to the performance of D-gluco-configured compounds with carbamate functionalities, the 1*N*-ONJ derivatives were expected to behave as ligands for galactose-specific lectins, which was exploited for the design of competitive lectin-glycosidase assays.^[125] In their study, C_{60} -fullerene was used as the scaffold to prevent the possible influence of orientational effects on binding modes. Moreover, they investigated the effects of arm length to clusters' inhibition potency by inserting six-carbon (C_6) and nine-carbon (C_9) spacers.

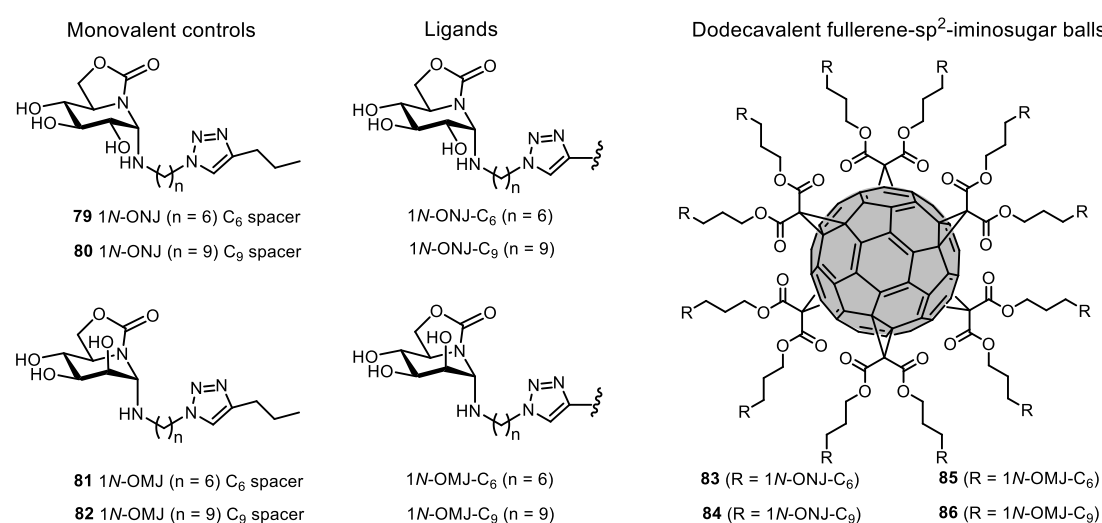


Figure 25 : Structures of dodecaivalent fullerene- sp^2 -iminosugar balls and the corresponding monovalent controls.

Their results of inhibitory assays are shown in Table 2. Barring the case of α -mannosidase (Jack bean), clusters with 1*N*-ONJ motifs mostly displayed detrimental or no effects for the affinity enhancements, yet the multivalent 1*N*-OMJ series significantly increased inhibitory potency. Multivalent presentation of mismatching inhitopes allows to switch on the inhibitory potency. Both multivalent 1*N*-ONJ series (**83**, **84**) and 1*N*-OMJ series (**85**, **86**) obtained excellent affinity enhancements against JB α -man.

Enzymes	D- <i>gluco</i> series				D- <i>manno</i> series			
	Mono C ₆ 79	Multi C ₆ 83	Mono C ₉ 80	Multi C ₉ 84	Mono C ₆ 81	Multi C ₆ 85	Mono C ₉ 82	Multi C ₉ 86
maltase (Baker's yeast)	2.6	18	5.3	49	NI ^[a]	67	227	104
isomaltase (Baker's yeast)	5.1	4.5	2.2	20	NI ^[a]	25	518	193
β -glucosidase (Bovine liver)	60	52	29	42	685	65	352	24
α -galactosidase ^[a]	NI ^[b]	NI ^[b]	NI ^[b]	41	NI ^[b]	78	NI ^[b]	104
α -mannosidase (Jack bean)	596	2.0	451	0.81	4.5	0.085	1.8	0.66

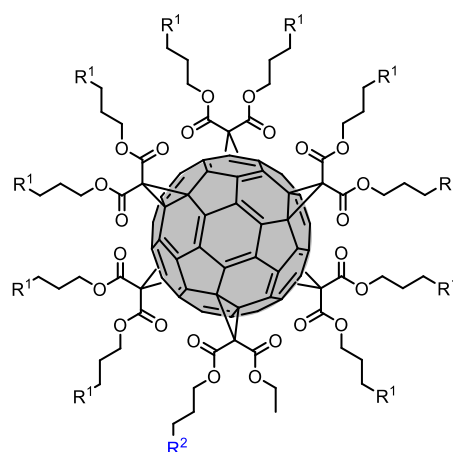
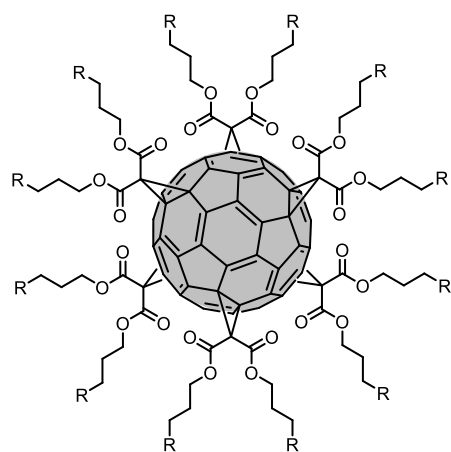
[a] The source of the α -galactosidase was not given in the paper.^[125] [b] NI : no inhibition detected at 2 mM.

Table 2 : Glycosidase inhibitory activities K_i [μ M] for monovalent controls 79-82 and dodecaivalent fullerene-sp²-iminosugar balls 83-86.^[125]

To further investigate the mechanisms of multivalent enzyme inhibition, S. P. Vincent *et al.* designed and synthesized two classes of homovalent and heterovalent glycosystems based on fullerene (Figure 26).^[129] The homovalent fullerene glycoconjugates carried twelve identical peripheral motifs, including α -D-mannopyranosyl, α -L-fucopyranosyl, β -D-galactopyranosyl, and β -lactosyl moieties. It is important to note here that those motifs are not inhibitors individually and that their glycosidic bond were not cleaved in presence of the glycosidases as checked by the authors. In contrast, the heterovalent derivatives are constructed with combinations of one copy of inhitope 1*N*-ONJ and ten identical copies of a glycoside motif (the same glycotopes as in homovalent clusters). The inhibitory activities of these glycomimetics were tested over α -glucosidase, maltase (yeast), isomaltase (yeast), β -galactosidase (*E. coli*) and α -mannosidase (Jack bean) (Table 3).^[129] The enzymes were selected thanks to their features of possessing open and accessible (α -mannosidase), narrow and deep (maltase and isomaltase), and conformationally flexible (β -galactosidase) binding sites. The aim of this study was to probe the contribution of the secondary sites of glycosidase in the inhibitory multivalent effect.

Homovalent [12:0] glycofullerenes

Heterovalent [10:1] glycofullerenes



87 (R = Man)

88 (R = Gal)

91 (R¹ = Man ; R² = 1N-ONJ-C₆)

92 (R¹ = Gal ; R² = 1N-ONJ-C₆)

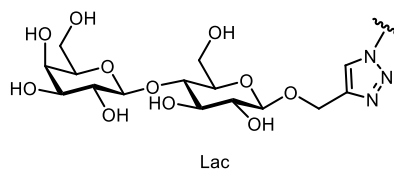
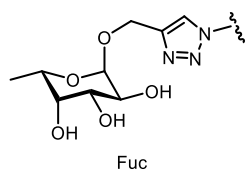
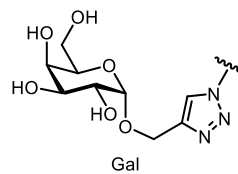
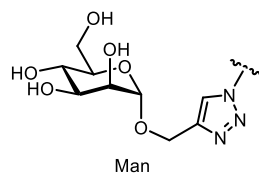
89 (R = Fuc)

90 (R = Lac)

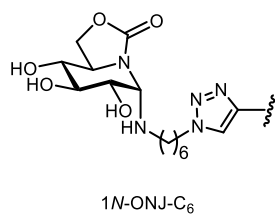
93 (R¹ = Fuc ; R² = 1N-ONJ-C₆)

94 (R¹ = Lac ; R² = 1N-ONJ-C₆)

Glycoside motifs



Inhitope



Monovalent model

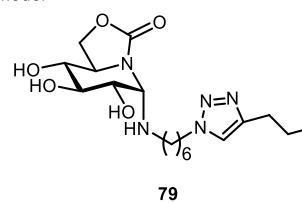


Figure 26 : Homovalent (87-90), heterovalent (91-94) glycosystems based on a C₆₀ core, and the monovalent model 79.

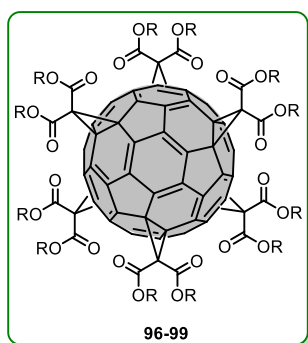
Enzymes	1 <i>N</i> -ONJ		Man		Gal		Fuc		Lac	
	mono	[12:0]	[12:0]	[10:1]	[12:0]	[10:1]	[12:0]	[10:1]	[12:0]	[10:1]
	79	83	87	91	88	92	89	93	90	94
maltase (yeast)	2.6	27	0.9	9.3	2.8	14.2	54	3.4	9.4	1.3
isomaltase (yeast)	5.1	4.5	5.0	33	9.6	23	205	19	65	3.5
β -galactosidase (<i>E.coli</i>)	-	-	1.3 ^[a] 2.3 ^[a]	7.5 ^[b]	1.8 ^[a] 11.0 ^[a]	3.2 ^[b]	25.1 ^[b]	1.6 ^[b]	7.1 ^[b]	1.7 ^[b] 3.7 ^[b]
α -mannosidase (Jack bean)	596	2.0	320	331	NI ^[c]	NI ^[c]	NI ^[c]	410	NI ^[c]	NI ^[c]

[a] Mixed or uncompetitive [b] inhibition modes were observed for β -galactosidase (*E. coli*). For the mixed mode inhibition, the K_i upper value belongs to the competitive type and K'_i lower value belongs to the uncompetitive type. [c] NI : no inhibition detected at 1 mM.

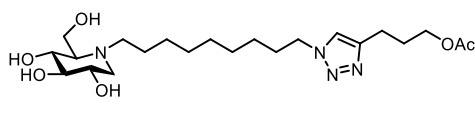
Table 3 : Glycosidase inhibitory activities K_i [μ M] for glycoconjugates 87-94.

Inhibitory results presented in Table 3 showed that multivalent glycofullerenes **87-94** weakly or did not inhibit JB α -man. Contrary to the observations for JB α -man, all the glycofullerenes displayed inhibitory activities towards the other three glycosidases. More interestingly, mixed or uncompetitive inhibition modes were observed for β -galactosidase (*E. coli*), due probably to the shielding of the conformationally flexible catalytic pocket with glycofullerene binding and further preventing the enzymatic progress.

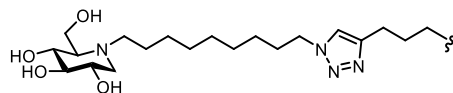
In the following years, Compain's and Nierengarten's teams kept on studying the mechanisms underlying the multivalent glycosidase inhibition by synthesizing more and more glycomimetics based on fullerene C₆₀. Figure 27 presented a set of DNJ-coated balls with incremental valency, i. e., 12-valent, 36-valent, 108-valent, and 120-valent derivatives. Remarkably, the 108-valent cluster **98** was constructed *via* a fast way of grafting twelve dendrons onto the hexa-substituted fullerene building block simultaneously.^[130] On the other hand, an ultra-fast synthetic procedure, based on attaching twelve fullerene macromonomers onto the fullerene core, was utilized to prepare the giant molecule **99** with 120 peripheral subunits.^[131,132] Table 4 described their inhibitory activities evaluated against a series of glycosidases.^[130] Dramatic multivalent inhibitory effects were observed with those multimeric glycofullerenes towards JB α -man, especially the 120-valent DNJ-coated superbball **99** ($rp/n \sim 1000$). Moreover, the giant iminosugar ball showed a mixed-type inhibition mode against JB α -man.



Monovalent model **95**

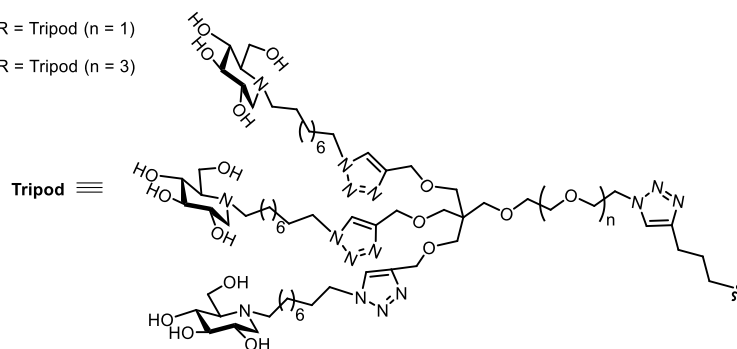


96 (12-valent) R =

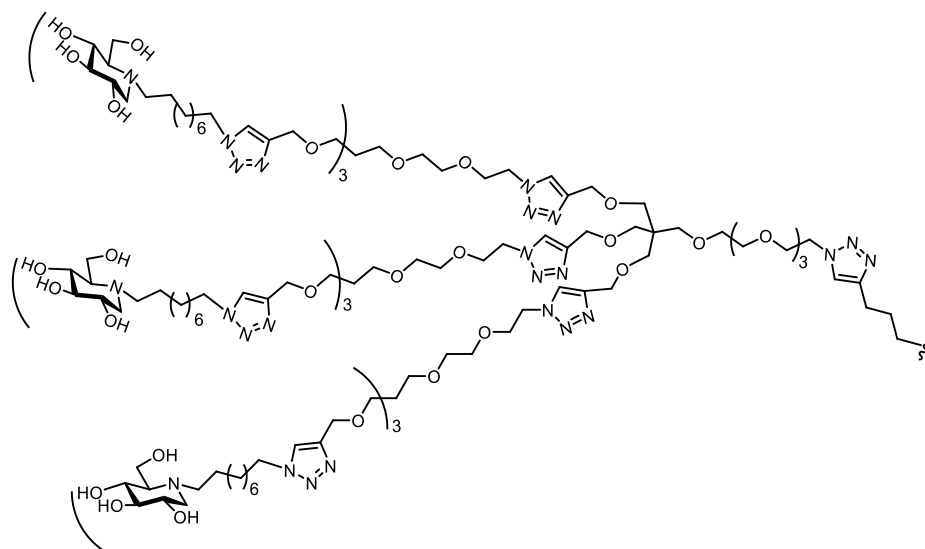


97a (36-valent), R = Tripod (n = 1)

97b (36-valent), R = Tripod (n = 3)



98 (108-valent) R =



99 (120-valent) R =

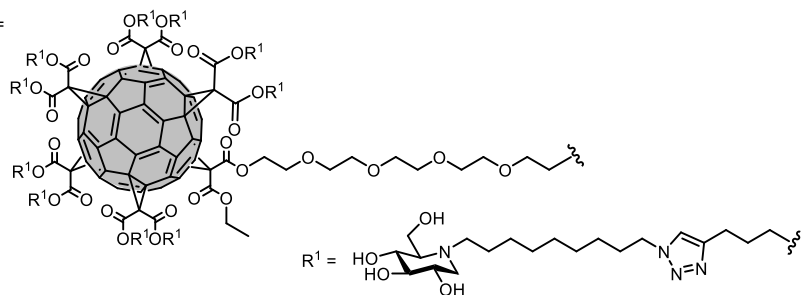


Figure 27 : Structures of multivalent glycoarchitectures **96-99** and a monovalent model **95**.

Enzymes	Mono 95	12-valent 96	36-valent 97a	36-valent 97b	108-valent 98	120-valent 99
maltase (yeast)	192	144	64	22	0.24	32
amyloglucosidase (<i>Asp. Niger</i>)	1.7	3	0.53	0.86	0.61	0.14
β -glucosidase (almonds)	15	136	25	224	6	87
α -galactosidase (green coffee beans)	351	30	42	103	11	44
β -galactosidase (<i>E. coli</i>)	NI ^[a]	NI ^[a]	27	50	8.6	60
α -mannosidase (Jack bean) ^[b]	204 (1)	0.099 (172)	0.069 (82)	0.064 (88)	0.0072 (262)	0.0018 ^[c] (944) 0.0042 ^[c]

[a] NI : no inhibition detected at 2 mM. [b] *rp/n* values are given in brackets. [c] Mixed-type inhibition, the competitive inhibition constant value (upper) and uncompetitive inhibition constant value (lower) are given.

Table 4 : Glycosidase inhibitory activities K_i [μ M] for monovalent model 95 and the multivalent fullerene derivatives 96-99.^[130]

III.3.3.2.2 Clusters based on β -cyclodextrin scaffold

Naturally occurring cyclodextrins (CDs) were discovered in 1891 by Villiers, and studied at the beginning of the 20th century.^[133] They are cyclic oligomers composed by α (1,4)-linked D-glucopyranose units, which are therefore commonly classified into α -, β -, and γ -cyclodextrin according to the comprised number of glucose units, i. e., six, seven, or eight, respectively. Due to the limited rotation of bonds between glucose units, CDs are conical or toroidal rather than cylindrical ring molecules, with the primary OH groups located on the narrow side and the secondary ones on the broader side. Furthermore, because of the presence of OH groups of glucose residues, the inner cavity of CDs is hydrophobic when the outer part is hydrophilic. This unique structure of CDs enables the inclusion of guest molecules in their internal apolar cavity attracts growing interest in various sectors, such as pharmaceutical, cosmetics, and biomedical fields.^[134]

Among all CDs, β -CD turns to be the most described in the literature and is an appealing scaffold for constructing multivalent glycoarchitectures. Its facial anisotropy, together with diverse methodologies of selective chemical functionalization, makes β -CD a privileged platform to build well-defined multivalent clusters in order to assess the effect of the number and spatial orientation of ligands in interaction with a given protein.^[135] After the first observation of a large multivalent effect with C_{60} -based dodecavalent "DNJ ball" **77**, a spectrum of β -CD-based (hetero)multivalent iminosugar architectures, with decorations of different peripheral motifs (DNJ, DMJ, 1*N*-ONJ), alkyl spacer lengths (C_6 or C_9), and spatial arrangement, have been synthesized and evaluated by our laboratory for the sake of further mechanistic study devoted to the inhibitory multivalent effect.

Figure 28 shows a library of hepta- to 21-valent β -CD-iminosugar conjugates. Their inhibitory activities against JB α -man are collected in Table 5.^[109] The quasi-globular 14-valent compound **106a** shares a similar valency, identical DNJ inhitope, and same C_6 spacer length with the C_{60} -based cluster **77**, but different inhibition profile, highlighting the impact of the scaffold on

inhibition potency. The multivalent effect of these β -CD-based series grew with the cluster valency and the alkyl spacer length, especially when reaching compound **106b** with 14 copies of DNJ and C₉ spacer length, giving the most potent multivalent effect of the series (of close to four magnitude orders of affinity enhancement and 610-fold on a valence-corrected basis).^[105] Comparison of the *rp/n* values of DNJ coated clusters **103a** and **103b** (7-valent), **106a** and **106b** (14-valent), showed a one magnitude order increase of multivalent effect related to the increase of the linker length. On the opposite, when clusters exposed DMJ as inhitopes, the structure with shorter linker (**105a**) obtained a higher *rp/n* value than one of the corresponding compound (**105b**) with longer linker. This observation perfectly indicated the linker length's contribution to inhibition result. The multivalent effects are less good with DMJ (**105**, **107**) which is a better head than DNJ (see *K_i* monovalent). Note that ligand spatial orientation caused a pronounced impact on *rp/n* values for iminosugars with C₉ spacer (compounds **106b** and **108b**), whereas the *rp/n* values of clusters **106a** and **108a** with C₆ spacer were similar. The multivalent presentation of the blank motif on the β -CD scaffold (structure **104**) was intentionally designed to assess a possible impact of β -CD and the triazole rings on the inhibition potency showing no inhibition as expected. The relatively compact bouquet-type 21-valent cluster **109** displayed the strongest affinity enhancement towards the J β -man (9900-fold), whereas its *rp/n* value of 470 is lower than the one (610) obtained for the 14-valent iminosugar **106b**.^[105,136] These results suggest that the multivalent inhibitory effect of β -CD-based multivalent glycoarchitectures evaluated against J β -man perhaps have reached a plateau despite the increase of the cluster valency.

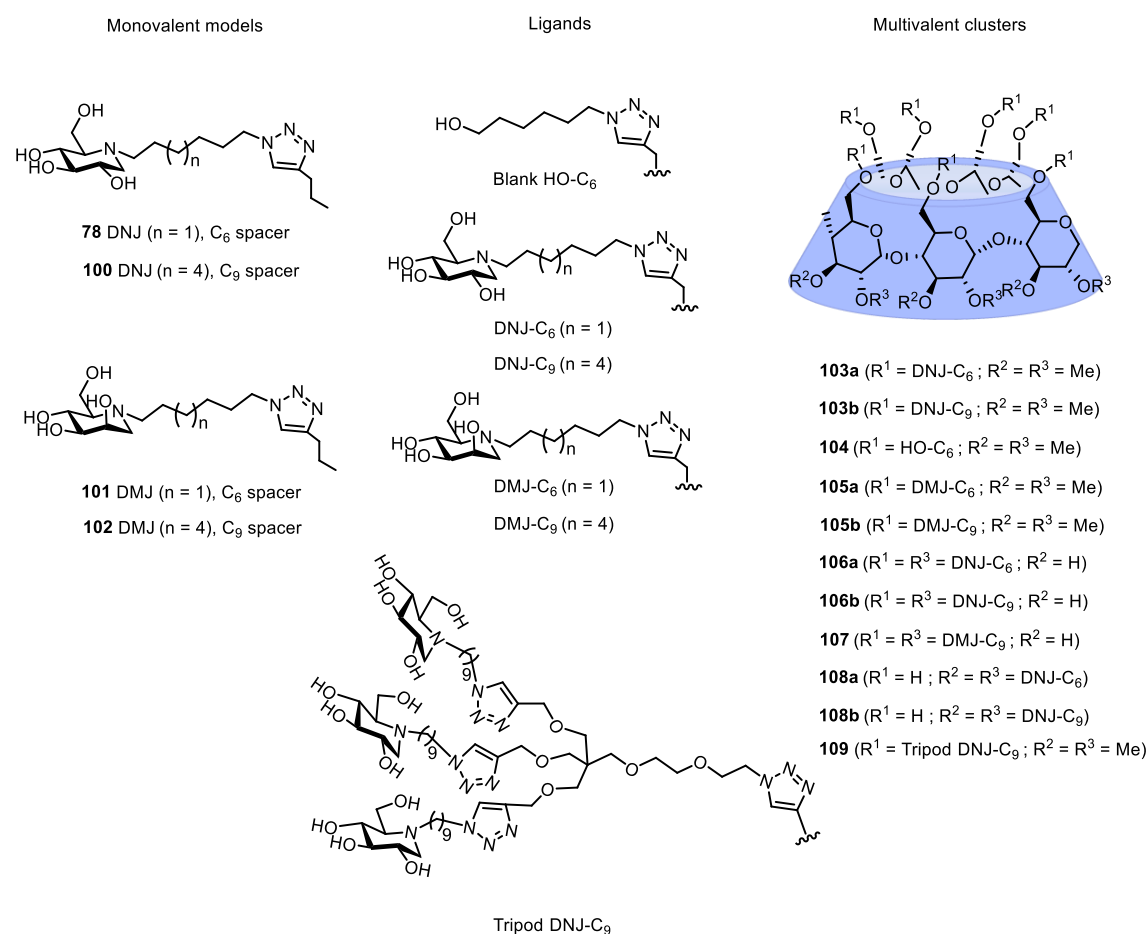


Figure 28 : β -CD based clusters and their monovalent models.^[109]

Compound	DNJ unit	DMJ unit	Linker length	K_i	rp	rp/n
78	1	-	C ₆	322	-	-
100	1	-	C ₉	188	-	-
103a	7	-	C ₆	7.7	42	6
103b	7	-	C ₉	0.36	522	75
106a	14	-	C ₆	0.5	644	46
106b	14	-	C ₉	0.022	8546	610
109	21	-	C ₉	0.019	9900	471
108a	14	-	C ₆	0.67	480	34
108b	14	-	C ₉	0.068	2765	197
101	-	1	C ₆	118	-	-
102	-	1	C ₉	111	-	-
105a	-	7	C ₆	0.49	241	34
105b	-	7	C ₉	0.73	152	22
107	-	14	C ₉	0.07	1586	113
104	-	-	C ₆	NI ^[a]	-	-

[a] NI : no inhibition detected at 2 mM.

Table 5 : Evaluation of glycosidase inhibitory activities (K_i [μ M]) for monovalent models **78, **100-102**, and multivalent derivatives **103-109** against JB α -man.^[109]**

In 2017, Ortiz Mellet *et al.* used also β -CD as scaffolds and further synthesized a collection of multivalent conjugates (Figure 29) incorporating 1*N*-ONJ and/or α -D-glucopyranoside (α -Glc) moieties to assess the impact of heteromultivalency in lectin recognition and glycosidase inhibition.^[137] Only the impact of heteromultivalency in glycosidase inhibition will be discussed in the following text. They evaluated the (hetero)multivalent inhibitory effect towards three multivalency-sensitive enzymes, i. e., α -mannosidase (Jack bean) (possessing a rather accessible catalytic site), maltase (yeast), and isomaltase (yeast) (both displaying narrow and deep catalytic sites). The idea behind this study was to distinguish distinct binding modes of the multivalent clusters and the enzyme : either with the active site or with secondary pockets. Table 6 gathered the inhibitory results of compound **79**, **110-120**. The monovalent model **79** showed potent inhibitory activities against maltase and isomaltase with K_i values of 2.6 μ M and 5.1 μ M, respectively, and low inhibition towards JB α -man. Pronounced affinity decreases were observed after connecting the 1*N*-ONJ inhitope with β -CD scaffold (compound **111**), which might be owing to the unfavorable impact caused by β -CD. Interestingly, the β -CD-based conjugates **113**, **115**, **117**, **119**, **120**, bearing multivalent presentation of 1*N*-ONJ, behaved as potent inhibitors (except compound **115** for α -mannosidase). Among the clusters bearing 1*N*-ONJ units, cluster **116**, with statistical repartition of 1*N*-ONJ and α -Glc units, was considered to have a 3.5 nominal valency of 1*N*-ONJ, and was used as the reference for evaluating the interaction of ligands with secondary pockets. It has indeed the lowest valency in 1*N*-ONJ units and its inhibition constant values measured against maltase and isomaltase (40 μ M and 65 μ M, respectively) were assumed to be 3.5-fold the formal contribution of each 1*N*-ONJ motif. The α -Glc-coated multivalent glycoconjugates **114** and **118** were not hydrolyzed and showed no or weak inhibitory potency. Comparing the rp/n values for maltase and isomaltase of heterocluster **115** with the related ones of homocluster **113**, shows that every single 1*N*-ONJ motif in heterocluster **115** is 4-fold (over maltase) or 2.7-fold (over isomaltase) more potent than that in homocluster **113**. The boosted inhibitory potency thanks to the simultaneous presentation of 1*N*-ONJ inhitope and α -Glc motif provided the first proof of heteromultivalent inhibitory effect. For the heterocluster **120**, a similar synergistic action was as well observed.

The monovalent compound **79** and the corresponding β -CD-based 1*N*-ONJ derivative **111** showed a poor or not measurable inhibitory profile against JB α -man. Whereas the

homoclusters **113** and **117** behaved as potent inhibitors towards the same glycosidase by taking advantage of the increased valency. Especially the homocluster **117** observed the highest rp/n value among this series.

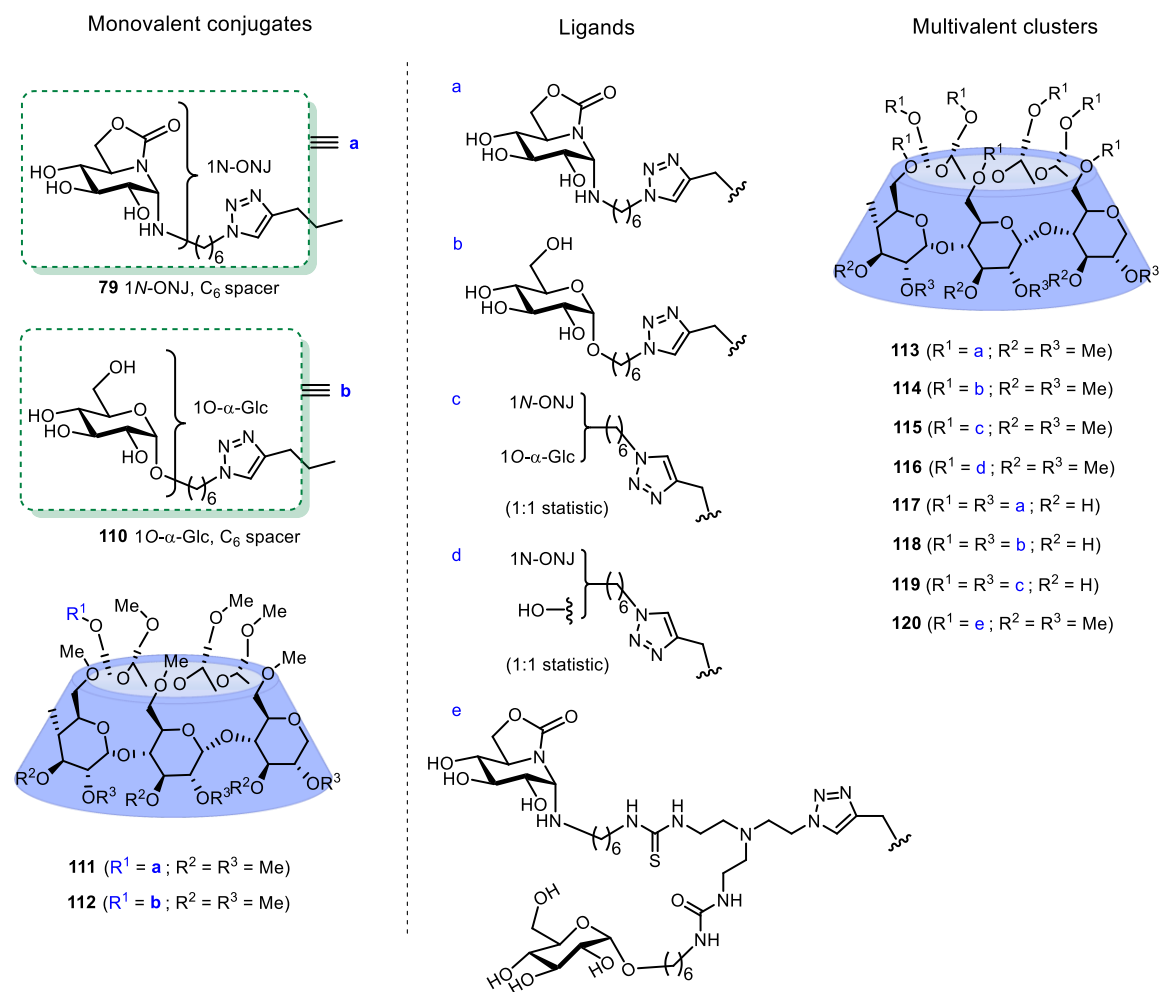


Figure 29 : Structures of (hetero)multivalent clusters **113-120** and monovalent conjugates **79, 110-112**.^[137]

Compound	Maltase (yeast)			Isomaltase (yeast)			α -Mannosidase (Jack bean)		
	K_i	$rp^{[a]}$	$rp/n^{[b]}$	K_i	$rp^{[c]}$	$rp/n^{[b]}$	K_i	$rp^{[d]}$	$rp/n^{[b]}$
79	2.6	-	-	5.1	-	-	596	-	-
110	ND ^[e]	-	-	ND ^[e]	-	-	NI ^[f]	-	-
111	53	-	-	61	-	-	NI ^[f]	-	-
112	ND ^[e]	-	-	ND ^[e]	-	-	NI ^[f]	-	-
113	2.9	48.2	6.9	1.9	119	17	23	25.9	3.7
114	NI ^[f]	NI ^[f]	NA ^[g]	NI ^[f]	NI ^[f]	NA ^[g]	590	1	NA ^[g]
115	1.4	100	28.6	1.4	162	46.3	506	1.2	0.34
116	40	3.5	1	65	3.5	1	35	17	4.8
117	1.7	82	5.9	2.0	113	8.1	2.5	238	17
118	524	0.27	NA ^[g]	326	0.7	NA ^[g]	351	1.7	NA ^[g]
119	4.2	33.3	4.8	5.6	40.5	5.8	70	8.5	1.2
120	0.82	171	24.4	1.6	142	20.3	5.1	117	16.7

[a] relative inhibition potency (rp) = K_i (monovalent reference)/ K_i (cluster), K_i (monovalent reference) is referred to the formal contribution per 1N-ONJ in structure **116** to the inhibitory activity towards maltase (i. e., K_i of 140 μ M). [b] rp/n = rp /number of ONJ units. [c] K_i (monovalent reference) is referred to the formal contribution per 1N-ONJ in structure **116** to the inhibitory activity towards isomaltase (i. e., K_i of 227 μ M). [d] K_i (monovalent reference) is referred to the monovalent control **79** (i. e., K_i of 596 μ M). [e] ND : not determined. [f] NI : no inhibition detected at 1 mM. [g] NA : not apply.

Table 6 : Inhibitory evaluation of compounds 79, 110-120 (K_i [μ M]).

In 2019, P. Compain *et al.* published a study devoted to the evaluation of the impact of inhitope affinity on the final multivalent effect. Two 14-valent β -CD-based glycoimidazoles **123**, **124** and their corresponding monovalent counterparts **121**, **122** were prepared (Figure 30).^[138] Those conjugates were evaluated as JB α -man inhibitors (Table 7). In contrast to monovalent models based on the DNJ inhitope, both D-gluco- and D-manno-configured monovalent glycoimidazoles are potent JB α -man inhibitors, with inhibition constants from the low μ M range to hundreds nM range. Notably, the rp/n values of 14-valent clusters **123** and **124** showed that the construction of inhitopes with better inhibiting abilities than DNJ motifs contributed to obtain low inhibition constants but did not lead to significant multivalent effects (for example, comparison of the inhibition results of 14-valent β -CD-based cluster **106b** to clusters **123** or **124**). Similarly, the monovalent C₉ DMJ **102** obtained lower inhibition constant against JB α -man than the monovalent C₉ DNJ **100** did (111 μ M vs. 188 μ M), whereas the rp/n value of 14-valent DMJ cluster **107** (113) is lower than DNJ cluster **106b** (610). The study results suggest that the strength of the multivalent inhibitory effect and the affinity of JB α -man with inhitope do not evolve in the same direction.

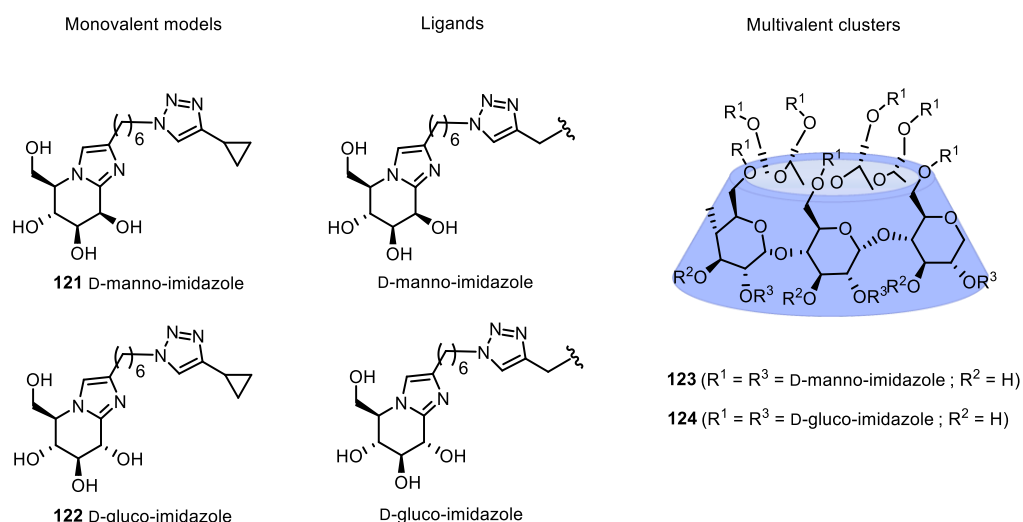


Figure 30 : Structures of β -CD-based glycoimidazoles **123**, **124** and the corresponding monovalent models **121**, **122**.^[138]

Compound	Valency	Inhitope	K_i (μM)	rp	rp/n	Inhibition mode
121	1	Manno-imidazole	0.11	-	-	Competitive
123	14	Manno-imidazole	0.002	55	4	Competitive tight binding
122	1	Gluco-imidazole	2.23	-	-	Competitive
124	14	Gluco-imidazole	0.006	372	26	Competitive tight binding

Table 7 : Inhibitory activities (K_i [μM]) for 14-valent glycoconjugates **123**, **124** and their corresponding monovalent counterparts **121** and **122** against $\text{JB}\alpha\text{-man}$.^[138]

III.3.3.2.3 Clusters based on porphyrin scaffold

In 2013, Gouin and co-workers designed a series of mono-, tetra-, and octavalent DNJ derivatives based on diverse platforms of porphyrin, calix[4]arene, glucose, galactose, trehalose, and γ -CD with identical C_3 spacer length (Figure 31).^[106,139]

Their inhibitory activities were evaluated towards a panel of glycosidases, including β -galactosidase (bovine liver), β -galactosidase (*E. coli*), α -galactosidase (green coffee), β -glucosidase (almonds pH 7.3), α -glucosidase (baker's yeast), α -mannosidase (Jack bean), β -mannosidase (helix pomatia), amyloglucosidase (*Aspergillus niger*). Significant affinity enhancements were again obtained towards $\text{JB}\alpha\text{-man}$ (Table 8).^[106,139] Among all the results in Table 8, the porphyrin-based 4-valent conjugate **130** showed the most outstanding (800-fold) improvement in binding affinity with $\text{JB}\alpha\text{-man}$ with a valency of only four, which highlighted the decisive influence of utilizing rigid scaffolds to achieve excellent multivalent effects. Further, the cluster **130** also displayed selectivity and increased inhibitory potency for Golgi α -mannosidase GMIIb (GM) over lysosomal α -mannosidase LManII (LM) (Table 9).^[106,139]

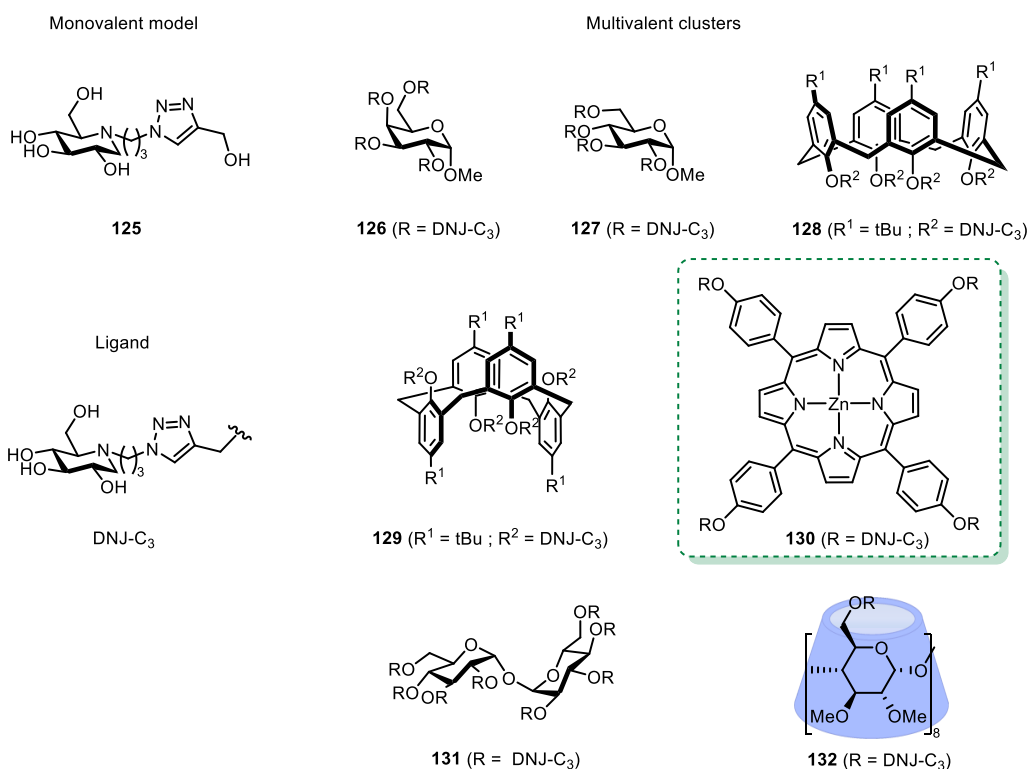


Figure 31 : Structures of mono-, tetra-, and octavalent DNJ derivatives base on diverse scaffolds and the corresponding monovalent model.^[106,139]

Compound	Valency	Scaffold	K_i (μM)	rp	rp/n
125	1	-	400	-	-
126	4	galactose	41	10	2.5
127	4	glucose	76	5	1.3
128	4	calix[4]arene	1.5	267	67
129	4	calix[4]arene	20	20	5
130	4	porphyrin	0.5	800	200
131	8	trehalose	21	19	2.4
132	8	γ -CD	23	17	2.2

Table 8 : Inhibitory activities (K_i [μM]) for DNJ clusters 126-132 and the monovalent reference 125 against JBA-man.^[106,139]

Compound	GM (μM)	LM (μM)
125	362	NI ^[a]
130	24	NI ^[a]

[a] NI : no inhibition detected at 1 mM.

Table 9 : Mannosidase inhibitory activities (K_i [μM]) for compound 125 and 130.^[106,139]

III.3.3.2.4 Clusters based on cyclopeptoid scaffold

Peptoids are oligomeric synthetic polymers of *N*-substituted glycines with high bioactivity and broad resistance to proteolytic decay. They are a readily accessible class and are attracting extensive interest as a useful molecular tool in the field of bioscience.^[140] The cyclopeptoids, that can be prepared by a protocol of head-to-tail condensation, gain advantages in terms of conformational rigidity in comparison to the corresponding linear forms.^[141] Of particular

interest is their potential as scaffolds as they can present multiple diverse chemical or bioactive groups, which have been investigated in the development of therapeutic agents.^[141] Moreover, increasing the size of cyclopeptoids armed with alkynes allows to have a pannel of clusters with incrementally increased valencies. These intriguing features make cyclopeptoids an ideal scaffold to both push and explore the threshold of inhibitory multivalent effects.^[5]

Our laboratory synthesized two sets of 6-10 and 14-48 valent cyclopeptoid-based iminosugar clusters **133a-135f** with different alkyl spacer lengths of C₆ or C₉ (Figure 32) thanks to the cyclopeptoids scaffolds from Irene Izzo's laboratory having the following valencies : 6, 8, 10, 12, 14, 16.^[5,142] The size of the scaffold grows along with the valency, which also relieves the crowded space of neighboring ligands for systems with higher-valencies. Those scaffolds were grafted either with azide armed DNJ ligands or with trivalent dendrons^[136] to reach valencies of the scaffold multiplied by 3. A nice scale of clusters with increasing valencies was thus obtained to run a systematic evaluation of the influence of valency, but also to obtain large multivalent effects and try to reach the highest effect. Their inhibitory potencies were evaluated against Jβ_α-man (Table 10), the glycosidase showing the best response to multivalent inhibitor to date.^[5]

For the first series of compounds (valencies of 6, 8, and 10), only modest but significant inhibitory activities were observed, the clusters with the C₉ alkyl chain being better. Among others, the 10-valent C₉ DNJ cluster **134c** showed the best multivalent effect (*rp/n* value of 3.8) which was however substantially lower than the one (*rp/n* of 75) of 7-valent β-CD-based DNJ cluster **103b** (with identical alkyl spacer length), suggesting a decisive impact of the scaffold on binding affinity enhancements (*via* size, rigidity and ligand spatial disposition).

The series of 18- to 48-valent DNJ derivatives **135a-135f**, with a valency increase of six ligand increments, were further prepared to probe the limit of the multivalent inhibitory effect. Interestingly, the 18-valent cluster **135a** showed a dramatic affinity enhancement compared to the 10-valent compound **134c** by adding eight DNJ units. Therefore, the 14-valent glycoconjugate **134d** was intentionally prepared to pinpoint from which valency a significant multivalent effect occurs. The outstanding *rp/n* value of 107 for cluster **134d** suggests the jump node could happen between 10- to 14-valent. Overall, an exponential increase of the *rp/n* is observed for the entire series. Cluster **134d** is the only one shifted from this general trend as it is better than the 18-valent cluster **135a**. The difference between those two clusters being that the ring size of **134d** is larger whereas **135a** is smaller but grafted with trivalent dendrons. Finally, it was found that the 36-valent DNJ cluster **135d** displayed the best inhibitory multivalent effect ever reported for an enzyme (*rp/n* = 4747).^[5] The further increase of the number of peripheral DNJ units led to a plateau effect in inhibiting potency, i. e., no higher affinity enhancement (on a valence-corrected basis) obtained for clusters **135e** and **135f**.

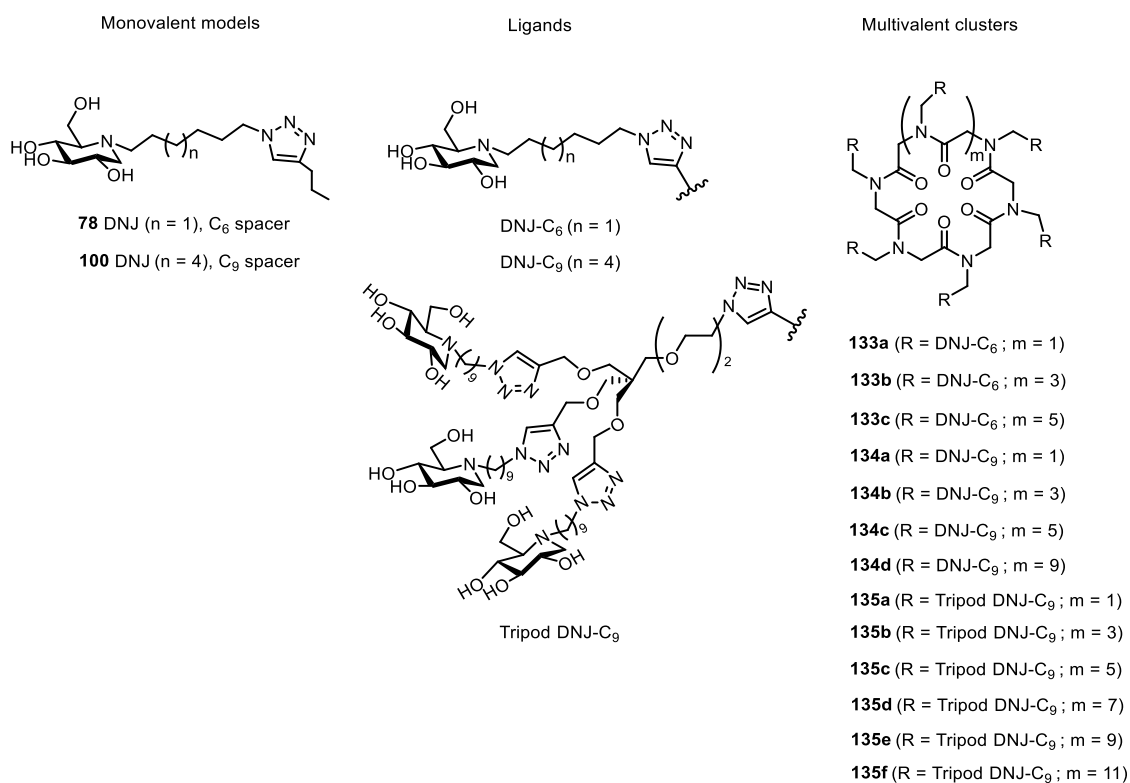


Figure 32 : Monovalent models **78**, **100** and multivalent cyclopeptoid-based DNJ derivatives **133a-135f**.

Compound	DNJ unit	Linker length	K_i (μM)	rp	rp/n
78	1	C ₆	322	-	-
133a	6	C ₆	65	4.9	0.8
133b	8	C ₆	21	15	1.9
133c	10	C ₆	15	21	2.1
100	1	C ₉	188	-	-
134a	6	C ₉	11	17	2.8
134b	8	C ₉	8	23	2.9
134c	10	C ₉	5	38	3.8
134d	14	C ₉	0.126	1492	107
135a	18	C ₉	0.142	1324	74
135b	24	C ₉	0.037	5081	212
135c	30	C ₉	0.0099	18990	633
135d	36	C ₉	0.0011	170909	4747
135e	42	C ₉	0.0015	125333	2984
135f	48	C ₉	0.0011	170909	3560

Table 10 : Inhibitory evaluation of compound **78**, **100**, **133a-135f** against JB α -man.^[5,142]

To understand the outstandingly large multivalent effect observed for cluster **135d** in JB α -man inhibition, four complementary techniques, including transmission electron microscopy (TEM), analytical ultracentrifugation sedimentation velocity (AUC-SV), native electrospray mass spectrometry (ESI-MS), and X-ray crystallography were used.^[5,104]

✓ **Results obtained with TEM (Transmission Electron Microscopy)**

JB α -man is a high-molecular-weight (around 220 kDa) zinc-enzyme, composed by two LH heterodimers.^[143] Each heterodimer possesses one active site and comprises two distinct chains, one heavy chain (H) of about 66 kDa, and one light chain (L) of about 44 kDa.^[143] Figure 33 (left) is the TEM picture of JB α -man alone showing clusters of around 10 \times 20 nm (red frame), which matches the size of one JB α -man (LH)₂.^[5] Correspondingly, the right picture in Figure 33 exhibits the complexes of JB α -man with **135d**. Blocks approximately 20 \times 20 nm (blue frame) were observed, indicating the existence of aggregates of double size compared to the enzyme alone.^[5] Although interesting, this qualitative result can not provide the binding mode, namely how many inhibitors are engaged into the 2 \times (LH)₂ aggregates.

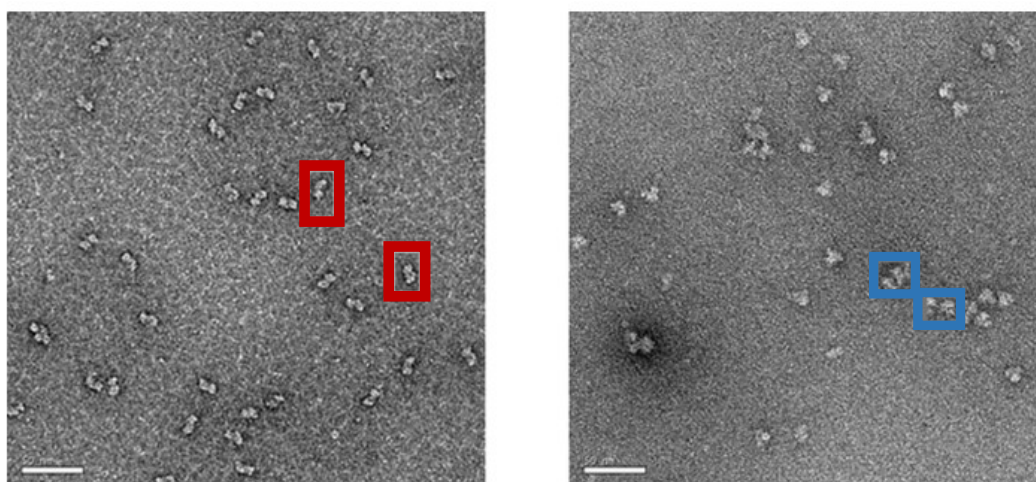


Figure 33 : EM pictures of JB α -man alone (left); complexes of JB α -man with cluster 135d (right); scale bars = 50 nm.^[5]

✓ **Result obtained with ESI-MS**

ESI is a “soft ionization” technique that overcomes the tendency of analytes to fragment during ionization.^[144] Thus, it is helpful for the production of ions from macromolecules. In addition, the ESI technique allows for the retention of solution phase information into the gas phase.^[144] ESI-tandem-MS facilitates the observation of molecular ion peaks of macromolecules. Our laboratory would like to further investigate the enzyme-inhibitor binding mode using the mass information obtained by ESI-MS for both JB α -man and JB α -man-inhibitor complexes. The ESI-MS^[5] spectra of the native enzyme (Figure 34A) and enzyme-inhibitor complexes (Figure 34B), presented three different multicharged ions patterns. For Figure 34A, the 17+, 29+, and 42+ ions are related to the heterodimer LH ($M_w = 121.3$ kDa), the homodimer (LH)₂ ($M_w = 242.3$ kDa), and the association of two homodimers (LH)₂ ($M_w = 484.9$ kDa), respectively. For Figure 34B in presence of the cluster **135d** ($M_w = 17.4$ kDa), the 18+, 32+, and 47+ ions correspond to the molecular masses of 121.3 kDa, 259.9 kDa, and 501.9 kDa, respectively. The last two masses are shifted by 17 kDa, which is the mass of the cluster. Ion 259.9 kDa is in adequacy with the calculated mass of the 1:1 enzyme-inhibitor complex, and 501.9 kDa suggests a 2:1 complex. However, this analysis is performed in gaz-phase, and the next analysis was performed in order to check that the result is the same in aqueous phase.

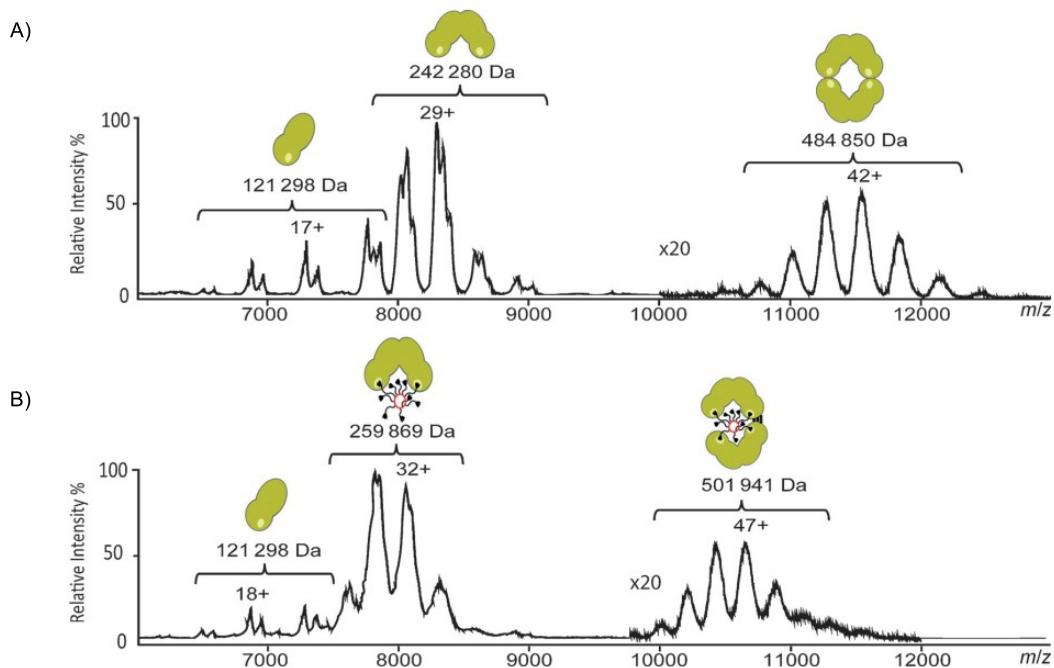


Figure 34: Native ESI-MS spectra for: A) JBα-man alone; B) complexes of JBα-man with cluster 135d. Multicharged ions patterns are labeled with the corresponding enzyme and enzyme-inhibitor complexes cartoons.^[5]

✓ **Result obtained with AUC-SV**

AUC-SV is a powerful method in aggregation analytics that provides sedimentation coefficients, shape information, molecular weights, *etc.*, with no prone to change the sample composition.

The solid line in Figure 35 shows the sedimentation coefficient distribution of JBα-man.^[5] The main species with a sedimentation coefficient value of 9.3 S corresponds to the homodimer (LH)₂, and the minor one at 13.4 S relates to the association of two homodimers (LH)₂. The dotted line (Figure 35) is the plot of the sedimentation coefficient distribution of enzyme-inhibitor complexes between JBα-man and **135d**.^[5] The reversible binding of inhibitor **135d** to the enzyme leads to a broader sedimentation coefficient distribution, and the value at about 14 S suggests a 2:1 enzyme : inhibitor complex.

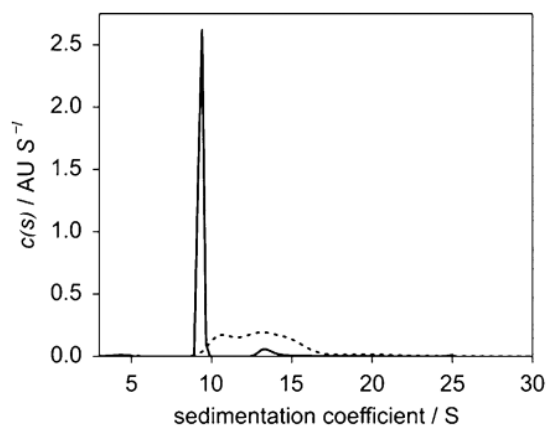


Figure 35 : The sedimentation coefficient distribution plot for JBα-man (solid line) and for enzyme-inhibitor complexes (dotted line).^[5]

✓ Result of X-ray crystallography

Our lab also reported the first high-resolution crystal structures of the JB α -man in apo and inhibited states.^[104] Figure 36 is the cartoon picture of the X-ray crystallographic structure of JB α -man in complex with the inhibitor **135d**. The X-ray structure showed that four iminosugar heads from one 36-valent cluster were reversibly linked to four active sites of two JB α -man molecules (electron density map at 2.0 Å resolution), and that the inhibitor core was at the center of the cavity (electron density map at 5.0 Å resolution). This result beautifully confirmed the formation of the 2:1 JB α -man : inhibitor sandwich that was initially postulated based on the EM, AUC-SV, and ESI-MS results.

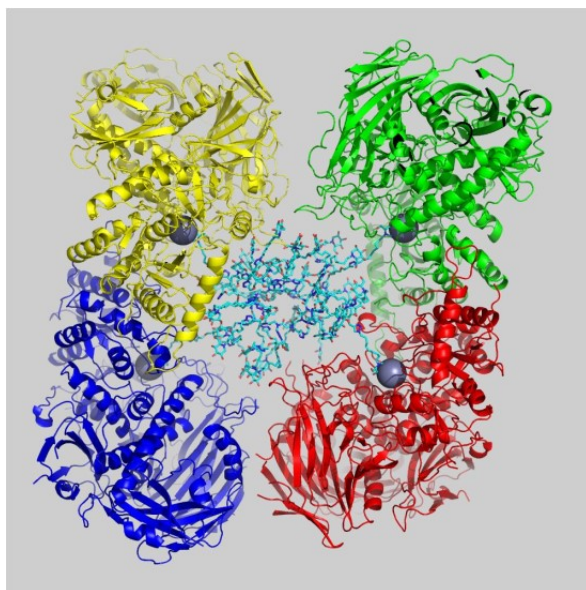


Figure 36: Ribbon representation of two enzymes, one formed by the green and red parts and a symmetry related one. At the center, the flexible 36-valent cluster **135d** (cyan) was modeled starting from the four well resolved DNJ in the four active site pockets.^[104]

Altogether those results suggest that the outstanding affinity enhancement of 36-valent cluster **135d** is due to a strong chelation effect resulting from the formation of a sandwich-type complex between one multivalent inhibitor **135d** and two JB α -man molecules.

III.3.3.2.5 Clusters based on calix[4]arene and calix[8]arene scaffolds

As CDs, calixarenes represent an essential class of macrocycles. They are formed *via* the reaction between phenols and aldehydes.^[145] Correspondingly, different families of calix[n]arenes can be defined based on the number of phenol residues,^[146] such as the cyclic molecules calix[4]arenes and calix[8]arenes which are constituted of four and eight phenol residues respectively, being connected through methylene bridges. Calixarenes were first used for their properties of encapsulation of neutral molecules and small ions (metal and ammonium cations and anions) in host-guest chemistry. Along with these applications, researchers who were encouraged by the low toxicity of these macrocycles started to undertake more biologically-oriented problems by developing calixarene derivatives as biomimetic receptors and as multivalent scaffolds.^[147]

Multivalent calixarene-based carbohydrate clusters (glycocalixarenes) have been extensively reported in the literature, and have shown enhanced affinity of interactions between glycans

and lectins.^[148] In 2012, Marradi *et al.* described the first examples of constructing multivalent iminosugars based on a calixarene platform (Figure 37, **136-137**).^[148] Four C_2 -symmetric 3,4-dihydropyrrrolidine units were linked to the lower rim of a SuO-activated (Su: succinimidyl) calix[4]arene in dendrimeric arrangements *via* amide bonds. However, the authors did not evaluate the glycosidase inhibitory properties for compounds **136** and **137**. The same year, a set of di- and tetravalent calixarene-based iminosugar derivatives (Figure 37, **138-141**) were synthesized and reported by Casnati, Goti, *et al.* Unfortunately, the inhibitory activities of the deprotected calixarene-iminosugar clusters could not be measured. Since the authors could not remove the benzyl protecting groups in the last step of the synthesis.^[149]

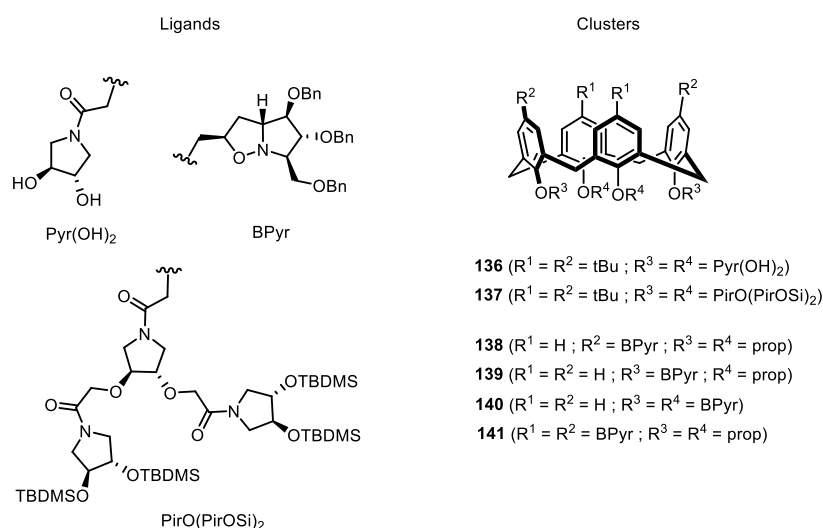


Figure 37 : Structures of calix[4]arene-based iminosugar clusters.^[148,149]

Subsequently, more extensive reports were focused on preparing diverse iminosugar clusters based on different conformers of calix[4]arene scaffolds (in a cone or 1,3-alternate conformation), or at different (lower and/or upper) rim of calix[4]arenes, or comprising different alkyl spacer length of the ligand (Figure 38).^[106,139,150-152] Only clusters **143-146**, **149** were tested as glycosidase inhibitors on a panel of enzymes (Table 11).

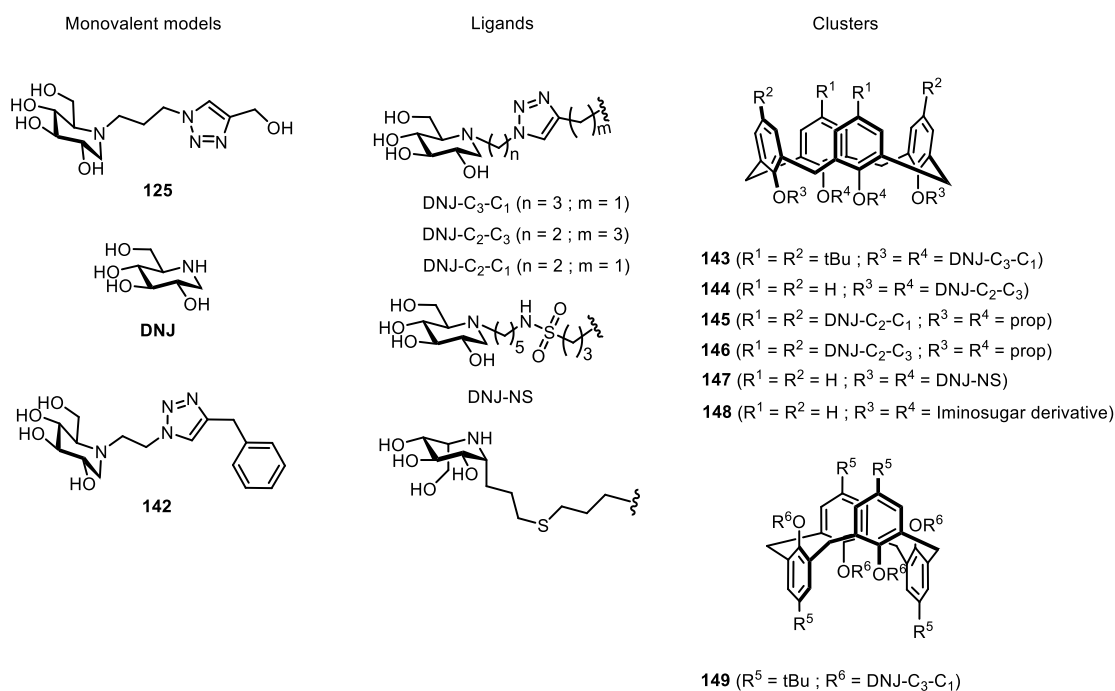


Figure 38 : Calix[4]arene-based iminosugar clusters and the corresponding monovalent models. [106,139,150–152]

Enzymes	Monovalent models			Calix[4]arenes (cone)				Calix[4]arene (1,3-alternate)
	DNJ	125	142	143	144	145	146	149
		C ₃ -C ₁	C ₂ -C ₁	C ₃ -C ₁	C ₂ -C ₃	C ₂ -C ₁	C ₂ -C ₃	C ₃ -C ₁
β-galactosidase ^[a]	42 ^[3]	NI ^[k]	ND ^[l]	38	ND ^[l]	ND ^[l]	ND ^[l]	58
β-galactosidase ^[b]	-	85	ND ^[l]	NI ^[k]	ND ^[l]	ND ^[l]	ND ^[l]	NI ^[k]
α-galactosidase ^[c]	-	55	11	24	24	948	18	36
β-glucosidase ^[d]	47 ^[3]	233	NI ^[k]	NI ^[k]	NI ^[k]	NI ^[k]	NI ^[k]	729
α-glucosidase ^[e]	25 ^[3]	NI ^[k]	NI ^[k]	585	NI ^[k]	NI ^[k]	NI ^[k]	45
α-mannosidase ^[f]	270 ^[3]	400	1940	1.5	73	6580	284	20
β-mannosidase ^[g]	-	NI ^[k]	ND ^[l]	NI ^[k]	ND ^[l]	ND ^[l]	ND ^[l]	NI ^[k]
glucoamylase ^[h]	2.1 ^[3]	45	ND ^[l]	43	ND ^[l]	ND ^[l]	ND ^[l]	11
α, α-trehalase ^[i]	42 ^[j]	ND ^[l]	15	ND ^[l]	47	57	NI ^[k]	ND ^[l]

[a] β-galactosidase from bovine liver. [b] Escherichia coli β-galactosidase. [c] α-galactosidase from green coffee. [d] β-glucosidase from almonds. [e] α-glucosidase from baker's yeast. [f] α-mannosidase from Jack bean. [g] β-mannosidase from helix pomatia. [h] glucoamylase from *Aspergillus niger*. [i] α, α-trehalase from porcine kidney. [j] the IC₅₀ value is noted here. [k] NI : no inhibition detected at 2 mM. [l] ND : not determined.

Table 11 : Glycosidase inhibitory activities *K_i* [μM] for monovalent controls DNJ, 125, 142 and for multivalent clusters 143-146, and 149. [106,139,150]

Compounds **125** and **142** are two monovalent references with different alkyl chain lengths (C₃ or C₂) between the triazole and the DNJ motif. The monovalent **125** was used to determine *rp* and *rp/n* for clusters with three carbon atoms between DNJ moiety and the triazole part, i. e., **143** and **149**. Correspondingly, the structure **142** was used to assess the *rp* and the *rp/n* values for clusters **144-146** who possess two carbon atoms between DNJ and the triazole. DNJ was as well helpful in evaluating different results of the inhibition tests. As a general trend, among

all the enzymes tested, this library of calix[4]arene-based DNJ derivatives showed best affinity enhancements towards JB α -man (except the case of cluster **145**) (Table 12). Cluster **143**, decorated with the most extended alkyl spacer (three carbon atoms) between DNJ and the triazole moiety, exhibited the best multivalent inhibitory effect of the series **143-146** and **149**.

Compound	Linker length	<i>rp</i>	<i>rp/n</i>
143	C ₃ -C ₁	267	67
144	C ₂ -C ₃	26.6	6.6
145	C ₂ -C ₁	0.29	0.07
146	C ₂ -C ₃	6.8	1.7
149	C ₃ -C ₁	20	5

Table 12 : Inhibitory evaluation of compound **143-146** and **149** against JB α -man.

Recently, our laboratory reported two sets of DNJ clusters with valency ranging from 6 to 24 and bear C₆ or C₉ linkers : one set is based on the larger calix[8]arene macrocycle platform (comparison to calix[4]arene macrocycle) to ensure a higher valency; the other one is based on a more rigid 1,5-xylylene bridged calix[8]arene scaffold (same size as previous calix[8]arene) to probe the impact of flexibility (Figure 39).^[153] The inhibitory activities of these clusters were determined on the model enzyme – JB α -man, and the results were presented in Table 13. The cluster **150a** with a C₆-length linker was instead a poor inhibitor of JB α -man, and the compound **151a**, constructed with the same alkyl spacer length, a similar number of DNJ units, but based on more rigid 1,5-xylylene bridged calix[8]arene scaffold, showed to be a potent inhibitor. In contrast, when it goes to C₉ length clusters **151b** and **150b**, the increase of scaffold rigidity does not contribute to dramatic affinity enhancement. These parameters suggest that the rigidity of the calix[8]arene platform plays a significant impact on inhibitory potency when clusters have shorter C₆ linker rather than C₉ linker. The compounds with C₉ linker **151b**, **150b**, **151c**, **150c**, no matter based on which scaffold, behaved as strong inhibitors, and the increasing valency boosted the inhibitory potency. The 24-valent displayed indeed the best multivalent inhibitory effect of the series **150a-151c**.

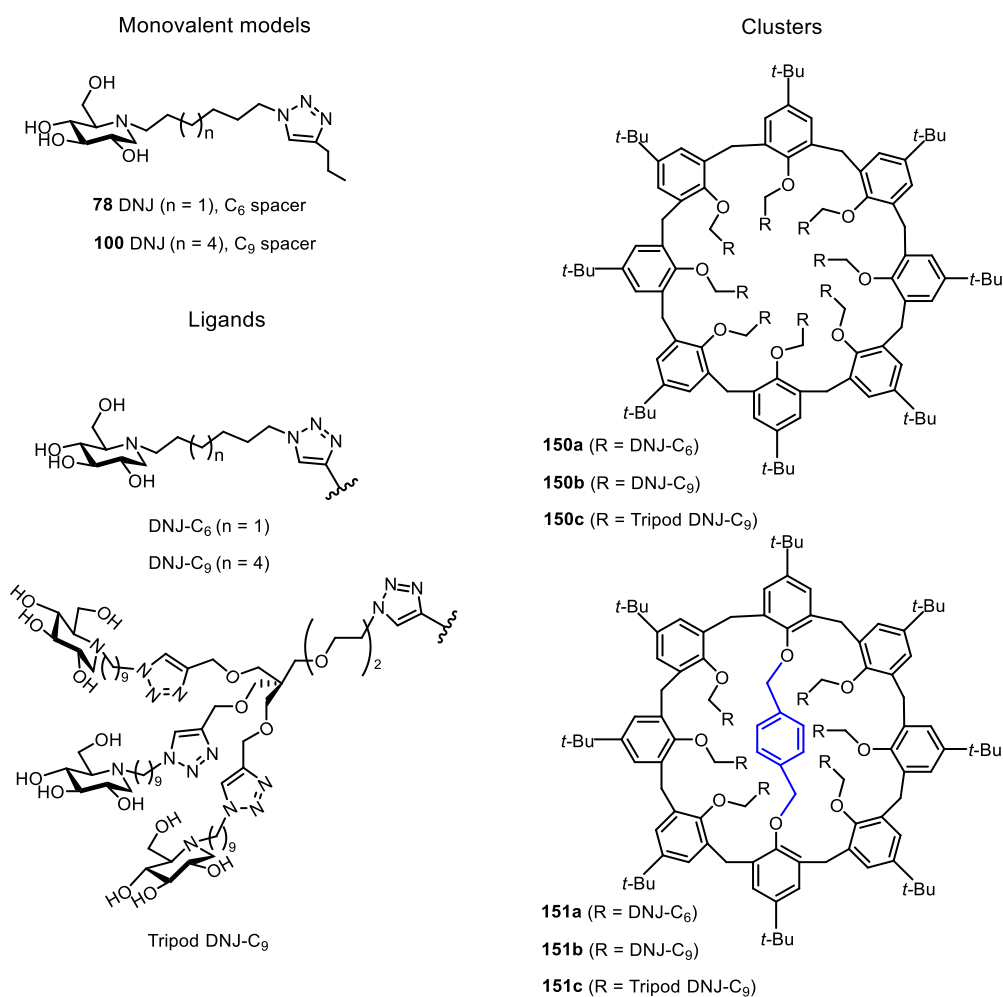


Figure 39 : Calix[8]arene based multivalent clusters and the corresponding monovalent models.^[153]

Compound	DNJ unit	Linker length	K_i (μM)	rp	rp/n
78	1	C ₆	322	-	-
100	1	C ₉	188	-	-
151a	6	C ₆	7.7	42	7
151b	6	C ₉	0.38	495	82
150a	8	C ₆	80	4	0.5
150b	8	C ₉	0.32	588	73
151c	18	C ₉	0.092 ^[a]	2043	113
150c	24	C ₉	0.213	3760	157

[a] mixed inhibition mode. [b] fast tight binding competitive inhibition mode.

Table 13 : Glycosidase inhibitory activities of iminosugar clusters and monovalent models towards JBA-man.^[153]

III.3.3.2.6 Others

There are also a diversity of multivalent systems synthesized based on other scaffolds, such as dendrimers,^[154,155] assemblies,^[156] and polymers.^[157] All these scaffolds (together with the ones mentioned above) have their intrinsic properties, like size, flexibility, rigidity, and other parameters, which are crucial for the presentation of inhitopes.

III.3.3.3 The more the better? Plateau effect displayed by cyclopeptoid based clusters and comparison with giant fullerenes

As shown from previous studies, the multivalent presentation of ligands (or inhitopes) does play a significant role in affinity/inhibition enhancement, as well as selectivity against enzymes. For example, the multivalent clusters **96-99** based on fullerene scaffold behave as potent inhibitors against JBA α -man compared to the corresponding monovalent counterpart **95** (Table 14). Their inhibition activities improve along with the increase of valency (except compound **96** which is already very good with a valency of 12), and the 120-valent **99** shows the highest affinity enhancement of 944-fold on a valence-corrected basis. However, more is not always better, or to quote Shakespeare, “too much of a good thing,” i. e., the increase of valency does not always lead to a higher multivalent inhibitory effect.

Compound	Valency	K_i (μ M)	rp	rp/n
95	1	204	-	-
96	12	0.099	2061	172
97a	36 ^[a]	0.069	2957	82
97b	36 ^[a]	0.064	3188	88
98	108	0.0072	28333	262
99	120	0.0018 ^[b] 0.0042 ^[b]	113333	944

[a] The two clusters differ by the length of their PEG spacer.^[130] [b] Mixed-type inhibition, the competitive inhibition constant value (upper) and uncompetitive inhibition constant value (lower) are given.

Table 14 : Glycosidase inhibitory activities of multivalent DNJ derivatives 96-99 and monovalent model 95 towards JBA α -man.^[130]

Take the cyclopeptoid based multivalent systems **134a-135f** for instance, from 6 to 36 valent, the inhibition activity exponentially increases with increasing valency, especially the 36-valent cluster **135d** representing an outstanding rp/n value of 4747, whereas the rp/n value decreases with increasing the valency to 42 and 48. Plotting $\log(rp/n)$ as a function of valency in Figure 40 intuitively reveals the tendency: multivalent effects increase with valency up to a plateau. Analogous plateau was detected when DNJ motif was grafted on β -CD scaffolds (clusters **103b**, **106b**, and **109**).

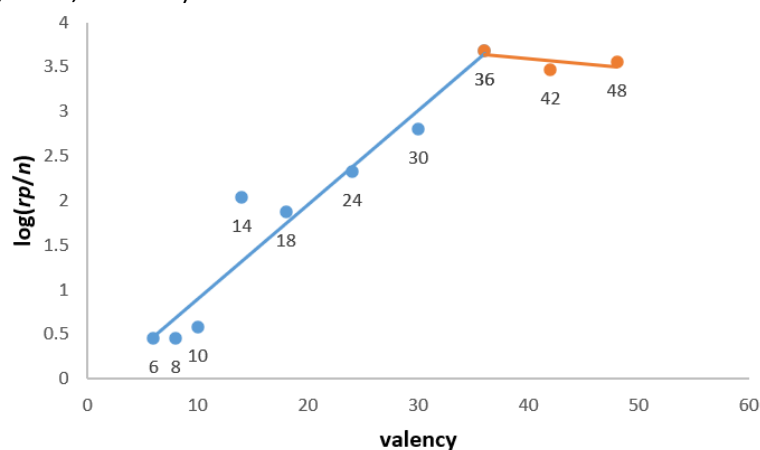


Figure 40 : Plot of $\log(rp/n)$ as a function of valency.

III.3.4 Mechanisms accounting for inhibitory multivalent effect

The mechanisms behind the inhibitory multivalent effect have been extensively investigated mostly from structure-activity relationship studies and with assistance of different physical techniques, including isothermal titration calorimetry (ITC),^[105] competitive lectin-enzyme assays,^[125] atomic force microscopy (AFM),^[106,139] dynamic light scattering (DLS),^[106,139] electron microscopy (EM),^[5] analytical ultracentrifugation sedimentation velocity (AUC-SV),^[5] native electrospray mass spectrometry (ESI-MS),^[5] transmission electron microscopy (TEM),^[158] and X-ray crystallography.^[104,154,159] The origin of the multivalent effect in glycosidase inhibition is far to be unequivocally elucidated. Several generally accepted binding modes have been proposed to explain this observed phenomenon, and are summarized in Figure 41.

As the interaction between inhibitor and enzyme is reversible and the processes of enzyme-inhibitor association/dissociation are fast enough, a statistical rebinding effect (Figure 41A) may account for the multivalent effect. Recapture of the multivalent ligand is favored by the high local ligand concentration. This process indirectly extends the lifetime of the enzyme-inhibitor complex, which thereby enhances the binding affinity. Chelate effect (Figure 41B) works when the enzyme presents multiple (or more than one) binding site, which decreases the overall dissociation rate and increases the functional affinity. Additionally, other unspecific interactions can occur in the regions of subsite other than the primary binding site. This binding mode is referred to as subsite binding effect (Figure 41C/a) that enhances the enzyme-inhibitor interactions. Further, non-specific interactions with non-catalytic subsites or aglycone sites may pose steric hindrances that hampers the access of substrate to enzyme's catalytic site (Figure 41C/b). Moreover, the clustering effect or aggregation effect is possible to happen when a simultaneous association of more than one enzyme is favored over one large multivalent inhibitor (Figure 41D), or with the formation of stabilized enzyme-inhibitor networks if the enzyme possesses a multimeric nature (Figure 41E).

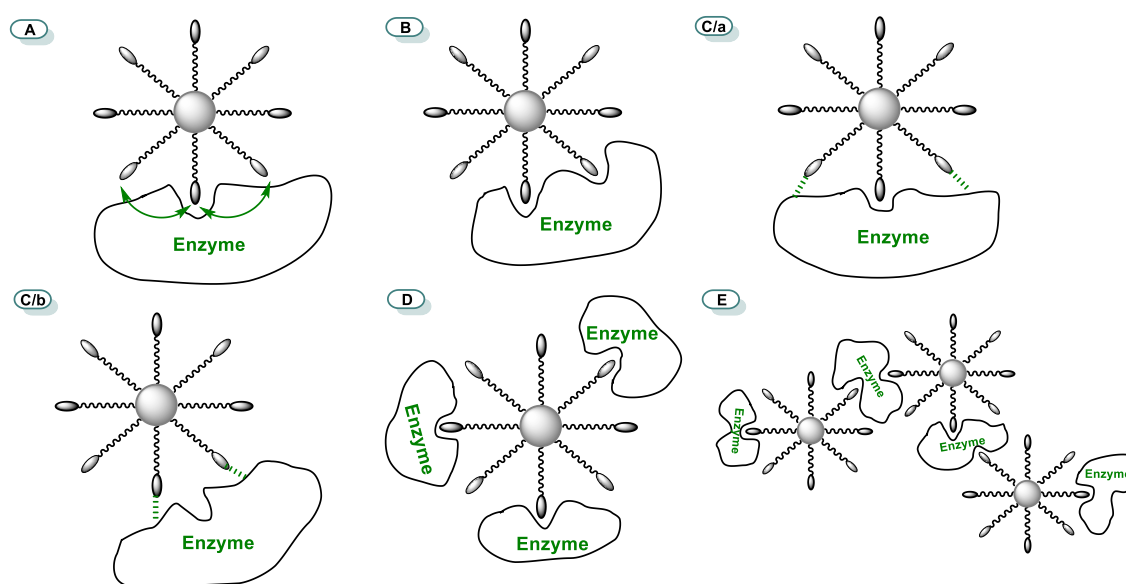


Figure 41 : Generally accepted binding models accounting for the multivalent inhibitory effect.

IV Objectives of this PhD

IV.1 Questions related to the chelate and the sliding effects

There are still remaining questions to be solved and space for improvements. What are the roles of the inhitopes that are not engaged in the active sites ? Are they usefull or not ? Which ones are taking part in the bind and recapture effect ? As the multivalent effect evaluation relies in dividing by the valency, it would be interesting to find the minimum amount of ligands needed to reach a high effect. Would it be possible to get a sandwich complex with only two DNJ heads on opposite directions if they have the right size to reach two active sites of 2 separate enzymes ? Could we optimize the cluster with only four DNJ heads reaching the four active sites to obtain an even larger multivalent effect ?

IV.2 Detailed objectives and strategy

As the cyclopeptoid-based 36-valent cluster **135d** gave the best inhibitory multivalent effect of the literature and its interaction with JBA-man was studied by different techniques, it was the best candidate to start our study. The idea was to gradually remove some inhibitory heads (such as using single arms instead of dendrons, removing some inhibitory heads...) to solve questions asked in Chapter I (IV.1) and maybe quantify some effects individually. The clusters envisioned for this PhD thesis are described in Figure 42. The corresponding scaffolds could be built following the sub-monomeric approach developed by I. Izzo (University Salerno).

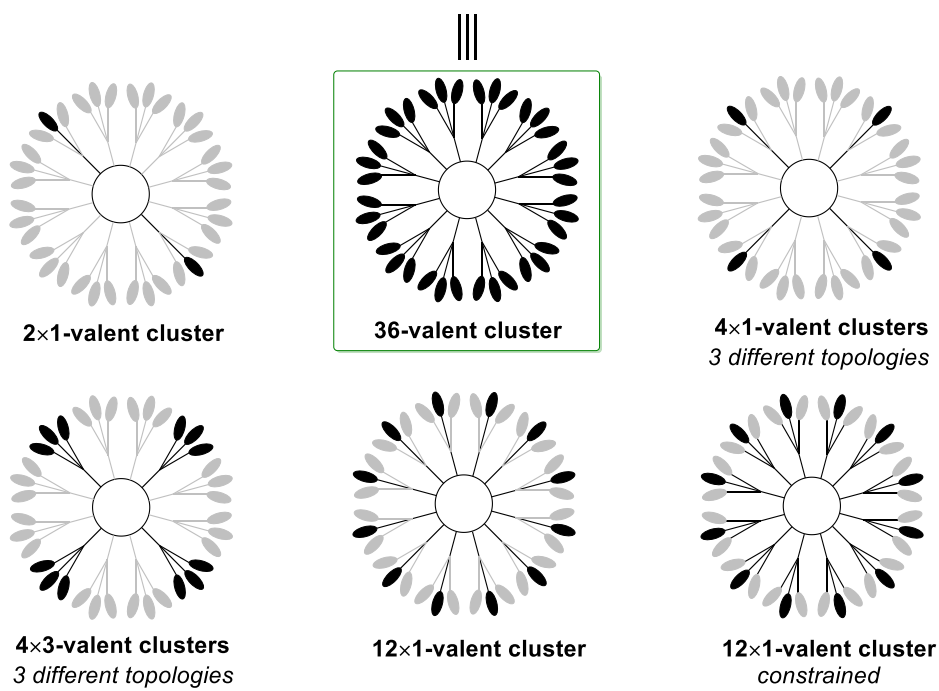
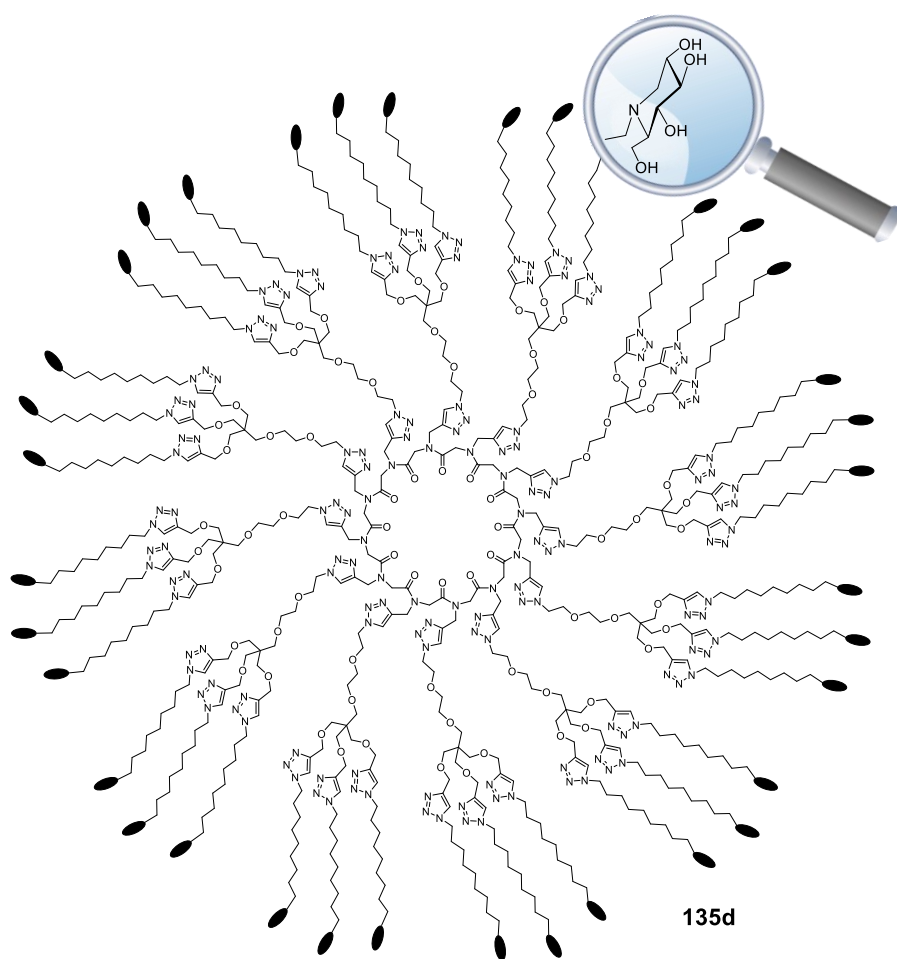


Figure 42 : Scenario of the novel clusters for this thesis.

A set of 2- and 12-valent clusters has been envisaged *via* CuAAC reaction with the scaffolds **I** to **V** prepared by our collaborators (Figure 43). Those new scaffolds have the exact size of core as the 36-valent cluster's one but contain only two (**I**), four alkynes with all possible distributions (**II**, **III**, **IV**) and twelve alkynes for **V**. The idea was to graft these cores with the same tripod ligand **152** (Figure 44)^[136] used for cluster **135d**, but also with a new monovalent clickable ligand **153** (Figure 44) having exactly the same characteristics in terms of length and nature of the arms. Finally, a last monovalent ligand **154** (Figure 44) was planned to be as close as possible to our 36-valent lead structure but with a valency of 12. The main idea was to obtain different simplified models of cluster **135d** allowing to decompose the impact of different structural factors on the multivalent effect.

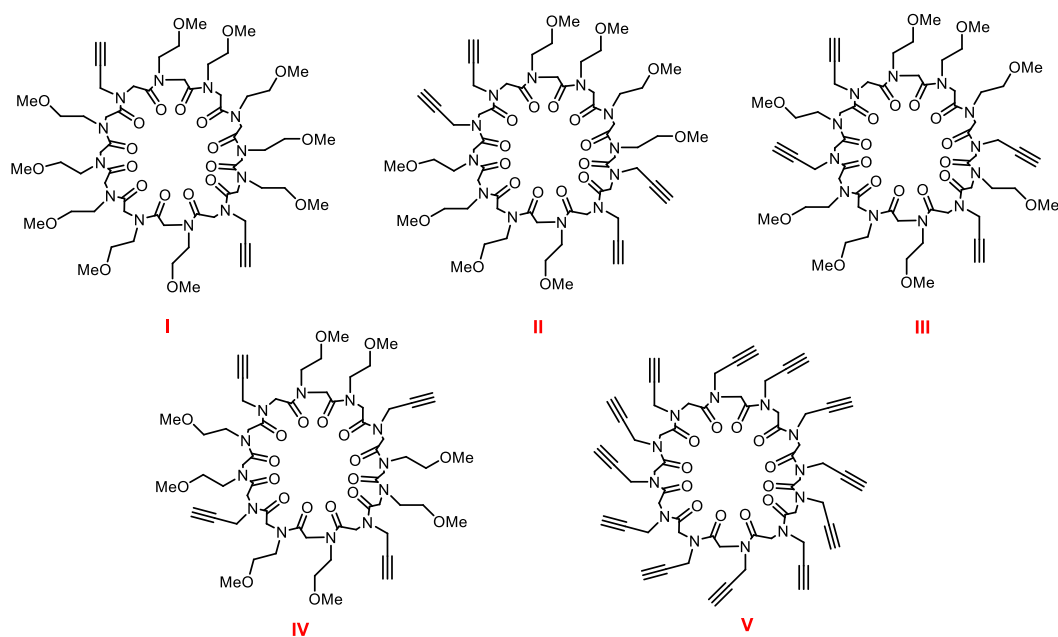


Figure 43 : Structures of the different platforms I to V.

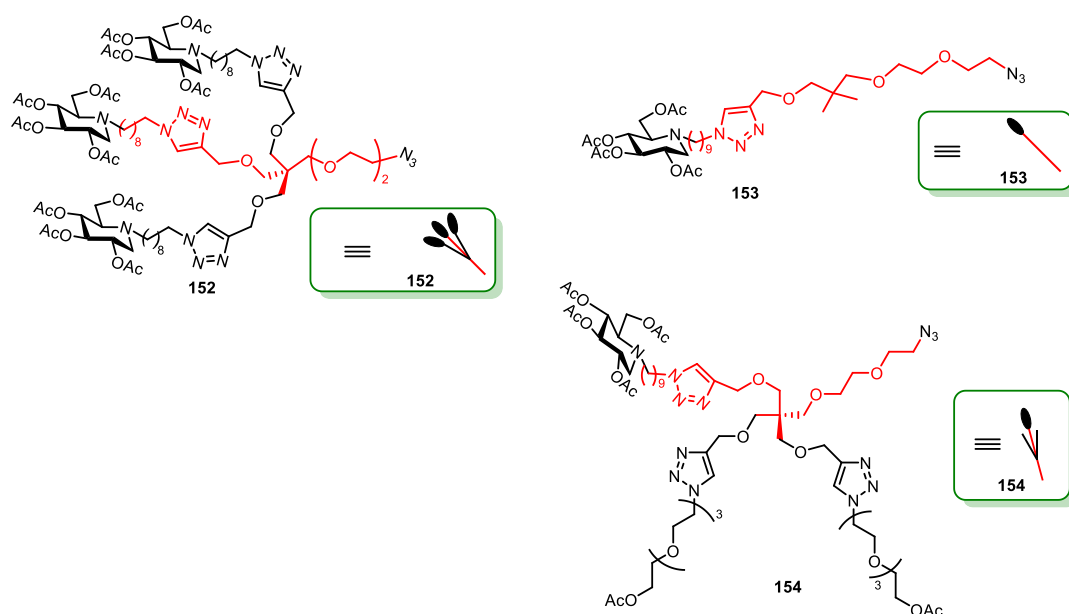


Figure 44 : Structures of clickable ligands 152 to 154.

To expand my expertise as a chemist, my second PhD objective was to develop a new synthetic methodology to access glycosyl cyanides by way of ring-opening of 1,6-anhydro sugars. In addition, this reaction could serve as a key step in the synthesis of functionalized C-glycoside inhibitors to build original multivalent inhibitors of carbohydrate-processing enzymes.

Chapter II :

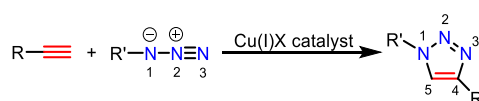
PREPARATION OF THE MAIN COMPONENTS
COMPOSING THE TARGETED CLUSTERS

This chapter will first introduce the key reaction to get clusters, i. e., CuAAC reaction, including what the CuAAC reaction is, how it is carried out, and its applications. The ligands required for the preparation of the target clusters will be also described.

I Cu(I)-catalyzed azide-alkyne cycloaddition

In 2001, H. C. Kolb, M. C. Finn and K. B. Sharpless defined “click chemistry” with a set of stringent criteria. The click reactions must be modular, insensitive to reaction conditions (light, air, temperature *et al.*), satisfying different scale requirements, easily purified by nonchromatographic methods, giving a stable and stereospecific product in high yields. It was also depicted as being “spring-loaded” for a “single trajectory,” i. e., nearly perfect reactions.^[160] Among the variety of click reactions satisfying those aforementioned stringent principles, Cu(I)-catalyzed azide-alkyne cycloaddition (CuAAC) reaction regioselectively yielding 1,4-disubstituted 1,2,3-triazoles has gained widespread attention. The debut of CuAAC started in 2002 when the groups of M. Meldal and K. B. Sharpless independently described a way to render the Huisgen 1,3-dipolar cycloaddition regioselective thanks to copper catalysis.^[161–163]

A CuAAC reaction comprises three indispensable components : azide, alkyne, and copper (pre)catalyst (Scheme 6). Scheme 6 only shows a generic form of CuAAC, e. g., without listing the exact copper catalyst or reaction conditions. In addition, with the discovery of various latent copper catalysts and specific reaction conditions, some types of internal alkynes could undergo CuAAC giving 1,4,5-trisubstituted 1,2,3-triazoles. For example, Nolan’s group developed [(NHC)CuBr] (NHC=N-heterocyclic carbene) complex catalyzing [3+2] cycloaddition of azides with a disubstituted alkyne,^[164] which illustrates that CuAAC is not limited to the terminal alkyne.



Scheme 6 : Generic form of Cu(I)-catalyzed azide-alkyne cycloaddition affording 1,4-disubstituted 1,2,3-triazoles.^[161,162]

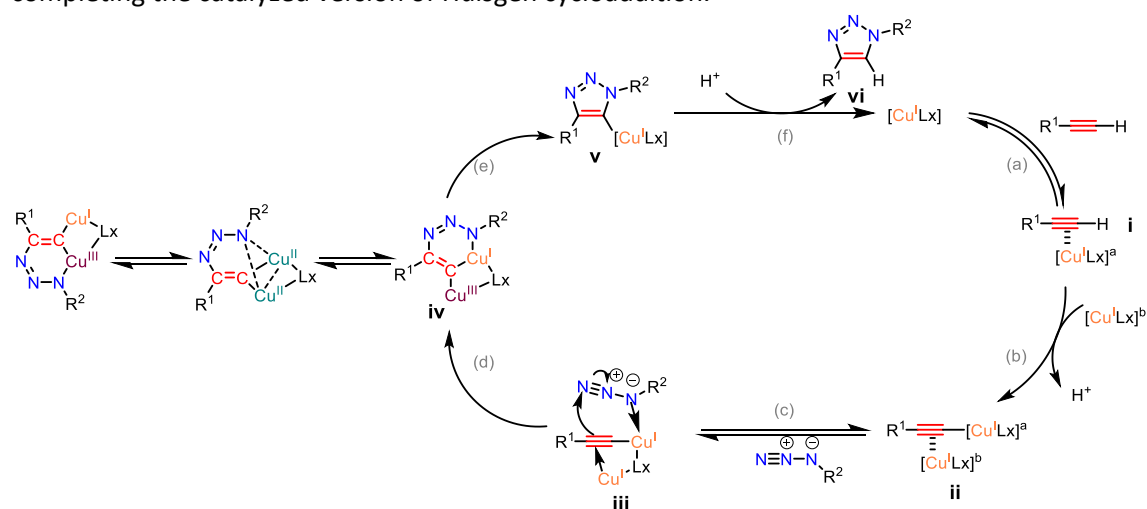
CuAAC is the catalyzed case of Huisgen 1,3-dipolar cycloaddition, which could accelerate as much as 7 orders of magnitude in comparison with the uncatalyzed thermal process.^[165] X. Y. Wang and Y. F. Hu’s group developed an extremely rapid and efficient CuAAC reaction between phenylacetylene and benzylazide, which was catalyzed by copper (I) acetate $[(CH_3CO_2Cu)_2]_n$, undertaken without solvent at ambient temperature and completed in 3 seconds.^[166] This is a perfect example illustrating how fast copper (I) could accelerate the rate of the azide-alkyne cycloadditions. Besides, the advantages of CuAAC reactions lie in the following aspects :

- i. high regioselectivity yielding only 1,4-disubstituted 1,2,3-triazole molecules and not the mixture of 1,4- and 1,5- isomers afforded in the non-catalyzed Huisgen reaction,
- ii. mild and convenient conditions (i. e., at mild temperature, occurring in water or alcoholic medium or solvent-free),
- iii. efficient and inexpensive catalyst combination (CuSO₄·5H₂O/sodium ascorbate).

The impressive performance of CuAAC reaction spurs its in-depth mechanistic investigations, development of novel catalysts, and subsequent applications.

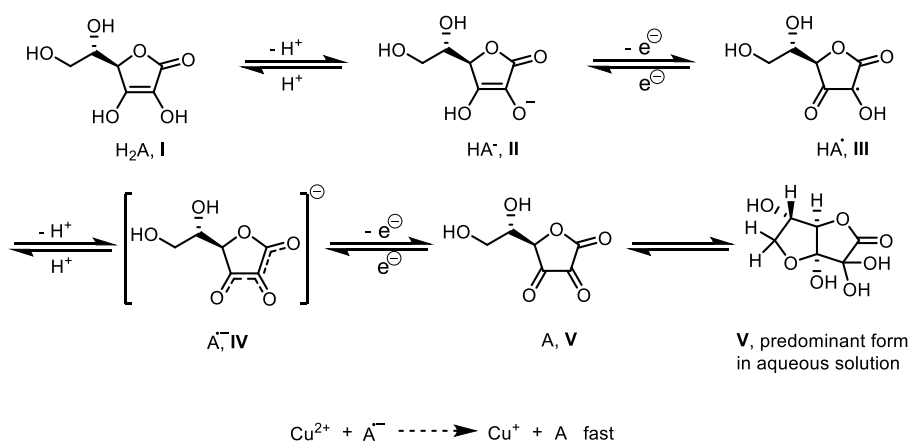
Fokin, Sharpless *et al.* initially proposed a monomeric copper acetylide complexes mechanism (the mononuclear mechanism) based on density functional theory (DFT) calculations.^[162] But

in 2013, Fokin and co-workers published the direct evidence of a dinuclear copper intermediate (Scheme 7, **iv**) within CuAAC reactions by copper isotope crossover method.^[167] Scheme 7 reveals the dinuclear mechanism of CuAAC.^[167] Briefly, it proceeds *via*: a) the initial coordination of copper(I) with the π -system of terminal alkyne forming the π -complex **i**, which lowers by 10 units of terminal alkyne $C-H$ pK_a ;^[168] b) deprotonation and formation of the σ -bound copper(I) acetylide facilitated by step (a), then a second copper atom positioned towards $C\equiv C$ bond to form the critical intermediate σ,π -di(copper) acetylide complex **ii** which was successfully isolated by L. Q. Jin and co-workers in the reaction;^[169] c) addition of organic azide providing the azide/alkyne/dimeric copper complex **iii** that was fished out and structurally characterized by F. D. Angelis's group for the first time through electrospray ionization mass spectrometry (ESI-MS);^[170] d) decreased electron density on $C\equiv C$ promotes the formation of metallacycle **iv** (along with oxidation of one copper from +1 to +3 state) which alleviates ring strains compared to the six-membered metallacycle initially proposed in the mononuclear mechanism;^[162] e) ring contraction to give the copper(I) triazolide **v** which also could be isolated as a viable intermediate of CuAAC reaction;^[171] f) protonation of **v** completing the catalyzed version of Huisgen cycloaddition.



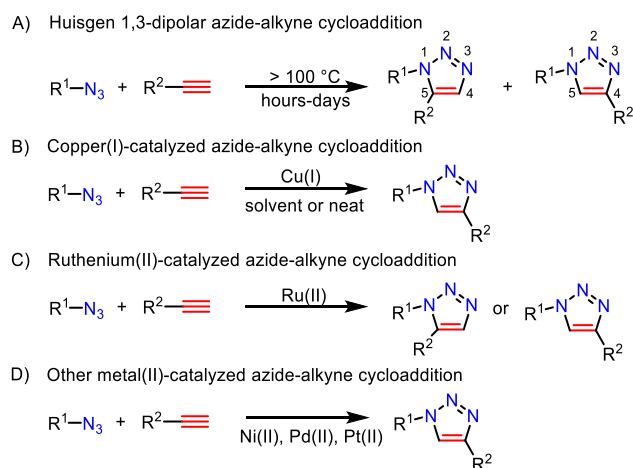
Scheme 7 : The dinuclear mechanism of CuAAC.^[172,167]

In the entire 1,4-disubstituted 1,2,3-triazole ring-formation process shown in Scheme 7, step (d) and (e) are fast, and the procedure of deprotonation of alkyne and protonation of copper(I) triazolide, namely proton-transfer, is the rate-determining step.^[173] The proton can be transferred directly from alkyne to copper(I) triazolide. Also, the proton-transfer could be facilitated by taking place in a protic solvent or accelerated by the addition of an exogenous base. In Sharpless and Fokin's catalyst combination $CuSO_4 \cdot 5H_2O$ /sodium ascorbate, sodium ascorbate is generally regarded as a reducing reagent to reduce the precatalyst copper(II) oxidative formation to copper(I) state (Scheme 8)^[174-176], whereas its potential property of acting as a general base catalyst (pK_a of ascorbic acid equals 4.1) is overlooked.^[172] Moreover, alkynes with relatively low pK_a , i. e., alkynes with electron-withdrawing substituents, showed faster rates of CuAAC reaction.^[172]



Scheme 8: Redox property of L-ascorbic acid and the reduction of copper(II) to copper(I).^[174–176]

There is no perfect catalyst always fulfilling the requirements for all types of Huisgen 1,3-dipolar cycloadditions. Even the classical Sharpless and Fokin's $\text{CuSO}_4 \cdot 5\text{H}_2\text{O}$ /sodium ascorbate catalyst has the drawback that large quantities of this system are needed for a reaction, and that copper maybe difficult to be removed after CuAAC completion. Therefore, investigating a better catalyst is also on the top-list of 1,3-dipolar Huisgen cycloaddition studies. Now, there are many catalysts based on not only copper^[177,178] but also other metals like ruthenium, silver, gold, and iridium, which were found to work efficiently.^[179] It is, however, interesting to note that different catalysts show alternative results *via* different mechanisms. Thermal Huisgen cycloaddition provides a mixture of 1,4- and 1,5- isomers, which requires elevated temperature and prolonged reaction time (Scheme 9A).^[180] Strikingly, in contrast to uncatalyzed Huisgen reaction, CuAAC reveals an excellent way of satisfying stringent criteria of "click chemistry" to afford regioselective 1,4-disubstituted 1,2,3-triazoles (Scheme 9B). Ruthenium-based catalysts are also versatile, which could be applied to yield either exclusive 1,4- or 1,5-regioisomers or mixtures of both (Scheme 9C).^[181] The results depend on the concrete structure of alkyne and the specific composition of Ru(II)-catalyst. Shown as Scheme 9D below, some other metals like Ni(II), Pd(II), Pt(II) enrich the types of metals that can catalyze 1,3-dipolar azide-alkyne regioselective conversion, forming 1,4-disubstituted 1,2,3-triazole products.^[182]



Scheme 9 : A) Thermal Huisgen 1,3-dipolar azide-alkyne cycloaddition; B) CuAAC; C) RuAAC; D) Other M(II)AAC

CuAAC offers a simple, robust but powerful method to form 1,2,3-triazole heterocycles. It boosts the development of heterocyclic chemistry and has extensive applications in medicinal chemistry, bioconjugation, surface modification, synthesis of polymers, *etc.*^[183–187] V. K. Tiwari and co-workers published a brilliant review demonstrating that CuAAC acts as a promising strategy in glycoscience to generate analogs of complex glycoconjugates such as glycopeptides, polysaccharides, glyco-macrocycles, glyco-arrays, glyco-dendrimers, glyco-clusters, and glycopolymers.^[188]

To illustrate the power of CuAAC, Figure 45 exhibits a gigantic 120-valent glycosidase inhibitor **99** obtained by a click – click strategy.^[130]

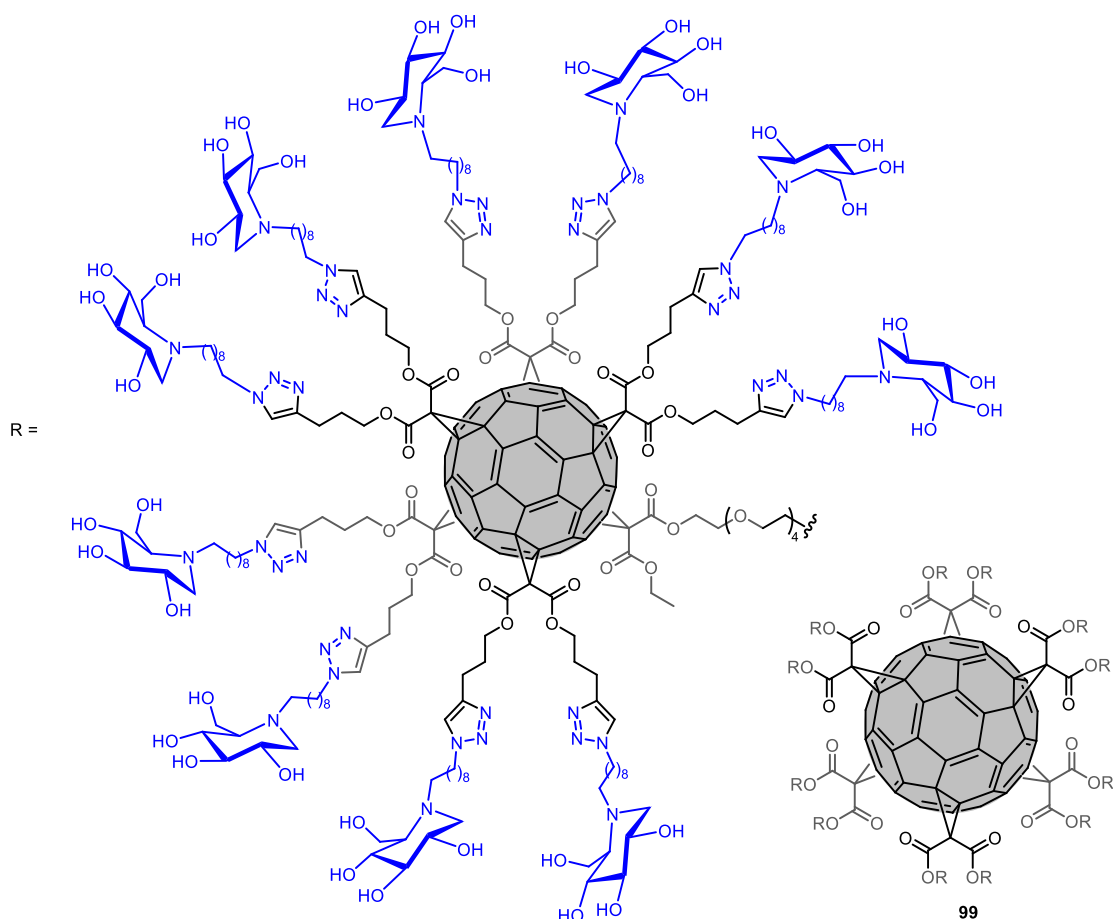


Figure 45 : A giant 120-valent cluster **99** based on a C₆₀ scaffold.

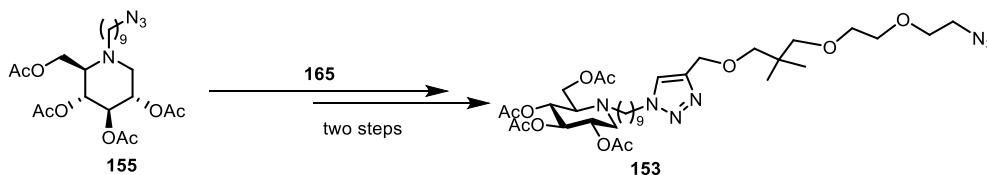
II Synthesis of three types of clickable ligands

II.1 Preparation of a monovalent-ligand related to the clickable tripod

Our structure-activity relationship study requiring to have access to a clickable tripod model exhibiting only one iminosugar head, we have synthesized compound **153** (Figure 44) with the following features :

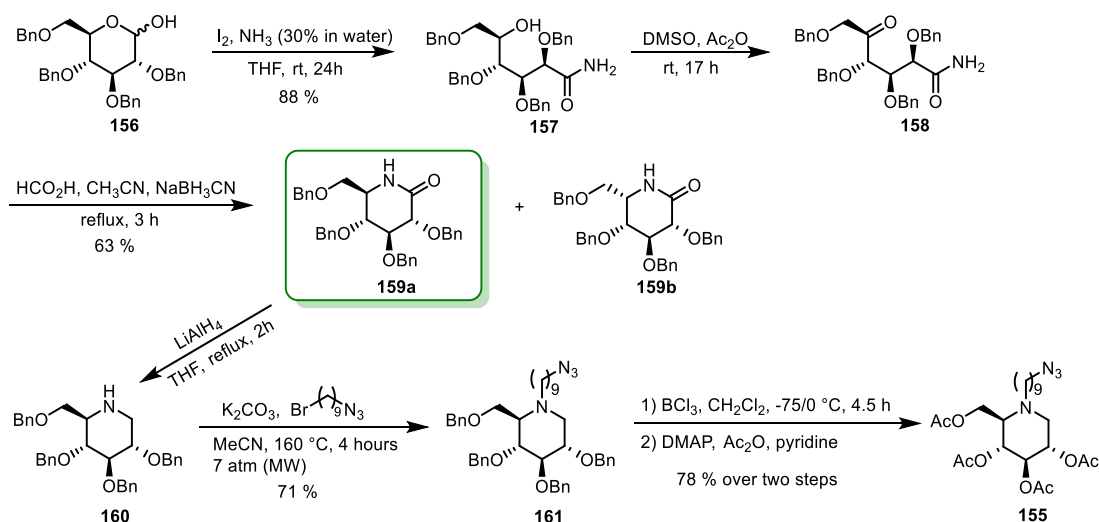
- i. same type of inhibiting epitope as the tripod **152**,
- ii. same dendron length as the tripod **152**.

The monovalent-ligand mimicking tripod was prepared by a convenient way based on CuAAC reaction of azide-armed azasugar building block **155** and an appropriate ethylene glycol chain with terminal alkyne. The strategy is depicted in Scheme 10.



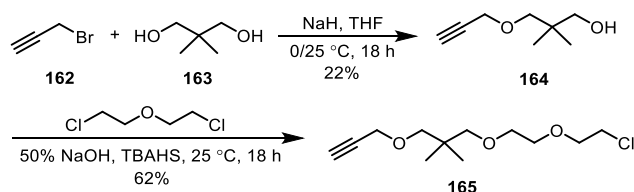
Scheme 10 : Synthesis of the clickable monovalent-ligand **153**.

The sequence forming azide-armed azasugar building block **155** started with the commercially available starting material, tetra-*O*-benzyl D-glucopyranose (**156**) as shown in Scheme 11.^[4,189,190] After the first step of oxidative amidation using iodine in 30% aqueous ammonia, the δ -hydroxy amide **157** was obtained in 88% yield. Due to the generation of explosive nitrogen iodide monoamine ($\text{NI}_3 \cdot \text{NH}_3$) during the oxidation, the operation was performed behind a safety shield. The OH group at position C-5 was subsequently oxidized to the corresponding keto amide **158** under the condition of Albright Goldman's reaction using DMSO/ Ac_2O , followed by intramolecular reductive amination giving a mixture of two diastereoisomeric lactams described by structures **159a** and **159b**. After purification with flash chromatography, the required diastereomer **159a** was obtained in a 63% yield. Lithium aluminium hydride (LAH) allowed the reduction of lactam **159a** to compound **160**, and then alkylation of **160** with 1-azido-9-bromo-nonane gave the *O*-benzylated **161**. To be smoothly removed in the final clusters, the *O*-protecting groups of **161** were replaced with acetyl groups in the next step. Benzyl protecting groups were selectively removed without causing degradation of the azide functional group. The *O*-debenzylation process was carried out with BCl_3 at low temperature efficiently. Subsequently, these free OH groups were peracetylated with Ac_2O /Pyridine to form the protected azide iminosugar building block **155**.



Scheme 11 : Synthesis of the azide azasugar building block **155**.

Thanks to my colleague Dr. Nicolas Kern's work, I got the compound **165** which was used to synthesize the clickable iminosugar **153**. It was prepared in a two-step sequence, starting with mono-propargylation of diol **163**, and followed by alkylation of the remaining free alcohol on structure **164** (Scheme 12).^[191]

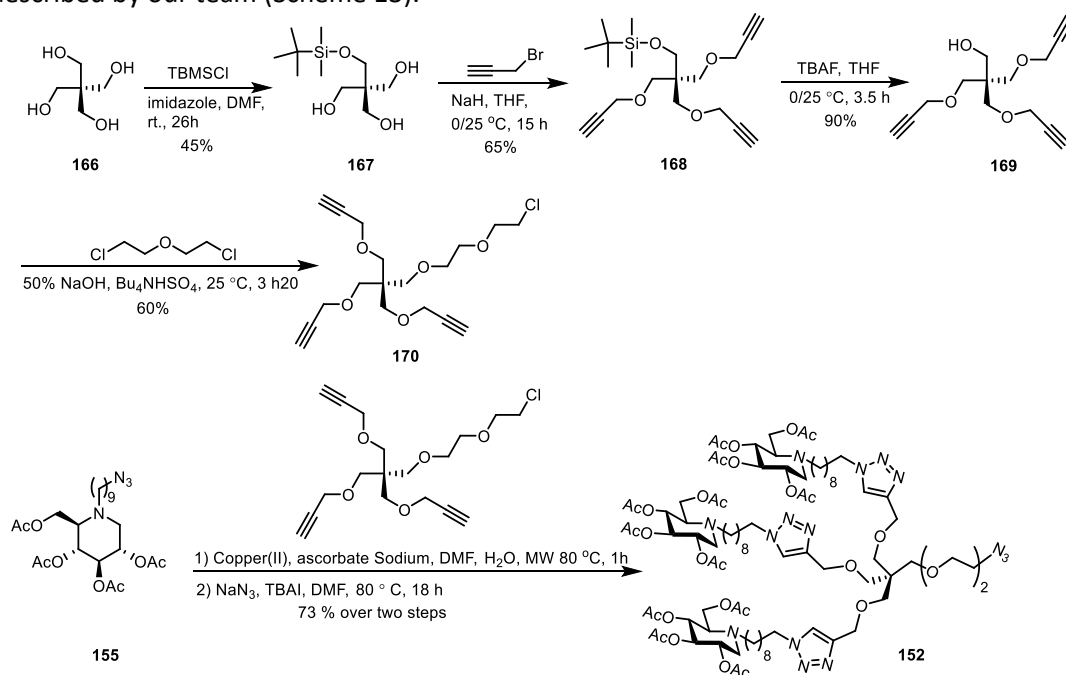


Scheme 12 : Synthesis of the ethylene glycol chain **165**.

With these two structures **155** and **165** in hand, the monovalent-ligand related to tripod **153** was prepared in two steps in 92% yield by CuAAC reaction assisted with microwave irradiation and chloride to azide conversion.

II.2 Preparation of the clickable tripod

The tripod bearing three inhibiting epitopes was also prepared following the protocol described by our team (Scheme 13).^[136]



Scheme 13 : Synthesis of the clickable tripod **152**.

Similar to the preparation of monovalent-ligand, the strategy to synthesize tripod **152** could also be divided into two sections, including synthesis of compound **155** and tripropargyl ether AB₃-type building block **170** (Scheme 13).

According to Mollard and Zharov's protocol,^[192] compound **170** was synthesized starting with commercially available pentaerythritol **166**. Then one of the four OH groups on structure **166** was monoprotected with 0.5 eq. of TBDMSCl in the presence of imidazole to give triol **167** in a moderate yield of 45%. Multi-silylated derivatives were observed as byproducts during the reaction. After that, triol **167** underwent tripropargylation, deprotection of TBDMS protecting

group by 5 eq. of TBAF, followed by alkylation with an excess of 2,2'-dichlorodiethyl ether to afford the desired compound **170**. During the addition of aqueous sodium hydroxide as the base for the alkylation, a solid phase appears in the flask, therefore, the transfer reagent and vigorous stirring are necessary for this step.

Finally, the tripod **152** was formed by clicking azide-armed iminosugar **155** with **170**, and then the chloride atom was substituted by azide with 10 eq of sodium azide. The entire yield over the two steps was 73%.

II.3 Preparation of the “hindered” monovalent-ligand related to the clickable tripod

To make a systematic evaluation concerning the influence of steric effects displayed when several inhitopes of a cluster interact with an enzyme, a “hindered” monovalent-ligand structure related to the tripod was designed. Its synthesis is described as follows.

II.3.1 Synthetic strategy

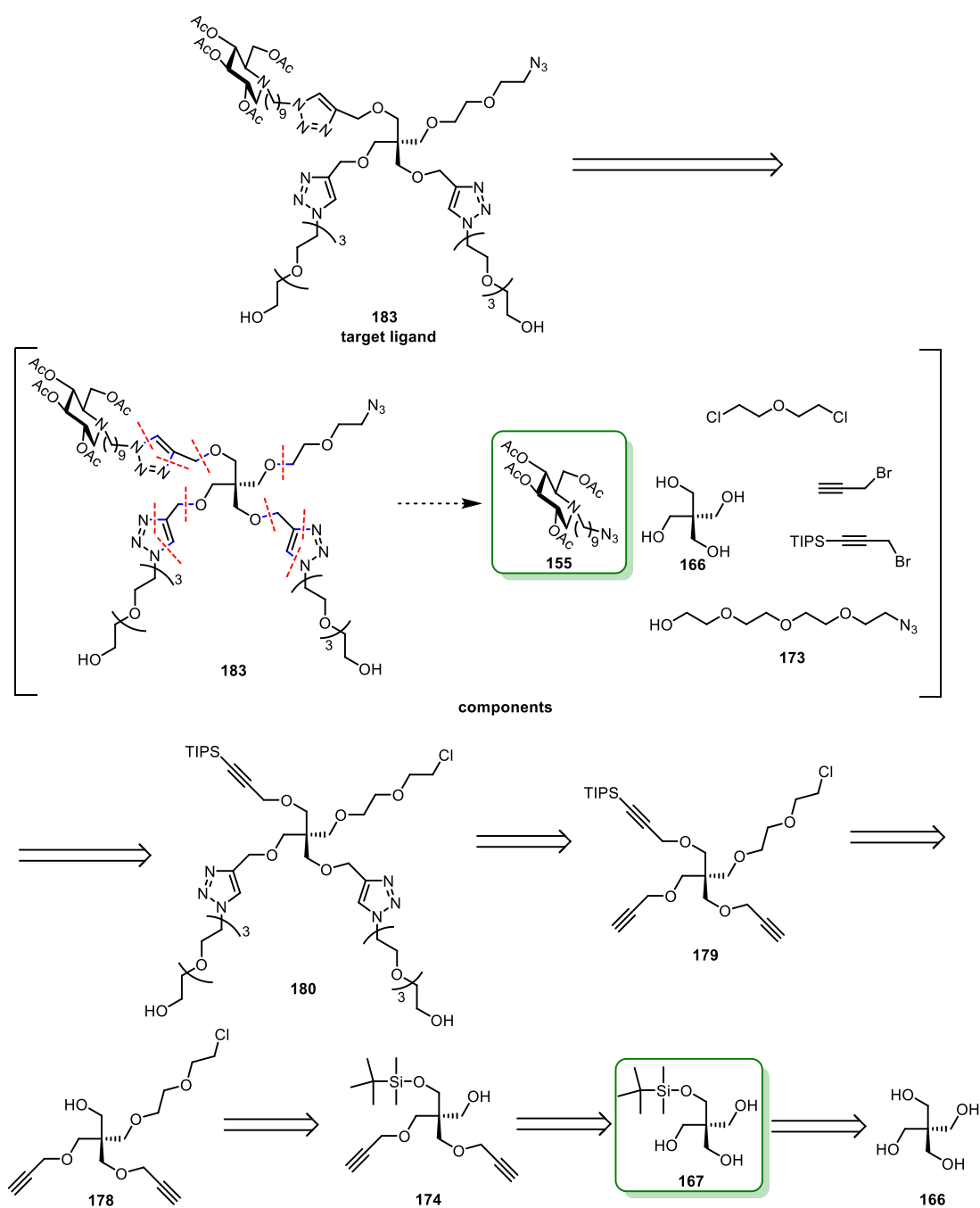
Since the new “hindered” monovalent-ligand structure was designed depending on the existing tripod **152**, then it should possess some characters as follows :

- i. same type of inhibiting epitope as the tripod but only one head for each ligand,
- ii. same dendron length as for the tripod,
- iii. similar hindrance compared to the tripod.

Keeping all these characteristics in mind, tetraethylene glycol was chosen to form the dendron chain with the same length and similar solubility as the tripod **152**.

To build the desired structure **183**, several points should be noticed :

The four identical OH groups of the starting material pentaerythritol have to be decorated with three different motifs (Scheme 14). One OH group will be used to introduce the PEG chain with a terminal azide group. Concerning the click reactions, two CuAAC reactions have to be performed in a successive manner to attach two different moieties : one containing the iminosugar inhitope and two containing the PEG chains. To achieve this, propargyl chains containing two different types of alkynes - one terminal alkyne and two alkynes protected with TIPS groups - will be introduced.



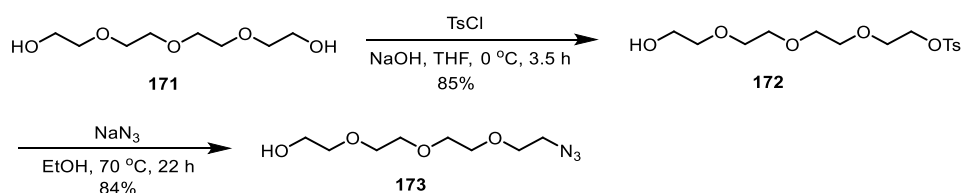
Scheme 14 : Retrosynthesis of the “hindered” monovalent-ligand.

In more details, two of the three OH groups are going to be functionalized with two identical terminal alkynes using propargyl bromide.^[138,193] After that, the remaining free OH group will be alkylated with 2,2'-dichlorodiethyl ether to form the pentaerythritol derivative bearing with two different building blocks. To insert the third distinct architecture on the dendritic pentaerythritol derivative, the TBDMS protecting group should be removed, followed by the reaction with a different alkyne. ii) The corresponding azido tetraethylene glycol would be clicked with those two identical terminal alkynes *via* CuAAC to provide the hindered arm mimetics of the target monovalent ligand. On the other hand, the protected alkynyl will be used to attach the sugar part **155** to finish the construction of the clickable “hindered”

monovalent inhitope **183**.

II.3.2 Synthesis of 2-{2-[2-(2-azidoethoxy)ethoxy]ethoxy}ethan-1-ol

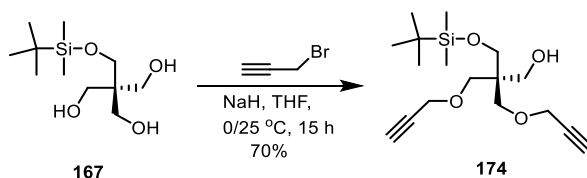
The azide **173** was prepared in two steps following G. -J. Boons's protocol.^[194] A large excess of commercially available tetraethylene glycol **171** was monoprotected by using *p*-toluenesulfonylchloride (TsCl) at 0 °C, giving **172** in 85% yield. Subsequently, the tosylate group of **172** was displaced with N₃ by adding sodium azide to afford **173** in a good yield of 84% that is comparable to the result described in G. -J. Boons's paper^[194](Scheme 15).



Scheme 15 : Synthesis of 2-{2-[2-(2-azidoethoxy)ethoxy]ethoxy}ethan-1-ol **173**.^[194]

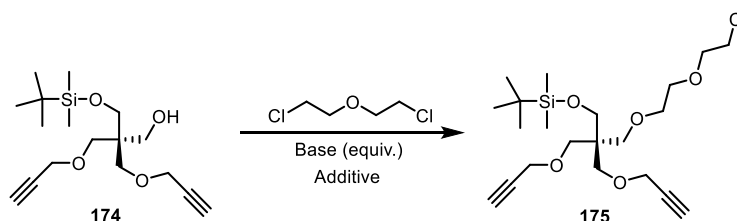
II.3.3 Synthesis of the “hindered” monovalent-ligand **183**

The dipropargyl ether **174** was obtained by treating **167** with 4 eq. of propargyl bromide in presence of 3 eq. of sodium hydride (Scheme 16). The amounts of propargyl bromide and sodium hydride were reduced here in comparison to protocols previously described.^[138,193] However, this step was accomplished in a good yield of 70%. The better proportion of dipropargyl ether over the tripropargylation one (5:1, whereas 3.5:1 as reported in previous works^[138,193]) certainly benefited from the portion-wise addition of 3 eq of sodium hydride, and 45 min later, dropwise addition of propargyl bromide.



Scheme 16 : Synthesis of the dipropargyl ether **174**.

The next step was not trivial due to the steric hindrance of the TBDMS group on **174** (Scheme 17). A similar reaction, alkylation of tripropargyl ether **170** with PEG, was presented in chapter two (II.2 section) using aqueous sodium hydroxide and TBAHS as transfer reagent. Using the same conditions than those described in Scheme 13, there was no desired product formed.



Scheme 17 : Alkylation of **174** with 2,2'-dichlorodiethyl ether (under conditions in Table 15).

A panel of reaction conditions (as shown in Table 15) were attempted for using 2,2'-

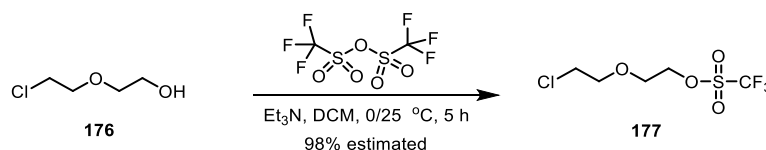
dichlorodiethyl ether as the alkylating agent, including the screening of different solvents, types of base, reaction temperatures, and duration times. Unfortunately, no targeted product was afforded.

Entry	174 (eq.)	Ether (eq.)	NaH ^a (eq.)	NaOH 50% aq (eq.)	Additive	t (°C)	Solvent	T	Result ^c
1	1	50	1.2	-	-	rt	THF	2.5d	-
2	1	50	1.2	-	-	60	THF	6h	-
3	1	50	2	-	-	120	THF	18h	-
4	1	50	1.2	-	TBAI	rt	DMF	1h	-
5	1	50	1.2	-	TBAI	65	DMF	1d	-
6	1	50	1.2	-	TBAI	80	DMF	1d	-
7	1	50	5	-	TBAI ^b	rt	THF	1d	-
8	1	50	5	-	TBAI ^b	40	THF	1d	-
9	1	50	5	-	TBAI ^b	75	THF	3h	-
10	1	60	-	2	TBAHS	rt	-	2.5d	-
11	1	60	-	2	TBAHS	70	-	1d	-

^a Sodium hydride was used as the base at 0 °C. ^b 0.1 eq MeOH was added as catalyst.^[195] ^c No desired product was observed.

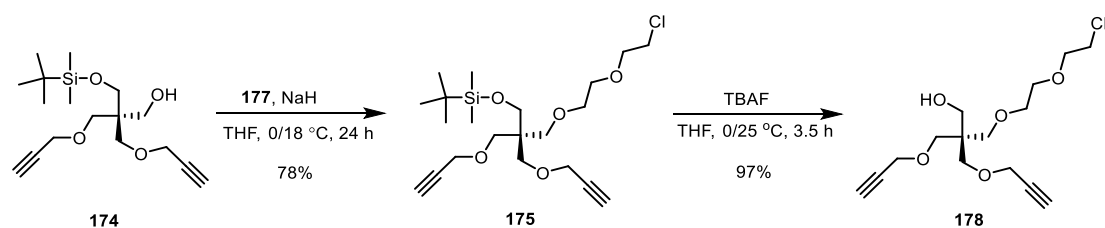
Table 15 : Attempts to alkylate **174** with 2,2'-dichlorodiethyl ether.

To complete the alkylation of **174**, an alternative alkylation reagent, 2-(2-chloroethoxy)ethyl trifluoromethanesulfonate that, possesses a better leaving group was tried.^[196] The triflate **177** was obtained by treating 2-(2-chloroethoxy)ethanol **176** with triflic anhydride using DCM as solvent.^[196,197] At the end of the reaction, **177** was formed as a crude compound (in an estimated 98% yield) and used without further purification (Scheme 18).



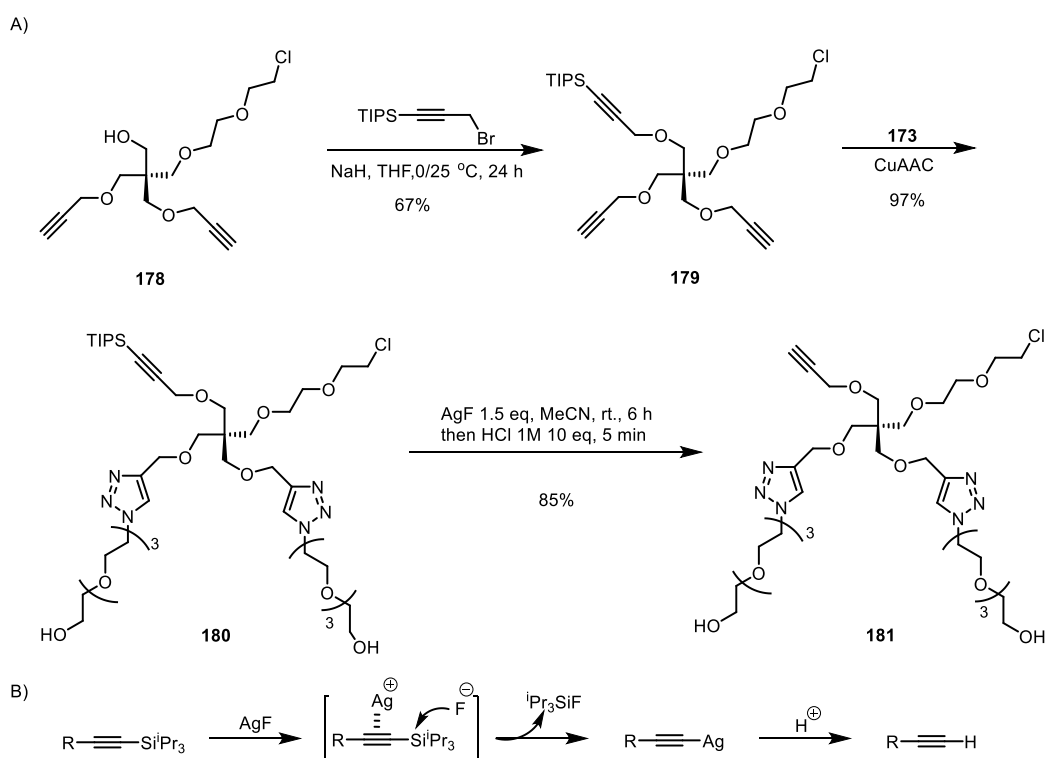
Scheme 18 : Synthesis of 2-(2-chloroethoxy)ethyl trifluoromethanesulfonate **177**.

Finally, **175** was obtained by treating alcohol **174** with **177** in a fair yield of 78%. This step is inspired by the A. Marinetti and co-workers' strategy described in 2006.^[196] Although their protocol is reproducible and reported in good yields, the amount and adding sequence of sodium hydride during the operation should be handled with attention. Slight excess of sodium hydride over the triflate **177** would be helpful for improving the yield. In my case, the 1.9:1.4 ratio of sodium hydride/**177** gave the best result. Moreover, we found that it was useless to increase the amount of sodium hydride after the addition of triflate. With **175** in hand, the TBDMS group was then deprotected by TBAF, giving **178** in almost quantitative yield (Scheme 19).



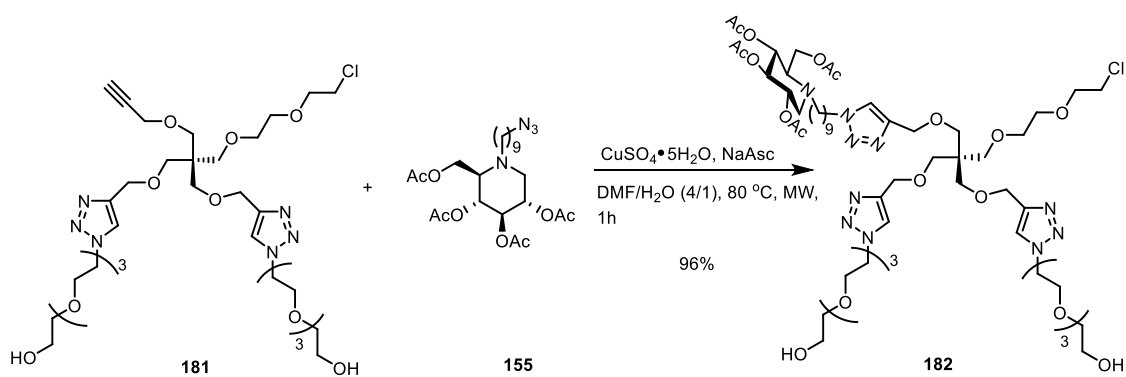
Scheme 19: Synthesis of the extended dipropargyl ether analogue **178**.

The synthesis to get the “hindered” monovalent-ligand **183** was continued (Scheme 20A). Compound **178** was first propargylated by TIPS protected propargyl bromide to give **179** in a good yield of 67%. Then, **179** was clicked with oligoethylene azide **173** affording expected compound **180** in excellent yields under the well-established CuAAC conditions. After that, the TIPS protecting group was removed following S. Kim’s strategy.^[198] It is an efficient and mild reaction. Silver fluoride serves as catalyst and reagent promoting the deprotection of **180** producing **181** with a terminal alkyne in an excellent yield of 85%. In the process, the interaction of cationic silver with C≡C bond facilitates the leaving of fluorinated TIPS, affording a silver acetylide intermediate, which is subsequently hydrolyzed by aqueous HCl (Scheme 20B).^[198] Therefore, the reaction should be performed in the dark.



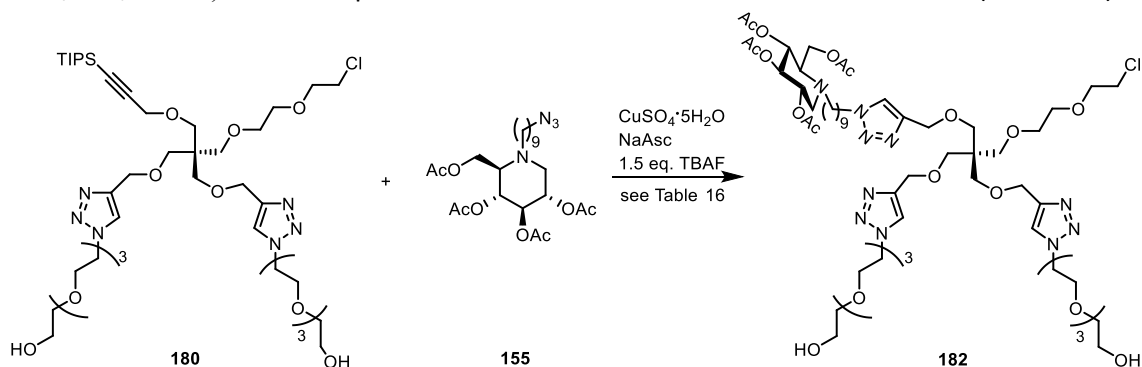
Scheme 20 : A) Synthesis of precursor **181** of the “hindered” monovalent-ligand. B) Mechanism of the deprotection of **180**.^[198]

The next step is the treatment of **181** with **155** under the aforementioned CuAAC conditions to introduce the unique inhibitory head into the dendron ligand, forming **182** in an excellent yield of 96% (Scheme 21).



Scheme 21 : Synthesis of a precursor **182** of the “hindered” monovalent-ligand.

An alternative way to get **182** from **180** (Scheme 22) was inspired by C. H. Larsen’s approach.^[199] The tandem copper-catalyzed and silyl deprotection in one step was tried. Unfortunately, in my case, no target compound **182** was observed using TBAF, CuSO₄·5H₂O/sodium ascorbate as the catalyst in protic solvents (*i*PrOH, *i*PrOH/MeOH, DMF/H₂O, MeOH). The attempted reaction conditions are summarized in Table 16 (see below).



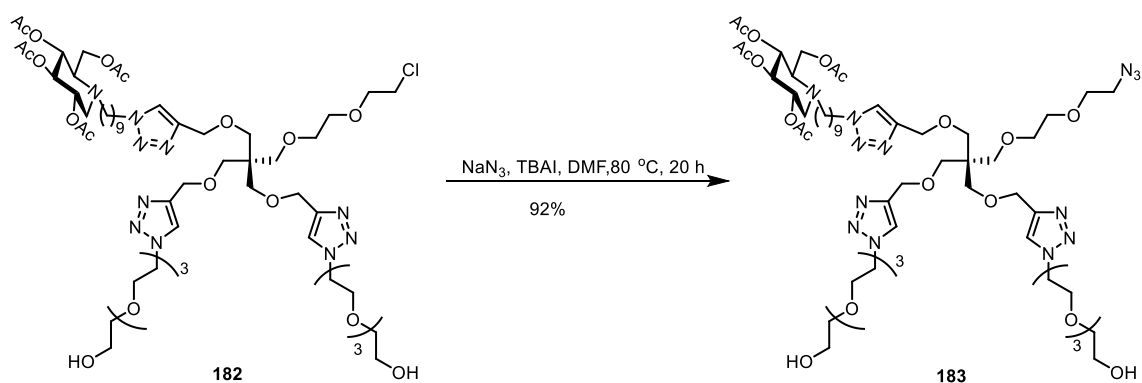
Scheme 22 : A tandem conversion to provide **182** from **180**.

Entry	180 (eq.)	155 (eq.)	Cu(II) (eq.)	NaAsc (eq.)	Solvent	t(°C)	T	Result ^c
1	1	1.1	0.1	0.2	<i>i</i> PrOH	60 ^a	2.5 h	-
2	1	1.1	0.1	0.2	<i>i</i> PrOH/MeOH (2:1)	60 ^b	18 h	-
3	1	1.1	0.1	0.2	DMF/H ₂ O(4:1)	80 ^a	1 h	-
4	1	1.1	0.1	0.2	MeOH	60 ^a	1 h	-

^a Assisted with microwave irradiation. ^b Conventional oil bath heating. ^c No desired product was observed.

Table 16 : Attempts to obtain **182** in one step from **180**.

An adequate amount of **182** was prepared through the step-wise protocol, namely deprotection of **180**, followed by click reaction with **155**. With **182** in hand, it only takes the last step to finish. The final compound **183** was constructed by replacing the Cl of **182** with N₃ in an excellent yield. Scheme 23 displays the detailed reaction conditions.



Scheme 23 : Synthesis of the “hindered” monovalent-ligand **183**.

II.4 Characterization of the “hindered” monovalent-ligand dendron **183**

II.4.1 ¹H NMR spectra

Owing to the symmetry of the compounds **181** and **183**, the “naked” PEG (polyethylene glycol) arms are equivalent, which facilitates their NMR analysis (Figure 46). The attribution of each proton of the molecules is realized by a refined analysis of the NMR spectra in two dimensions, including COSY (correlation spectroscopy), HSQC (heteronuclear single quantum correlation), and HMBC (heteronuclear multiple-bond correlation spectroscopy). The signals of 1-deoxynojirimycin derivative **155** and the clickable compound **181** are basically not affected by the click reaction, except the protons close to the azide group (H-15 for **155**) shifted to around 4.3 ppm (H-15 for **183**) and the terminal alkyne (H-20 for **181**) shifted to approximately 4.6 ppm (H-18 for **183**). Crucially, the typical resonance arising from the proton of the 1,2,3-triazole ring generated by clicking the compound **155** with **181** is clearly observed at 7.5 ppm (H-16 for **183**), proving the success of the CuAAC reaction.

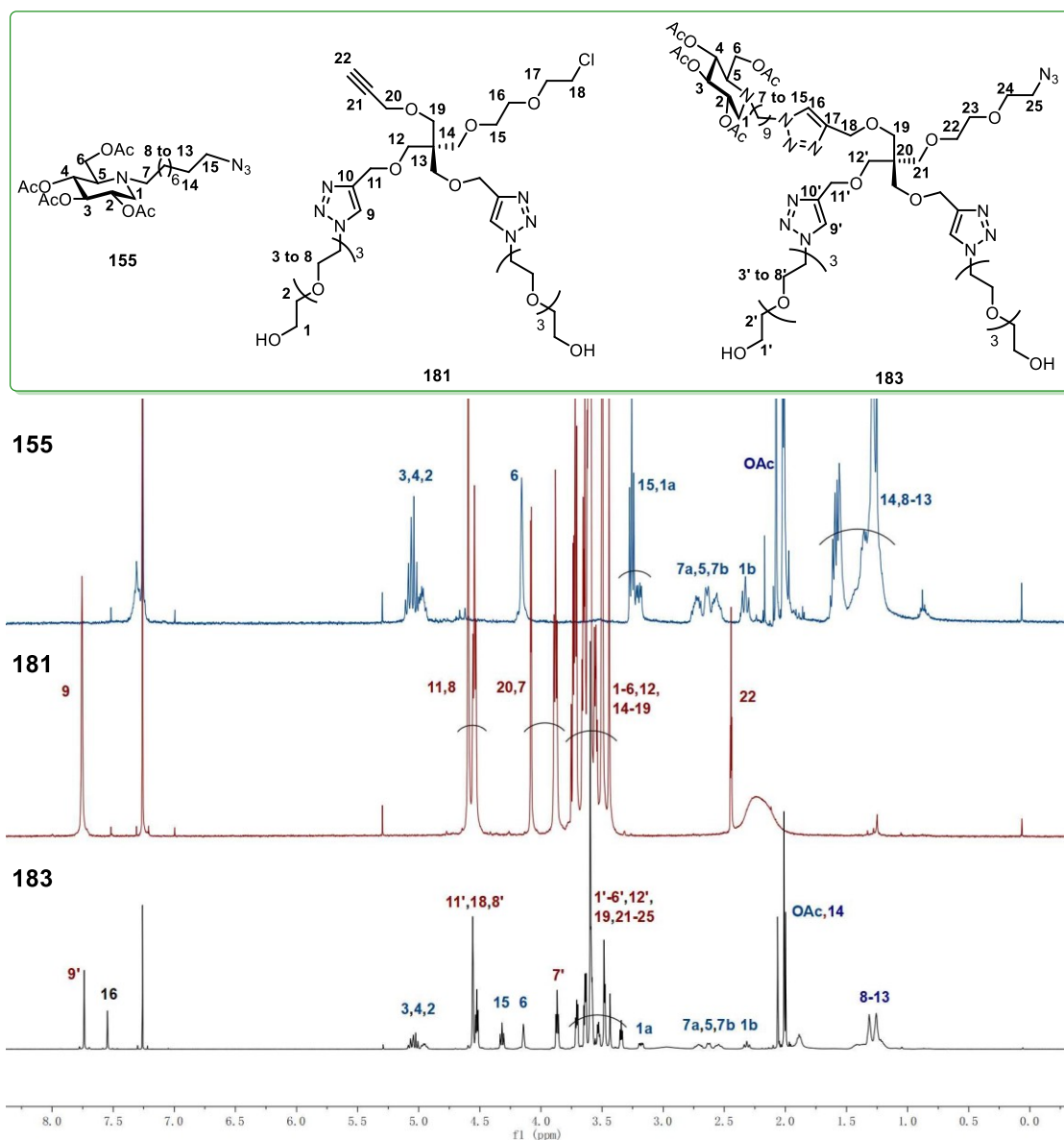


Figure 46 :¹H NMR spectra of molecules 155, 181, 183 in CDCl₃.

II.4.2 Infra-Red spectrum

The typical absorption features of **183** are also seen in the Infra-Red (IR) spectrum (Figure 47). The IR spectrum below shows the specific absorption bands of the hydroxyl function at 3457 cm⁻¹, azide function at 2106 cm⁻¹, acetate at 1744 cm⁻¹. The absorption band around 3300 cm⁻¹ corresponding to the alkyne is not present in the “hindered” dendron **183**.

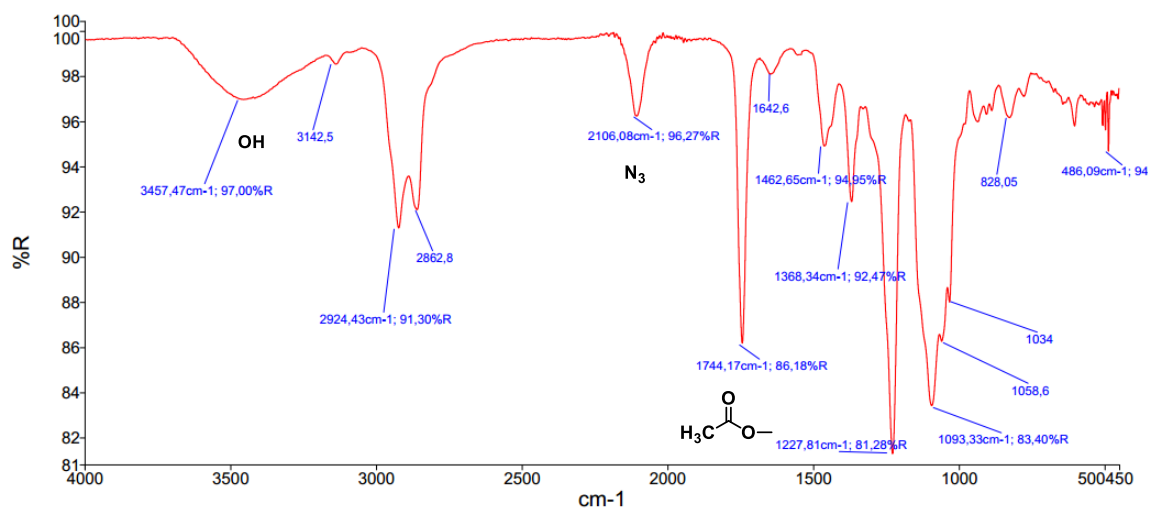


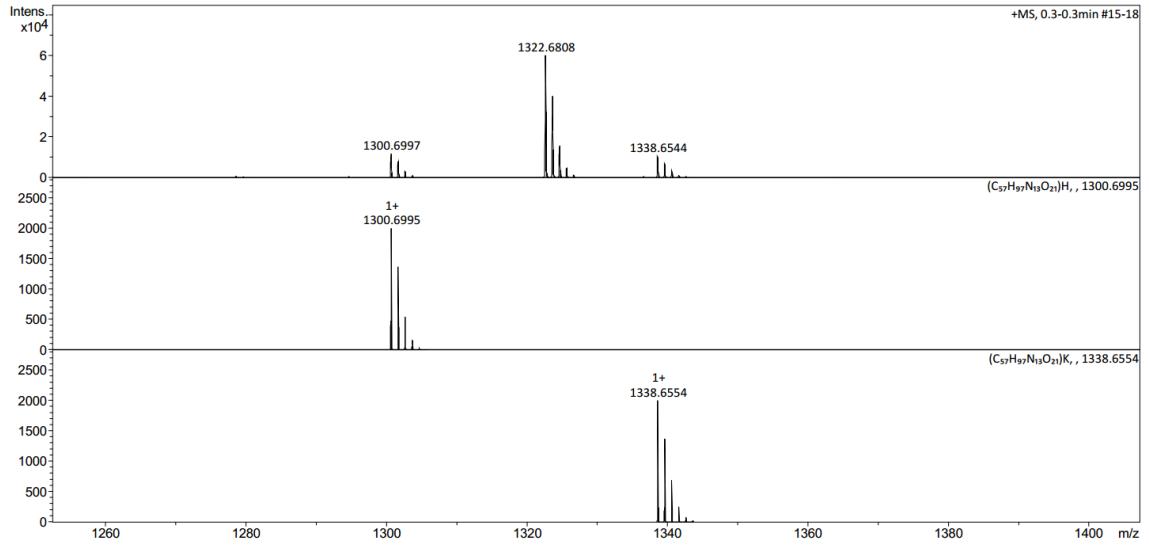
Figure 47 : Infra-red spectrum of **183**.

II.4.3 Mass spectra

To further confirm the structure of **183**, mass spectra *via* electrospray ionization (ESI) were recorded under different conditions (Figure 48). The expected molecular ion peaks were clearly observed: m/z 1300.6997 [M + H]⁺ (calculated for C₅₇H₉₈N₁₃O₂₁ : 1300.6995), m/z 1322.6808 [M + Na]⁺ (calculated for C₅₇H₉₇N₁₃NaO₂₁ : 1322.6814), m/z 1338.6544 [M + K]⁺ (calculated for C₅₇H₉₇KN₁₃O₂₁ : 1338.6554).

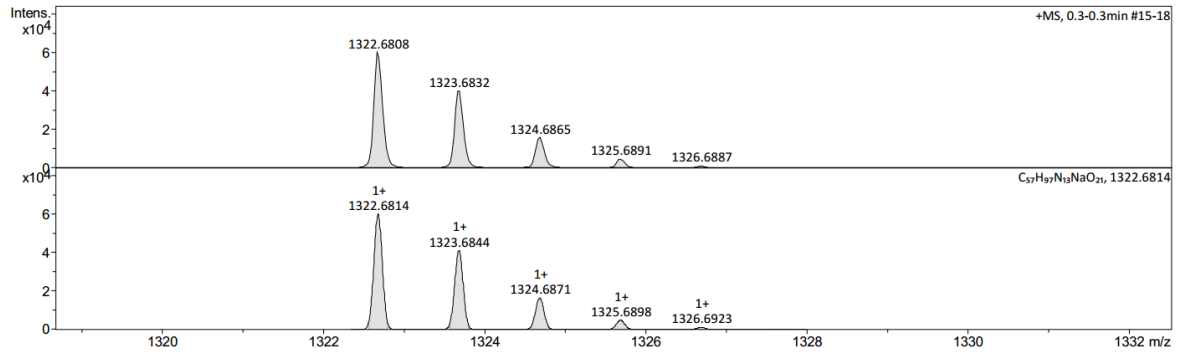
Acquisition Parameter

Source Type	ESI	Capillary	4500 V	Nebulizer	0.3 Bar	Set Hexapole RF	330.0 Vpp
Ion Polarity	Positive	Dry Heater	200 °C	Dry Gas	3.0 l/min	Set Capillary Exit	150.0 V



Acquisition Parameter

Source Type	ESI	Ion Polarity	Positive	Set Corrector Fill	52.4 V
n/a	n/a	n/a	n/a	n/a	n/a
Scan Begin	50 m/z	n/a	n/a	Set Reflector	1800.0 V
Scan End	3000 m/z	n/a	n/a	Set Flight Tube	8600.0 V
		n/a	n/a	Set Detector TOF	1996.2 V



Meas. m/z #	Ion Formula	m/z err [ppm]	Mean err [ppm]	rdB	N-Rule	e ⁻ Conf	mSigma	Std I	Std Mean m/z	Std I VarNorm	Std m/z Diff	Std Comb Dev
1322.680800	1 C57H97N13NaO21	1322.681418	0.5	0.9	15.5	ok even	8.7	8.6	n.a.	n.a.	n.a.	n.a.

Figure 48 : Mass spectra (ESI) of 183.

Chapter III :

CLUSTERS SYNTHESIS AND STRUCTURE-
ACTIVITY RELATIONSHIPS STUDY OF
MULTIVALENT EFFECT WITH JACK BEAN α -
MANNOSIDASE

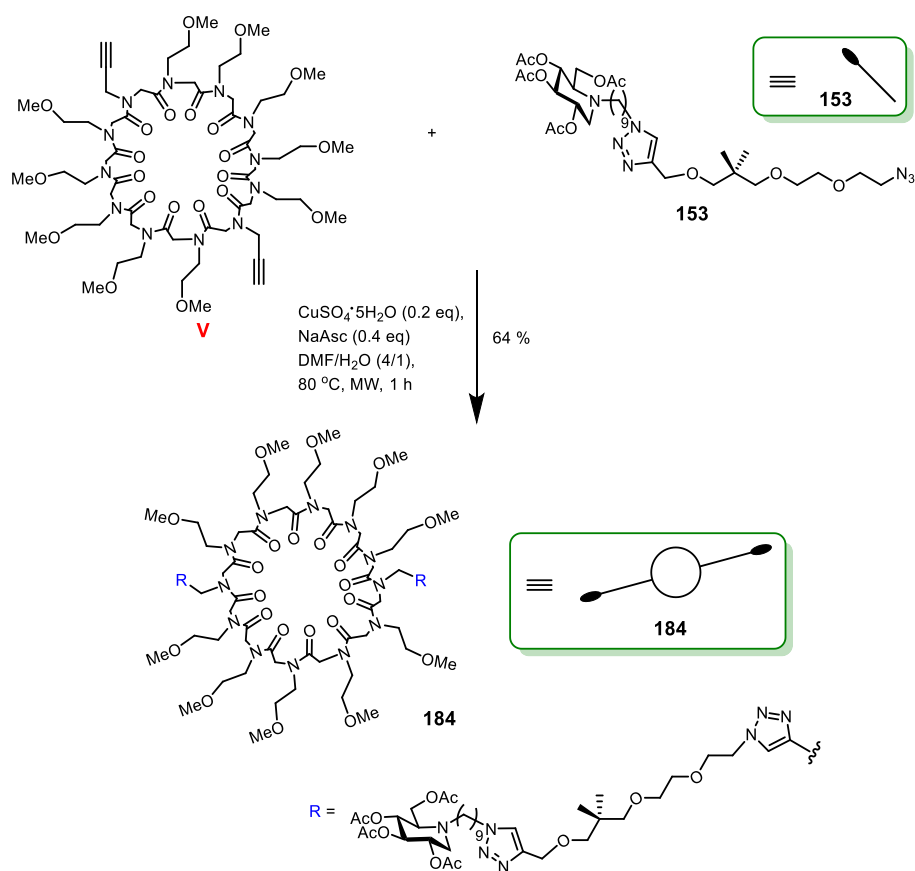
I. Synthesis of multivalent cyclopeptoid-based clusters

With the clickable ligands prepared in chapter II and the Prof. Izzo's scaffolds in hand, all the building blocks were available to synthesize the library of multivalent iminosugar designed for our SAR study. The two key steps to afford them were the CuAAC coupling reaction and the final deprotection, namely the *O*-deacetylation step using basic type resin amberlite IRA400.^[200]

I.1 Click coupling between the prepared ligands and various cyclopeptoid scaffolds

I.1.1 Synthesis of the *O*-acetylated 2×1-valent glycomimetic

The smallest 2×1-valent inhibitor **184** (Scheme 24) related to this set of iminosugar-cyclopeptoid conjugates was synthesized. It is a divalent iminosugar with : i) the same type of ligand as the 4×1-valent series; ii) the same size of the scaffold as all the clusters described in this chapter (I.1 section). The reaction was performed by treating the platform **V** and ligand **153**, with $\text{CuSO}_4 \cdot 5\text{H}_2\text{O}$ (0.2 eq.) and NaAsc (0.4 eq.) under microwave irradiation at 80 °C for 1 h. Thanks to that, it's an easy-going reaction, and the crude mixture is relatively clean. The purification by flash chromatography was efficiently done and glycomimetic **184** was obtained in 64% yield.



Scheme 24 : Synthesis of the 2×1-valent glycomimetic **184**.

➤ Characterization of the *O*-acetylated 2×1-valent glycomimetic **184**

i. ¹H NMR spectra

Owing to the high symmetry of **184**, both the peripheral DNJ subunits and the alkyl chains are equivalent, which simplifies the ¹H NMR spectrum (Figure 49). The signals corresponding to the terminal iminosugars and the alkyl chain (H-1 to H-23 for **184**) are basically aligned with the ones of starting material **153**. Although of low intensity, the typical resonance arising from the protons (H-26 for **184**) of the 1,2,3-triazole ring can be quickly identified by their chemical shift, which is around 8.0-7.6 ppm. On the other hand, the typical resonance of H-28 for **184** could not be clearly observed due to its low intensity (representing less than 3% of the total protons) and similar shift as protons 18 and 15 (for **184**). Although the amount of H-30, H-31, and H-32 represents 5%-8% of the total protons, respectively, it is still hard to clearly attribute them due to their similar chemical shifts with other protons (for example, H-31 and H-32 have similar shifts than H-21 to H-23).

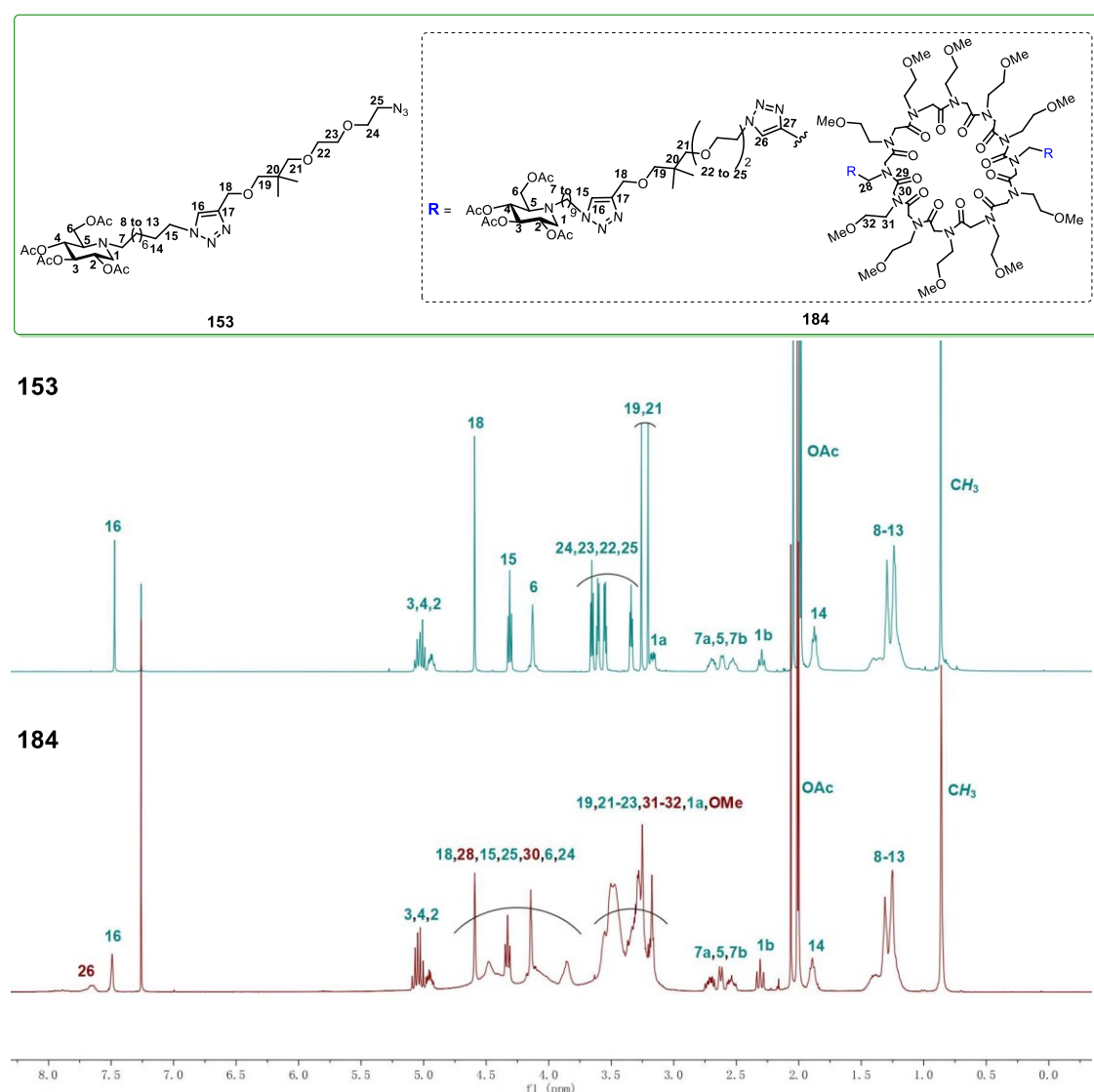


Figure 49 : ¹H NMR spectra of molecules **153** and **184** in CDCl₃.

ii. Infra-Red spectrum

In addition to NMR analyzes, the IR spectrum provides information as well (Figure 50). The absorption band at 1747 cm^{-1} indicates the acetate groups, and the signal at 1673 cm^{-1} corresponds to the amide function from the cyclopeptoid platform. The IR data also confirmed that no unreacted terminal alkyne functions (3300 cm^{-1}) remained in the final structure of **184**.

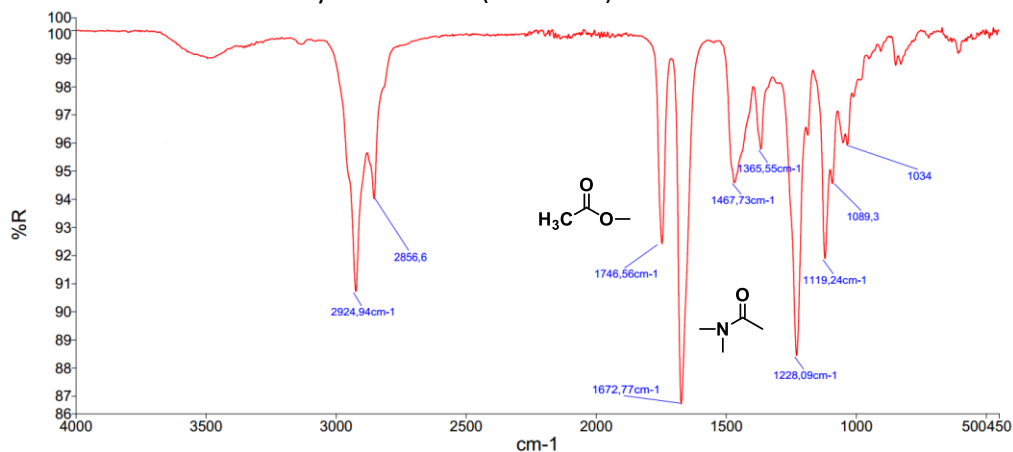


Figure 50 : Infra-red spectrum of **184**.

iii. Mass spectrum

The ESI mass spectrum (Figure 51) demonstrates the molecular ion peak at m/z 2886.5168 $[M + K]^+$, which is in adequacy with the calculated mass 2886.5252 for $C_{130}H_{218}KN_{26}O_{44}$. This data further demonstrates the effectiveness of the CuAAC reaction.

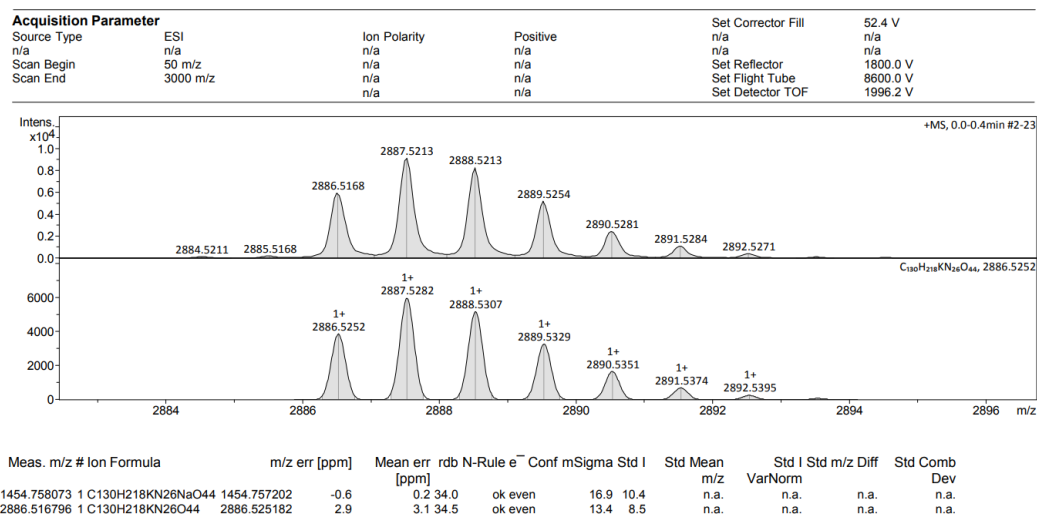


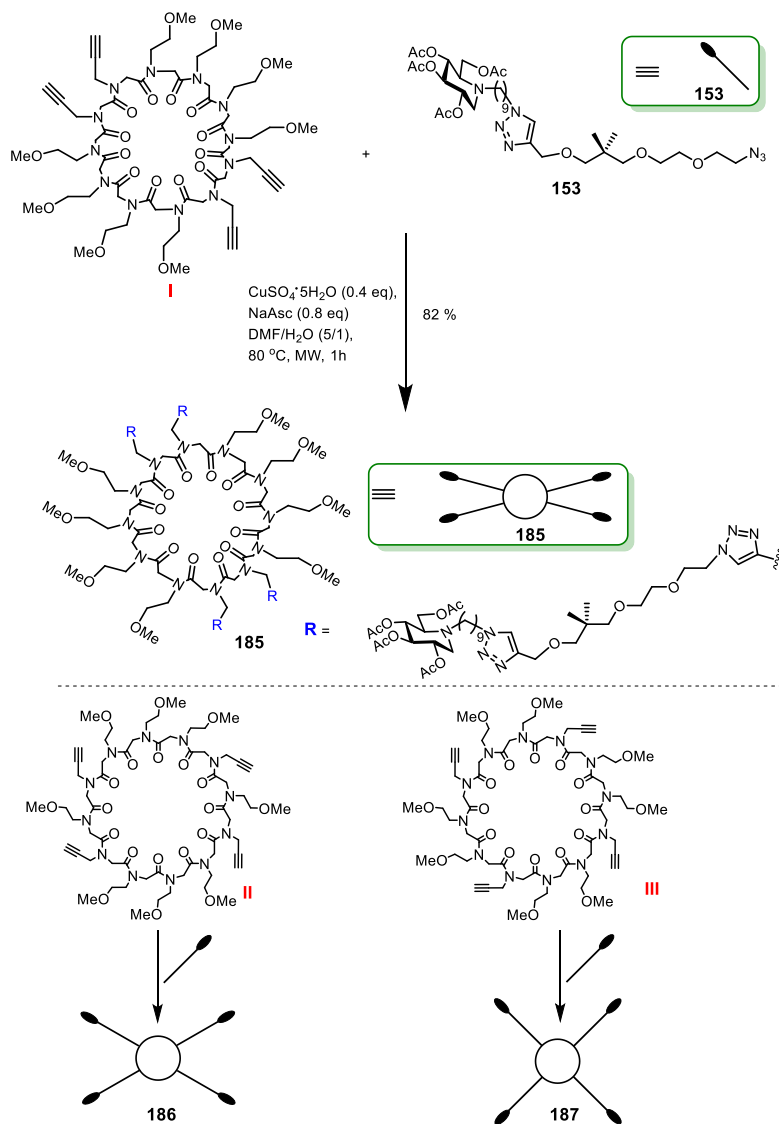
Figure 51 : Mass spectra (ESI) of **184**.

1.1.2 Synthesis of the *O*-acetylated 4×1 and 4×3-valent clusters

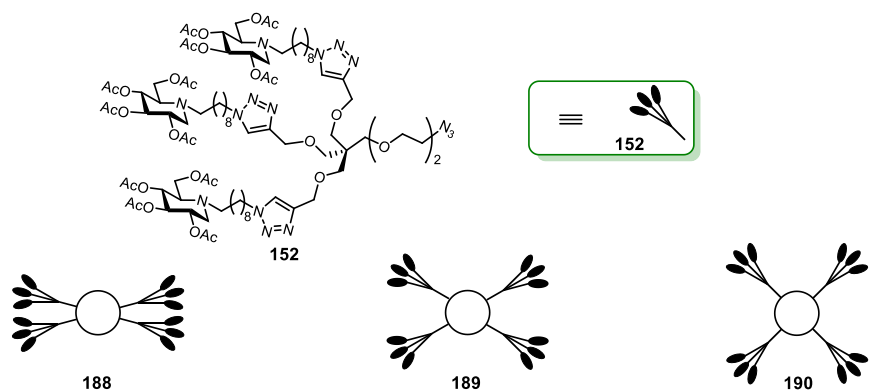
Scheme 25 exhibits the process to obtain *O*-acetylated 4×1 and 4×3-valent iminosugars. Chemical structures of both mono- and tripod ligands, the three types of scaffolds, and the six clusters are given together with their schematic representation to clarify their differences and use simplified drawings in the next paragraphs. Due to the two reasons that the amount of

final inhibitor for the inhibitory test is 10-15 mg, and the ligands and scaffolds are precious, each *O*-acetylated glycomimetic was prepared in a limit amount of around 60 mg.

a) 4×1-valent clusters



b) 4×3-valent clusters



Scheme 25: Synthesis of the *O*-acetylated clusters based on cyclopeptoid scaffolds: a) scheme for the synthesis of 4×1-valent clusters; b) 4×3-valent clusters

The specific reaction conditions and outcomes of that set of clusters shown in Scheme 25 are summarized in Table 17. The iminosugar clusters were obtained in 55% to 82% yields and no significant differences were observed between the CuAAC reactions performed with the mono- or trivalent clickable iminosugars except for scaffold III (72% versus 55%).

Product	Platform	CuSO ₄ ·5H ₂ O (eq.)	NaAsc (eq.)	DMF/H ₂ O (v/v)	T (°C)	t	Yield (%)	Valency
185	I	0.4	0.8	5/1	80	1h	82	4×1
186	II	0.4	0.8	5/1	80	1h	68	4×1
187	III	0.4	0.8	5/1	80	1h	72	4×1
188	I	0.4	0.8	5/1	80	50min	79	4×3
189	II	0.4	0.8	5/1	80	1h	63	4×3
190	III	0.4	0.8	5/1	80	1h	55	4×3

Table 17 : Conditions and results of the CuAAC for generating the desired clusters.

➤ **¹H NMR spectra for selected *O*-acetylated 4×1 and 4×3-valent clusters**

All the *O*-acetylated 4×1 and 4×3-valent clusters have symmetry elements, and their ¹H NMR spectra are in full agreement with their symmetrical structures. Figure 52 exhibits ¹H NMR spectra of selected 4×1 and 4×3-valent clusters **185**, **188** with the 2×1-valent glycomimetic **184** (Figure 49). The comparison reveals the chemical shifts of **185** and **188** are essentially the same as those of **184**, except for the absence of methyl signal in the proton NMR of **188** (there is no methyl group in **188** structure). The other clusters not shown here also have similar ¹H NMR spectra as **184**, and the integral values for all protons are consistent with the theoretical calculations.

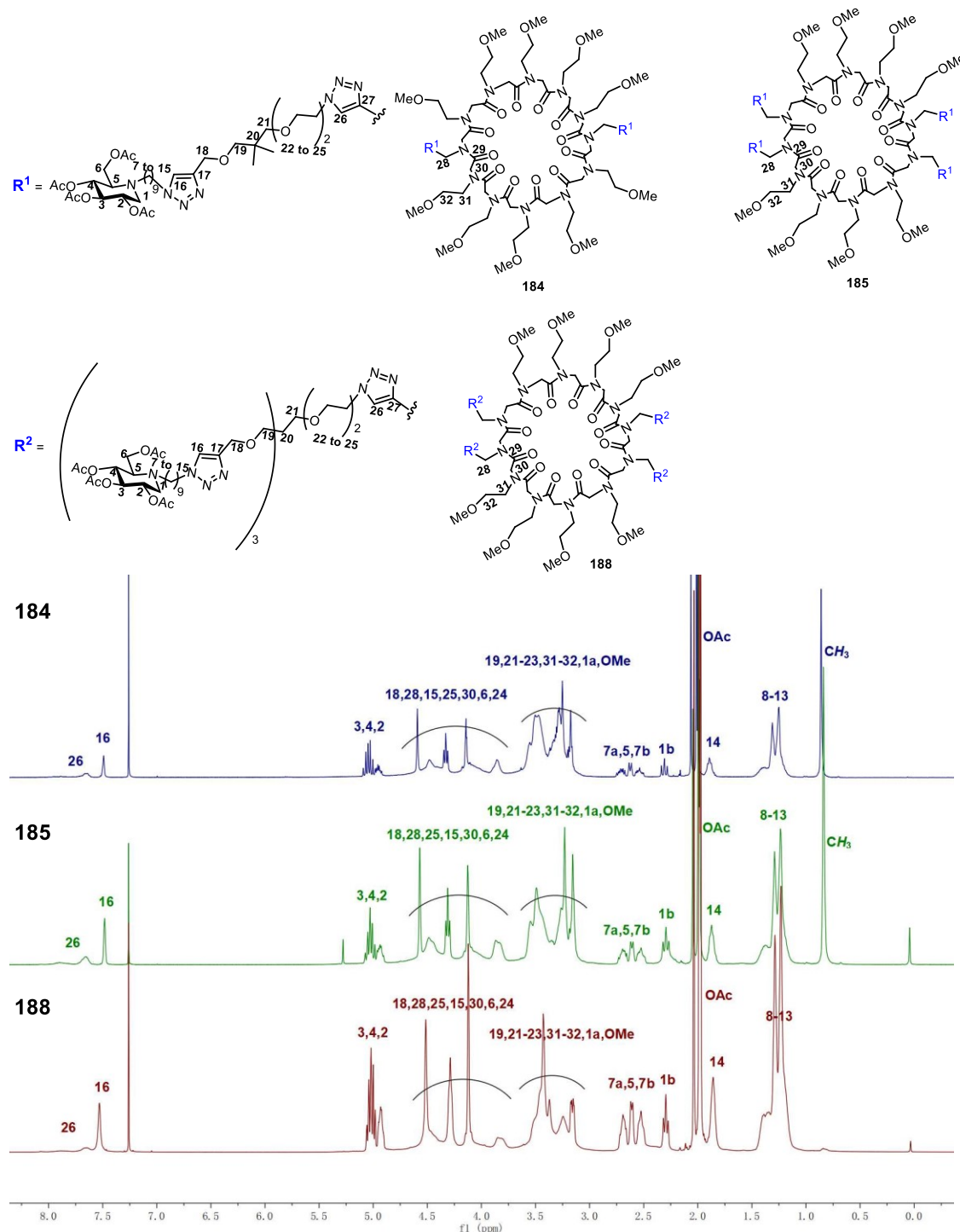
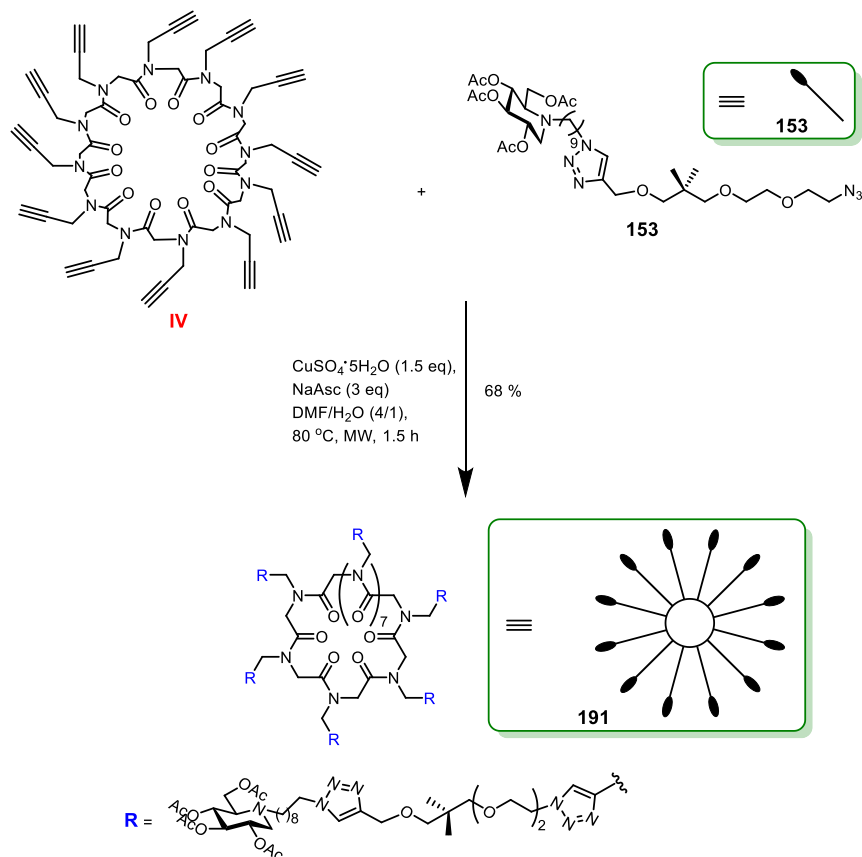


Figure 52 : ¹H NMR spectra of molecules 184, 185, and 188 in CDCl₃.

I.1.3 Synthesis of the *O*-acetylated 12×1-valent cluster

The CuAAC reaction of scaffold **IV** with the clickable ligand **153** was performed by my colleague Dr. N. Kern. The mixture was heated at 80 °C assisted with microwave irradiation for 1.5 h. After that, it was quenched and purified to afford the desired compound **191** in 68% yield (Scheme 26).



Scheme 26 : Synthesis of the *O*-acetylated 12×1-valent cluster.

➤ **^1H NMR spectra of **153** and **191****

This 12×1-valent cluster **191** has a highly symmetrical structure, the symmetry of which belongs to the C_{12} group. Therefore, all its peripheral DNJ subunits and the arms are equivalent, allowing rapid identification of its structure. The chemical shifts corresponding to the protons of the DNJ part and the alkyl chain (H-1 to H-24 for **191**) remain essentially unchanged compared to **153** (Figure 53). The typical resonances (around 8.2-7.6 ppm) arising from the protons (H-26 for **191**) of the 1,2,3-triazole ring formed by grafting the ligands onto the 12-valent scaffold are observed, which shows the success of the CuAAC reaction. Moreover, the integral values for total protons are consistent with the calculated ones.

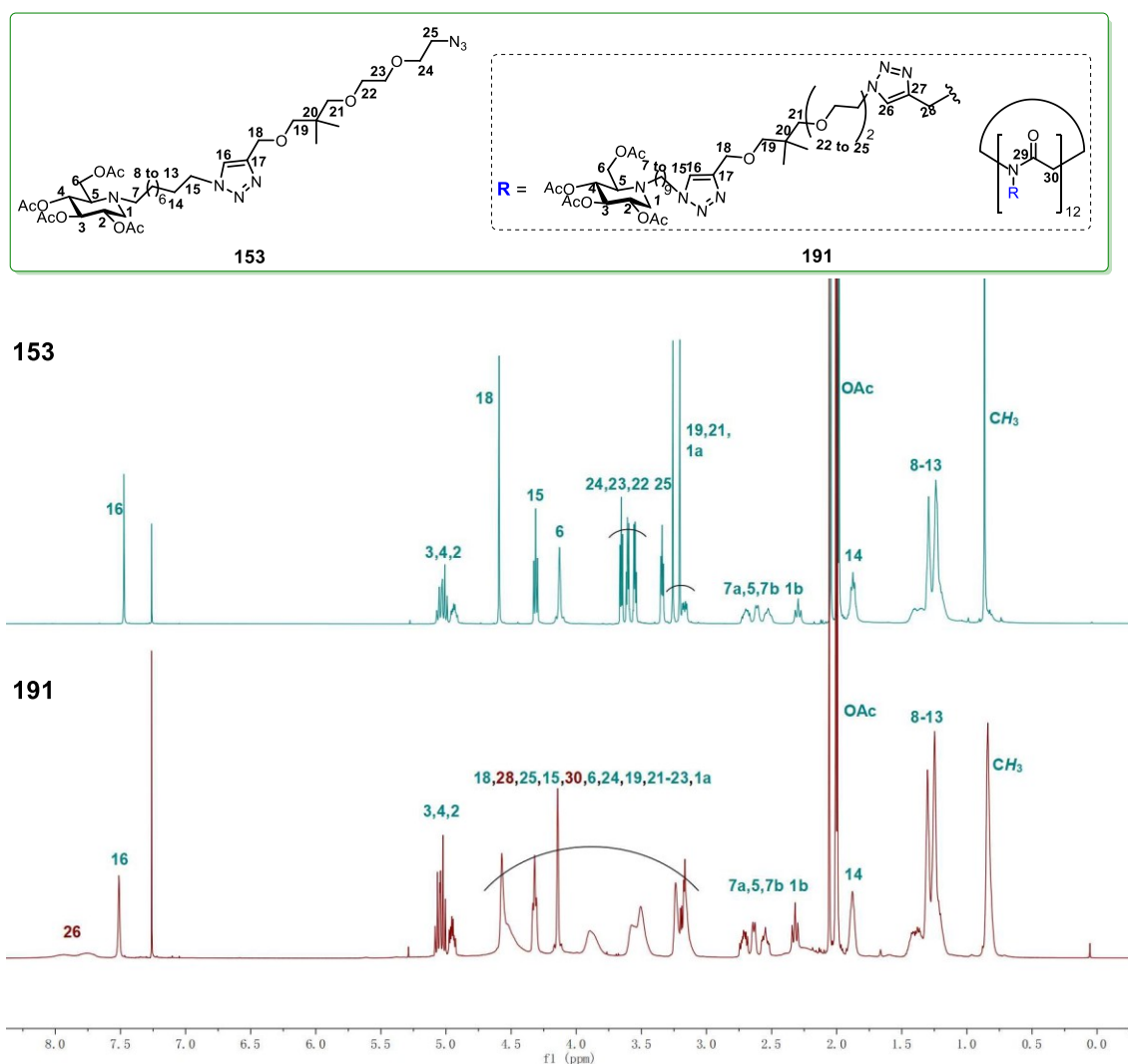
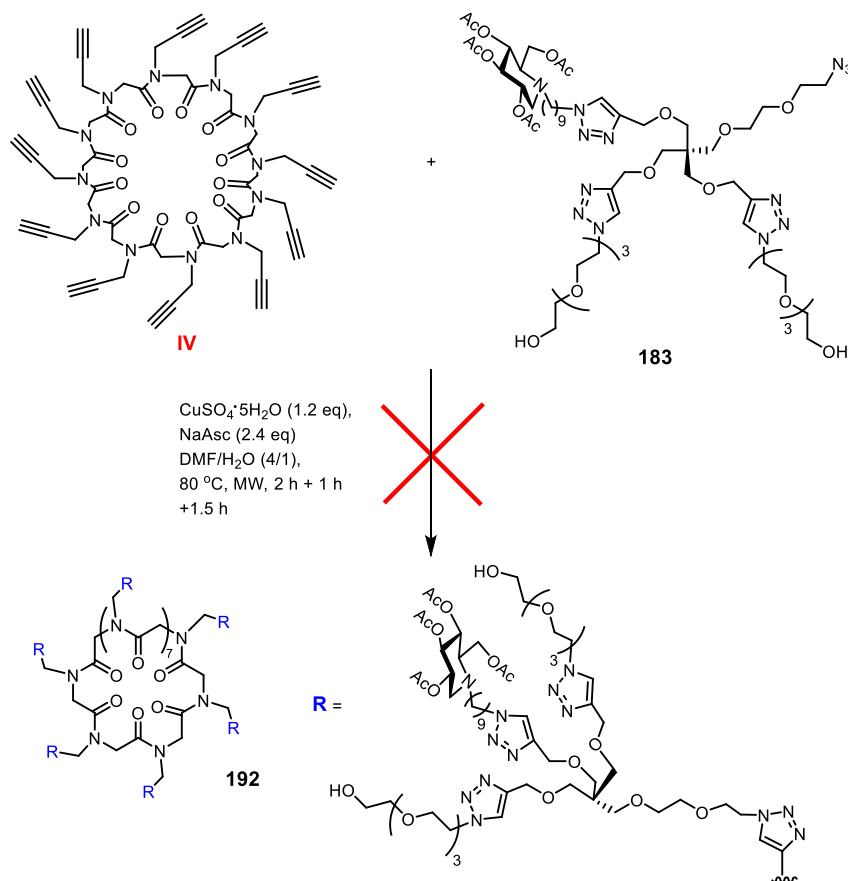


Figure 53 : ^1H NMR spectra of molecules 153, 191 in CDCl_3 .

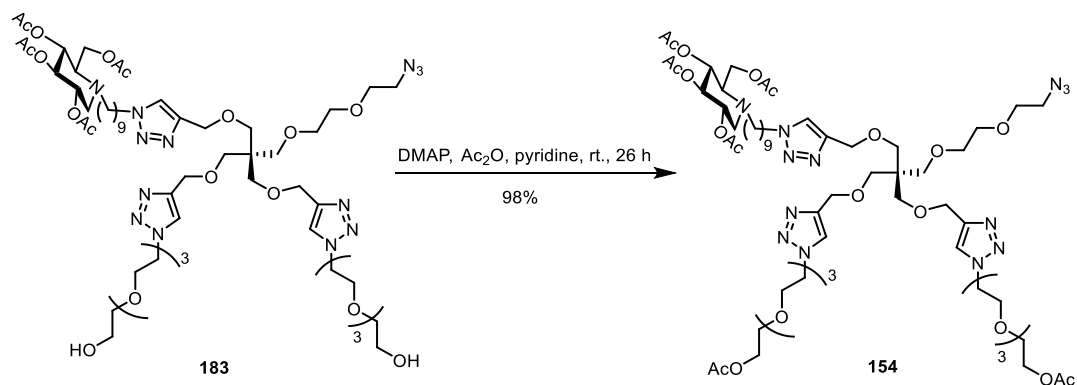
I.1.4 Synthesis of the *O*-acetylated “hindered” 12×1-valent cluster

To obtain the “hindered” 12×1-valent glycomimetic, the clickable monovalent ligand **183** was attempted to be grafted onto scaffold **IV** via CuAAC reaction (Scheme 27). The construction was performed by treating platform **IV** with ligand **183** in the presence of the catalyst combination of $\text{CuSO}_4 \cdot 5\text{H}_2\text{O}$ (1.2 eq.) + NaAsc (2.4 eq.) (the amount of $\text{CuSO}_4 \cdot 5\text{H}_2\text{O}$ is 0.1 eq./alkyne moiety and NaAsc equals 0.2 eq./alkyne moiety). There still remained substantial ligand as shown by TLC in the mixture after heating under microwave irradiation at 80 °C for 2 h. Therefore, the duration time was prolonged two times (1 h and 1.5 h), in order to maximize the conversion of starting materials into the target compound. The reaction solution was eventually quenched and then purified by flash chromatography to give a set of individual compounds, including ligand and some partially clicked intermediates. Unfortunately, no desired cluster **192** was observed by NMR, Electrospray Ionization Mass Spectrometry (ESI-MS) or Matrix-Assisted Laser Desorption Ionization (MALDI). It was presumed that the water-soluble azido arm is surrounded by the two hydrophilic arms (with free OH groups), which would prevent the effective collision of the azido groups with the terminal alkynes on scaffold **IV**.



Scheme 27 : CuAAC reaction of the “hindered” mono-valent ligand with scaffold IV.

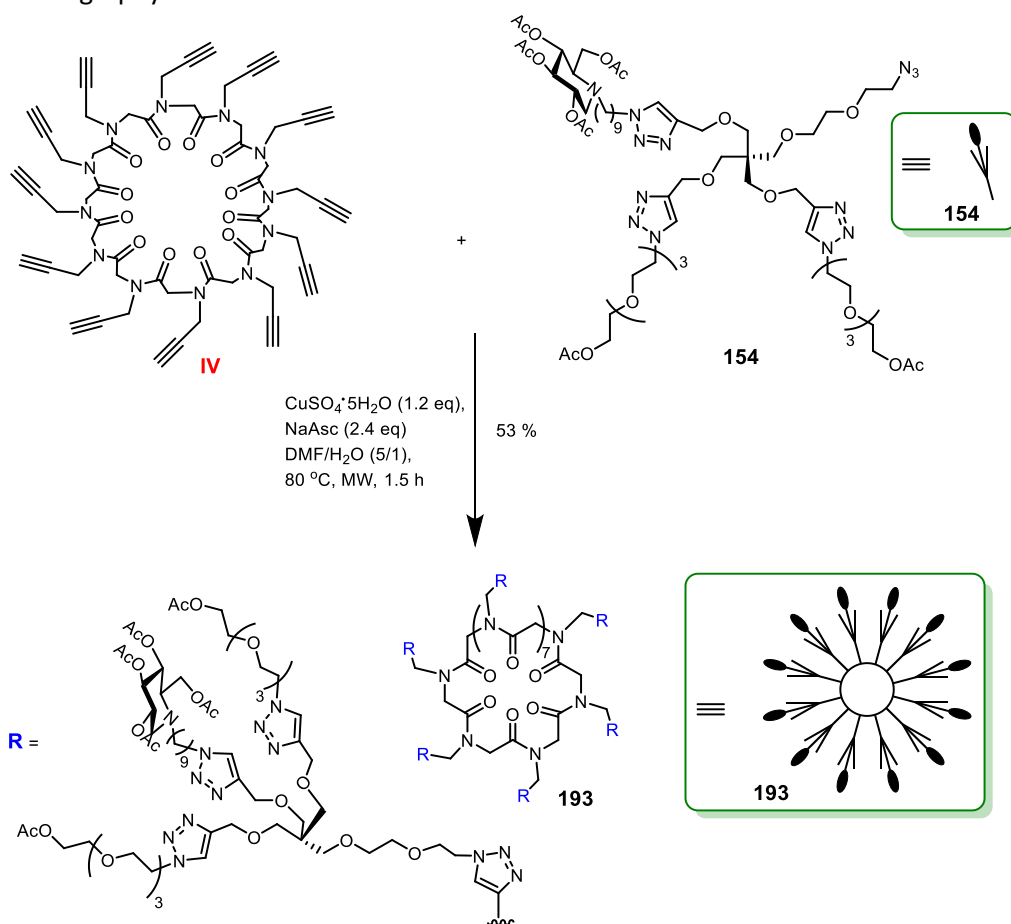
Inspired by previous work where the OH group on sugar unit is protected with acetyl groups, the ligand **183** underwent the same strategy of *O*-acetylation (see Scheme 28). Firstly, **183** and 0.26 eq. of DMAP were dissolved in pyridine, then an excess amount of Ac_2O was added dropwise to the mixture. For this reaction, the solvent pyridine also acted as a base. The reaction mixture was kept stirring at room temperature to afford the *O*-protected ligand **154** in an excellent yield of 98%.



Scheme 28 : *O*-acetylation of **183** to afford **154**.

Compound **154** was then grafted onto the 12-valent platform **IV** via CuAAC reaction (Scheme 29). The reaction mixture was heated under microwave irradiation at $80\text{ }^\circ\text{C}$ and then was

tracked by TLC. It showed two spots on TLC, among which there was the excess of ligand **154**; the other one below was new-formed during the reaction. The target iminosugar-cyclopeptoid conjugate **193** was obtained in a moderate yield of 53% after purification by flash chromatography.



Scheme 29 : Synthesis of the *O*-acetylated neo-cluster **193**.

➤ Characterization of the *O*-acetylated “hindered” 12×1-valent cluster

i. ^1H NMR spectra

The “hindered” 12×1-valent cluster **193** also has a symmetrical structure (belongs to the C_{12} group of symmetry), and as a result, all the “hindered” monovalent-ligand dendrons are equivalent. The typical resonances of the monovalent-ligand dendron are not affected after grafting onto the central core (Figure 54). Due to their low intensity resulting from dilution among the immense size of peripheral dendrons, the signals for H-26, H-28 and H-30 are under the baseline between 8.4-7.7 ppm (H-26) and 4.5-3.4 ppm (H-28 and H-30) and could not be clearly observed. Importantly, the integral value of the total protons matches the calculated one, indicating also the effectiveness of the click reaction.

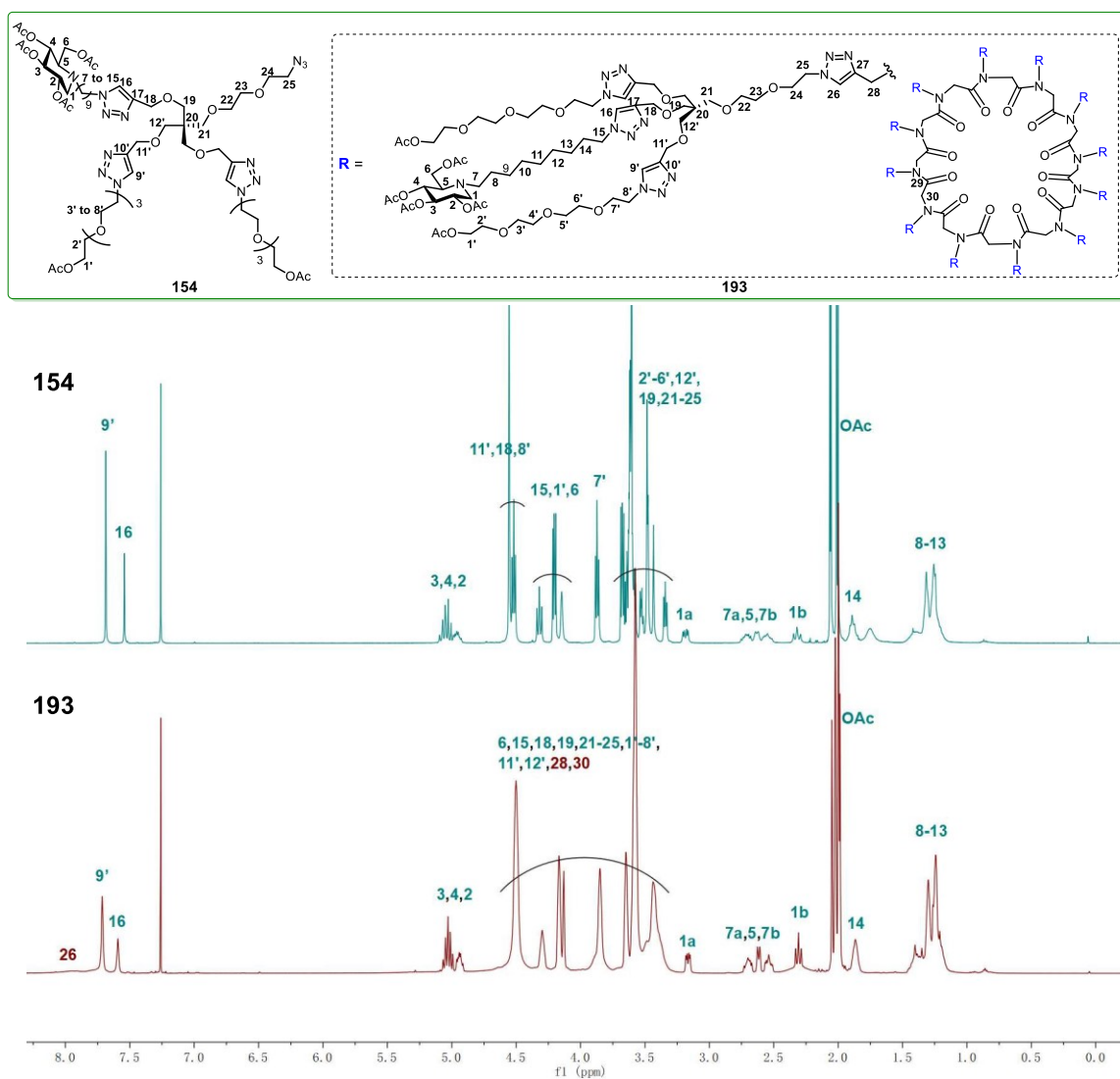


Figure 54 : ^1H NMR spectra of molecules **154**, **193** in CDCl_3 .

ii. Infra-Red spectrum

The CuAAC reaction between “hindered” monovalent-ligand dendron **154** and the 12-valent platform **IV** may result in a mixture of partially clicked products, however, it was not the case as, no alkyne functions (3300 cm^{-1}) were detected by IR (Figure 55) on the purified product. The typical absorption bands at 1741 cm^{-1} and 1673 cm^{-1} corresponding to the acetate and amide function, respectively, were clearly seen in the IR spectrum.

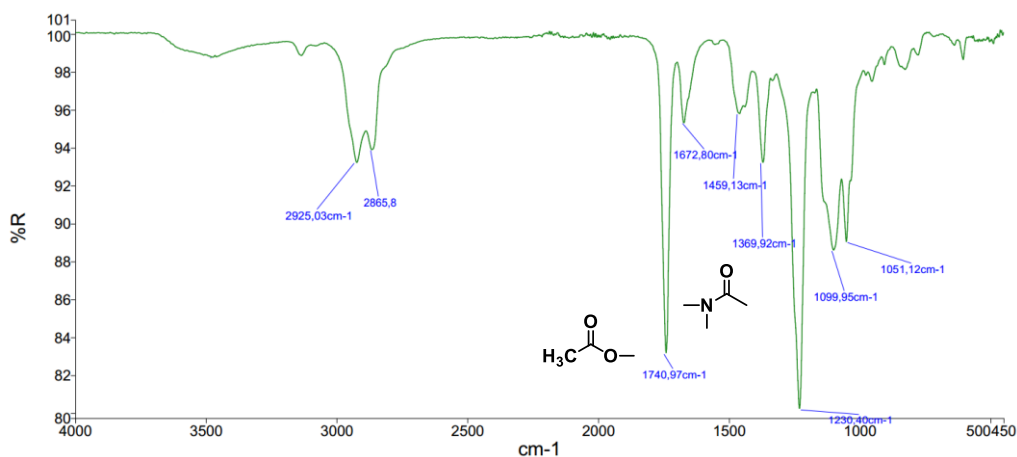


Figure 55 : Infra-red spectrum of 193.

iii. Mass spectra

The ESI mass spectrum further proved the success of the clicking of the 12-valent platform **IV** with the twelve “hindered” monovalent-ligand dendrons. Figure 56 collected signals corresponding to different states of charge are in adequacy with the calculated values.

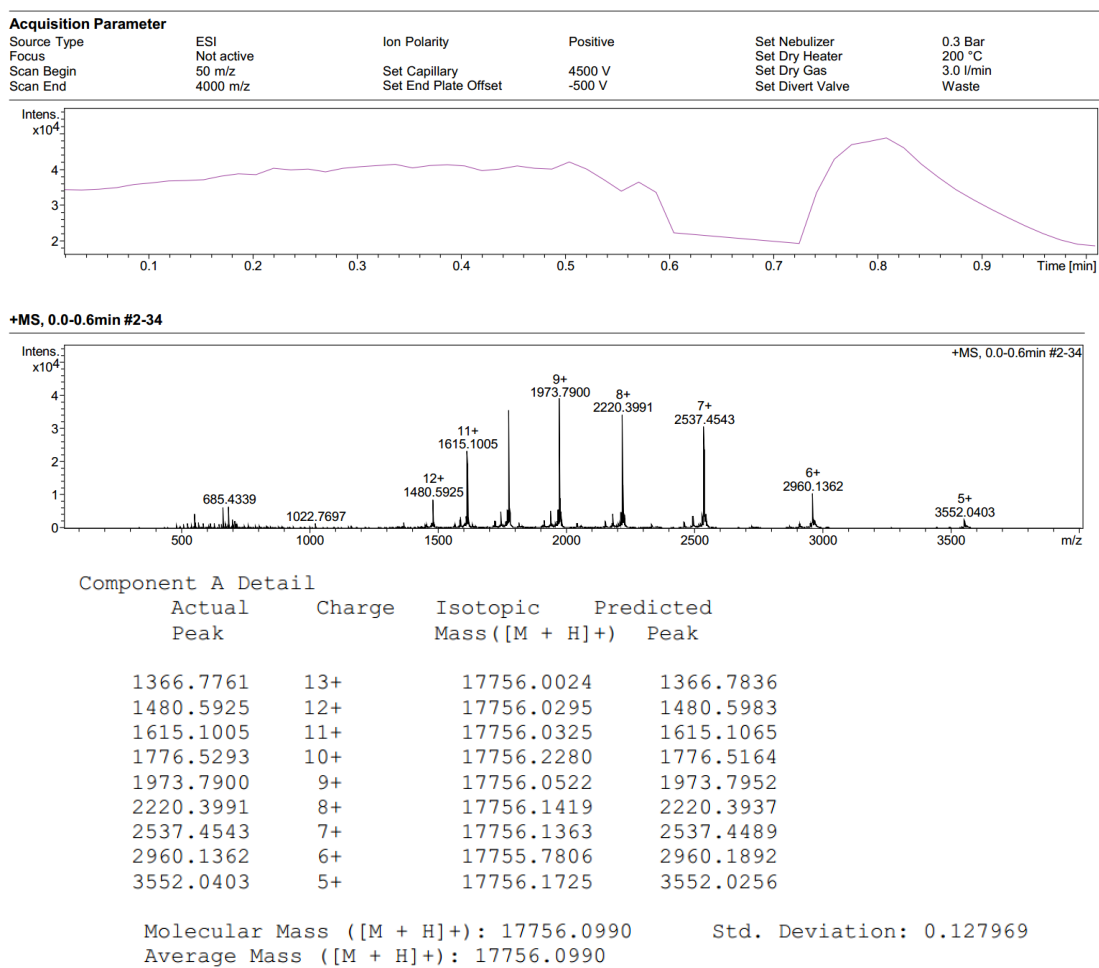
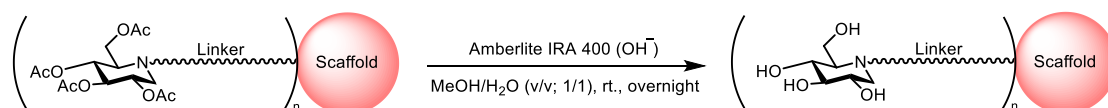


Figure 56 : Mass spectrum (ESI) of 193 corresponding to different states of charge.

I.2 Deprotection of acetyl groups on the clusters

The acetyl protecting groups on the clusters were removed by using IRA 400 (OH⁻) resin, which affords the polyhydroxylated compounds in quantitative yields (see Scheme 30 and Table 18) in mild conditions. At the end of the deprotection, it only entails filtration of the resin and rinsing with 20 mL MeOH/H₂O (1/1). The multivalent clusters at this stage have the required purity to do the following biological tests.



Scheme 30 : *O*-deacetylation of different clusters.

OAc cluster	Valency	Scaffold	Ligand	OH cluster	Yields
184	2×1	V	153	194	in quant.
185	4×1	I	153	195	in quant.
186	4×1	II	153	196	92%
187	4×1	III	153	197	in quant.
188	4×3	I	152	198	in quant.
189	4×3	II	152	199	in quant.
190	4×3	III	152	200	90%
191	12×1	IV	153	201	in quant.
193	12×1	IV	154	202	in quant.

Table 18 : Summary of the numbers of clusters and corresponding *O*-deacetylated compounds.

Taking the deprotection of 2-valent **184** (the simplest cluster) and “hindered” 12×1-valent **193** (the most complicated cluster) as examples, Figure 57 shows the proton NMR spectra of the *O*-acetylated (top) and *O*-deacetylated (bottom) 2-valent clusters. Similarly, Figure 58 displays the proton NMR spectra of the *O*-acetylated (top) and *O*-deacetylated (bottom) “hindered” 12×1-valent clusters **193** and **202**. The signals of acetyl protons at around 2.0 ppm all disappear after treating **184** and **193** with IRA 400 (OH⁻) resin in mild conditions. Moreover, as can be seen from the ¹H NMR spectra, the *O*-deacetylation is clean and no further purification is needed.

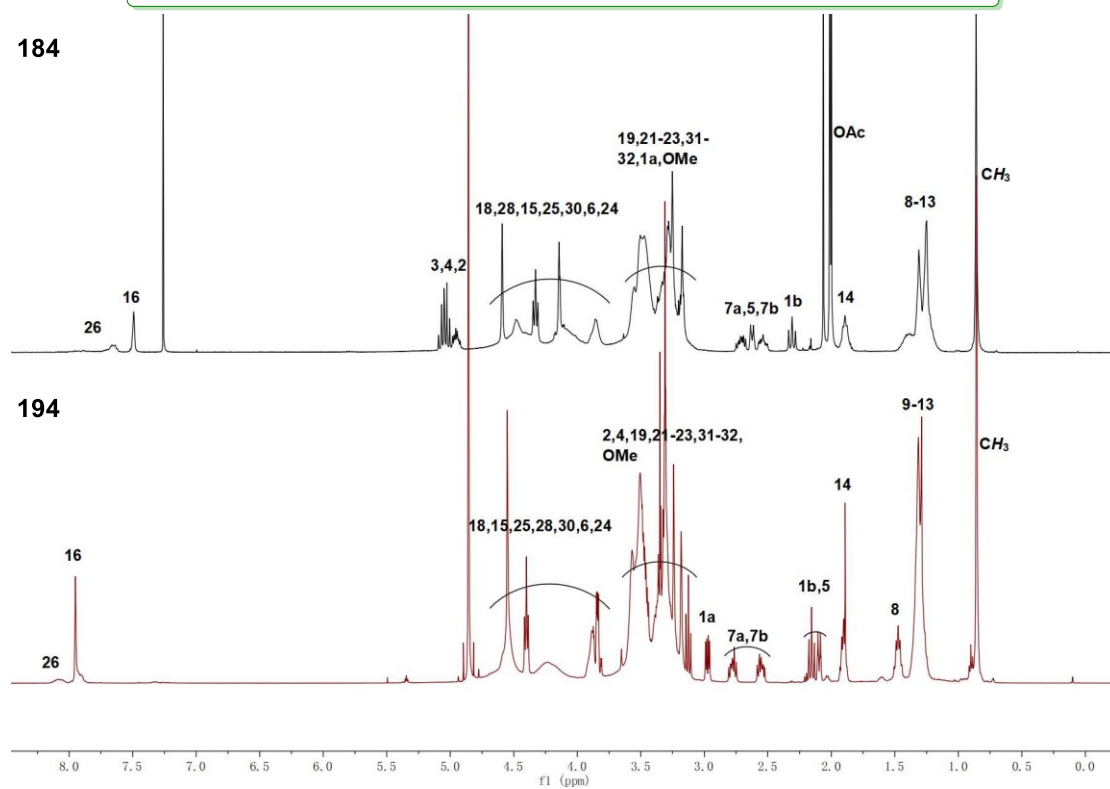
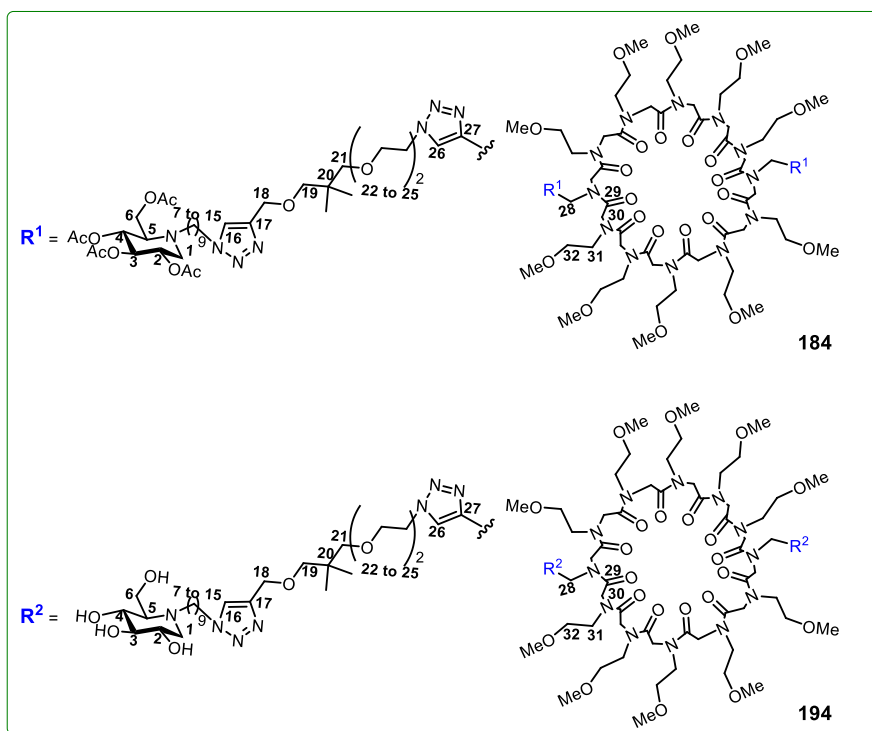


Figure 57 : ^1H NMR spectra of molecules 184 (in CDCl_3) and 194 (in MeOD).

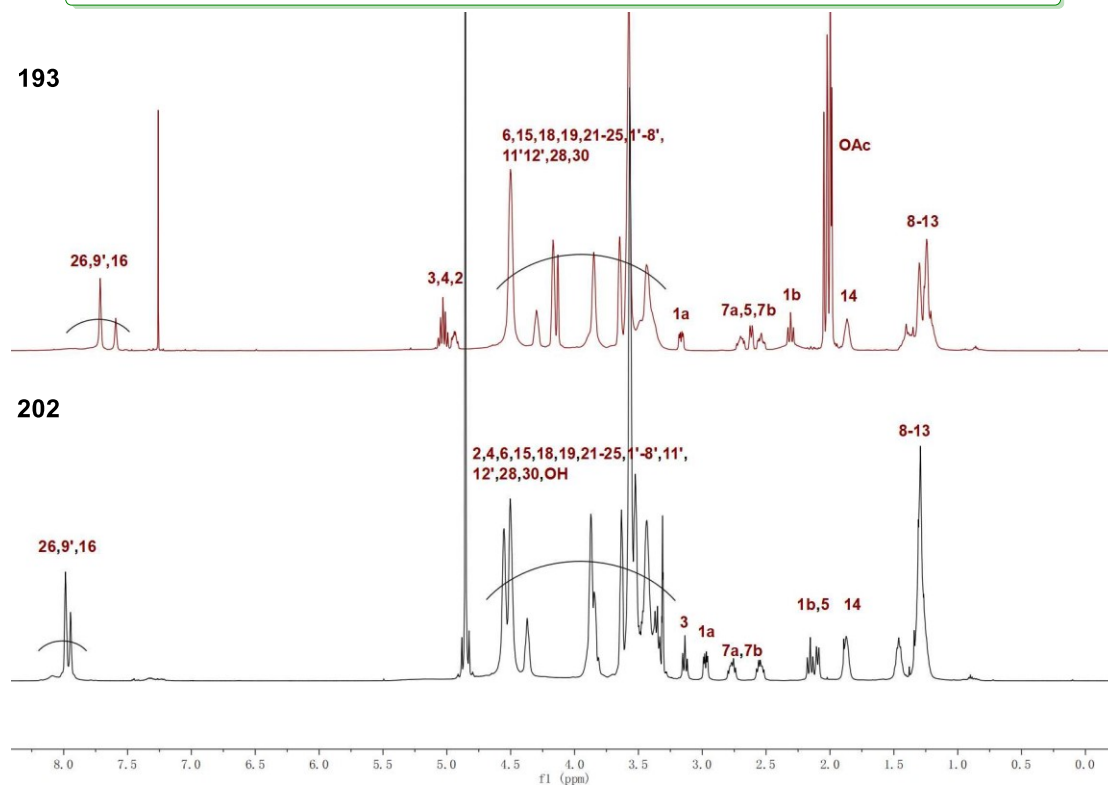
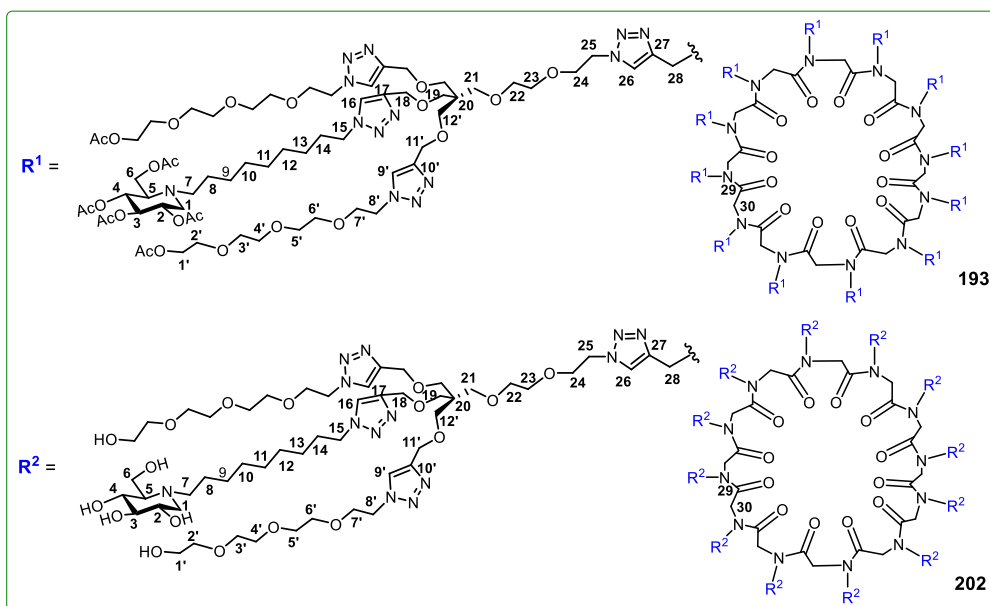
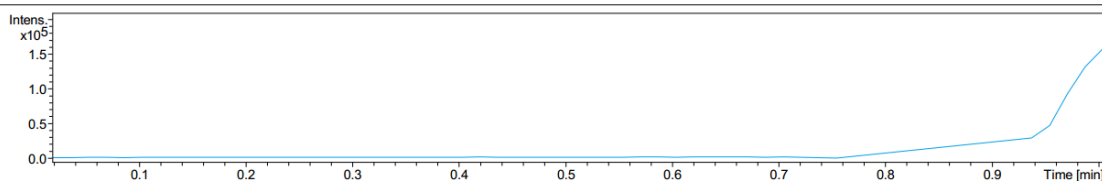


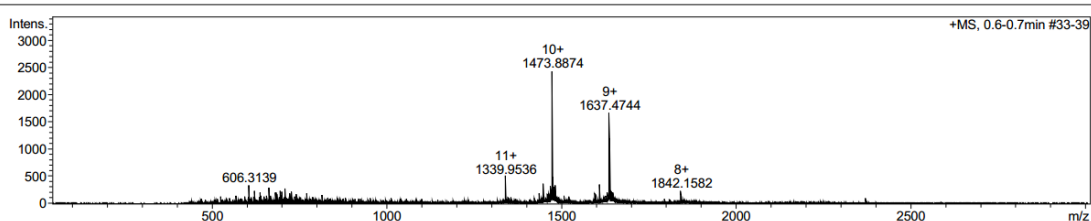
Figure 58 : ¹H NMR spectra of molecules **193** (in CDCl₃) and **202** (in MeOD).

The mass spectrum (ESI) (Figure 59, below) further confirmed the structure of **202** (deprotection of **193**) with signals corresponding to different states of charge. The deprotection of **193** confirms the applicability of this *O*-deacetylation strategy (Scheme 30).

Acquisition Parameter					
Source Type	ESI	Ion Polarity	Positive	Set Nebulizer	0.3 Bar
Focus	Not active	Set Capillary	4500 V	Set Dry Heater	200 °C
Scan Begin	50 m/z	Set End Plate Offset	-500 V	Set Dry Gas	3.0 l/min
Scan End	3000 m/z			Set Divert Valve	Waste



+MS, 0.6-0.7min #33-39



Component	Molecular Mass	Molecule	Absolute Abundance	Relative Abundance
A	14729.5835	14729.5835	[M + H] ⁺	4831 100.00

Compound Mass Spectrum Deconvolution Report

Component A Detail

Actual Peak	Charge	Isotopic Mass ([M + H] ⁺)	Predicted Peak
1339.9536	11+	14729.4165	1339.9688
1473.8874	10+	14729.8085	1473.8649
1637.4744	9+	14729.2113	1637.5157
1842.1582	8+	14730.2149	1842.2047

Molecular Mass ([M + H]⁺): 14729.5835 Std. Deviation: 0.298063
Average Mass ([M + H]⁺): 14729.5835

Figure 59 : Mass spectrum (ESI) of 202 (from 193 deacetylation).

II. Biological evaluation

The inhibition constants (K_i) of the synthesized iminosugar clusters were determined against the commercially available JB α -man. Two significant parts compose this chapter. Firstly, some basic concepts concerning enzyme kinetics will be presented, which lay bioassay's theoretical foundation. As there are plenty of symbols mentioned in this section, Table 19 (see below) summarizes the standardized notation throughout this thesis. In the second part, I will give the results from the biological tests I performed myself.

Symbols	Definitions
E	enzyme
S	substrate
P	product
I	inhibitor
[E]	free enzyme concentration in the equilibrium
[E₀]	total enzyme concentration
[S]	free substrate concentration in the equilibrium
[I]	free inhibitor concentration in the equilibrium
k_{cat}	rate constant for ES → E + P
K_m	Michaelis Menten constant
K_m^{app}	the apparent Michaelis Menten constant
K_i	inhibition constant
V_{max}	maximal velocity
V_{max}^{app}	the apparent maximal velocity
IC₅₀	half maximal inhibitory concentration

Table 19 : Symbols and definitions related to enzyme kinetics in this section.

II.1 Basics of enzyme kinetics

II.1.1 Michaelis-Menten equation^[201]

An enzyme (E) accelerates the conversion of a substrate (S) to product (P) swiftly and specifically. The kinetic study of this reaction relies on an assay where we measure how fast a given amount of substrate is consumed or the product is formed, i. e., the measurement of reaction velocity. Thus, the test requires that the changes of concentration of a substrate or a product could be followed by spectral changes (using UV or visible absorption spectroscopy or fluorimetry). As for chemical reactions, for an enzymatic reaction, we measure the initial velocity because it is constant. The initial velocity is the beginning rate measured under the condition that the substrate concentration does not fall visibly (less than 20% conversion is needed). Along with the substrate consuming, or product concentration increasing, the plot of product against time becomes curved (Figure 60). It is, therefore, essential to measure the velocity before the noticeable substrate depletion.

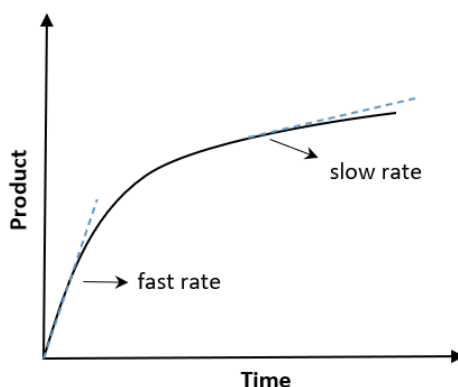
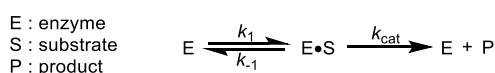


Figure 60 : The general trends of an enzymatic reaction.

In our case, the simple mechanism of the well-studied enzyme-catalyzed reaction $S \rightarrow P$ is used. It is a reaction that converts a single substrate into a single product. The route for this reaction proceeds through i) the formation of the $[E \cdot S]$ complex by binding the substrate with the enzyme at the active site; ii) the conversion of the $[E \cdot S]$ complex to the single product along with releasing the enzyme catalyst (Scheme 31). The little k_1 , k_{-1} and k_{cat} are rate constants. Michaelis and Menten expressed the reaction speed in the form of Equation 1, which is derived from a steady-state assumption that the rate of $[E \cdot S]$ formation equals the speed of its decomposition.



Scheme 31 : General mechanism of the enzyme-catalyzed single substrate to single product reaction.

Equation 1 : Equation of Michaelis-Menten.

$$V = \frac{V_{max}[S]}{K_m + [S]} = k_{cat}[E \cdot S] \quad K_m = \frac{k_{-1} + k_{cat}}{k_1}$$

The Michaelis-Menten equation also reflects the relationship of the initial velocity with the corresponding substrate concentration (Figure 61). When the substrate concentration $[S]$ is equal to zero ($[S]=0$), from the Equation 1, there is no initial velocity. As the initial $[S]$ is increased (but not at very high concentration, i. e., $[S] \ll K_m$), the more and more free enzyme is bound with the substrate in the formation of the enzyme-substrate $[E \cdot S]$ complex, which promotes the reaction velocity to increase linearly. When $[S]=K_m$, then $V=1/2 V_{max}$. The term K_m could be defined as the substrate concentration required to produce a rate of one-half of V_{max} . It also equals the sums of rate constants (k_{-1} , and k_{cat}) divided by k_1 . The smaller the K_m is, the stronger the enzyme interacts with the substrate. Keeping increasing the initial $[S]$ to a point where all the enzyme is occupied with or saturated by the substrate, and you would find that the reaction velocity no longer goes higher and approaches V_{max} . At this point, $[S] \gg K_m$.

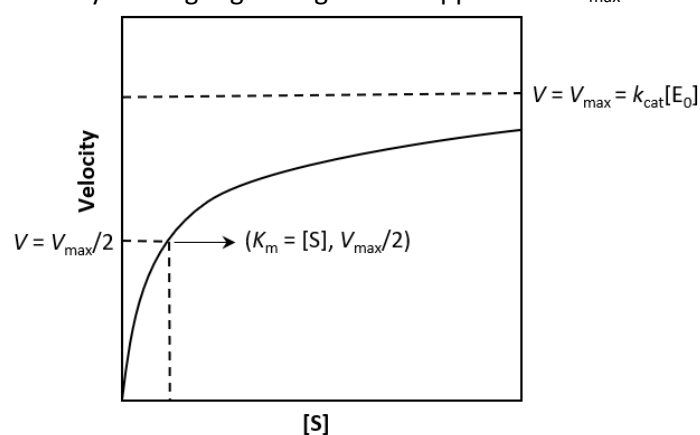


Figure 61 : The effect of initial substrate concentration on the initial velocity of an enzymatic reaction. When a) $[S] \ll K_m$, $V = V_{max}[S]/K_m$; b) $[S] \gg K_m$, $V = V_{max}$; c) $[S] = K_m$, $V = V_{max}/2$.

The two critical parameters of the enzyme K_m and V_{max} can be measured by graphical methods. Lineweaver-Burk graph ($1/V$ is the y-axis, $1/[S]$ is the x-axis), Eadie-Hofstee graph (V is the y-axis, $V/[S]$ is the x-axis), and Hanes-Wolf graph ($[S]/V$ is the y-axis, $[S]$ is the x-axis) are all

plotted to transform of the Michaelis-Menten equation into linear plots. Each one of these plots provides a straight line which intersects with x, y-axis. The Lineweaver-Burk plot is shown in Figure 62. The x-intercept gives the value of $-1/K_m$, which has the same units as $1/[S]$. Similarly, the V_{max} could be calculated from the y-intercept of the Lineweaver-Burk plot.

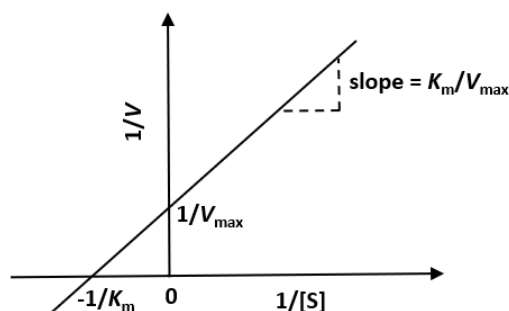


Figure 62 : Graph of Lineweaver-Burk.

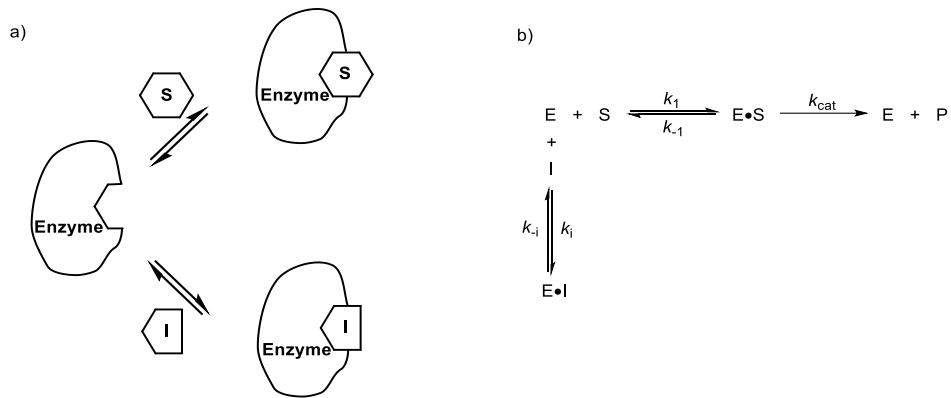
II.1.2 The different inhibition modes and their kinetics

Enzymes could become deactivated or denatured by elevated temperature, treatment with chemical reagents, or other means. Alternatively, their activities could be decreased or inhibited (without being denatured) in a reversible or an irreversible way by interacting with inhibitors, natural or synthetic. An irreversible inhibitor causes irreversible intervention *via* the formation of a covalent bond between the enzyme and the inhibitor. The enzyme's activity could not be restored by dialysis or other simple methods. In contrast, the inhibitory behavior through non-covalent bonds to form the enzyme-inhibitor complex is defined as reversible inhibition, which is not stable and could be recovered.

The series of multivalent inhibitors presented in chapter three all interact reversibly with the enzyme JB α -man by electrostatic interactions, formation of hydrogen bonds and chelation of the zinc ion in the active site^[104] as other clusters based on the reversible competitive DNJ inhibitor. Looking further into reversible inhibition, it can be classified into three types : competitive inhibition, non-competitive inhibition, and uncompetitive inhibition. Their respective particularities will be described in the following text.

- **Competitive inhibition**

An inhibitor competitively binds to the enzyme and hampers the binding of the substrate with the enzyme's active site (Scheme 32). The competitive inhibitor usually has structural similarity with the substrate but is not modified in the enzyme-catalyzed reaction.



Scheme 32 : a) Competitive inhibition (S: Substrate, I: Enzyme); b) Equations for competitive inhibition

In presence of an inhibitor that affects the enzymatic reaction velocity, a new parameter, the inhibition constant K_i (Equation 2), is needed to describe the dissociation equilibrium of the $[E \cdot I]$ complex. The smaller the K_i , the more tightly an inhibitor binds to an enzyme.

Equation 2 : Definition of inhibition constant K_i .

$$K_i = \frac{[E][I]}{[E \cdot I]}$$

For the equilibrium shown in Scheme 32b, the total concentration of enzyme $[E_0]$ could be expressed as :

$$[E_0] = [E] + [E \cdot S] + [E \cdot I],$$

and according to the steady-state approximation :

$$K_m = \frac{k_{-1} + k_{cat}}{k_1} = \frac{[E][S]}{[E \cdot S]},$$

velocity formula of an enzymatic reaction with the addition of the competitive inhibitor can be derived (see Equation 3).

Equation 3 : Expression of the initial velocity of an enzymatic reaction in the presence of the competitive inhibitor.

$$V = \frac{V_{max}[S]}{[S] + K_m \left(1 + \frac{[I]}{K_i}\right)}$$

From the expression of Equation 3, it is apparent that K_m is increased by a factor of $(1 + [I]/K_i)$, and the V_{max} is not affected by the existence of the competitive inhibitor. Furthermore, Equation 3 can be simplified to Equation 1 when the inhibitor concentration is 0. Figure 63 exhibits the Michaelis-Menten competitive inhibition graph.

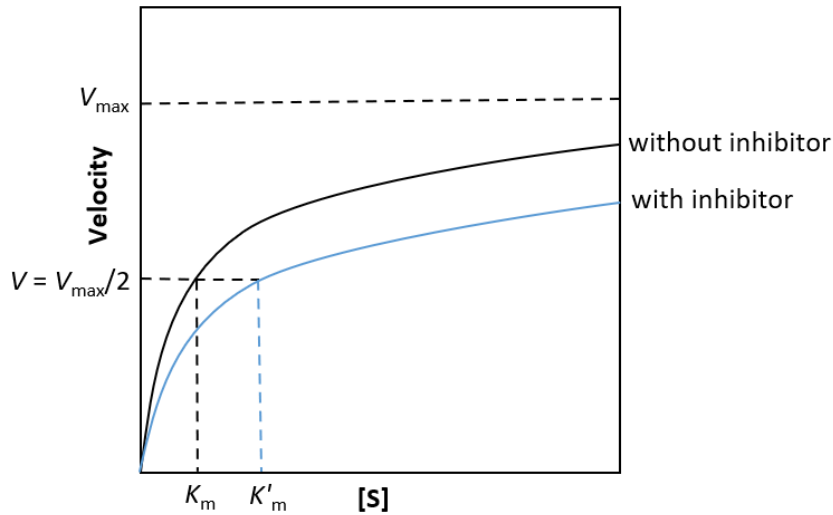


Figure 63 : Graph of Michaelis-Menten competitive inhibition.

Taking the reciprocal of Equation 3, the Lineweaver-Burk plotting (double reciprocal of $1/V$ vs. $1/[S]$) transforms Equation 3 into Equation 4, and plotting Equation 4 can give a straight line. Figure 64 represents different straight lines at different inhibitor concentration. We can highlight two hallmarks of competitive inhibition from Figure 64: i) the addition of inhibitor will not affect the value of V_{max} which could be calculated from the intercept on the y-axis (the inhibitory effect is prevented by a high concentration of substrate); ii) the inhibitor only affects the slope of the line - the more amount of inhibitor, the bigger the slope -, which is called the slope effect.

Equation 4 : Lineweaver-Burk transform for competitive inhibition pattern.

$$\frac{1}{V} = \frac{K_m(1 + \frac{[I]}{K_i})}{V_{max}[S]} + \frac{1}{V_{max}}$$

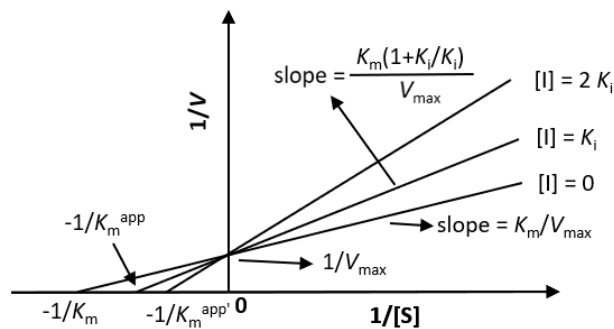


Figure 64 : Lineweaver-Burk competitive inhibition graph.

After having verified the competitive inhibition pattern, the next step is the determination of K_i value. Lineweaver-Burk or Dixon are the two notable graphic methods which are generally used.

The Lineweaver-Burk graph does not give the inhibition constant directly (Figure 64), but provides the value of K_m^{app} from its slope (Equation 5). Nevertheless, we can obtain the K_i

based on plotting a secondary graph involving the slope of the Lineweaver-Burk graph *versus* the different inhibitor concentration (Figure 65). The x-intercept gives the value of $-K_i$ in Figure 65.

Equation 5 : Slope of the graph Lineweaver-Burk.

$$\text{Slope}_{\text{LB}} = \frac{K_m^{\text{app}}}{V_{\text{max}}} = \frac{K_m(1 + \frac{[I]}{K_i})}{V_{\text{max}}} = \frac{K_m}{V_{\text{max}}K_i} [I] + \frac{K_m}{V_{\text{max}}}$$

$$K_m^{\text{app}} = K_m(1 + \frac{[I]}{K_i})$$

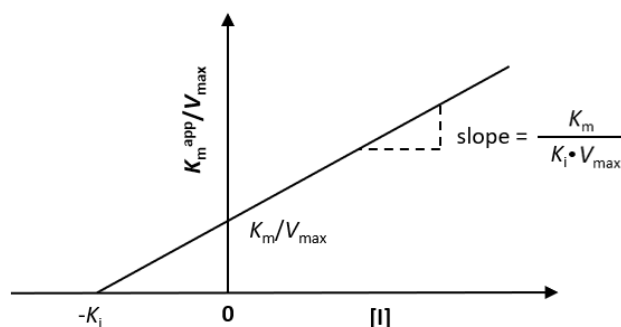


Figure 65 : Determination of competitive inhibition constant K_i based on the re-plotted Lineweaver-Burk graph.

Different from the Lineweaver-Burk graphic method, Dixon diagram offers faster and more direct access to the inhibition constant K_i . Plotting the inverse of the initial velocity $1/V$ as a function of the inhibitor concentration for a series of different $[S]$ generates straight lines intersecting at one point whose abscissa equals $-K_i$ value (see Figure 66). To simplify the calculations, multiple values of K_m are chosen as the set of $[S]$ values.

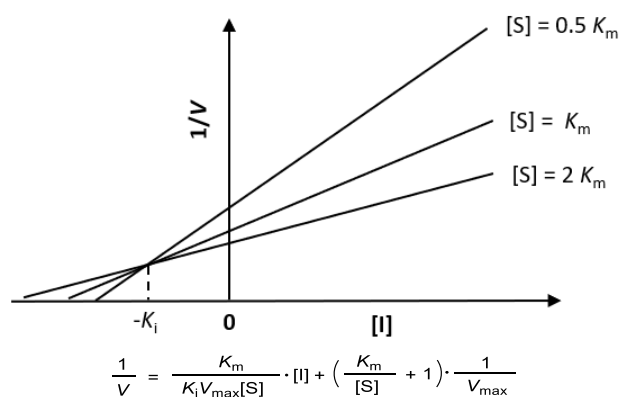
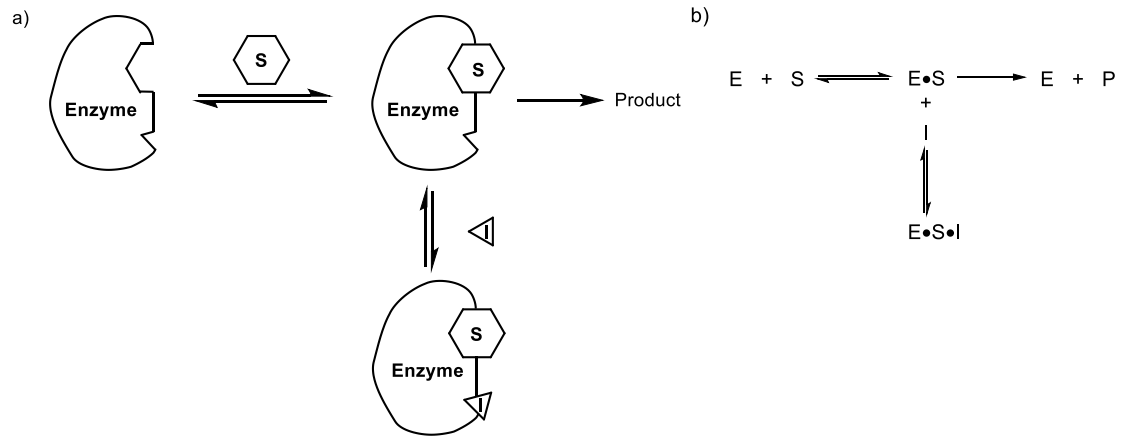


Figure 66 : Dixon graph for competitive inhibition.

- **Uncompetitive inhibition**

An Uncompetitive inhibitor is an inhibitor that only binds to the enzyme-substrate complex (Scheme 33) and exerts more its function at high substrate concentration. There is no necessity that an uncompetitive inhibitor has a similar structure to the substrate.



Scheme 33 : a) Uncompetitive inhibition (S: Substrate, I: Enzyme); b) Equations for uncompetitive inhibition.

Under the Michaelis-Menten mechanism, the initial velocity expression (see Equation 6) of uncompetitive inhibition can be derived by a similar process as competitive inhibition. We can find that both V_{max} and K_m are reduced by a factor of $(1+[I]/K_i)$. Two types of graphs, Michaelis-Menten and Lineweaver-Burk, in Figure 67 intuitively show us the influence of uncompetitive inhibitor on enzymatic reaction. The Lineweaver-Burk graph (Figure 67b) indicates that different inhibitor concentrations only affect the value of y-intercept, which is called the intercept effect and is distinct from the slope effect.

Equation 6 : Expression of the initial velocity of an enzymatic reaction in the presence of the uncompetitive inhibitor.

$$V = \frac{V_{max}[S] / (1 + \frac{[I]}{K_i})}{[S] + K_m / (1 + \frac{[I]}{K_i})}$$

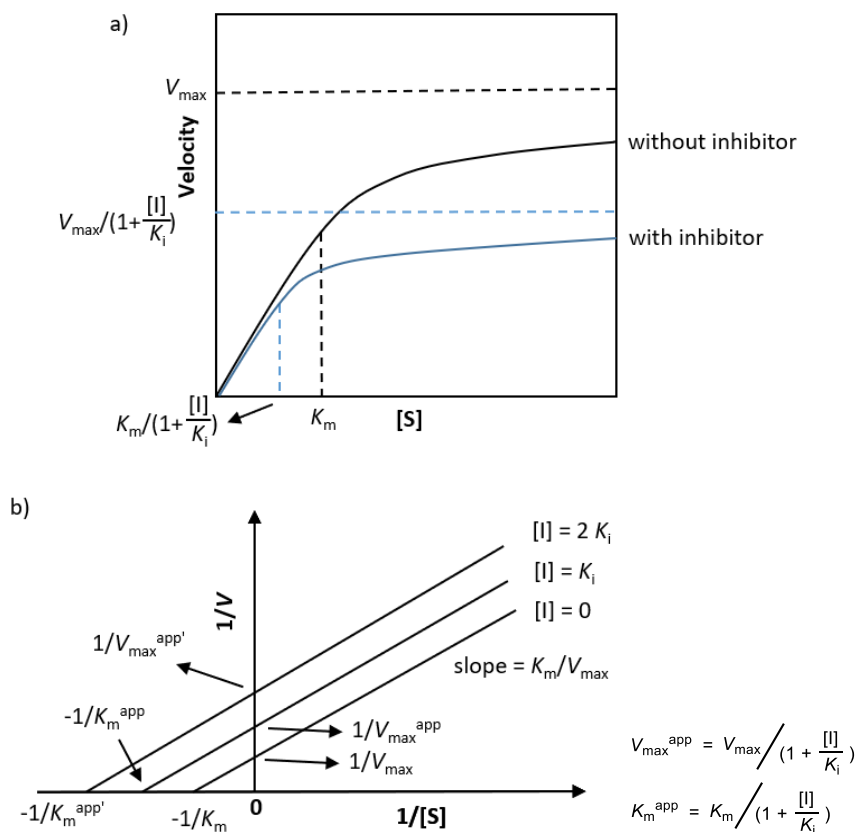


Figure 67 : a) Graph of Michaelis-Menten uncompetitive inhibition; b) Lineweaver-Burk uncompetitive inhibition graph.

Similar to the way to determine the K_i value of competitive inhibition, the uncompetitive inhibition constant can also be obtained by the graphical method. Plotting $1/K_m^{app}$ as a function of the inhibitor concentration or $1/V_{\max}^{app}$ versus the inhibitor concentration gives a straight-line intersecting with the x-axis at $-K_i$ (Figure 68). It is easy to figure out both $1/K_m^{app}$ and $1/V_{\max}^{app}$ values from the intercepts of the Lineweaver-Burk graph (Figure 67b).

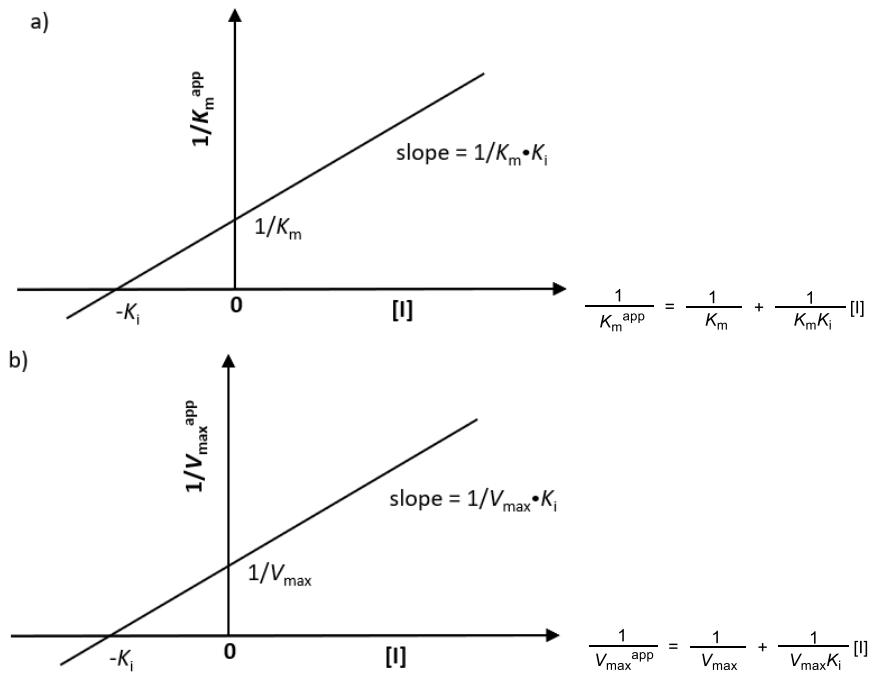
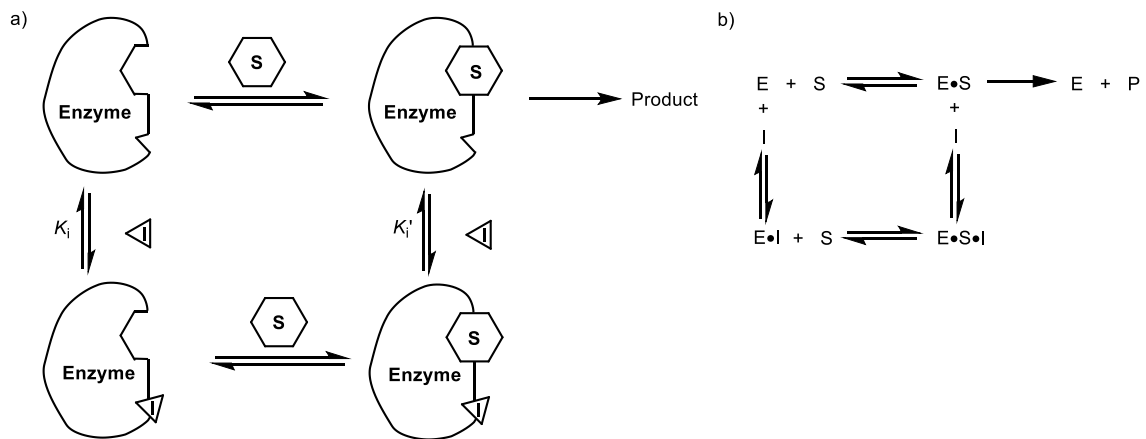


Figure 68 : a) Plot of $1/K_m^{app}$ vs. $[I]$; b) Plot of $1/V_{max}^{app}$ vs. $[I]$.

• **Non-competitive inhibition**

If an inhibitor binds to both the enzyme and the enzyme-substrate $[E \cdot S]$ complex preventing the formation of product, the inhibition and the inhibitor belong to the non-competitive type (Scheme 34). The inhibitor does not need to possess a similar chemical structure as the substrate molecule owing to the substrate and the inhibitor interact with the enzyme on different sites.



Scheme 34 : a) Non-competitive inhibition (S : Substrate, I : Enzyme); b) Equations for non-competitive inhibition.

From the expression of Scheme 34, we can find that the non-competitive type of inhibition is observed as a combination of competitive inhibition and uncompetitive inhibition. Therefore, the equation of its initial velocity is more complicated and shown in Equation 7. Nevertheless, it is not rigorous to use a generic term mixed inhibition to refer to this combinatorial inhibition.

Different values of K_i and K_i' would generate a distinct transformation of Equation 7, which is corresponding to a certain inhibition pattern.

Equation 7: Expression of the initial velocity of an enzymatic reaction in the presence of the non-competitive inhibitor.

$$v = \frac{V_{\max}[S] / (1 + \frac{[I]}{K_i'})}{[S] + K_m (1 + \frac{[I]}{K_i}) / (1 + \frac{[I]}{K_i'})}$$

When $K_i = \infty$, Equation 7 is simplified to uncompetitive inhibition (Equation 6); when $K_i' = \infty$, it would have the same expression as competitive inhibition (Equation 3). Apart from these two infinities, the inhibitory process shows non-competitive inhibition (simple) type when $K_i = K_i'$, and non-competitive inhibition (mixed) type when $K_i \neq K_i'$. In the case of $K_i = K_i'$, i. e., non-competitive simple inhibition, the K_m is not affected by the inhibitor. The non-competitive inhibition (mixed) could be further classified into two cases: $K_i < K_i'$ and $K_i > K_i'$. Figure 69 displays the graphic expression of non-competitive simple inhibition.

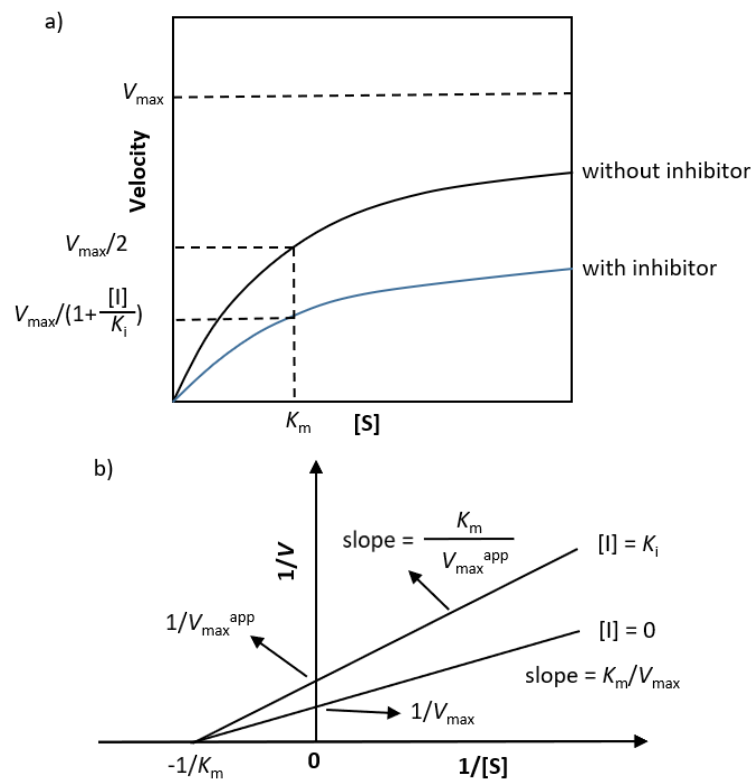


Figure 69 : a) Graph of Michaelis-Menten non-competitive inhibition (simple); b) Lineweaver-Burk non-competitive inhibition (simple) graph.

The K_i value of non-competitive inhibition (simple) can be obtained by plotting a second graph: $1/V_{\max}^{app}$ as a function of the inhibitor concentration which generates a straight-line intersecting with the x-axis at $-K_i$ (Figure 70) based on the y-intercepts from Lineweaver-Burk plot (Figure 69b).

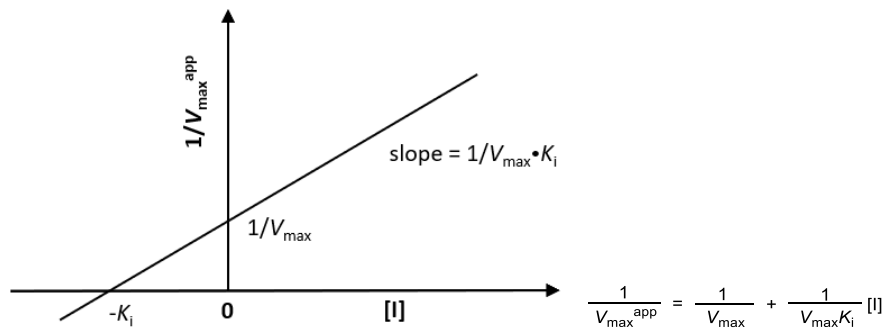


Figure 70 : Plot of $1/V_{\max}^{\text{app}}$ vs. $[I]$.

The two Lineweaver-Burk graphs in Figure 71 below reveal the tendencies of non-competitive inhibition (mixed) to affect the K_m values.

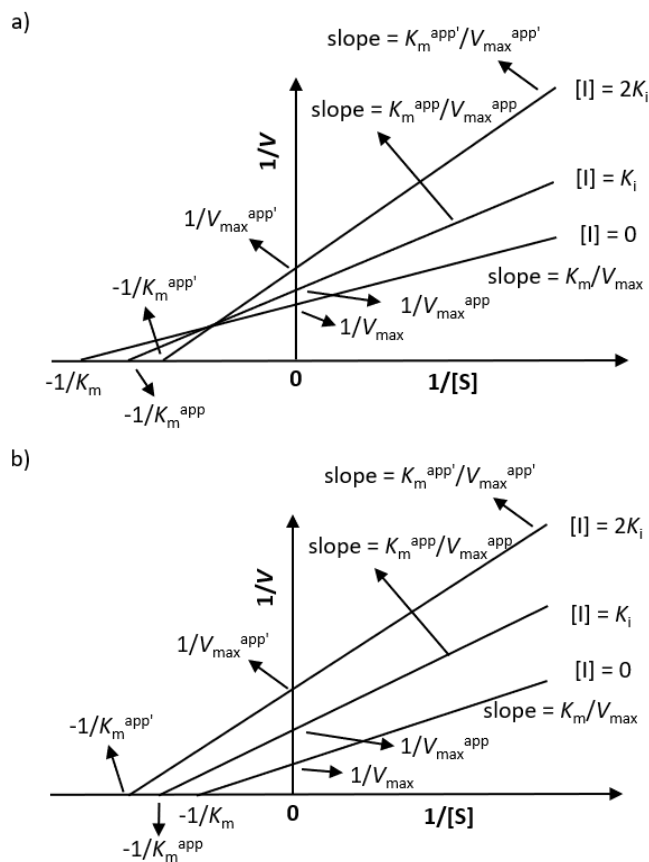


Figure 71: a) Lineweaver-Burk non-competitive inhibition (mixed) graph when $K_i < K_i'$; b) Lineweaver-Burk non-competitive inhibition (mixed) graph when $K_i > K_i'$.

Figure 72 displays the way to determine the non-competitive inhibition (mixed) constants K_i and K_i' . Plotting $1/V_{\max}^{\text{app}}$ as a function of the inhibitor concentration gives a straight-line intersecting with the x-axis at $-K_i'$ (Figure 72a), and $K_m^{\text{app}}/V_{\max}^{\text{app}}$ versus the inhibitor concentration gives a straight-line crossing the abscissa axis at $-K_i$ (Figure 72b).

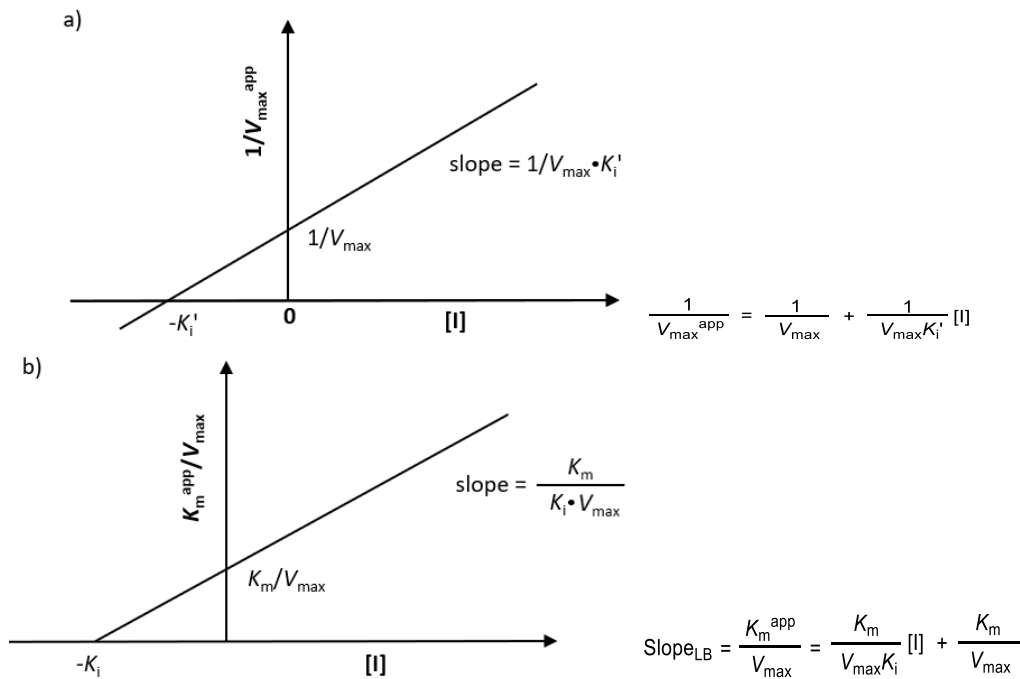


Figure 72 : a) Plot of $1/V_{\max}^{\text{app}}$ vs. $[I]$; b) Plot of $K_m^{\text{app}}/V_{\max}^{\text{app}}$ vs. $[I]$.

- **Tight-binding inhibition**

Last but not least, it should be noticed that besides those three inhibition patterns discussed above, other possibilities exist and we will only focus on tight-binding inhibition. Correspondingly, the inhibitor is named as tight-binding inhibitor. This class of inhibitors binds tightly and sometimes in nearly stoichiometric proportion with their target enzymes, which leads to the depletion of inhibitor concentration by the formation of the $[E \cdot I]$ that cannot be neglected anymore (i. e., $[I] \neq [I_0]$) since lower inhibitors concentrations are used during the inhibition assays. Further, it is suggested that the assumptions of steady-state approximations should not be adopted when the inhibition constant K_i is less than 1000 times the total enzyme concentration.^[202–204]

Hence, it is necessary to find an alternative and right method to analyze these untraditional inhibitors; otherwise, the actual mode of inhibition mechanism could be misinterpreted. For example, the natural ribonuclease inhibitor was initially described as a classical non-competitive inhibitor by double-reciprocal plots. After a wide range of examinations by Turner *et al.*, the proteins were corrected to be tight-binding competitive inhibitors.^[205] According to Morrison and coworkers' in-depth mathematical study, it can be generally stated that the double-reciprocal plots for tight-binding competitive inhibitors appear similar to those of classical non-competitive and this could be misleading.^[204]

There are several ways to identify the tight-binding inhibition. As a tight-binding inhibitor combines the enzyme in a stoichiometric proportion, hence the plot of IC_{50} (half maximal inhibitory concentration) as a function of total enzyme concentration at a fixed $[S]$ gives a straight line, which is a reliable method to determine the tight-binding inhibition.^[204]

Further, a tight-binding inhibitor can be classified into three types, namely tight-binding competitive inhibitor, tight-binding non-competitive inhibitor, and tight-binding uncompetitive inhibitor. Each type exhibits its features, which are demonstrated clearly by R. A. Copeland.^[204] Rather than present this work again, I would like to highlight the determination for the K_i value of a tight-binding competitive inhibitor, which is related to my

following biological test.

In 1969, Morrison derived a general initial steady-state rate equation which describes the fractional rate as a function of total inhibitor concentration (at fixed enzyme and substrate concentrations).^[204,206] However, strictly speaking, Morrison's equation is merely a generic template for the rate equation of any enzymatic reaction in the presence of tight-binding inhibitors. It can be used only when the generic terms in the equation are specialized for a particular catalytic and inhibition mechanism. Morrison's equation are the seminal sparks that promote the survey of functionalized "Morrison equation" equivalents. Until now, there exist various algebraic forms derived from the abstract template (the Morrison's equation), such as Cha's equation (1975),^[207] Greco & Hakala's equation (1979),^[208] and Copeland's equation (2000).^[204]

Among those variants, Cha's equation^[207] 8 (see below) is exclusively suitable for competitive inhibition of Michaelis-Menten mode^[209], and by which we can deduce the inhibition constant K_i by non-linear regression.

Equation 8 : Expression of velocity for tight-binding competitive inhibition constant determination.

$$V_i = \frac{V_0([E_0] - [I] - K_i^{app} + \sqrt{([E_0] - [I] - K_i^{app})^2 + 4[E_0]K_i^{app}})}{2[E_0]}$$

$$K_i^{app} = K_i \left(1 + \frac{S}{K_m}\right)$$

In the formula, V_i represents the initial rate in the presence of the inhibitor, and V_0 is the initial rate observed in the absence of the inhibitor.

II.2 Enzymatic assay results

After the discovery of strong multivalent effects on glycosidases,^[4,109] our lab has explored the maximum level of affinity enhancement against JB α -man with the help of clusters based on cyclopeptoid scaffolds and 1-deoxynojirimycin (DNJ) inhibitor head. Among this series, the 36-valent DNJ **135d** displayed the best multivalent effect with JB α -man and showed the largest binding enhancement reported on a glycosidase so far. To make comparisons with the previous inhibitory results, the enzymatic evaluation of novel series of cyclopeptoid-minosugar conjugates have also been carried on JB α -man by spectrophotometrical measurement.

The determination of K_i depends on three steps :

- K_i range determination by plotting the inverse of the initial velocity $1/V$ as a function of the inhibitor concentration at one $[S]$ generates a straight line which could indirectly give a rough K_i value calculated from the IC_{50} ,
- assessment of the inhibitory pattern *via* the secondary graph from the Dixon plot or Lineweaver-Burk graph,
- determination of the exact K_i value through either Dixon plot, the double-reciprocal Lineweaver Burk plot or the Morrison equation.

First of all, the enzymological assays were launched for the divalent and 4x1-valent iminosugar-cyclopeptoid inhibitors. The simplified structures of *O*-deacetylated clusters and the graphic results are exhibited in the following text.

- Inhibitor **194**

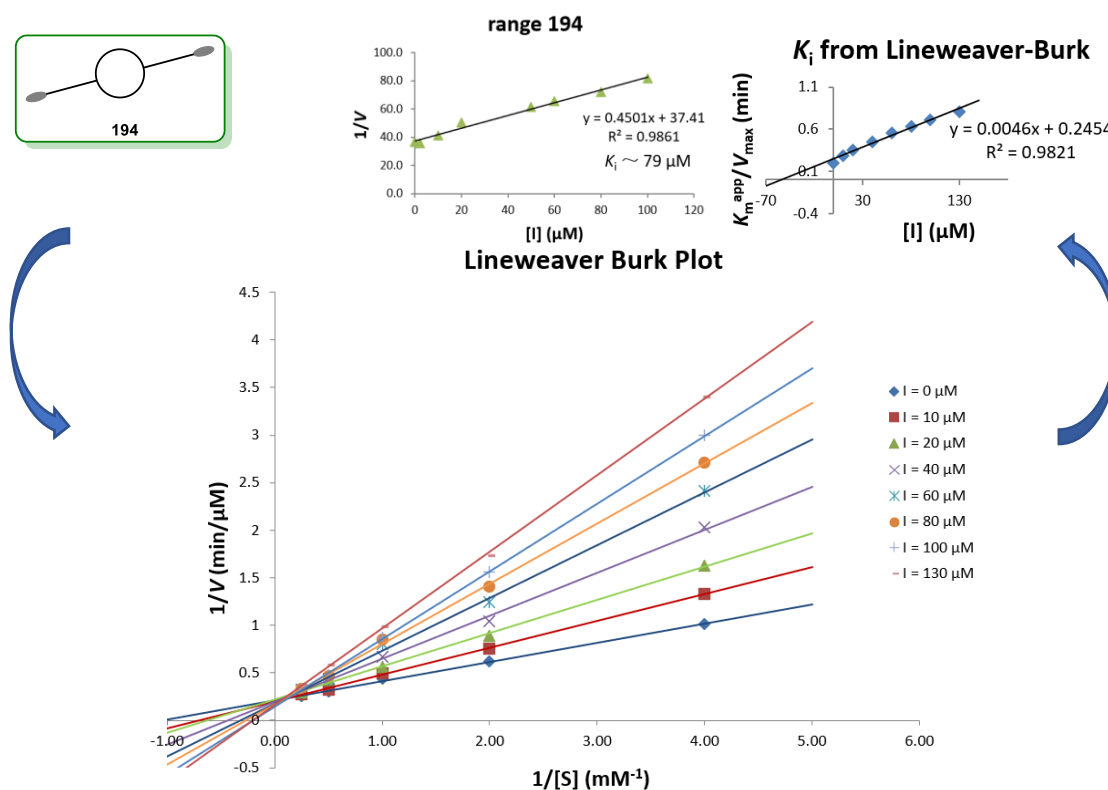
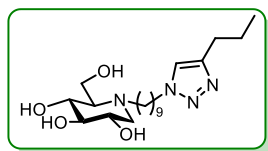


Figure 73 : Simplified structure and inhibitory activity of 194; Lineweaver Burk plot reveals a competitive inhibition pattern and $K_i = 54 \mu\text{M}$.



100 $K_i = 188 \mu\text{M}$

Figure 74 : Monovalent control.^[189]

The inhibitory activity K_i of **194** against $\text{JB}\alpha$ -man equals $54 \mu\text{M}$ and the relative inhibition potency (rp) over monovalent control **100** (Figure 74) is 3, which means no multivalent effect. This compound is interesting because bind-and-recapture effect is not possible due to diametral remoteness and it highlights the importance of statistical rebinding again. The low rp observed indicates also that no aggregation effect may have been obtained and that **194** is not able to link two different enzymes.

- Inhibitor **195**

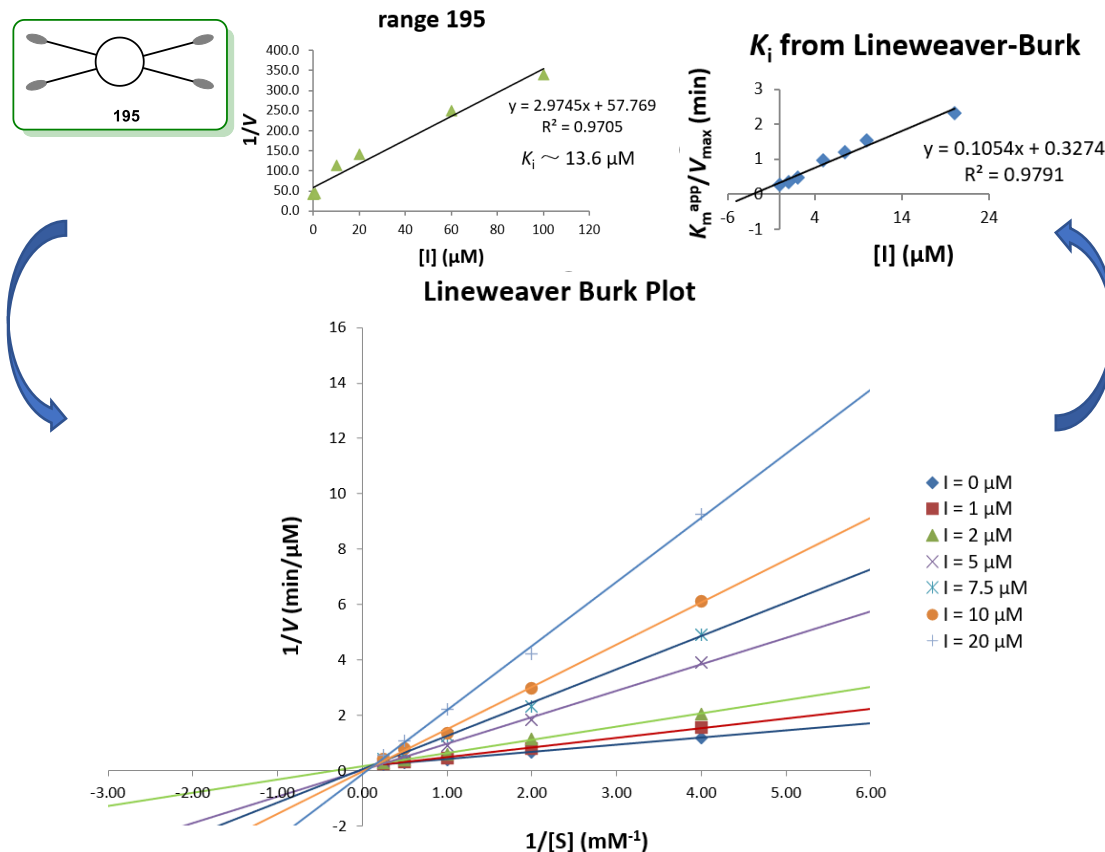


Figure 75 : Simplified structure and inhibitory activity of **195**; Lineweaver Burk plot reveals the competitive inhibition pattern and $K_i = 3.1 \mu\text{M}$.

• Inhibitor 196

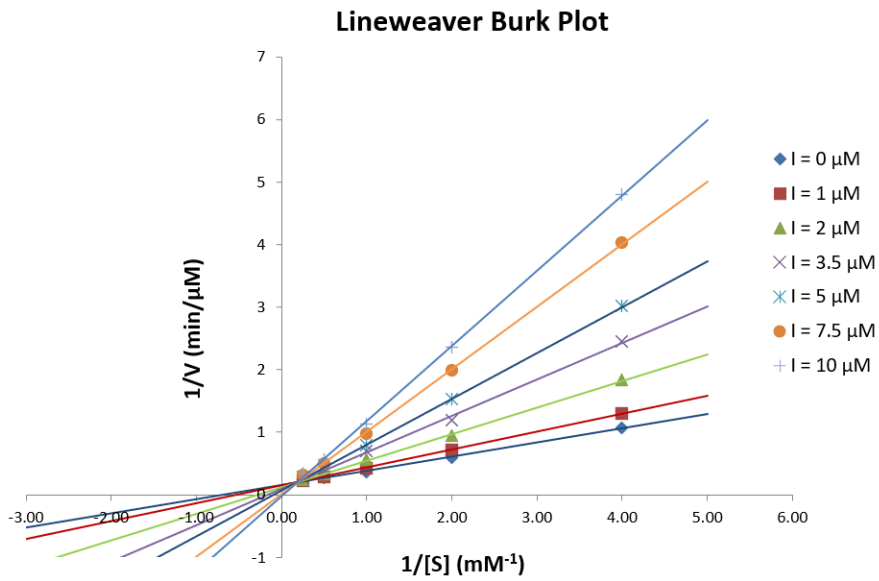
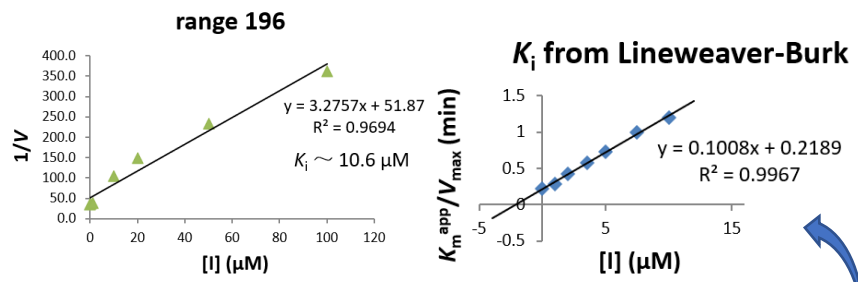
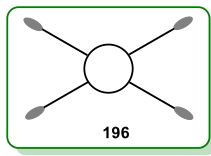


Figure 76 : Simplified structure and inhibitory activity of 196; Lineweaver Burk plot reveals the competitive inhibition pattern and $K_i = 2.2 \mu\text{M}$.

• Inhibitor **197**

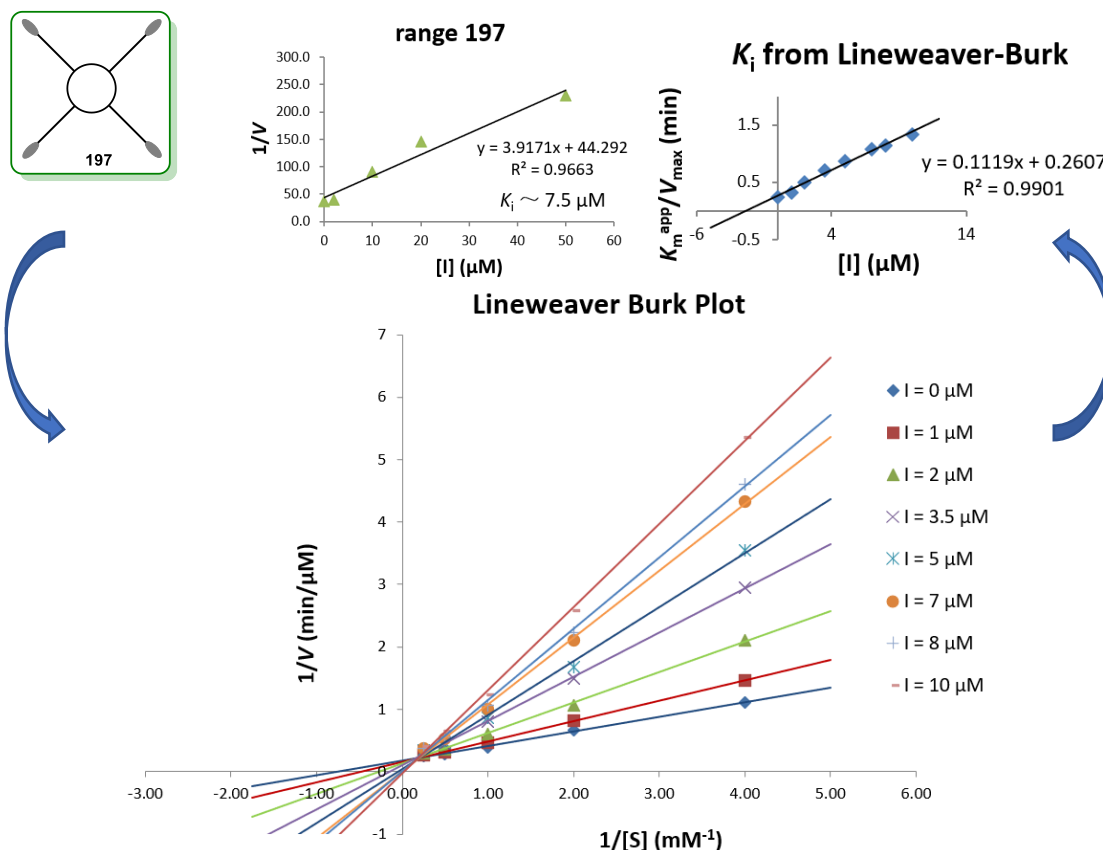


Figure 77 : Simplified structure and inhibitory activity of 197; Lineweaver Burk plot reveals the competitive inhibition pattern and $K_i = 2.3 \mu\text{M}$.

The crossing on the vertical axis of Lineweaver Burk plots reveals that these three inhibitors all share competitive inhibition mode. Further, the three inhibition constants were obtained through secondary Lineweaver Burk plots. To quantify the affinity enhancement (i. e., rp) gained by the multivalent structures, these inhibitory activities were subsequently compared with the K_i of the monovalent control **100** (Figure 74). The inhibition constants, the relative inhibition potency (rp) over monovalent control **100** as well as valency-corrected relative inhibition potency (rp/n) are shown in Table 20.

Compound	DNJ units	K_i^a (μM)	rp	rp/n
100	1	188	-	-
195	4	3.1	61	15
196	4	2.2	85	21
197	4	2.3	82	20

^a K_i obtained from triplicate assays.

Table 20 : Inhibitory activity (K_i , μM) and relative inhibition potency of iminosugar clusters and against $\text{JB}\alpha\text{-man}$.

Figure 78 makes an at-a-glance comparison of the valency-corrected relative inhibition potency (rp/n) of these series of 4x1-valent inhibitors.

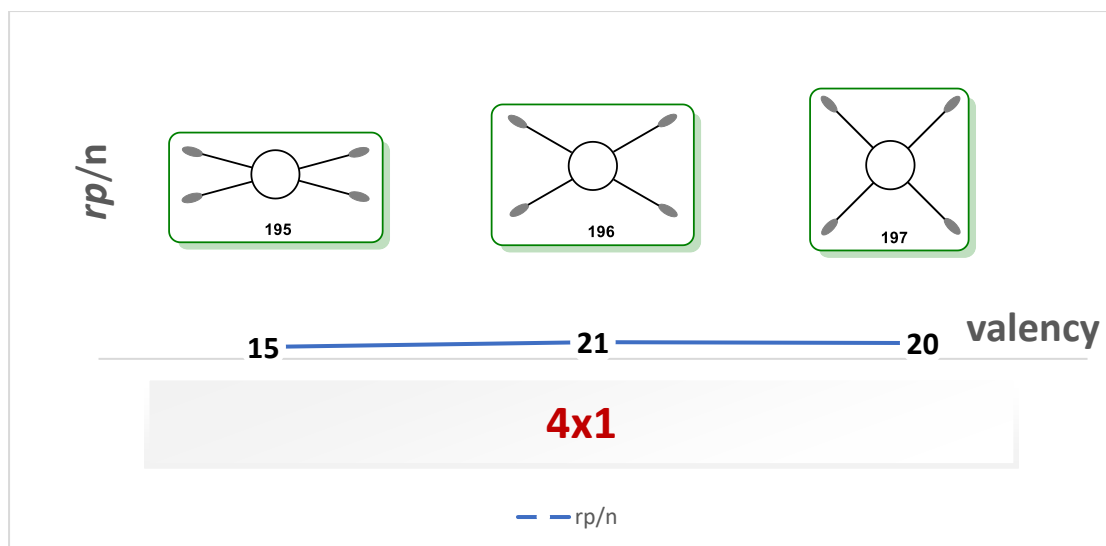


Figure 78 : Valency-corrected relative inhibition potency (rp/n) of the 4x1-valent inhibitors.

From the results in Figure 78, all 4x1-valent iminosugar-cyclopeptoid conjugates do display similar multivalent effects. There is no best geometry. They are all equivalents. Moreover, they do not reach high rp/n values expected from a chelate effect.

Thereafter, the inhibitory activities of the 4x3-valent iminosugar-cyclopeptoid inhibitors were evaluated *via* the same operations. While the Dixon plots and the secondary graphs of Lineweaver-Burk demonstrate apparent non-linearity, these three 4x3-valent clusters were recognized to be fast tight-binding competitive inhibitors as observed before in the lab by Maeva Pichon.^[111,138] Their inhibition constants K_i were thus calculated by Cha's equation, and the graphic results of the 4x3-valent inhibitors are presented as follows.

- Inhibitor 198

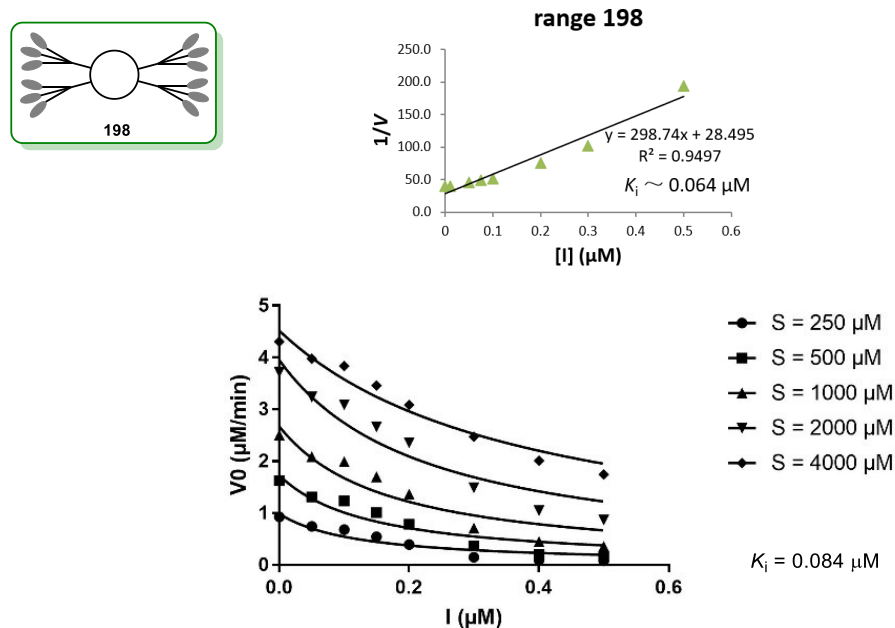


Figure 79 : Simplified structure and inhibitory activity of 198; Lineweaver Burk plot reveals the tight-binding competitive inhibition pattern and $K_i = 0.084 \mu\text{M}$.

• Inhibitor 199

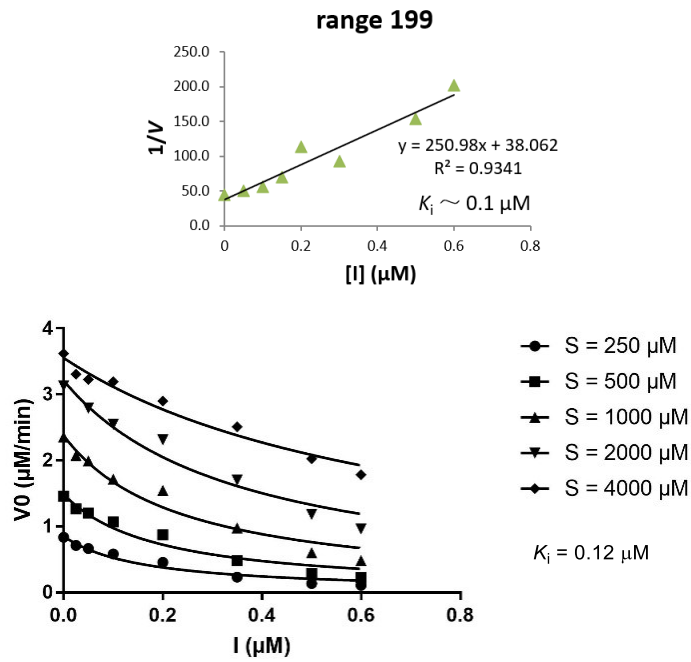
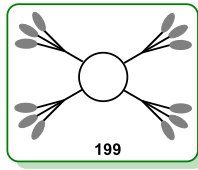


Figure 80 : Simplified structure and inhibitory activity of 199; Lineweaver Burk plot reveals the tight-binding competitive inhibition pattern and $K_i = 0.12 \mu\text{M}$.

• Inhibitor 200

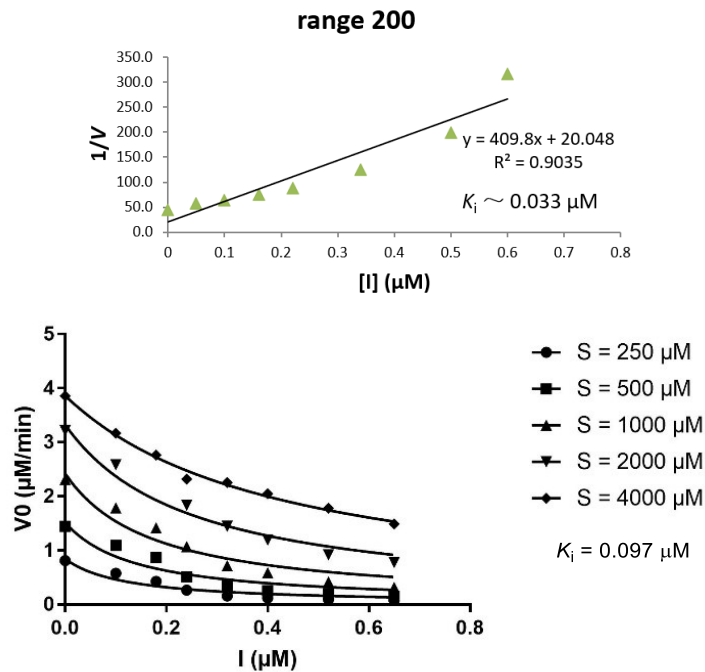
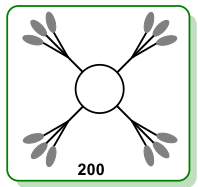


Figure 81 : Simplified structure and inhibitory activity of 200; Lineweaver Burk plot reveals the tight-binding competitive inhibition pattern and $K_i = 0.097 \mu\text{M}$.

Dixon plots for inhibitors 198-200 were not straight lines but curve ones. Plot of enzyme

velocity as a function of inhibitor concentration were then used (Figure 79-81) for non linear regression. The solid curves drawn through the data points represent the best fit to the Morrison equation used to obtain K_i values for the tight binding inhibitors **198-200**. The relative inhibition potency (rp) of these three clusters was evaluated over the same monovalent control **100** (Figure 74). Table 21 collects the results, including inhibition constants, the relative inhibition potency (rp), and valency-corrected relative inhibition potency (rp/n).

Compound	DNJ units	$K_i^a(\mu\text{M})$	rp	rp/n
100	1	188	-	-
198	12	0.084	2238	187
199	12	0.12	1567	131
200	12	0.097	1938	162

^a K_i obtained from triplicate assays.

Table 21 : Inhibitory activity (K_i , μM) and relative inhibition potency of iminosugar clusters and against JBA-man.

The valency-corrected relative inhibition potency (rp/n) of these 4x3-valent inhibitors was displayed in Figure 82 to make comparisons with each other visually. All these three inhibitors behaved very similarly.

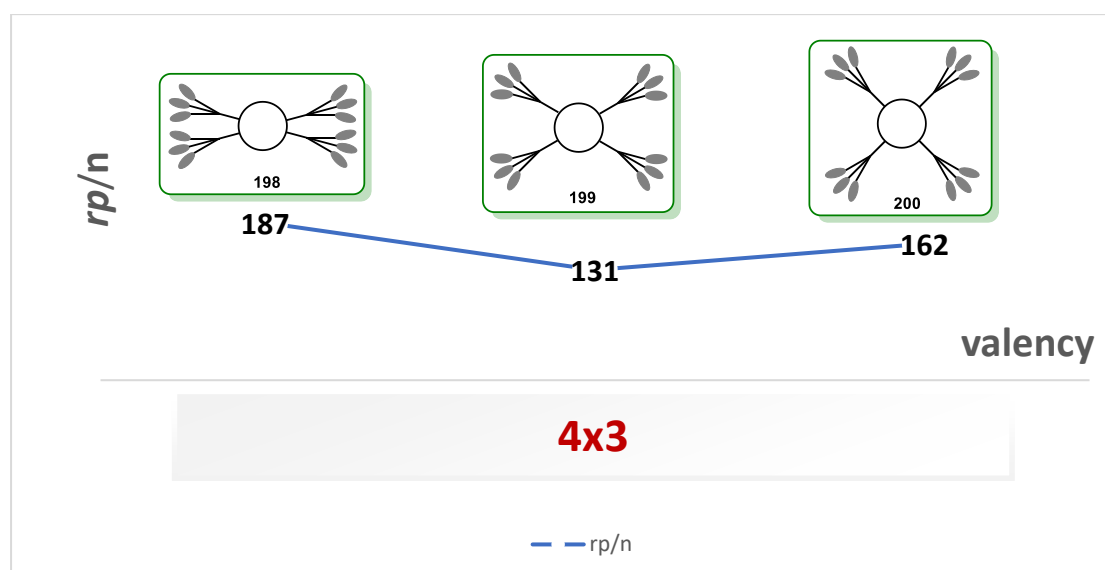


Figure 82 : Valency-corrected relative inhibition potency (rp/n) of the 4x3-valent inhibitors.

The inhibitory activities (with K_i in range of 0.084-0.12 μM) and multivalent effects (with rp/n in range of 131-187) of these 4x3-valent inhibitors are one magnitude order better than 4x1-valent clusters (K_i in range of 2.2-3.1 μM and rp/n in range of 15-21). It is hypothesized that the partially restored bind-and-recapture effect^[108] of the 4x3-valent inhibitors **198-200** leads to this improvement. The increased local concentration of inhibiting epitopes close to the enzyme active site “prolongs” the lifetime of bound state. However, the rp/n values obtained remain one order of magnitude under the one (rp/n of 4700) observed with 36-valent cluster **135d**. For all clusters derived from the 4-valent scaffolds, **195-197** and **198-200**, the inhibition constants are close when their valences are equal. Therefore, it is deduced that there is no influence of spatial orientation. The flexibility of the arms allows the same good positioning

whatever the special orientation originating at the central core.

Then, the determination of inhibition constants for the other two 12-valent (the 12×1 and “hindered” 12×1 valent) glycoclusters were conducted. Interestingly, the “regular” 12×1-valent inhibitor shows competitive tight-binding with the enzyme JBα-man, while the “hindered” one behaves as a generic competitive inhibitor. Their results are introduced individually.

- Inhibitor **201**

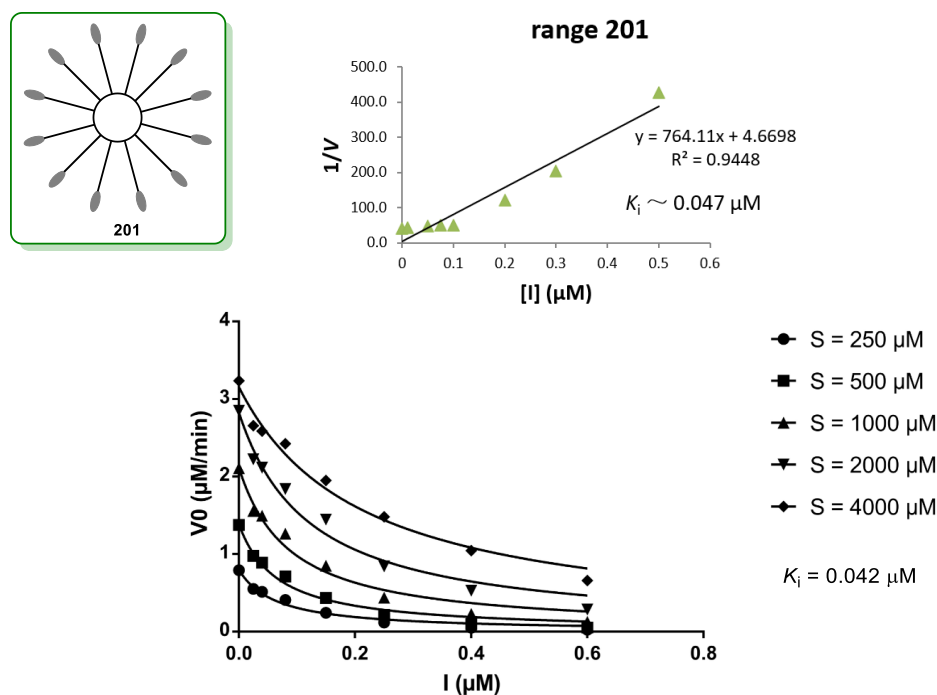


Figure 83 : Simplified structure and inhibitory activity of 201; Lineweaver Burk plot reveals a tight-binding competitive inhibition pattern and $K_i = 0.042 \mu\text{M}$.

Its inhibitory activity K_i against JBα-man equals $0.042 \mu\text{M}$, the relative inhibition potency (rp) over monovalent control **100** is 4476, and the relative inhibition potency per iminosugar is 373. Compared with the inhibitory potency and the multivalent effect of 4×3-valent inhibitors, the 12×1-valent one exhibits a slight better affinity enhancement. At that time we hypothesized that the slight improvement gained with cluster **201** over clusters **198-200**, and the strong gain obtained with 36-valent cluster **135d** might be due to a steric effect:^[210] the filling of the cluster into the enzyme cavity could indeed sterically hamper the access of the substrate.

To explore further this steric effect and the bind-and-recapture effect, the inhibition potency of inhibitor **202** was determined.

- Inhibitor **202**

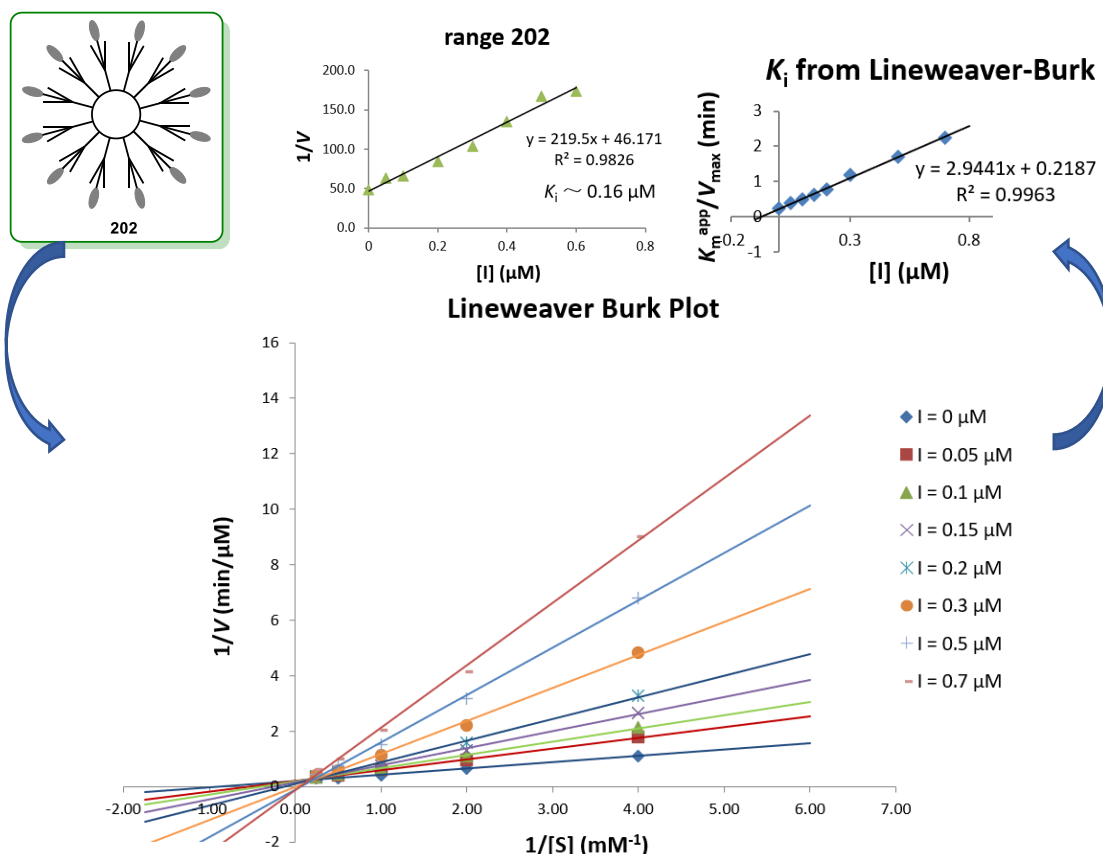


Figure 84 : Simplified structure and inhibitory activity of **202**; Lineweaver Burk plot reveals a competitive inhibition pattern and $K_i = 0.074 \mu\text{M}$.

The inhibition constant of **202** against $\text{JB}\alpha\text{-man}$ is $0.074 \mu\text{M}$ and the relative inhibition potency (rp) over monovalent control **100** is 2540. It does not show a significant disparity by comparing it to the 12-valent cluster **201**. Reducing the overall flexibility of the 12-valent cluster by adding 24 “naked” arms to obtain a more hindered system did not lead to rp/n closer to the one observed for the 36-valent cluster **135d**. This means that the hypothesis was wrong and another explanation is needed to explain the enhancement obtained for **201**.

Figure 85 summarizes all the valency-corrected relative inhibition potency (rp/n) of the novel inhibitors synthesized in this thesis. By comparing the rp/n of each cluster, we can find (to repeat for emphasis) that :

- i) different spatial orientations of the inhitops (inhibiting epitopes) do not influence the inhibitory potency;
- ii) reducing the overall flexibility of the cluster by adding “naked” arms does not improve the multivalent effect.

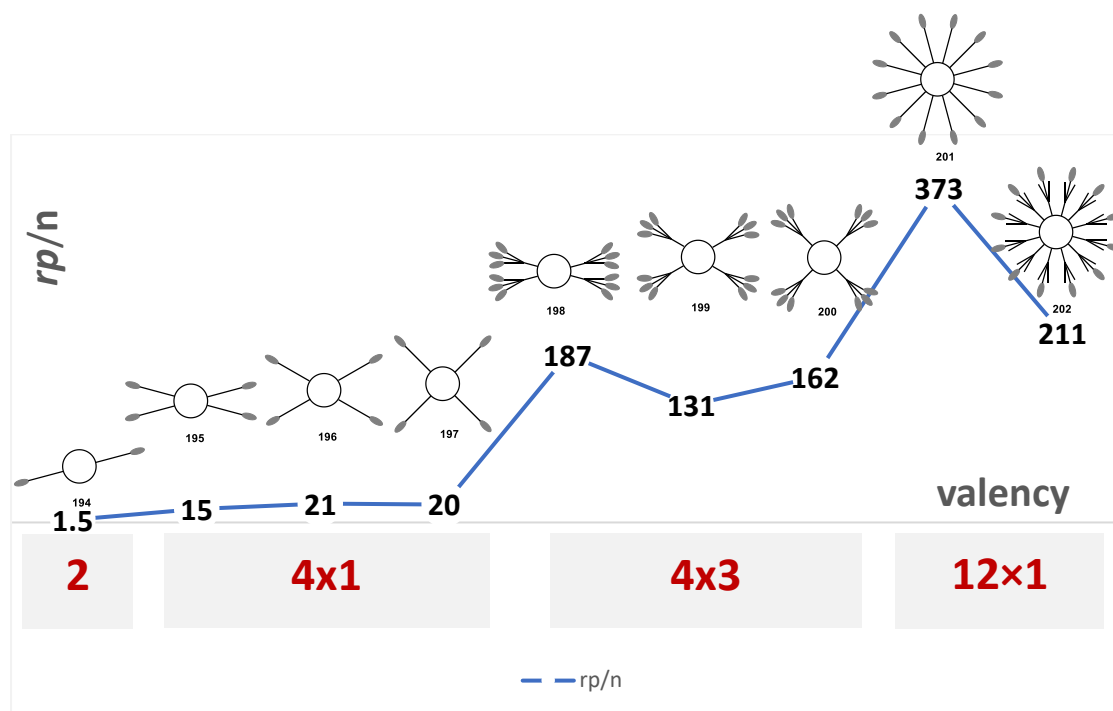


Figure 85: Valency-corrected relative inhibition potency (rp/n) of cyclopeptoid-based DNJ clusters 194-202.

II.3 Mechanistic studies based on analytical ultracentrifugation

The stoichiometry of enzyme/inhibitor complexes was evaluated by analytical ultracentrifugation sedimentation velocity (AUC-SV). AUC was developed in the 1920s by Theodor Svedberg,^[211] and became a central technique for characterizing biomolecules and studying their physicochemical properties, in particular for characterization of the formation of aggregates, heterogeneity of a sample, intermolecular interactions, size distribution in samples, *etc.* The basic principle of AUC is to combine the application of a centrifugal force with the simultaneous real-time observation of the resulting redistribution of the sample.^[211] AUC of interacting proteins can reveal the protein complexes characterizations regarding to their stoichiometries (including self-association, mixed self- and hetero-association), kinetic and thermodynamic constants. Among many specialized centrifugation techniques, AUC-SV is a powerful method that provides sedimentation coefficients, shape information, molecular weights, *etc.*, and is not prone to change the sample composition.

Thanks to the collaboration with the team from the IGBMC analysis department, we got the sedimentation coefficients of the JBA-man alone and the ones of enzyme-inhibitor mixtures with compounds **197**, **200**, **201**, **202**, **194** and also a 14-valent mannoimidazole **123** (see Figure 86) from my colleague Dr. M. M. Pichon. This compound, with a tight-binding competitive character has a K_i of 2nM.^[138]

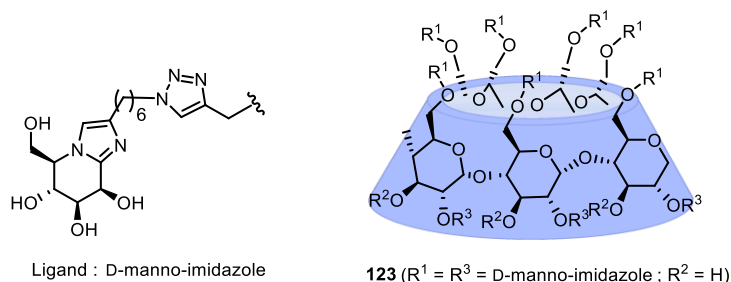


Figure 86 : Structure of 14-valent mannoimidazole **123**.

The results obtained are plotted in Figure 87. Observation of the plots reveals different areas : 8.45 S - 11 S, 11 S - 13 S and 13 S - 16.6 S. Their respective normalized percentage was calculated from their integration and is given in Table 22. The sedimenting species between 8.5 S and 11 S corresponds to the tetramer $(\text{LH})_2$ with a molar mass estimate around 210 kDa, whereas the species of double mass corresponding to the 2:1 enzyme-inhibitor was found at 13.4 S in our previous study.^[5] The sedimentation peaks between species $(\text{LH})_2$ and $2x(\text{LH})_2$ correspond to dissociations/re-associations of the $2x(\text{LH})_2$ complex during sedimentation.^[212] The frictional ratio is the same for all oligomers of a sample and informs about the dynamics. Experiments with frictional ratios close to 1 are in dynamic equilibrium, whereas those with values close to 1.3 are not. Cluster **135d** showed the broader and most dynamic system of species, with a frictional ratio at 0.85. The clusters tested here have more distinct peaks and are all less dynamics than **135d**.

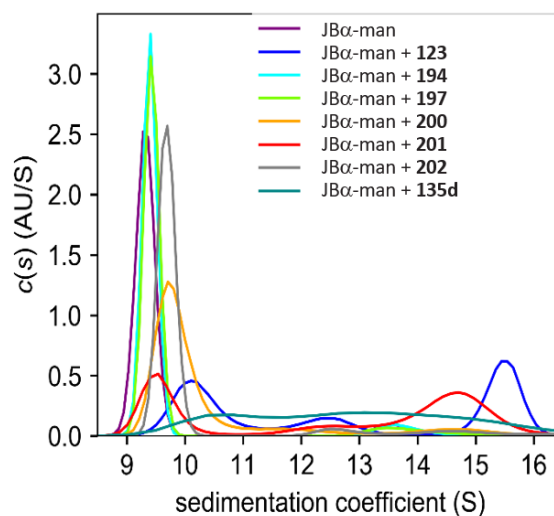


Figure 87 : Sedimentation coefficient distributions $c(s)$ of $\text{JB}\alpha\text{-man}$ (purple), $\text{JB}\alpha\text{-man} + 123$ (blue), $\text{JB}\alpha\text{-man} + 194$ (cyan), $\text{JB}\alpha\text{-man} + 197$ (chartreuse), $\text{JB}\alpha\text{-man} + 200$ (orange), $\text{JB}\alpha\text{-man} + 201$ (red), $\text{JB}\alpha\text{-man} + 202$ (gray), $\text{JB}\alpha\text{-man} + 135d$ (darkcyan).

Sample	Valency	Frictional ratio	peak integration	peak integration	peak integration	K_i (nM)	Rp/n
			(%) 8.45 S - 11 S	(%) 11 S - 13 S	(%) 13 S - 16.6 S		
JB α -man	/	1.35	92	0	8	/	/
E + 123	14	1.06	38	18	44	2	4
E + 194	2	1.31	92	0	8	54000	1.7
E + 197	4	1.32	92	0	8	2300	20
E + 200	4x3	1.09	83	8	9	97	161
E + 201	12	1.09	36	10	54	42	373
E + 202	12	1.35	89	4	7	74	212
E + 135d	36	0.85	21	33	46	1.1	4747

Table 22 : Summary of data concerning the different clusters. Inhibition constants, rp/n , frictional ratios and integration of the area under the curve for different sedimentation coefficients ranges relative to the total signal and normalized with the signal integration from 8.6 S to 11 S.

Among them, only **123** and **201** can form $2x(LH)_2$ complexes with their peaks between 14 S - 15 S and 15 S - 16 S, respectively. It is worthy to note that for a similar mass, the sedimentation coefficient can vary depending on the shape, with higher values for more compact species according to the Svedberg equation.

From the table and plots, most of the new clusters are associated with the enzyme in a 1:1 fashion, except **201**, which has the highest percentage of enzyme-inhibitor complex 2:1. The 36-valent cluster favors the formation of dynamic species in solution as shown by the frictional factor, however with more dissociation/association as shown by the higher amount of species between the 1:1 and 2:1 complexes. The 36-valent cluster is the one favoring the most the bind-and-recapture mechanism probably because it has the highest density of inhitopes. Since **201** allows formation of the enzyme-inhibitor 2:1 in a ratio similar to the one of the 36-valent cluster, it seems that the incredible power of the 36-valent does not only come from the cross-linking but also from a very favored bind-and-recapture mechanism. Those new data however are not sufficient to explain several points. Why the three 12-valent clusters, having similar inhibition constants gave such different trends in AUC-SV (different frictional ratio and different integrations) ? Why does the hindered cluster **202**, which is in a structural point of view between **201** and 36-valent **135d** has a K_i almost twice less good than **201** ? To tackle those new questions, a collaboration has been started with a specialist in modelisation.

Chapter IV :

SYNTHESIS OF GLYCOSYL CYANIDES BY
RING-OPENING OF 1,6-ANHYDRO SUGARS
WITH TMSCN

I Introduction

C-glycosides - also referred to as C-glycosyl compounds^[6] as recommended by IUPAC - are an essential group of hydrolytically stable glycomimetics. They have attracted an increasing interest due to the presence of many naturally occurring C-glycosides showing valuable biological activities, such as antibacterial, antitumor, antiviral properties.^[6-8] In 2016, our team designed the first examples of multivalent C-glycosides based on C₆₀-fullerene or β -cyclodextrin cores to study the mechanisms underlying the multivalent effects observed in glycosidase inhibition (Figure 88).^[9] In connection with this study, we were particularly interested in developing a new approach towards glycosyl cyanides from 1,6-anhydrosugars. First because anomeric cyanation is one of the most simple, practical C-extension methods to access C-glycosides. Secondly, 1,6-anhydrosugars offer numerous advantages as sugar donors.^[213] Ring-opening reaction with cyanide nucleophiles is expected to provide a direct access to C-glycoside precursors bearing a free hydroxyl group at the C-6 position, limiting protecting group manipulations and enabling the design of convergent synthetic strategies. In this chapter, we report our efforts to develop a new method for the stereoselective synthesis of glycosyl cyanides by means of cyanide nucleophilic ring-opening of 1,6-anhydro sugars.

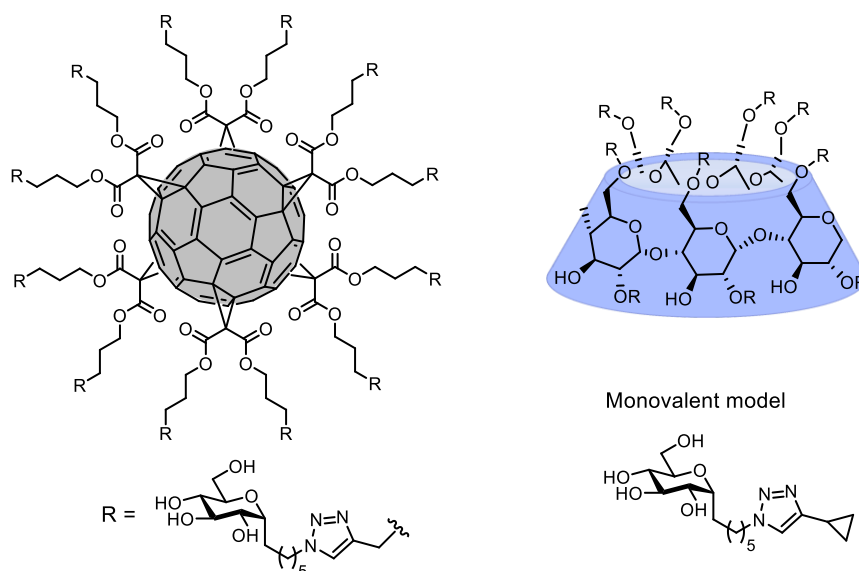
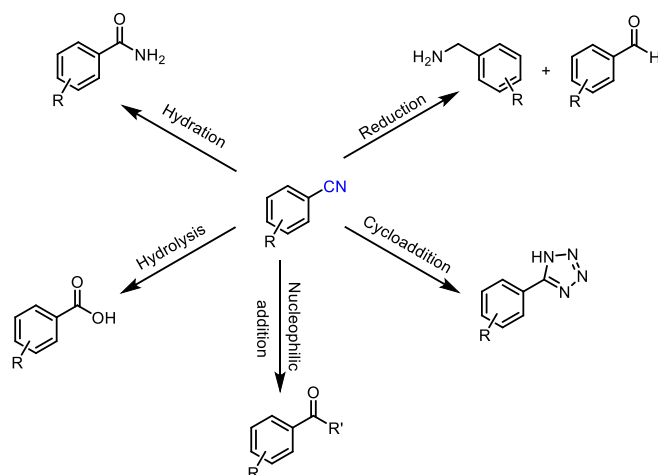


Figure 88: First examples of multivalent C-glycosides based on C₆₀-fullerene or β -cyclodextrin cores.^[9]

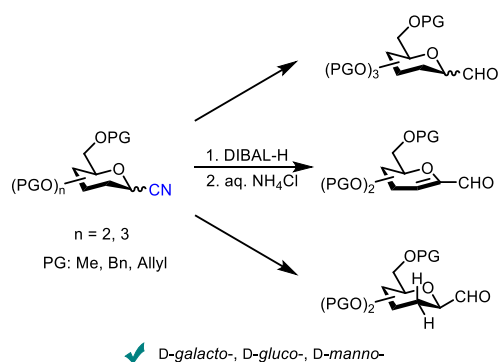
I.1 Synthetic strategies to access glycosyl cyanides

The nitrile (or cyano) group serves as an integral part of structural motifs in dyes, agrochemicals, pharmaceuticals, electronic materials, and is also found in natural products.^[214] Moreover, this versatile functional group may be transformed into other key functionalities comprising amines, aldehydes, carboxylic acid, amides, heterocycles, and ketones *via* different processes including reduction, hydrolysis, hydration, cycloadditions, and nucleophilic additions (Scheme 35).^[214,215]



Scheme 35: Examples of cyano (or nitrile) group transforming into other functionalities.^[214]

It is well known that the anomeric carbon atom is a key position in carbohydrates. The introduction of a versatile nitrile group at this position affords valuable intermediates for the synthesis of C-glycosides, i. e., glycomimetics in which the C-O acetal linkage in natural O-glycosides has been substituted for a more stable C-C bond. For example, S. Sipos and I. Jablonkai described a convenient way to prepare 1-C-glycosyl aldehydes by reductive hydrolysis of glycosyl cyanides employing complex aluminum-hydrides (Scheme 36).^[216]



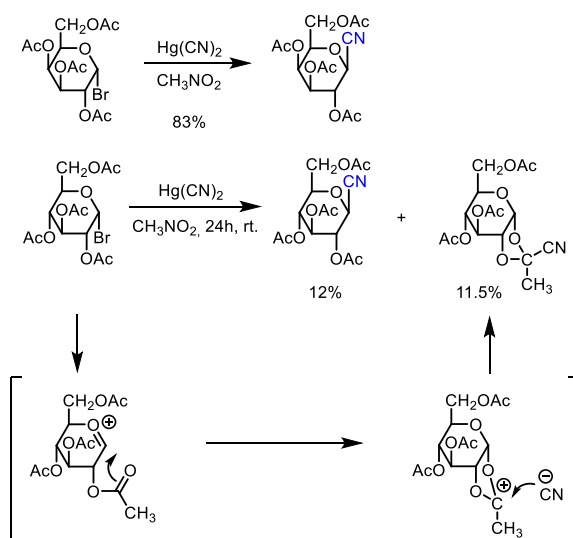
Scheme 36: Preparation of 1-C-glycosyl aldehydes by reductive hydrolysis of glycosyl cyanides.^[216]

Due to the obvious interest of glycosyl cyanides as intermediates in the preparation of C-glycosyl compounds, efficient methods have been actively investigated for the cyanation of the anomeric position over the past decades. Representative examples of the main strategies developed to access glycosyl cyanides are presented below.

✓ Reaction of activated glycosides with various cyanation sources

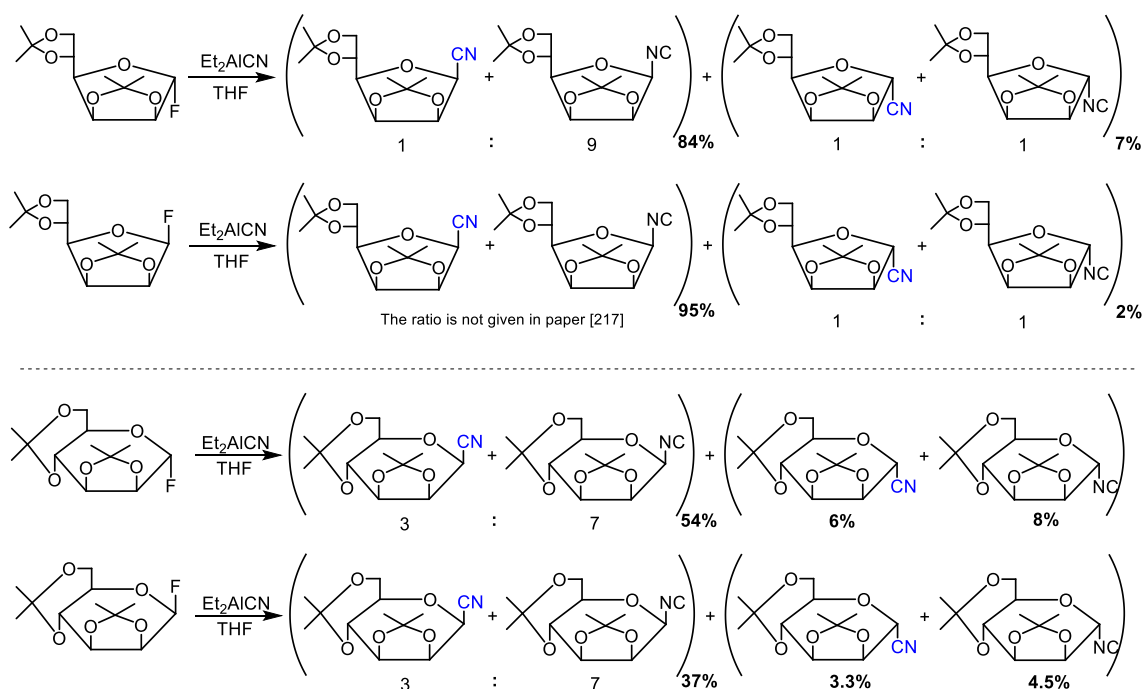
Glycosyl halides are often chosen as activated electrophilic sugar donors for generating glyconitriles.^[7,217–219] It should be noted that the nature of the halogen substituent significantly impact the stereochemical outcome and applicability of the reaction conditions.

The reaction of 2,3,4,6-tetra-O-acetyl- α -D-galactopyranosyl bromide with mercuric cyanide in nitromethane solution provided 2,3,4,6-tetra-O-acetyl- β -D-galactopyranosyl cyanide in 83% yield, whereas, under similar conditions, its C-4 epimer gave 2,3,4,6-tetra-O-acetyl- β -D-glucopyranosyl cyanide in only 12% yield and 3,4,6-tri-O-acetyl-1,2-O-(1-cyanoethylidene)- α -D-glucopyranose as the by-product in 11.5% yield (Scheme 37).^[218,220]



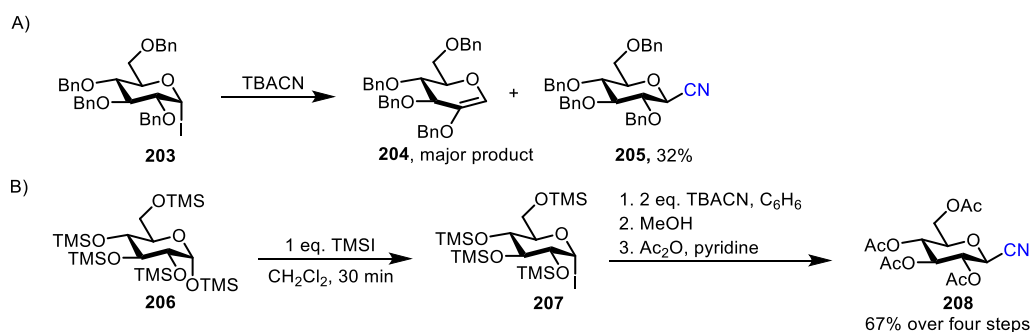
Scheme 37: Examples of glycosyl cyanide synthesis from per-*O*-acetylated glycosyl bromides.^[218,220]

Glycosyl fluorides have been also used as sugar donors to access glycosyl cyanides. In 1991, K. N. Drew and P. H. Gross first reported the synthesis of fully protected glycosyl cyanides by treatment of 2,3:5,6-di-*O*-isopropylidene-*D*-mannofuranosyl fluoride and 2,3:5,6-di-*O*-isopropylidene-*D*-mannopyranosyl fluoride with Et_2AlCN in THF (Scheme 38).^[217] Their protective group strategy completely excluded the formation of cyanoethylidene side products due to neighboring group participation as shown above. However, this process generated a mixture of both anomers of furanosyl cyanides and isocyanides (i. e., a four-component mixture of α -CN, α -NC, β -CN, and β -NC) which could not be separated according to the authors.^[217]



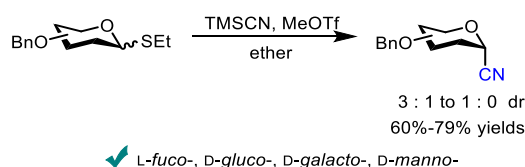
Scheme 38: Examples of glycosyl cyanide synthesis from acetal protected glycosyl fluorides.^[217]

Displacement of glycosyl iodide by a cyanide source (such as tetrabutylammonium cyanide) could also provide glycosyl cyanides.^[7] However, this process is strongly dependent of the choice of the protecting groups. For example, the reaction of per-*O*-benzylglucosyl iodide **203** with TBACN gave the unwanted *endo*-glycal **204** as the major product (Scheme 39A).^[219] The cyanation reaction could be significantly improved by changing benzyl groups to silyl groups. The higher electron-donating capability of the latter protecting groups may suppress the side elimination reaction by decreasing the acidity of the C-2 hydrogen (Scheme 39B).^[7]



Scheme 39: Examples of glycosyl cyanide synthesis from differently protected glycosyl iodides.^[7,219]

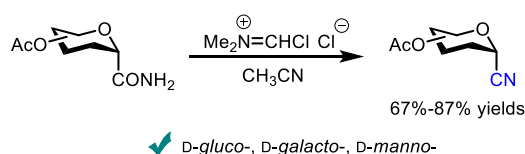
In addition to glycosyl halides, other activated glycosides, such as thioglycosides, can also act as sugar donors to produce glycosyl cyanides. In 1997, Y. Igarashi and co-workers synthesized several α -glycosyl cyanides in the *L-fuco* and *D-gluco* series using TMSCN and MeOTf in ether (Scheme 40).^[221] In contrast to the processes described above from glycosyl halides,^[7,217–219] this method produced glyconitriles mainly in α -form. It should be noted, however, that this approach showed modest stereocontrol in the *D-galacto* and *D-manno* series.



Scheme 40: Examples of glycosyl cyanide synthesis from thioglycosides.^[221]

✓ Dehydration of corresponding amides to obtain glycosyl cyanides

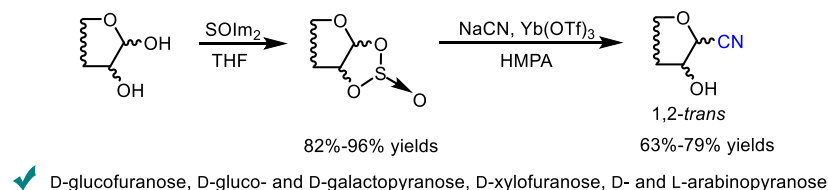
In 1983, G. Grynkiewicz and J. N. Bemiller disclosed a way to obtain aldopyranosyl cyanides by dehydrating the corresponding amides (Scheme 41).^[222] Peracetylated-2,6-anhydroheptonamides were thus dehydrated using *N*-(chloromethylene)-*N*-methylmethanaminium chloride, generated *in situ* from oxalyl chloride and *N,N*-dimethylformamide, to give α -glycopyranosyl cyanides in good yields.^[222] The drawback of this method is that the precursor of the glycosyl cyanides were prepared in low yields by photochemical addition of formamide to 2,3,4,6-tetra-*O*-acetyl-hex-1-enitols.^[223,224]



Scheme 41: Examples of glycosyl cyanide synthesis *via* amide dehydration.^[222]

✓ S_N2 -ring opening of 1,2-*O*-sulfinyl sugars

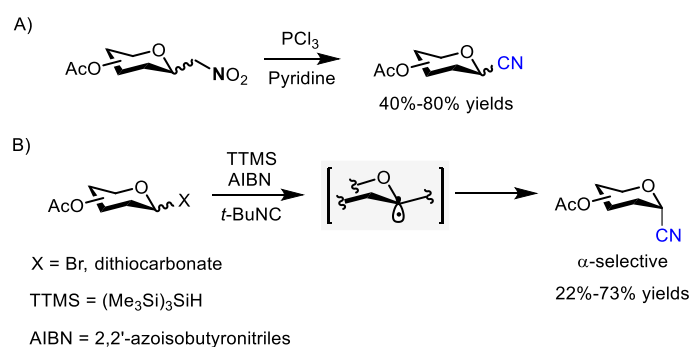
S_N2 -ring opening of 1,2-*O*-sulfinyl monosaccharides using sodium cyanide in the presence of a catalytic amount of ytterbium triflate is an efficient strategy for the efficient stereoselective synthesis of 1,2-*trans*-glycosyl cyanides (Scheme 42).^[225] In addition, the ring-opening reaction releases a free hydroxyl group at C-2 position which is ready for further decoration. The sulfinyl starting materials were prepared from the corresponding 1,2-diols in 82% to 96% yields.^[225] The synthesis of the 1,2-diol precursors may require multi-step preparation from relatively expensive glycal starting materials *via* reaction sequence involving deacetylation, benzylation, and dihydroxylation.^[225]



Scheme 42: Examples of glycosyl cyanide synthesis by S_N2 -ring-opening of 1,2-*O*-sulfinyl sugars.^[225]

✓ Miscellaneous

In addition to the methods mentioned above, it has been shown that glycopyranosyl cyanides could be obtained by reduction of C-glycopyranosyl nitromethanes using PCl_3 and pyridine (Scheme 43A),^[226] or by way of pseudoanomeric radicals generated from glycosyl dithiocarbonates or glycosyl bromides (Scheme 43B).^[227] The latter approach provides α -cyanoglycosides in high diastereoselectivity. Both methods employed per-*O*-acetylated sugar donors.



Scheme 43: A) PCl_3 -mediated reduction of C-glycosyl nitromethanes.^[226] B) Glycosyl radical cyanation.^[227]

1.2 Recent developments in the ring-opening of 1,6-anhydro sugars

1,6-Anhydrosugars have shown immense value as important synthons to synthesize a wide range of biologically potent glycoconjugates, oligosaccharides, antibiotics and natural products. Their unique [3.2.1] bicyclic skeleton, controlled by the 1,6-anhydro bridge, leads to

a rigid 1C_4 conformation, which contrasts with the corresponding hexopyranoses adopting usually a 4C_1 conformation (Figure 89).^[228] As well, this particular framework provides opportunities for high regio- and stereocontrol in diverse reactions. The dual protection at both C-1 and C-6 positions saves protecting group manipulations and the release of the primary hydroxyl group at C-6 allows its direct functionalization or orthogonal protection.^[228] In recent years, newer methodologies for ring-opening reactions of 1,6-anhydro sugars have been extensively investigated, and will be briefly presented according to the nucleophiles involved in the ring-opening process, comprising *N*-nucleophiles, *C*-nucleophiles, *S*-nucleophiles, and other nucleophiles.^[213] We will focus on methods that are directly related to our objective of developing a cyanide ring-opening of 1,6-anhydro sugars.

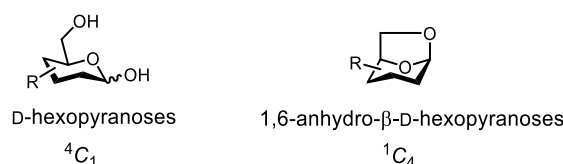
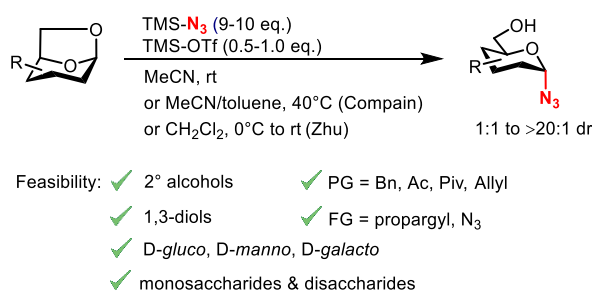


Figure 89: 4C_1 conformation for D-hexopyranoses and 1C_4 conformation for 1,6-anhydro- β -D-hexopyranoses.

➤ Ring-opening with *N*-nucleophiles

In the early 1990's, Furuhashi and co-workers reported the first example of ring-opening reactions for 1,6-anhydro sugars with *N*-nucleophiles to access 5-fluorouracil nucleosides in the presence of SnCl_4 .^[229] More than 20 years later, further nucleophilic ring-opening reactions of this type were based on using TMSN_3 as the *N*-nucleophile source to generate glycosyl azides. These compounds are valuable and powerful carbohydrate building blocks in organic and medicinal chemistry. They have indeed found many applications in the synthesis of *N*-glycopeptides, triazolyl glycoconjugates, or amino sugars.^[230,231] A stereocontrolled synthesis of α -glycosyl azides by ring-opening of 1,6-anhydro sugars was described by our team and the group of Zhu (Scheme 44).^[232,233] The optimal reaction conditions were a combination of TMSOTf as the Lewis acid catalyst with a large excess of trimethylsilyl azide (TMSN_3). Meanwhile, the reaction scope of this methodology was investigated, observing moderate to high levels of diastereoselectivity.



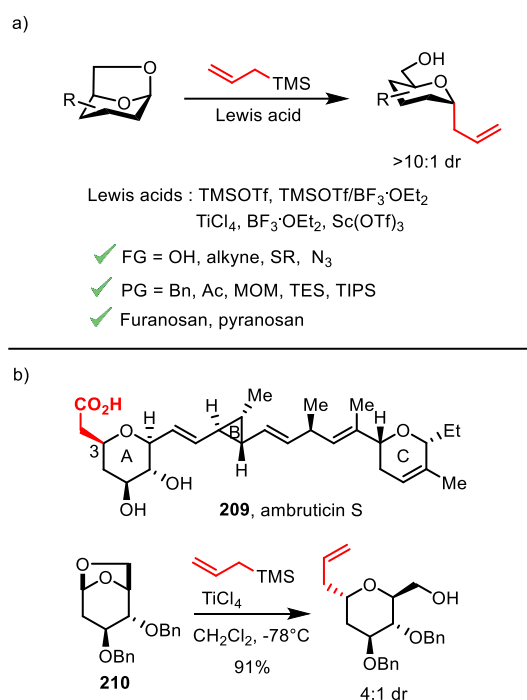
Scheme 44: Ring-opening of 1,6-anhydro sugars with TMSN_3 .^[232,233]

➤ Ring-opening with *C*-nucleophiles

As mentioned above, *C*-glycosides constitute an important class of glycomimetics and are unlikely to be hydrolyzed by enzymes. The ring-opening of 1,6-anhydro sugars with *C*-nucleophiles provides an efficient way to afford highly diastereoselective *C*-glycosides with a

free OH at C-6.

Allylation of 1,6-anhydro sugars in the presence of Lewis acid (Scheme 45a) is indeed a feasible and popular way to introduce a versatile alkene group that allows further decoration of the aglycon part.^[213] For example, the total synthesis of (+)-ambruticin S (**209**) by Martin and co-workers hinged on TiCl₄-mediated allylation of dibenzyl anhydro sugar **210**. Further installation of the carboxymethyl side chain at C-3 position completed the construction of the A-ring subunit of (+)-ambruticin S (Scheme 45b).^[234]



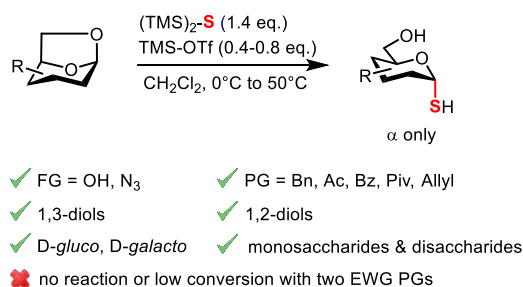
Scheme 45: a) Ring-opening of 1,6-anhydro sugars with TMS-allyl;^[213] b) Example of allyl C-glycosides as building blocks.^[234]

➤ Ring-opening with S-nucleophiles

Thioglycosides, replacing the glycosidic oxygen atom of *O*-glycosides with a sulfur atom, are valuable glycomimetic derivatives that have received considerable attention in efforts to construct glycomimetics of interest. As the *S*-glycosidic bond has a higher resistance to both chemical and enzymatic hydrolysis than the *O*-glycosidic bond, *S*-glycosides have been used as inhibitors of enzymes.^[235] Moreover, this class of glycomimetics has been found in a plethora of drugs, biologically active agents, and natural products.^[235,236] In addition, 1-thioglycosides are routinely used as glycosylation donors in building diverse glycosidic linkages.^[237] Owing to the importance of this key building blocks in glycoscience, the methods for their construction have attracted much attention and have been extensively explored. Ring-opening of 1,6-anhydrosugars in the presence of a proper sulfide source allows access to thioglycosides.

For instance, in 2008, the group of Zhu reported a direct and stereospecific method for the synthesis of α -glycosyl thiols by 1,6-anhydrosugars ring-opening reactions.^[238] The reactions were performed with commercially available bis(trimethylsilyl)sulfide as the sulfide source and catalyzed by TMSOTf, leading to α -glycosyl thiols in excellent yields. In 2011, Zhu and co-workers described the applicability of this method to a wide range of substrates, differing in sugar units, protecting and functional group patterns, and glycosidic linkages (Scheme 46).^[239]

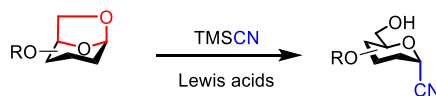
Almost all reactions were highly stereoselective and proceeded in good to excellent yields, except for the less reactive substrates carrying two electron-withdrawing acetyl groups.



Scheme 46: Strategy for the synthesis of glycosyl thiols by ring-opening reactions of 1,6-anhydrosugars. [213,238,239]

In general, as the examples described above, TMSOTf catalyzed ring-opening reactions of 1,6-anhydrosugars with various trimethyl silyl nucleophiles tend to be α -selective. In order to explain the observed diastereoselectivities, Zhu postulated a concerted S_N2 substitution mechanism for the ring-opening of 1,6-anhydrosugars by (TMS)₂S.^[239] Alternatively, the α -selectivity observed may be explained by postulating a preferential nucleophilic attack along axial trajectories on the most reactive/favored half-chair of the glycosyl cation intermediate (See part III.2 of the present chapter).

Based on literature precedents mentioned above and our own research, our objective was to develop a new access to glycosyl cyanides based on TMSCN ring-opening of 1,6-anhydrosugars (Scheme 47).



Scheme 47: Our project : synthesis of α -glycosyl cyanides by TMSCN ring-opening of 1,6-anhydrosugars.

II Stereoselective ring-opening of 1,6-anhydro sugars for the synthesis of glycosyl cyanides

II.1 Principal methods for the synthesis of 1,6-anhydro sugars

1,6-Anhydro- β -D-glucopyranose **211** (Figure 90) is the longest known and most readily available compound among the 1,6-anhydro- β -D-hexopyranoses series. Tanret first prepared it as a well-defined compound in 1894.^[240] 1,6-Anhydro- β -D-glucopyranose is also referred to as levoglucosan which coins from “levo” - levorotatory optical activity -, “gluco” for glucose configuration, and “an” (for anhydro). Levoglucosan **211** preparation can be achieved on a kilogram scale by pyrolysis of starch under reduced pressure.^[241] On the other hand, the corresponding D-mannosan **212** could be obtained in only 8% yield by pyrolysis of ivory nut meal.^[228,242] The pyrolytic strategies display many drawbacks including the concomitant formation of diverse by-products which render the isolation of the target 1,6-anhydro sugars

difficult. Consequently, alternative synthetic methods to prepare these types of sugars more reliably and cleanly have been developed.

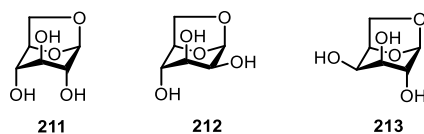
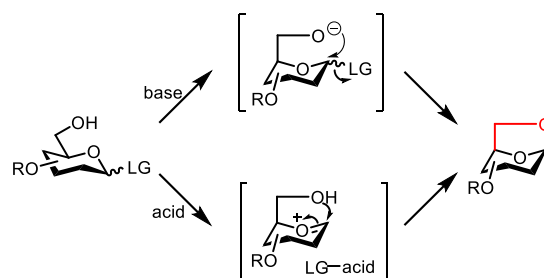


Figure 90: Configuration of common 1,6-anhydro- β -D-hexopyranoses.

The existing strategies for synthesizing 1,6-anhydrohexopyranoses on the basis of intramolecular 1,6-cyclization of hexoses and their derivatives can be broadly classified into three main categories.

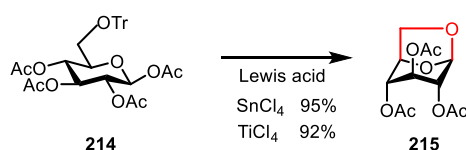
✓ **Leaving group at the anomeric position under basic or acidic conditions**

1,6-Cyclizations of hexoses carrying a good leaving group at the anomeric position can be achieved under basic conditions *via* an alkoxide intermediate or under acidic conditions through an oxocarbenium ion intermediate (Scheme 48).



Scheme 48: Synthesis of 1,6-anhydrohexopyranoses under basic or acidic conditions.

Treating the relevant phenyl glycosides with alkali is one of the often adopted methods to afford levoglucosan **211** and D-galactosan **213** (excluding D-mannosan **212**).^[228] 1,6-Cyclizations can also proceed smoothly under acidic conditions, and various Lewis acids have been used to facilitate the reactions. Rao and Nagarajan studied for example the use of anhydrous SnCl_4 and TiCl_4 to prepare the acetyl-protected levoglucosan **215** in excellent yields of 95% and 92%, respectively (Scheme 49).^[243]

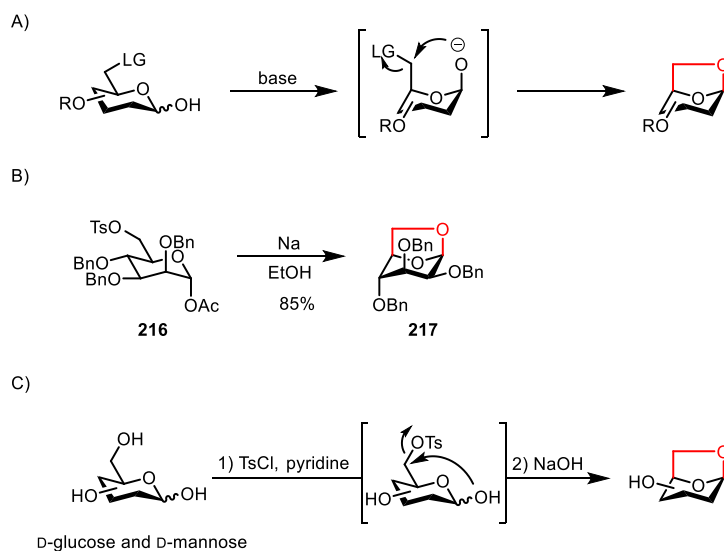


Scheme 49: Preparation of levoglucosan derivative **215** using SnCl_4 or TiCl_4 .^[243]

✓ **Leaving group at C-6**

Alternatively, treatment of substrates bearing a leaving group at C-6 position under basic conditions provides the expected anhydrosugar products *via* intramolecular nucleophilic displacement (Scheme 50A). This method is handy for synthesizing D-mannose **212**, which cannot be afforded through alkaline degradation of glycosides. Sondheimer and co-workers produced the desired 1,6-anhydro-2,3,4-tri-*O*-benzyl- β -D-mannopyranose **217** by treating the

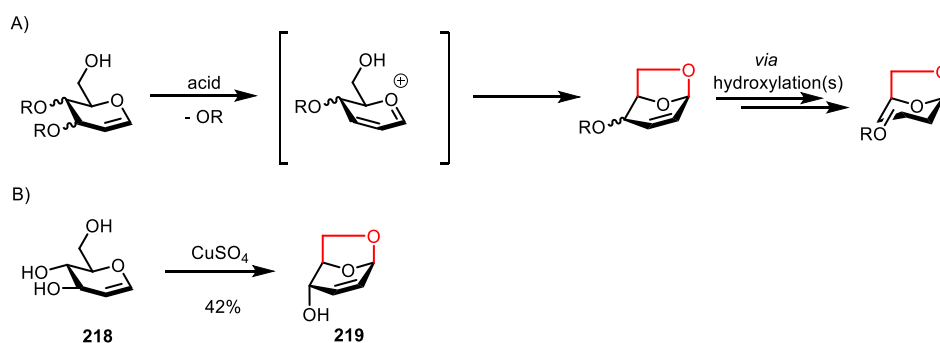
precursor **216** with sodium ethoxide in an 85% yield (Scheme 50B).^[244] Fraser-Reid described an efficient strategy to prepare levoglucosan **211** and D-mannosan **212** starting from totally unprotected D-glucose and D-mannose, respectively. The reactions occurred first with regioselective 6-O tosylation, followed by intramolecular nucleophilic displacement of the tosyl group leading to the desired 1,6-cyclisation (Scheme 50C).^[245,246]



Scheme 50: Synthesis of 1,6-anhydropyranoses by intramolecular displacement of a leaving group at C-6 position under basic conditions.^[244–246]

✓ **1,6-cyclisation via intramolecular Ferrier rearrangement of glycols**

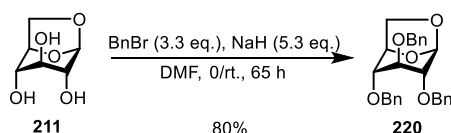
1,6-Anhydro sugars can also be provided by intramolecular Ferrier rearrangement (Scheme 51A). For example, Oberdorfer and co-workers obtained the bridged glucoside **219** (42% yield) via 1,6-cyclisation of **218** in the presence of a considerable excess of anhydrous cupric sulfate (Scheme 51B).^[247]



Scheme 51: Synthesis of 1,6-anhydropyranoses by intramolecular Ferrier rearrangement of glycols.^[247]

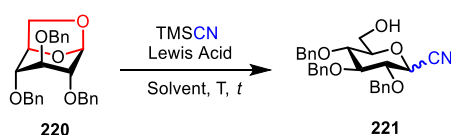
II.2 Exploring cyanide ring-opening of 1,6-anhydrosugars and identification of optimized reaction conditions

The known fully benzylated levoglucosan **220**^[248] (Scheme 52) was chosen as the model substrate to test the feasibility of our project for two main reasons. First, it only takes a single step to prepare **220** from commercially available levoglucosan **211** upon treatment with NaH and benzyl bromide in DMF solution.^[249] Secondly, levoglucosan **220** was used by our team for optimization studies in the development of a new access towards α -glycosyl azides,^[232] allowing interesting comparison studies between both systems (cyanation *versus* azidation).



Scheme 52: Synthesis of perbenzylated levoglucosan **220**.

Based on previous related studies on the synthesis of α -glycosyl azides,^[232,233,250] the feasibility of our approach was first evaluated with TMSCN as the cyanide source in combination with TMSOTf as the Lewis acid (Scheme 53). First attempts performed in MeCN from 1,6-anhydro-D-glucose **220**^[248] using 0.5-1 equiv. of TMSOTf and 5-10 equiv. of TMSCN provided the desired glucosyl cyanide **221** in modest yields and with a low degree of stereocontrol (Table 23, entries 1-3). A first screening revealed that the choice of the solvent is a key factor in controlling the efficiency and stereoselectivity of the ring-opening process. The first significant improvements were indeed obtained with CH₂Cl₂. Running the reaction in CH₂Cl₂ instead of MeCN led to diastereomeric ratios of up to 6.4:1 and to higher yields, but required prolonged reaction times (entries 4-7). The loss of stereocontrol observed with acetonitrile is in line with its participating role as a nucleophile and, as a consequence, the probable formation of α -glycosyl nitrilium intermediates.^[251] Lowering the excess of TMSCN (from 5 to 2 equiv.) had a detrimental impact on the reaction time and the yield (entries 5 and 6). High stereoselectivity was obtained in toluene (entries 8-13). In the presence of 0.5 equiv. of TMSOTf and 5 equiv. of TMSCN, α -glucosyl cyanide **221** was obtained as a single diastereoisomer in 78% yield at 40 °C (entry 8). Adjusting the concentration to 0.2 M (entry 9) provided a good balance between shorter reaction time, high yield and diastereomeric control (entries 8-10). Other reaction conditions involving higher temperatures or lower Lewis acid loading were screened without improving the efficiency of the process (entries 11-12). The use of a mixture of toluene and MeCN (5 : 1) led to slightly lower yields and stereoselectivities without reducing the reaction time (entry 13). Lower stereocontrol was observed with ZnI₂. This Lewis acid had to be used in stoichiometric quantities to maintain good yields (entries 14-16). The use of BF₃·OEt₂ or Sc(OTf)₃ resulted in lower diastereoselectivities and isolated yields (entries 17-19), whereas degradation of the starting material was observed with stoichiometric amount of TiCl₄ at -40 °C (entry 20).



Scheme 53: TMSCN-ring-opening of 1,6-anhydro-D-glucose **220** under different conditions (see table 23).

Entry ^a	TMSCN [equiv.]	Lewis acid ^b	Solvent	t [h]	T[°C]	Yield ^c (%)	α/β ratio ^d
1	10	TMSOTf (0.5)	MeCN	4.5	0-rt	56	1:1
2	5	TMSOTf (0.5)	MeCN	4	0-rt	57	1:1.3
3	5	TMSOTf (1)	MeCN	2.5	0-rt	54	1:1.2
4	5	TMSOTf (1)	CH ₂ Cl ₂	72	0-rt	86	6.1:1
5	5	TMSOTf (0.5)	CH ₂ Cl ₂	73	0-rt	75	6.4:1
6	2	TMSOTf (0.5)	CH ₂ Cl ₂	144	0-rt	36	4.2:1 ^e
7	5	TMSOTf (0.5)	CH ₂ Cl ₂	76	Δ	73	6.8:1 ^e
8	5	TMSOTf (0.5)	toluene	75	0/rt/40	78	α only
9 ^f	5	TMSOTf (0.5)	toluene	47	0/rt/40	84	88:1 ^e
10 ^g	5	TMSOTf (0.5)	toluene	25	rt-40	79	27:1
11	5	TMSOTf (0.25)	toluene	168	0/rt/40	88	92:1 ^e
12	5	TMSOTf (0.5)	toluene	52	0/rt/60	19	α only ^e
13	5	TMSOTf (0.5)	toluene ^h	70	0/rt/40	80	9:1
14	5	ZnI ₂ (1)	CH ₂ Cl ₂	20	0-rt	83	2.6:1
15	5	ZnI ₂ (1)	toluene	19	0-rt	85	8.6:1
16	5	ZnI ₂ (0.5)	toluene	24	0-rt	~50	7.5:1 ^e
17	5	BF ₃ .OEt ₂ (1)	MeCN	0.5	0	19	1:2.8 ^e
18	5	BF ₃ .OEt ₂ (1)	CH ₂ Cl ₂	0.5	0	23	1:1.6 ^e
19	5	Sc(OTf) ₃ (1)	toluene	23	-78-rt	46	1.4:1 ^e
20	5	TiCl ₄ (1)	toluene	0.5	-40	^j	^j

^a Reactions performed at a concentration of 0.1 M unless otherwise stated. ^b Number of equivalents in parentheses. ^c isolated yields of **221**. ^d Determined by ¹H NMR of the crude reaction mixture. ^e Determined after separation of the anomers on silica gel. ^f Reaction performed at a concentration of 0.2 M. ^g Reaction performed at a concentration of 0.3 M. ^h Reaction performed in a 5:1 (v/v) mixture of toluene/MeCN. ⁱ Degradation products were observed on TLC and NMR spectra.

Table 23: Optimization of the ring-opening reaction.^[a]

III Scope investigation of the ring-opening reaction

The scope of the reaction was then studied on diverse 1,6-anhydrosugars with various protecting group patterns and structural complexity in the *D-gluco*, *D-manno*, and *D-galacto* series (Figure 91).

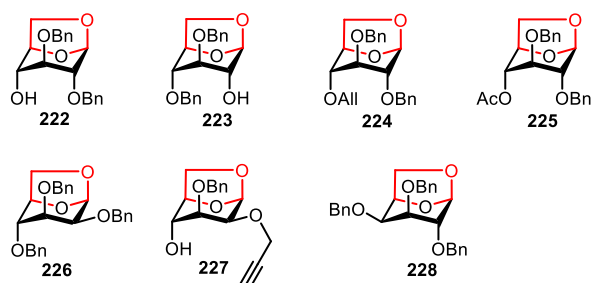
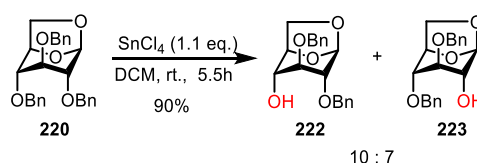


Figure 91: Prepared 1,6-anhydrosugars for scope extension.

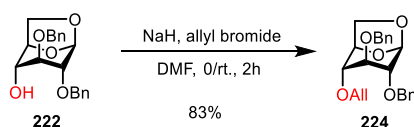
III.1 Synthesis of 1,6-anhydrosugar substrates

In order to investigate the effect of stereochemistry at C-2 and C-4 positions on the ring-opening reactions, the partially unprotected levoglucosan substrates **222** and **223** were synthesized. According to Ohruï and co-workers' protocol, regioselective de-*O*-benzylation of fully benzylated levoglucosan **220** catalyzed by SnCl₄ gave regioisomers **222** and **223** in high yields (Scheme 54).^[252]



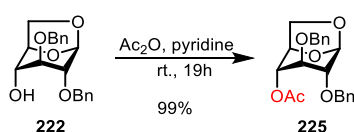
Scheme 54: Regioselective de-*O*-benzylation of fully benzylated levoglucosan **220**.^[252]

The free OH group at C-4 in compound **222** was allylated with allyl bromide in the presence of NaH,^[253] to give the desired 1,6-anhydrosugar **224** to investigate further the scope of protecting groups in ring-opening conditions (Scheme 55).



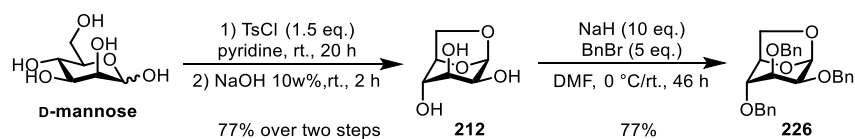
Scheme 55: Allylation of compound **222**.^[253]

In addition, the free OH group at C-4 of compound **222** was acetylated using Ac₂O/Pyridine 1:2 (v/v), forming the corresponding acylated 1,6-anhydrosugar **225** in 99% yield (Scheme 56), to assess the influence of electron-withdrawing protecting groups on the ring-opening process.



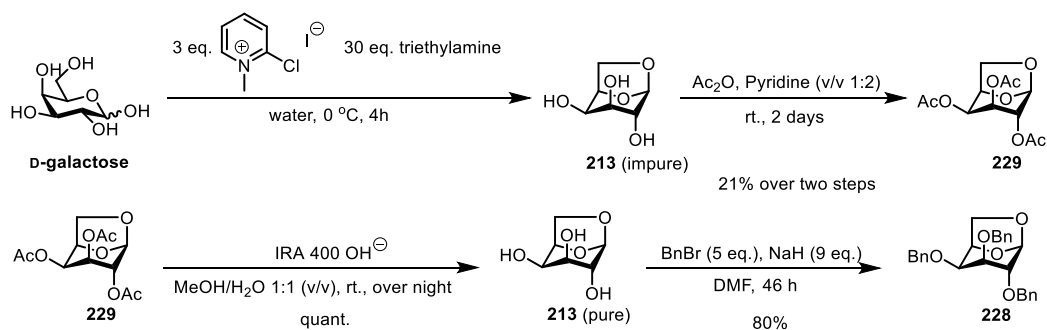
Scheme 56: Synthesis of partially acylated 1,6-anhydrosugar **225**.

Commercially available D-mannose was converted into D-mannosan **212** (Scheme 57).^[246] Subsequently, **212** was perbenzylated under classical conditions to give the expected 1,6-anhydrosugar **226** in 77% yield.



Scheme 57: Synthesis of perbenzylated 1,6-anhydrosugar **226**.

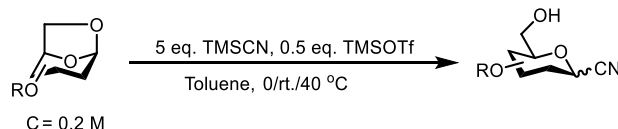
The corresponding perbenzylated 1,6-anhydrogalactopyranose **228** was prepared as well. To get access to unprotected D-galactosan **213**, we followed the one-step protocol described by Tanaka *et al.*, starting from commercially available D-galactose through an intramolecular dehydration reaction. We, however, used 2-chloro-1-methylpyridinium iodide as dehydrative condensing agent instead of 2-chloro-1,3-dimethyl imidazolium chloride (Scheme 58).^[254] Although the reaction for synthesizing D-galactosan **213** proceeded under relatively mild conditions without employing any protecting group, the removal of the excess of 2-chloro-1-methylpyridinium iodide and protonated triethylamine proved difficult. The presence of these unconsumed reagents was highly detrimental to the following benzylation step. Therefore, the obtained impure D-galactosan **213** was peracetylated to facilitate the purification step. Pure D-galactosan **213** obtained after basic deacetylation was then treated with benzyl bromide in the presence of NaH to give the desired 1,6-anhydrosugar **228**.



Scheme 58: Synthesis of substrate in D-manno series.

III.2 Substrate scope studies

With the optimized conditions in hands (Table 23, entry 9) (Scheme 59), the scope of the ring-opening reaction was examined (Table 24). The 1,6-anhydropyranose substrates were selected to enable investigation of the impact of the carbohydrate configurations and protecting group pattern on the outcome of the cyanation reaction.



Scheme 59: Optimized condition for the ring-opening reaction.

We were pleased to see that our procedure could be applied successfully to partially

unprotected analogues of 1,6-anhydro-D-glucopyranose **220** (entries 2-3). The 4-OH-free anhydro sugar **222** could be converted directly into the corresponding α -glucosyl cyanide **230 α** in good yields and high stereocontrol (entry 2). In contrast, TMSOTf-mediated ring-opening of the parent 2-OH-free analogue **223** led to the formation of the expected glucosyl cyanide **231 α** as the major product along with the corresponding 2-O-silylated compound **231' α** (entry 3). The silylated **231' α** was easily and quantitatively converted into **231 α** in the presence of 3N aqueous HCl solution in THF. After merging the two batches, glucosyl cyanide **231** was eventually obtained in 96% yields. Interestingly, 4-O-allyl levoglucosan **224** could be transformed into the corresponding cyanide **232 α** within a shorter time and in excellent yields and high α -selectivity (entry 4). The presence of an electron-withdrawing protecting group was found to have a detrimental effect on the efficiency of the process leading to a slow conversion of 4-OAc levoglucosan **225** (entry 5). The presence of the acetate group is likely to disfavour the formation of the putative oxocarbenium intermediate generated during the ring-opening process. The reaction scope was then evaluated on *D-galacto*- and *D-manno*-configured 1,6-anhydropyranoses to evaluate the influence of the configuration at C-2 and C-4 on the efficiency and the stereochemical outcome of the cyanation reaction (entries 6-8). Good yields up to 87% could be obtained for both series of anhydrosugars. The interest of the ring-opening process within the context of click chemistry was for example demonstrated with the synthesis of 2-propargyl mannosyl cyanide **235** (entry 7).^[160] However, as previously observed for related process leading to the formation of mannosyl azides,^[232] the ring-opening of 1,6-mannopyranosyl derivatives proceeded with significant loss of stereoselectivity (entries 6-7). A much better stereocontrol was achieved in the *D-galacto* series as shown with α -galactosyl cyanides **236** which were obtained with a good d.r. of 5:1 (entry 8). It should be noted, however, that the α/β -glycosyl cyanides synthesized in this study could be, in most cases, easily separated by flash chromatography on silica gel.

Entry ^a	Substrate	Product	Time (h)	Yield ^b (%)	α/β ratio ^c
1			48	84	88:1
2			49	75	25:1 ^d
3			63	61 35	9:1 ^d > 20:1 ^c
4			31	93	48:1 ^d
5				4	- ^e
6			72	63	1:1.4 ^d
7			163	81	1:2.3
8			196	87	5:1 ^d

^a Reaction conditions: 1,6-anhydro sugar/TMSCN/TMSOTf (1:5:0.5) in toluene at 40°C. ^b Isolated yields. ^c Determined after separation of the anomers on silica gel. ^d Determined by ¹H NMR of the crude reaction mixture. ^e Degradation products were observed on TLC and NMR spectra.

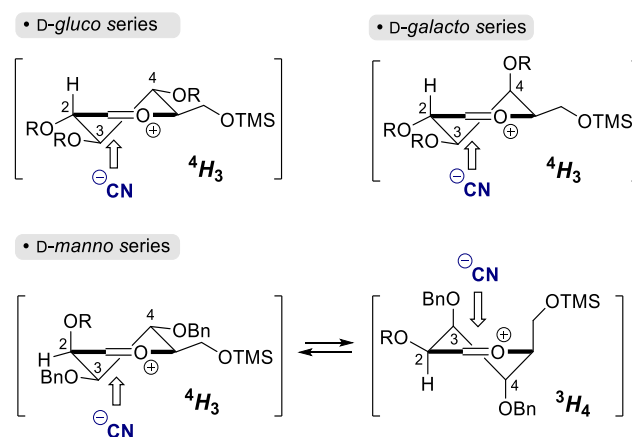
Table 24: Scope of 1,6-anhydro sugar ring-opening.^a

It should also be noted that the typical absorption band of C≡N (2000-2300 cm⁻¹ region) is not observed in the IR spectra of the glycosyl cyanides synthesized. This phenomenon which was noted previously is typical of α -cyano ethers.^[218,222,255] Analysis of both NMR and mass spectra for compounds **221**, **230-236**, however, demonstrated unambiguously the structures of the products obtained.

The stereochemical outcome of the cyanation reaction is consistent with the Woerpel model.^[256-258] The α -stereoselectivity observed in the *D-gluco* and *D-galacto* may be explained by preferential nucleophilic attack along axial trajectories on the most favoured/reactive half chair of the glycosyl oxocarbenium ion intermediate (Scheme 60). This approach minimizes torsional strain during the transition to the final chair conformation and is sterically

unhindered. In the *D-gluco* and *D-galacto* series, the 4H_3 conformers are strongly favoured by two main factors. Firstly, the hydroxymethyl side chain at C-5 is in the favoured pseudoequatorial position and, secondly, the electron-donating C-2 carbon-hydrogen bond is axial, maintaining the stabilizing hyperconjugation with the 2p orbital on the electrophilic carbon atom.^[259–261] In the *D-galacto* series, the 4H_3 conformation is further stabilized by the axial position of the electronegative C-4 alkoxy group, the electron density of which being donated to the positively charged endocyclic oxygen.^[260,261]

Switching from the *D-gluco* to the *D-manno* series by formal inversion of the configuration at C-2 led to partial destabilization of the 4H_3 conformers while increasing 3H_4 conformer stability (Scheme 60). Cyanide addition may thus also occur in the axial direction of the alternate 3H_4 conformers leading to a substantial proportion of β -D-mannosyl cyanide product. An alternative rationale for the α -stereoselectivity of the cyanation reaction could be also forwarded based on the ability of the electronegative, sterically undemanding cyano group to induce an anomeric effect.^[262] This possibility was however ruled out by an equilibration experiment performed on β -glycosyl cyanide **221 β** . Under typical ring-opening conditions (Table 23, entry 15), no epimerization of the anomeric center was observed after 2 days.



Scheme 60: Stereoselective nucleophilic attack on intermediate glycosyl oxocarbenium ion conformers.

IV Conclusion

In conclusion, we have developed a new access to glycosyl cyanides by way of TMSCN ring-opening of 1,6-anhydro sugars in 55 to 93% yields with good to high stereoselectivity in the *D-gluco* and *D-galacto* series. The level of stereocontrol was found to be strongly dependent of the solvent used and of the stereochemistry of the anhydrosugar substrates. A much lower stereoselectivity was indeed observed in the *D-manno* series or when MeCN is used as a solvent instead of toluene. Further exploration of the substrate scope of this reaction as well as its applications in the field of glycoscience represent the next immediate prospects of this present work.

General Conclusion

This thesis's main objective was to understand better the mechanism underlying the multivalent effect in glycosidase inhibition and to explore the minimum amount of ligands needed to reach a high effect.

To achieve this goal, we have prepared a set of cyclopeptoid-based clusters with a progressively reduced number of ligands. All the scaffolds of the novel clusters have the exact size as the one of the 36-valent cluster **135d** but contain only two (**I**), four alkynes with all possible distributions (**II**, **III**, **IV**), or twelve alkynes for **V** (Figure 43). Another key point of this structure-activity relationships study was the choice of three clickable ligands : the same tripod ligand **152** (Figure 44)^[136] used for cluster **135d**, a new monovalent ligand **153**, and a new “hindered” monovalent ligand **154**. The clickable monovalent iminosugar **153** has the same inhibiting epitope and dendron length as the ligand tripod **152**. Meanwhile, the new “hindered” monovalent ligand is also structurally related to the tripod, possessing the same inhibiting epitope as the tripod but only one inhitope for each clickable ligand, same dendron length, and similar hindrance compared to the tripod. The grafting of those ligands **152-154** onto multivalent scaffolds (**I** to **V**), respectively, were based on the efficient CuAAC reaction.

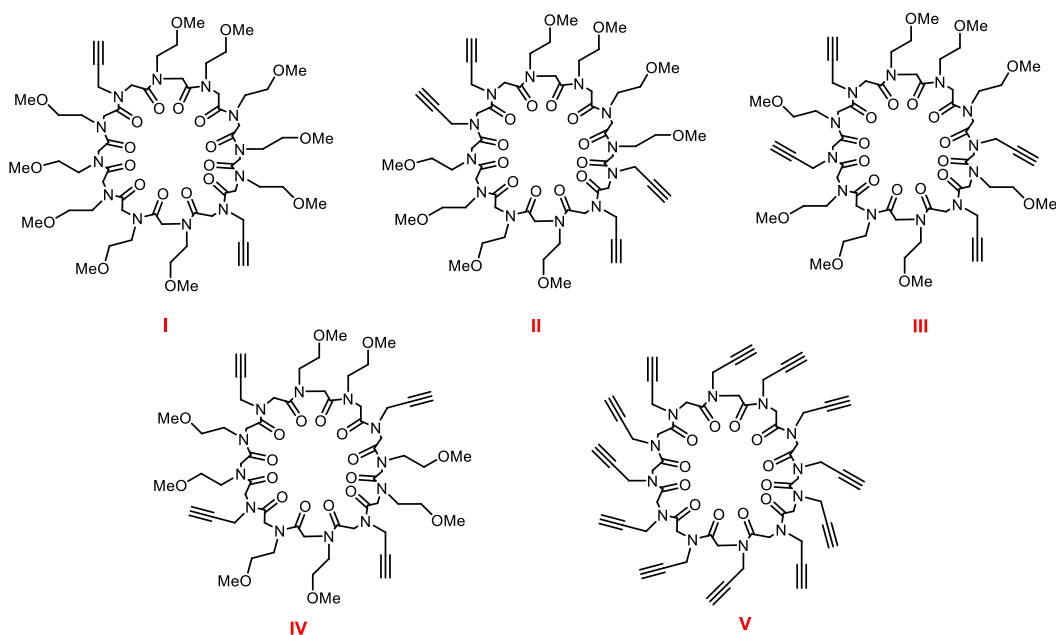


Figure 43: Structures of the different platforms I to V.

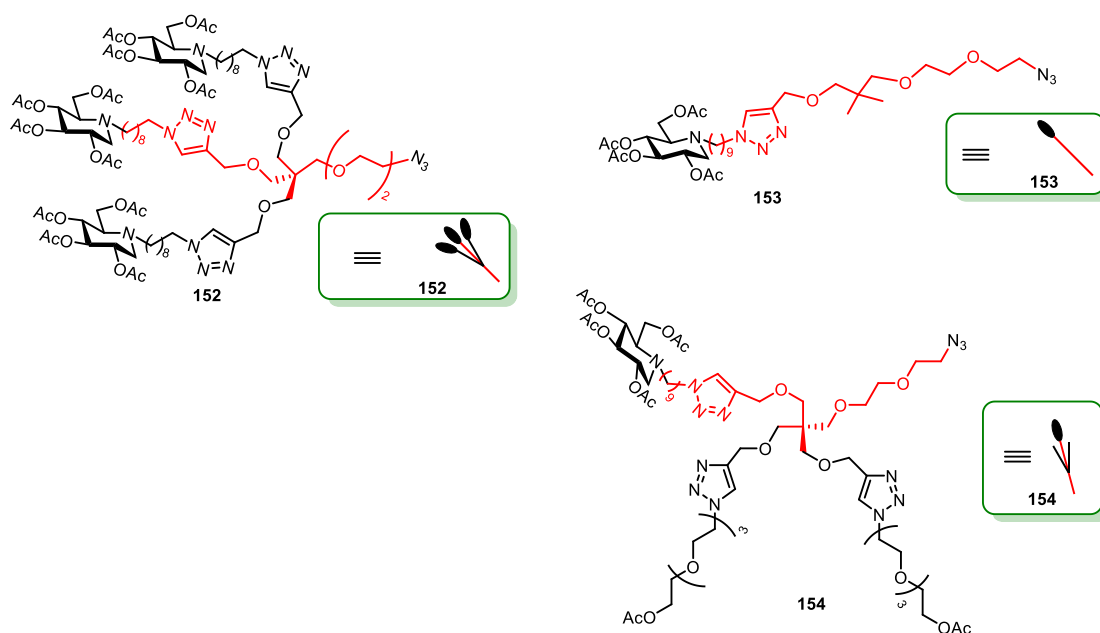


Figure 44: Structures of clickable ligands 152 to 154.

Inhibition assays performed on JBA-man showed that the divalent compound **194** had a K_i of 54 μM (Figure 92). All 4x1-valent inhibitors display similar inhibitory activities with K_i in the range of 2.2-3.1 μM . The K_i values of 4x3-valent inhibitors are around 0.1 μM . The 12x1-valent compound **201** and the “hindered” 12-valent compound **202** are the more potent inhibitors with K_i values of 0.042 μM and 0.074 μM , respectively.

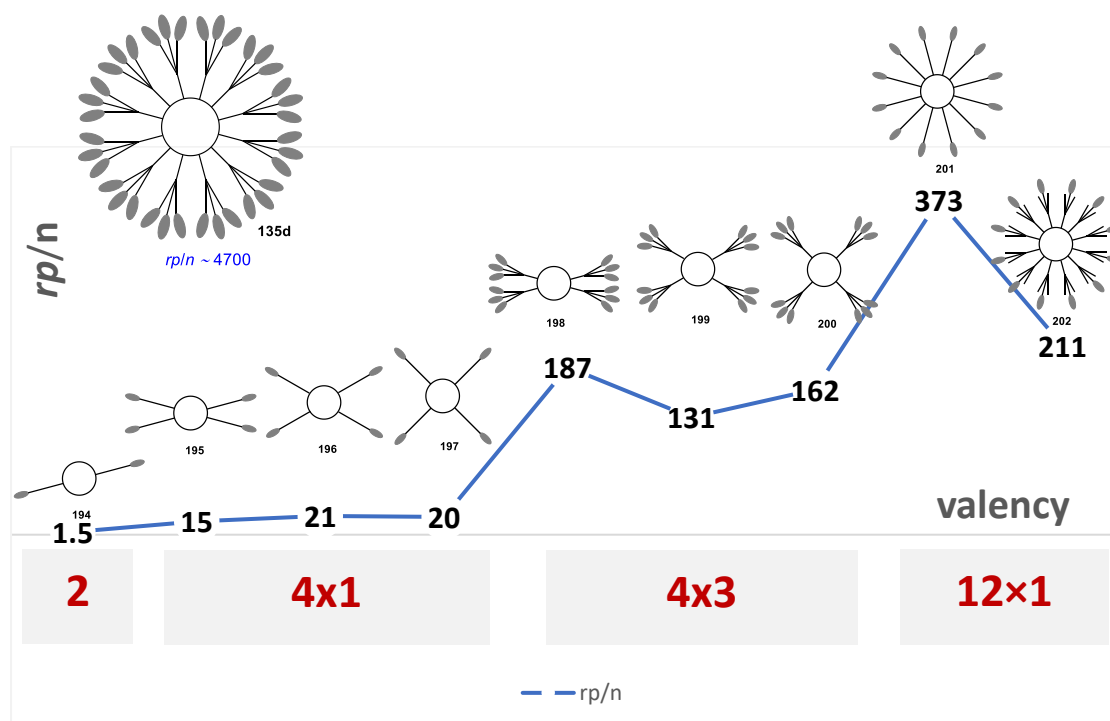


Figure 92: Valency-corrected relative inhibition potency (rp/n) of the novel inhibitors designed for the SAR study.

The stoichiometry of enzyme/inhibitor complexes was evaluated by analytical ultracentrifugation sedimentation velocity (AUC-SV). Among the results of the evaluated inhibitors (including 2-, 4-, 4×3-, 12-, and the “hindered” 12-valent clusters), only the 12×1-valent compound **201** forms a 2:1 enzyme-inhibitor complex.

Our study shows that the bind-and-recapture effect significantly impacts rp/n increment comparable to the one generated by the chelate effect. Indeed, despite the fact that the 36-valent cluster **135d** and its 12-valent closely related analog **201** have the same linker and scaffold size and, in addition, form a 2:1 complex, their rp/n values differ by one order of magnitude. More work remains to be done to understand this point fully. In particular, the data from AUC analysis can not explain the similar inhibitory activities of 4×3- and 12×1-valent clusters to each other, nor the large gap of inhibition potent between the “regular” 12-valent cluster **201** and the 36-valent cluster **135d**. To address the remaining perplexing points, a collaboration has been started with an expert in molecular modelling.

In connection with previous work performed in the group,^[9] we have developed a new method for the stereoselective synthesis of glycosyl cyanides by means of TMS-CN ring-opening of 1,6-anhydro sugars. Anomeric cyanation is indeed one of the most simple, practical C-extension methods to access C-glycosides. By this procedure, 1,6-anhydro sugars in the *D-gluco* and *D-galacto* series (with different protecting group patterns) can be converted into the corresponding cyanides in good to high α -selectivities, and the glycosyl cyanides were obtained in yields up to 93%. However, this method shows a much lower stereoselectivity but good yields in the *D-manno* series. The scope of the reaction should be further explored from 1,6-anhydrosugars with different functional groups and structural complexity. This method offers opportunity to synthesize multimeric inhibitors of carbohydrate-processing enzymes based on functionalized C-glycoside inhitopes.

Résumé de la thèse

Chapitre I : Les glycosidases et leur inhibition

Les enzymes dont les substrats sont des sucres représentent une famille majeure de protéines pour la plupart des organismes et environ 1 à 3 % des gènes de leurs génomes sont consacrés à leur codage.^[12] Parmi ces enzymes, les glycoside hydrolases (EC 3.2.1.-), plus communément appelées glycosidases, occupent une grande proportion et sont responsables de la catalyse de l'hydrolyse des liaisons glycosidiques. Après un descriptif de leurs mécanismes réactionnels,^[17,18,20,21] les grandes familles d'inhibiteurs réversibles de ces enzymes ont été parcourues^[35,26] avant de présenter le concept de multivalence qui est utilisé dans la nature pour atteindre des interactions fortes à partir de nombreuses interactions faibles.^[87,88]

La multivalence comme principe d'organisation chimique et de coopération pour l'inhibition des glycosidases. Ce concept a été intuitivement reconnu par les chimistes comme représentant une stratégie attrayante pour la conception de ligands présentant une spécificité de liaison élevée pour leurs récepteurs. La suramplification de l'affinité au-delà d'un effet statistique est appelée « effet cluster » ou « effet multivalent ».^[87] Après la découverte d'un effet multivalent puissant sur les enzymes avec un fullerène (C₆₀) portant 12 fois un inhibiteur réversible, la 1-déoxynojirimycine (DNJ),^[4] notre laboratoire a exploré le niveau maximal d'augmentation de l'affinité sur l' α -mannosidase de Jack Bean (JB α -man) à l'aide de clusters basés sur des plateformes cyclopeptoïdes portant plusieurs copies de la DNJ. La valence du cluster a été augmentée progressivement en utilisant une stratégie click basée sur des dendrons trivalents porteurs d'un azote^[136] et de plateformes cyclopeptoïdes propargylées de taille croissante.^[130,142] Dans cette série, le cluster **135d** (Fig. 42) ayant une valence de 36, a montré l'effet multivalent le plus puissant de la littérature pour une glycosidase.^[108-109,264-265] Cet effet exceptionnel a été expliqué par la formation d'un complexe de type sandwich entre un inhibiteur multivalent et deux enzymes par différentes techniques complémentaires.^[5] Notre laboratoire a également rapporté récemment les premières structures cristallines à haute résolution de la JB α -man dans les états apo et inhibé par le cluster 36-valent (Fig. 93).^[104] La structure cristallographique aux rayons X a montré que quatre têtes iminosucres du cluster 36-valent se lient à quatre sites actifs de deux molécules de JB α -man, confirmant ainsi la formation du complexe JB α -man/inhibiteur 2:1.

Objectifs de cette thèse. Il restait encore des questions non résolues et un potentiel d'amélioration. Quel est, par exemple, le rôle des iminosucres du cluster 36-valent non engagés dans le site actif ? Quels sont ceux qui participent à l'effet de glissement ? Quel est l'impact de l'encombrement stérique sur l'accessibilité des sites actifs ? Puisque seules quatre DNJ sont liées aux différents sites actifs, peut-on optimiser le système avec un cluster de valence 4 et obtenir un effet multivalent encore plus important ? Serait-il possible d'obtenir un complexe sandwich avec seulement deux têtes de DNJ dans des directions opposées si elles ont la bonne taille pour atteindre deux sites actifs de deux enzymes distinctes ? Comme le cluster 36-valent **135d** basé sur un noyau cyclopeptoïde a conduit au meilleur effet multivalent inhibiteur de la littérature et que son interaction avec JB α -man a été étudiée par différentes techniques, il était le meilleur candidat pour commencer une étude de type relations structure-activité (SAR). L'idée était d'éliminer progressivement certaines têtes inhibitrices pour répondre à ces questions et peut-être quantifier certains effets individuellement. Les clusters synthétisés au cours de cette thèse sont décrits dans la figure 42.

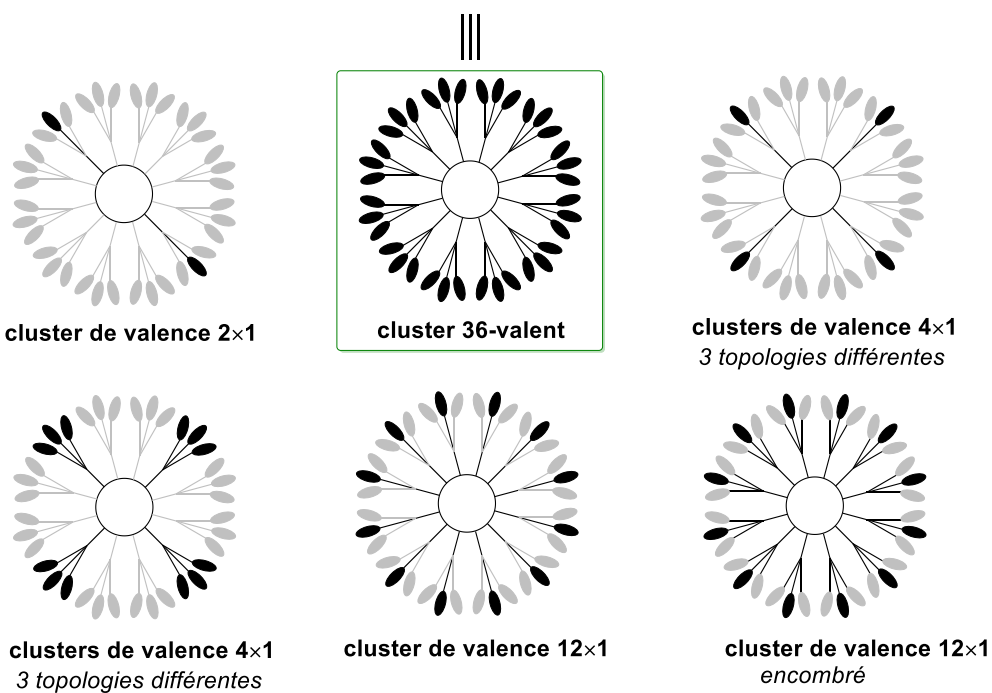
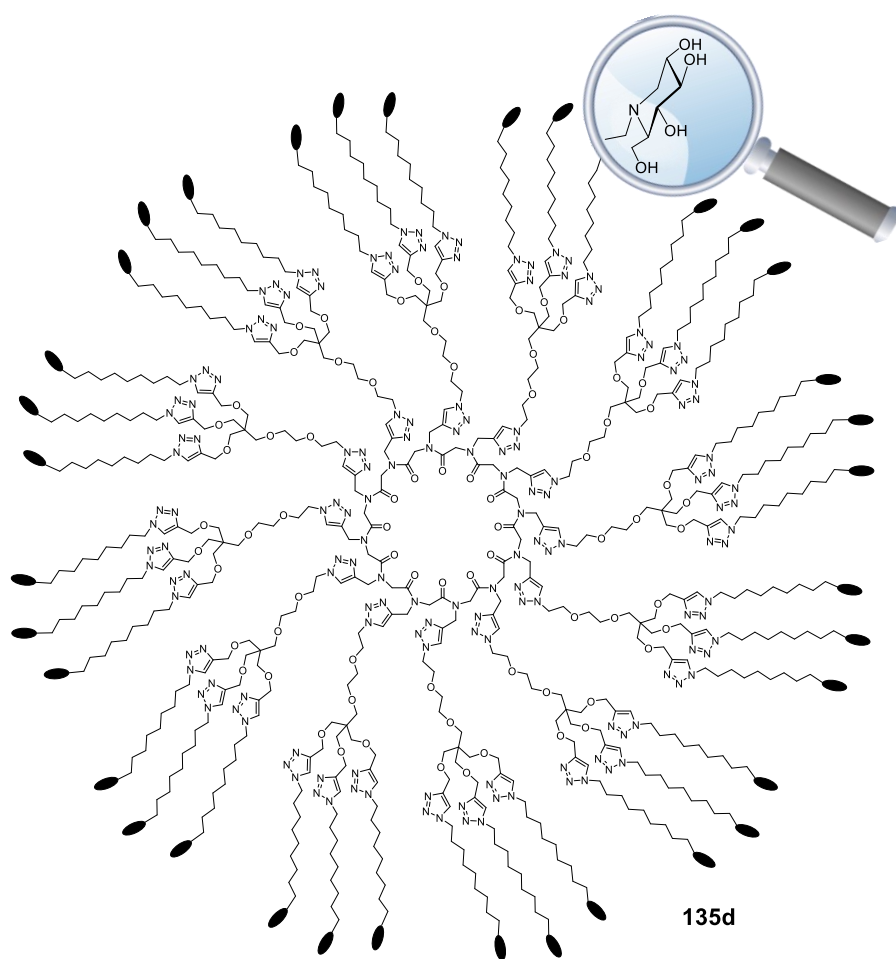


Figure 42 : Présentation des nouveaux clusters synthétisés au cours de cette thèse.

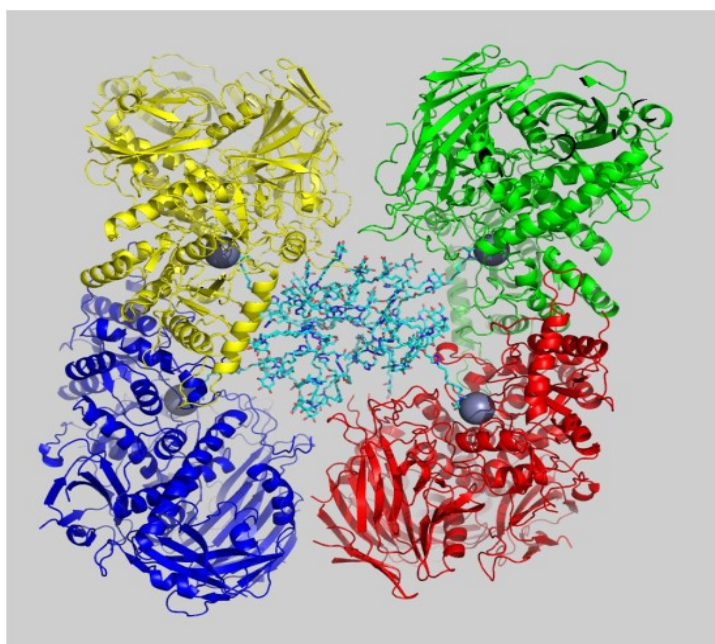


Figure 93. Représentation de deux enzymes de JB α -man, l'une formée par les parties verte et rouge et sa symétrique bleue et jaune. Au centre, le cluster flexible 36-valent 135d (cyan) modélisé à partir des quatre DNJ bien résolues au sein des quatre poches du site actif.^[104]

Chapitre II : Synthèse des principaux éléments composant les clusters ciblés

Cet ensemble de clusters 2, 4 et 12-valents a été envisagé *via* une cycloaddition catalysée au Cu(I) entre un azoture et un alcyne (CuAAC) entre les plateformes I à V préparées par approche sub-monomérique par nos collaborateurs de l'équipe du Pr. I. Izzo (Université de Salerne) (Figure 43). Ces nouvelles plateformes cyclopeptoides ont exactement la même taille que celle du cluster 36-valent mais ne contiennent que deux alcynes (I), quatre alcynes avec toutes les distributions possibles (II, III, IV) ou douze alcynes pour V.

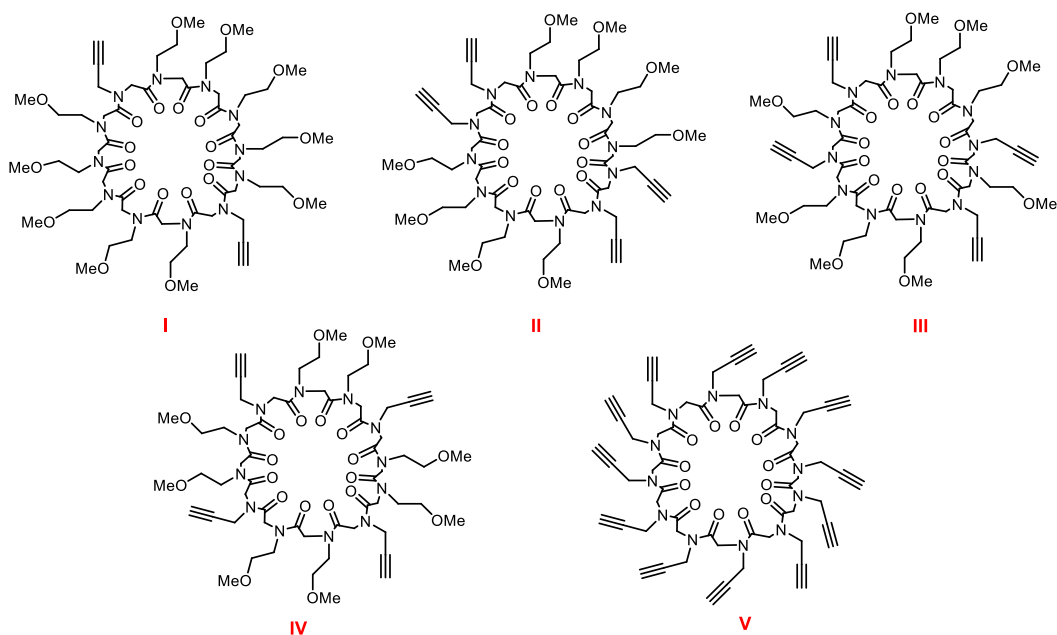


Figure 43 : Structures des différentes plateformes I à V.

L'idée était de les greffer avec le même ligand tripode utilisé pour le cluster **135d**^[5,136] mais aussi avec un nouveau ligand cliquable monovalent ayant exactement les mêmes caractéristiques (longueur et nature du bras). Enfin, un dernier ligand monovalent a été prévu pour être le plus proche possible de la structure du 36-valent mais avec une valence de 12 et une seule tête inhibitrice sur les trois présentes dans le tripode afin de pouvoir étudier les relations structure-activité.

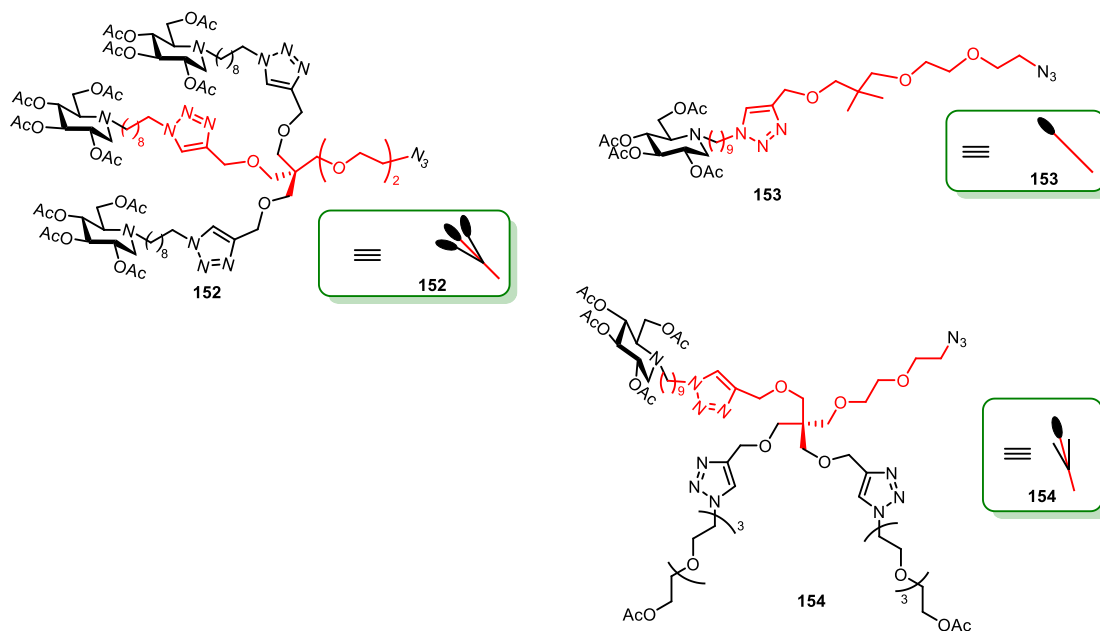


Figure 44 : Structures des ligands cliquables 152 à 154.

Tout d'abord, la tête inhibitrice cliquable **155** (Schéma 60) dérivée de la DNJ a été synthétisée en 7 étapes à partir du tetra-*O*-benzyl D-glucopyranose commercial selon la procédure usuelle

mise au point au laboratoire.^[189,190] Le bras **165** a également été préparé en deux étapes, par mono-propargylation du diol **163** suivie de l'alkylation de l'alcool restant (schéma 60).^[191] Ce dernier a été cliqué au dérivé **155** de la DNJ puis le chlorure a été substitué par un azoture avec un rendement de 92% pour ces deux étapes.

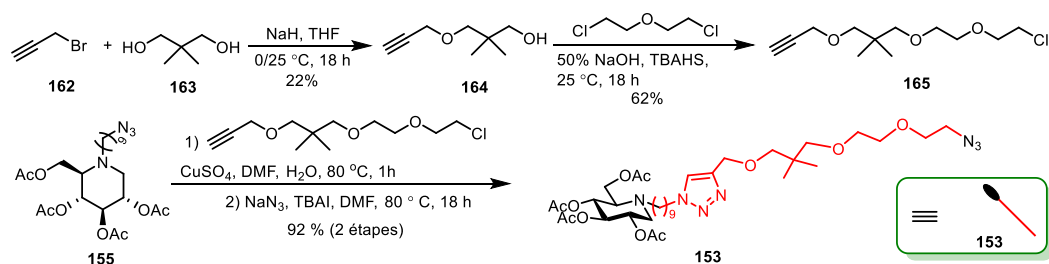


Schéma 61 : Synthèse du ligand **153** porteur d'un azoture.

Le tripode **152** portant trois inhitopes a également été préparé selon le protocole décrit par notre équipe.^[136]

Enfin, le ligand monovalent **154** ayant un encombrement similaire à celui du tripode a été également préparé. Pour ceci il a fallu distinguer 3 positions du pentaerythritol, afin d'y greffer les deux chaînes responsables de l'encombrement, le ligand DNJ **155** et le lien oligoéthylène glycol porteur de l'azoture final (schéma 62).

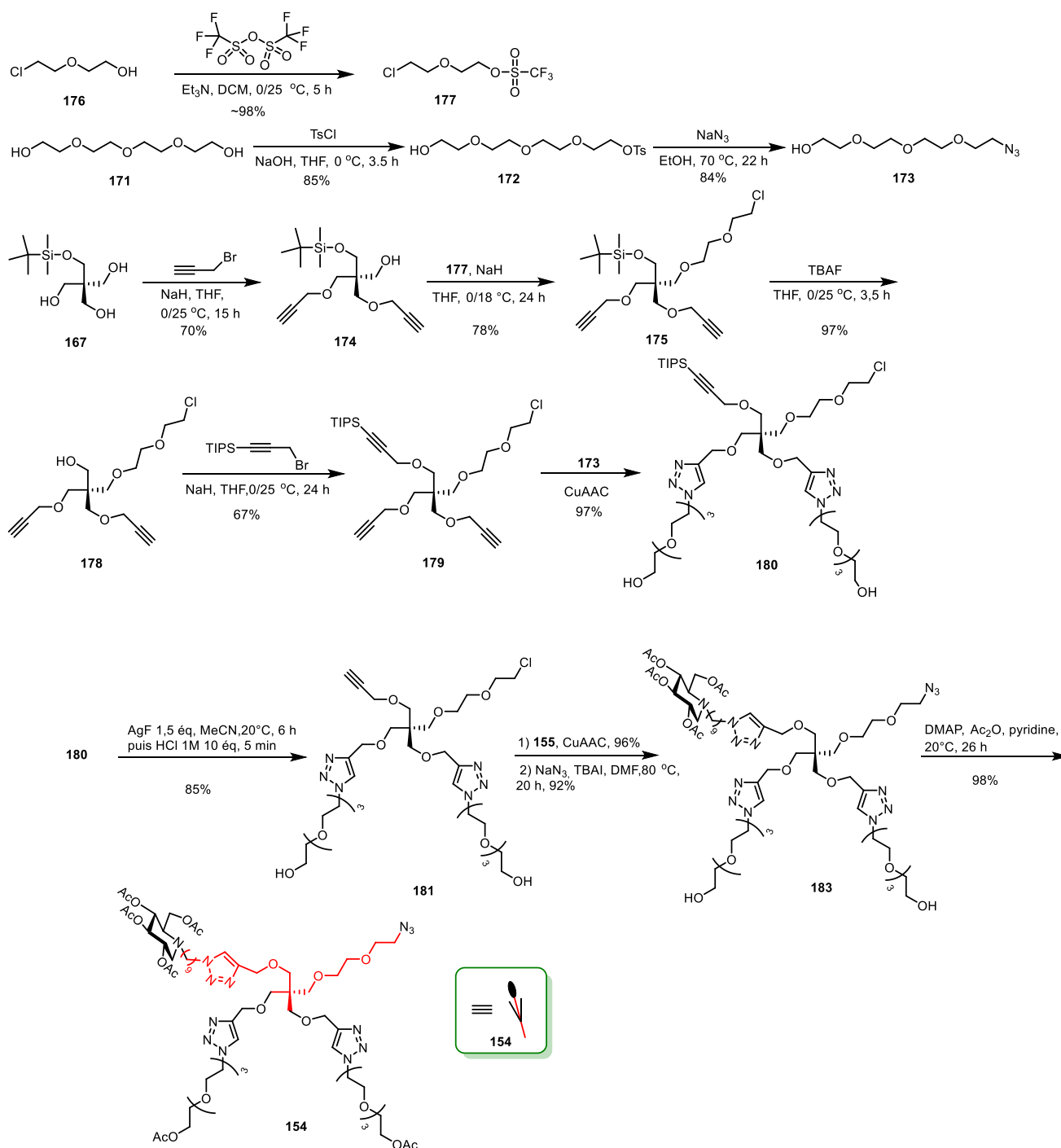


Schéma 62 : Synthèse du ligand encombré 154.

L'azoture **173**, mime des deux bras du tripode sans tête inhibitrice a été préparé en deux étapes en suivant le protocole de G. -J. Boons.^[194] Le composé **172** a été obtenu avec un rendement de 85% par monotosylation grâce à un large excès de tétraéthylène glycol. Le tosylate a ensuite été substitué par un azoture pour donner **173** avec un bon rendement de 84% (Schéma 15).

L'éther dipropargylique **174** a été obtenu à partir du pentaerythritol monosilylé **167** en jouant sur les proportions des réactifs.^[138,193] En réduisant encore plus les proportions de réactifs que lors de travaux précédents^[138] et grâce à l'addition par portions de 3 éq. d'hydrure de sodium,

suivie 45 min plus tard, de l'addition goutte à goutte de 4 éq. bromure de propargyle a conduit à un rendement de 70% (Schéma 62). L'étape suivante n'a pas été triviale en raison de l'encombrement stérique du groupe TBDMS sur **174**. Un panel de différentes conditions de réaction (en utilisant de l'hydroxyde de sodium aqueux et du TBAHS comme agent de transfert de phase ou l'hydrure de sodium dans le THF ou le DMF) a été testé pour tenter d'alkyler **174** directement avec le 2,2'-dichlorodiéthyl éther, cependant le produit désiré n'a pas été formé. En revanche, l'utilisation d'un meilleur groupement partant a été couronnée de succès avec l'alkylation de **174** par le trifluorométhanesulfonate **177** avec un rendement de 78%. Cette étape est inspirée de la stratégie d'A. Marinetti.^[196] Le groupement TBDMS a ensuite été déprotégé par TBAF, donnant **178** avec un rendement quasi quantitatif (Schéma 62). Le composé **178** a ensuite été propargylé par du bromure de propargyle protégé par un groupement TIPS pour conduire à **179** avec un rendement de 67%, puis **179** a été cliqué avec l'azoture d'oligoéthylène **173** donnant le composé **180** avec un excellent rendement dans les conditions classiques de CuAAC. Après cela, le groupe protecteur TIPS a été retiré suivant la stratégie de S. Kim^[198] avec un excellent rendement de 85% afin de pouvoir réagir par CuAAC avec la tête inhibitrice munie d'un azoture **155**. En effet, la désilylation *in situ* par du TBAF dans les conditions de CuAAC n'avait pas fonctionné malgré l'essai de différentes combinaisons de solvants et chauffages.

Chapitre III : Synthèse des clusters et étude des relations structure-activité de l'effet multivalent avec l' α -mannosidase de Jack Bean

Synthèse des clusters. Avec les ligands cliquables préparés dans le chapitre II et les échafaudages du Pr. Izzo en main, les différents précurseurs étaient disponibles pour synthétiser la bibliothèque d'iminosucres multivalents conçus pour notre étude SAR. Les deux étapes clés pour les obtenir ont été la réaction de CuAAC et la déprotection finale, à savoir l'étape de *O*-désacétylation en utilisant la résine basique amberlite IRA400(OH⁻).^[200] L'étape de CuAAC a été effectuée dans les conditions classiques avec des rendements allant de 53 à 82 % (tableau 25).

Produit	Plateforme	Ligand	CuSO ₄ ·5H ₂ O (éq.)	NaAsc (éq.)	DMF/H ₂ O (v/v)	T (°C)	Durée (h)	Rdt (%)	Valence
184	V	153	0.2	0.4	4/1	80	1	64	2×1
185	I	153	0.4	0.8	5/1	80	1	82	4×1
186	II	153	0.4	0.8	5/1	80	1	68	4×1
187	III	153	0.4	0.8	5/1	80	1	72	4×1
188	I	152	0.4	0.8	5/1	80	0.83	79	4×3
189	II	152	0.4	0.8	5/1	80	1	63	4×3
190	III	152	0.4	0.8	5/1	80	1	55	4×3
191	IV	153	1.5	3	4/1	80	1.5	68	12×1
192	IV	154	1.2	2.4	5/1	80	1.5	53	12×1

Tableau 25 : Conditions et rendements de la CuAAC pour générer les clusters peracétylés.

Seule la réaction avec le ligand encombré **183** s'est soldée par un échec dans ces conditions. En effet, en présence de 1,2 éq. de CuSO₄·5H₂O et de 2,4 éq. d'ascorbate de sodium, une large

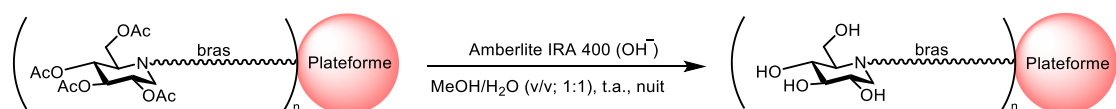


Schéma 30 : O-Désacétylation des différents clusters.

Cluster-OAc	Valence	Plateforme	Ligand	Cluster-OH	Rendements
184	2×1	V	153	194	quant.
185	4×1	I	153	195	quant.
186	4×1	II	153	196	92%
187	4×1	III	153	197	quant.
188	4×3	I	152	198	quant.
189	4×3	II	152	199	quant.
190	4×3	III	152	200	90%
191	12×1	IV	153	201	quant.
193	12×1	IV	154	202	quant.

Tableau 18 : Bilan des O-désacétylations et des composés finaux correspondants.

Evaluation biologique. Les constantes d'inhibition (K_i) ont ensuite été mesurées par spectrophotométrie à l'aide d'un lecteur de plaques 96 puits sur la JB α -man commerciale. Ces valeurs ont été comparées à celle du dérivé monovalent correspondant **100** afin de déterminer l'inhibition relative (rp) par rapport à ce dernier ainsi que la puissance d'inhibition relative corrigée en fonction de la valence (rp/n) (tableau 26).

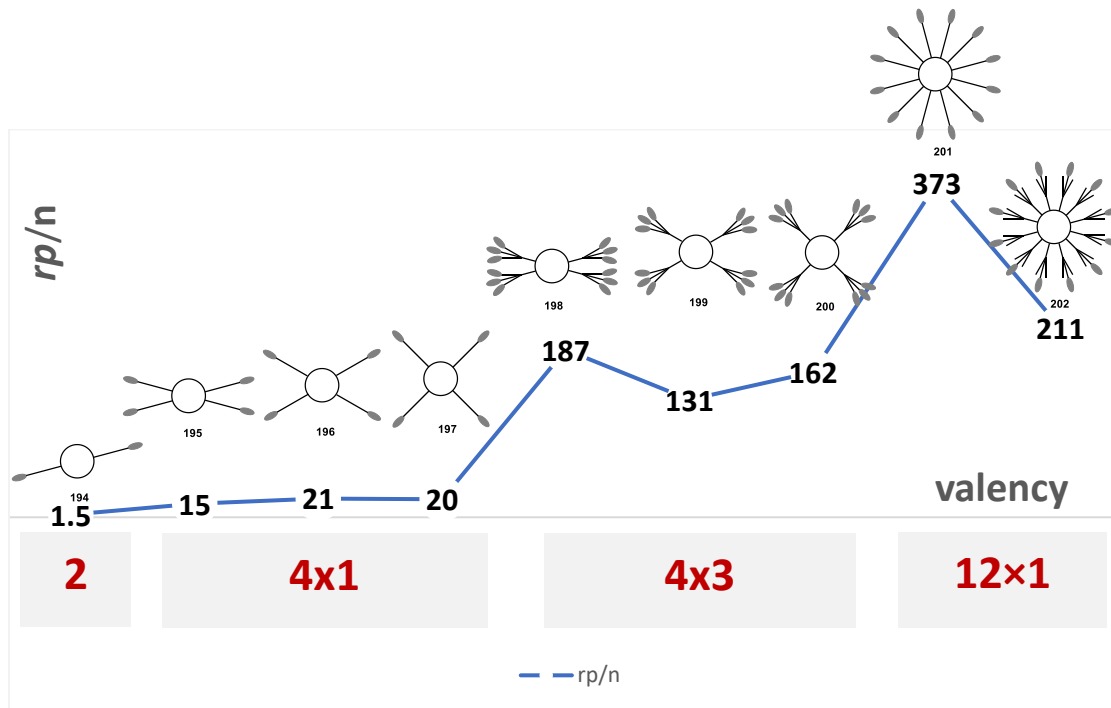


Figure 88: Récapitulatif des nouveaux inhibiteurs conçus pour l'étude SAR et de leur puissance d'inhibition relative corrigée par la valence (rp/n) .

Tous les inhibiteurs sont compétitifs. Pour les inhibiteurs les plus puissants (12 valents), la concentration en inhibiteur étant plus faible et par conséquent moins nettement supérieure à celle de l'enzyme, la concentration en inhibiteur libre doit prendre en compte la fraction qui est prise dans le complexe enzyme/inhibiteur. Les données ont donc été modélisées par le modèle « tight-binding » compétitif. Les résultats sont présentés sur la figure 88 et dans le tableau 26.

La stœchiométrie du complexe JBa-man/inhibiteur a été étudiée par ultracentrifugation analytique afin de savoir quels sont les clusters qui permettent la formation du sandwich 2:1.

Composé	Nombre DNJ	$K_i^{[a]}$	$rp^{[b]}$	$rp/n^{[c]}$	Stœchiométrie E/I
100	1	188	-	-	n.d.
194	2	54	3.5	1.7	1 :1
195	4	3.1	61	15	n.d.
196	4	2.2	85	21	n.d.
197	4	2.3	82	20	1 :1
198	12	0.084	2238	187	n.d.
199	12	0.12	1567	131	n.d.
200	12	0.097	1938	162	n.d.
201	12	0.042	4476	373	2 :1
202	12	0.074	2540	212	1 :1
135d	36	0.0011	170,000	4747	2 :1

[a] K_i (μM) obtenus en triplicats.

[b] Puissance d'inhibition relative (rp) = K_i (référence monovalente) / K_i (cluster).

[c] rp/n = rp /nombre d'unités DNJ.

Tableau 26. Constante d'inhibition (K_i en μM), augmentation d'affinité relative (rp), augmentation d'affinité relative par unité DNJ (rp/n) et stœchiométrie des clusters d'iminosucres avec l' α -mannosidase de Jack Bean obtenue par AUC-SV.

Discussion. D'après les résultats du tableau 26, l'inhibiteur divalent ne présente pas d'effet multivalent significatif et ne permet pas la formation du complexe sandwich malgré le fait qu'il soit théoriquement possible du point de vue de la géométrie et des distances. Ce résultat montre que le cross-linking entre deux enzymes ne peut pas se mettre en place sans l'apport entropique d'un autre mécanisme. Tous les inhibiteurs 4x1-valents présentent des effets multivalents similaires ($rp/n \sim 15-20$) suggérant que la géométrie centrale a peu d'influence sur l'interaction des inhibiteurs périphériques avec l'enzyme, ce qui peut s'expliquer par la flexibilité des bras qui compenserait la géométrie centrale différente pour les quatre clusters. De plus, ils ne permettent pas la formation de complexes 2:1 soulignant à nouveau le fait que la taille optimale de la plateforme et des espaceurs n'est pas un critère suffisant pour permettre la formation de ces agrégats. Lorsque l'effet de glissement est partiellement rétabli avec les clusters 4x3-valents **198-200**, en raison de l'augmentation de la concentration locale des inhibiteurs à proximité du site actif de l'enzyme, une augmentation d'un ordre de grandeur du rp/n est observée. Cependant, les valeurs de rp/n obtenues ici restent inférieures d'un ordre de grandeur à celle observée avec le cluster **135d** de valence 36. Pour les deux séries de clusters dérivés des plateformes tétravalentes, **195-197** et **198-200**, la position des bras au niveau de la plateforme n'a pas d'influence significative sur les valeurs d'inhibition observées, la flexibilité de leurs bras semble suffire à compenser une orientation éventuellement imparfaite de ces derniers. De façon remarquable, le cluster **373** est le meilleur de la série et se distingue également des autres en permettant la formation d'un complexe sandwich 2:1. En revanche, son rp/n reste quand même un ordre de grandeur en dessous de celui du 36-valent. C'est le cluster qui bénéficie de la symétrie la plus élevée avec une géométrie radiale semblant déterminante ici. Enfin, le cluster encombré **202** ayant une structure intermédiaire entre le **201** et le **135d**, ne se situe pas entre ces deux ni en termes d'affinité avec l'enzyme ni en termes de capacité à former des agrégats. L'encombrement apporté par les bras oligoéthylène glycol du cluster **202** ne semble donc pas apporter de bénéfice supplémentaire puisque son rp/n est inférieur à celui du 12-valent **51** réfutant ainsi

l'hypothèse de travail (encombrement stérique empêchant le substrat d'atteindre le site actif). Des simulations de dynamique moléculaire sont en cours afin de tenter d'expliquer ces résultats (collaboration avec Martin Spichy, LIMA).

Chapitre IV. Synthèse de cyanures de glycodides par ouverture de cycle 1,6-anhydro sur des sucres avec TMSCN

Le dernier chapitre de cette thèse repose sur un projet de méthodologie permettant un accès aisé à des C-glycosides. Ces derniers constituent un groupe essentiel de glycomimétiques stables face à l'hydrolyse. Ils ont suscité un intérêt croissant en raison de la présence de nombreux C-glycosides naturels présentant des activités biologiques intéressantes, telles que des propriétés antibactériennes, antitumorales et antivirales.^[6-8] En 2016, notre équipe a conçu des C-glycosides multivalents basés sur des noyaux fullerène ou β -cyclodextrine afin d'étudier les mécanismes sous-jacents aux effets multivalents observés dans l'inhibition des glycosidases.^[9] En lien avec cette étude, nous étions particulièrement intéressés par le développement d'une nouvelle approche vers les cyanures de glycosyle à partir de 1,6-anhydrosucres. Tout d'abord parce que la cyanation anomérique est l'une des méthodes d'insertion de carbone les plus simples et les plus pratiques pour accéder aux C-glycosides. Deuxièmement, les 1,6-anhydrosucres offrent de nombreux avantages en tant que sucres donneurs.^[213] La réaction d'ouverture de cycle avec des cyanures devrait fournir un accès direct aux précurseurs de C-glycosides portant un groupe hydroxyle libre en position C-6, limitant les manipulations de groupes protecteurs et permettant la conception de stratégies de synthèse convergentes.

Dans la littérature, les différentes stratégies d'accès aux cyanures de glycosides existantes reposent sur la cyanation d'halogénures de glycosyle à l'aide de différentes sources telles que $\text{Hg}(\text{CN})_2$,^[218,220] Et_2AlCN ,^[217] TBACN ^[219] ou la cyanation de thioglycosides par TMSCN.^[221] La déshydratation d'amides en position anomérique,^[222] la réduction de nitrométhane en position anomérique,^[226] l'ouverture de 1,2-O-sulfinyl^[225] par du cyanure de sodium ou la cyanation de radicaux anomériques en sont quelques exemples.^[227]

En outre, les 1,6-anhydrosucres ont montré leur potentiel en tant que précurseurs clés pour synthétiser une large gamme de glycoconjugués, d'oligosaccharides, d'antibiotiques et de produits naturels. Leur squelette bicyclique [3.2.1] unique, contrôlé par le pont 1,6-anhydro, conduit à une conformation ${}^1\text{C}_4$ rigide, qui contraste avec les hexopyranoses correspondants adoptant généralement une conformation ${}^4\text{C}_1$.^[228] La double protection des positions 1 et 6 permet d'éviter les manipulations des groupes protecteurs et conduit à la libération de l'alcool primaire en C-6 permettant sa fonctionnalisation directe ou sa protection orthogonale.^[228] De nouvelles méthodes d'ouverture de cycle 1,6-anhydro ont été récemment mises au point et sont décrites dans une revue récente.^[213]

Entrée ^a	TMSCN [équiv.]	Acide de Lewis ^b	Solvant	t [h]	T[°C]	Rendement ^c (%)	Ratio α/β
1	10	TMSOTf (0.5)	MeCN	4.5	0-t.a.	56	1:1
2	5	TMSOTf (0.5)	MeCN	4	0-t.a.	57	1:1.3
3	5	TMSOTf (1)	MeCN	2.5	0-t.a.	54	1:1.2
4	5	TMSOTf (1)	CH ₂ Cl ₂	72	0-t.a.	86	6.1:1
5	5	TMSOTf (0.5)	CH ₂ Cl ₂	73	0-t.a.	75	6.4:1
6	2	TMSOTf (0.5)	CH ₂ Cl ₂	144	0-t.a.	36	4.2:1 ^e
7	5	TMSOTf (0.5)	CH ₂ Cl ₂	76	Δ	73	6.8:1 ^e
8	5	TMSOTf (0.5)	toluène	75	0/t.a./40	78	α
9 ^f	5	TMSOTf (0.5)	toluène	47	0/t.a./40	84	88:1 ^e
10 ^g	5	TMSOTf (0.5)	toluène	25	t.a.-40	79	27:1
11	5	TMSOTf (0.25)	toluène	168	0/t.a./40	88	92:1 ^e
12	5	TMSOTf (0.5)	toluène	52	0/t.a./60	19	α ^e
13	5	TMSOTf (0.5)	toluène ^h	70	0/t.a./40	80	9:1
14	5	ZnI ₂ (1)	CH ₂ Cl ₂	20	0-t.a.	83	2.6:1
15	5	ZnI ₂ (1)	toluène	19	0-t.a.	85	8.6:1
16	5	ZnI ₂ (0.5)	toluène	24	0-t.a.	~50	7.5:1 ^e
17	5	BF ₃ .OEt ₂ (1)	MeCN	0.5	0	19	1:2.8 ^e
18	5	BF ₃ .OEt ₂ (1)	CH ₂ Cl ₂	0.5	0	23	1:1.6 ^e
19	5	Sc(OTf) ₃ (1)	toluène	23	-78-t.a.	46	1.4:1 ^e
20	5	TiCl ₄ (1)	toluène	0.5	-40	j	j

^a Réactions réalisées à une concentration de 0,1 M, sauf indication contraire. ^b Nombre d'équivalents entre parenthèses. ^c rendement isolé en composé **221**. ^d Déterminé par RMN ¹H sur le brut réactionnel. ^e Déterminé après séparation des anomères sur gel de silice. ^f Réaction effectuée à une concentration de 0,2 M. ^g Réaction effectuée à une concentration de 0,3 M. ^h Réaction effectuée dans un mélange 5:1 (v/v) de toluène/MeCN. ⁱ Des produits de dégradation ont été observés par CCM et par RMN.

Tableau 23: Optimisation de la réaction d'ouverture de cycle.

Inspirés par ces précédents, nous avons testé différentes conditions d'ouvertures du pont 1,6-anhydro du levoglucosan perbenzylé **220**, utilisé comme substrat modèle, par TMSCN, en présence de différents catalyseurs et solvants répertoriés dans le tableau 23.

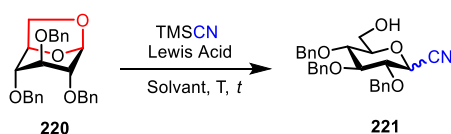
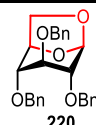
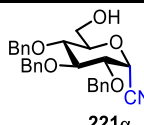
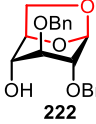
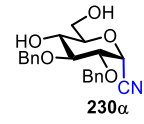
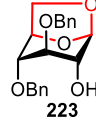
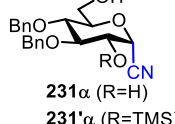

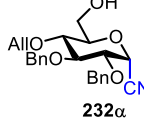
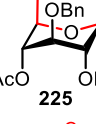
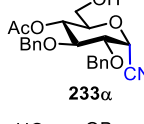
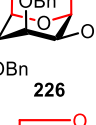
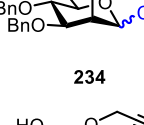
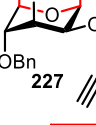
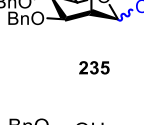
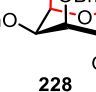
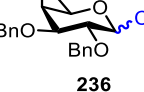


Schéma 53: Ouverture du cycle anhydro par le TMSCN sur le substrat modèle 1,6-anhydro-D-glucose **220** dans différentes conditions (voir tableau 23).

Les entrées 8 et 11 en présence d'une quantité catalytique (0,5 ou 0,25 éq.) de TMSOTf dans le toluène conduisent aux meilleures diastéréosélectivités avec cependant des durées de réaction assez longues. L'entrée 9, avec sa concentration deux fois plus élevée, a été considérée comme étant le meilleur compromis entre une durée raisonnable et des rendements/diastéréosélectivités élevés. Les autres catalyseurs conduisaient à des sélectivités moindres et le choix du toluène a été crucial pour une sélectivité maximale.

Dans un second temps, le champ d'application de la réaction a été étudié sur divers 1,6-anhydrosucres dans les séries *D-gluco*, *D-manno* et *D-galacto* en présence de différents groupes protecteurs (tableau 24).

Notre procédure a pu être appliquée avec succès aux analogues partiellement non protégés du 1,6-anhydro-D-glucopyranose **220** (entrées 2-3). L'anhydro **222** avec son alcool libre en position 4 a pu être converti directement en cyanure d' α -glucosyle **230 α** avec un bon rendement et une sélectivité élevée (entrée 2). En revanche, l'ouverture par le TMSOTf de l'analogue **223** avec l'alcool libre en position 2 a conduit à la formation du cyanure de glucosyle **231 α** attendu et du composé 2-O-silylé **231' α** correspondant (entrée 3). Ce dernier a été quantitativement converti en **231 α** en présence d'une solution aqueuse de HCl 3N dans le THF. En rassemblant les deux lots, le cyanure de glucosyle **231** a finalement été obtenu avec un rendement de 96%. D'autre part, le 4-O-allyl levoglucosan **224** a pu être converti en **232** dans un temps plus court et avec d'excellents rendements et une haute sélectivité en anomère α (entrée 4). La présence d'un groupe protecteur électro-attracteur s'est avérée néfaste avec une conversion très lente du 4-OAc levoglucosan **225** (entrée 5). En effet, La présence du groupe acétate est susceptible de défavoriser la formation du possible intermédiaire oxocarbénium généré lors de l'ouverture du cycle. Le champ d'application a ensuite été évalué sur des 1,6-anhydropyranoses de configuration *D-galacto* et *D-manno* afin d'évaluer l'influence de la configuration en C-2 et C-4 sur l'efficacité et la sélectivité de la réaction (entrées 6-8). De bons rendements allant jusqu'à 87% ont pu être obtenus pour les deux séries d'anhydrosucres. L'intérêt de cette réaction d'ouverture de cycle dans le contexte de la chimie click a été démontré avec la synthèse du cyanure de 2-propargyl mannopyranosyle **235** (entrée 7).^[160] Cependant, comme observé précédemment pour la formation d'azotures en série *D-manno*,^[232] l'ouverture de cycle des 1,6-mannopyranosyles a eu lieu avec une perte significative de stéréosélectivité (entrées 6-7). Un bien meilleur stéréocontrôle a été obtenu dans la série *D-galacto* comme le montre l'entrée 8, avec le cyanure d' α -galactosyle **236** obtenus avec un bon d.r. de 5:1. Même si la sélectivité de la réaction n'est pas complète, les α/β -glycosyl cyanides synthétisés dans cette étude ont pu être, dans la plupart des cas, facilement séparés par chromatographie flash sur gel de silice.

Entrée ^a	Substrat	Produit	durée (h)	Rendement ^b (%)	Ratio α/β^c
1	 220	 221 α	48	84	88:1
2	 222	 230 α	49	75	25:1 ^d
3	 223	 231 α (R=H) 231' α (R=TMS)	63	61 35	9:1 ^d > 20:1 ^c
4	 224	 232 α	31	93	48:1 ^d
5	 225	 233 α		4	- ^e
6	 226	 234	72	63	1:1.4 ^d
7	 227	 235	163	81	1:2.3
8	 228	 236	196	87	5:1 ^d

^a Conditions de la réaction : 1,6-anhydro/TMSCN/TMSOTf (1:5:0,5) dans le toluène à 40°C. ^b Rendements isolés. ^c Déterminés après séparation des anomères sur gel de silice. ^d Déterminés par RMN ¹H du brut réactionnel. ^e Produits de dégradation observés sur CCM et spectres RMN.

Tableau 24 : Champ d'application de l'ouverture du pont 1,6-anhydro.

La diastéréosélectivité de la réaction de cyanation est cohérent avec le modèle de Woerpel.^[256-258] La stéréosélectivité α observée dans les séries *D-gluco* et *D-galacto* peut s'expliquer par une attaque nucléophile préférentielle le long de trajectoires axiales sur la demi-chaîne la plus favorisée/réactive de l'intermédiaire oxocarbénium (Schéma 60). Cette approche – la moins encombrée – minimise également les effets de torsion pendant la transition vers la conformation chaise finale. Dans les séries *D-gluco* et *D-galacto*, les conformères ⁴H₃ sont fortement favorisés par deux facteurs principaux. Premièrement, la chaîne latérale hydroxyméthyle en C-5 est en position pseudo-équatoriale et deuxièmement, la liaison carbone-hydrogène donneuse d'électrons en C-2 est axiale, ce qui maintient l'hyperconjugaison stabilisante avec l'orbitale 2p sur l'atome de carbone électrophile.^[259-261] Dans la série *D-galacto*, la conformation ⁴H₃ est encore plus stabilisée par la position axiale de

l'alcoxy électrodonneur en position 4.^[260,261]

Le passage de la série *D-gluco* à la série *D-manno*, avec l'inversion formelle de la configuration en C-2, a conduit à une déstabilisation partielle des conformères 4H_3 tout en augmentant la stabilité des conformères 3H_4 (Schéma 60). L'addition du cyanure peut donc se produire dans la direction axiale des deux conformères possibles conduisant à une proportion substantielle de produit β . Une autre justification de la stéréosélectivité α de la réaction de cyanation pourrait également être proposée, basée sur la capacité du groupe cyano électronégatif et peu encombré à induire un effet anomérique.^[262] Cette possibilité a toutefois été écartée par une expérience d'équilibration réalisée sur l'isomère β **221**. Dans les conditions typiques d'ouverture de cycle (tableau 23, entrée 15), aucune épimérisation du centre anomérique n'a été observée après 2 jours.

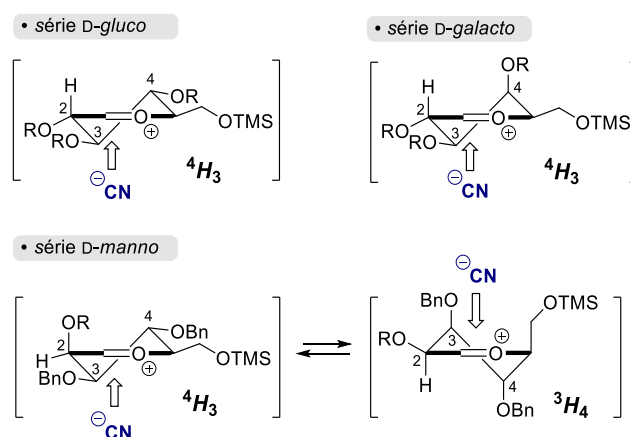


Schéma 60 : Attaque nucléophile stéréosélective sur des conformères de l'ion oxocarbénium.

En conclusion, nous avons développé un nouvel accès aux cyanures de glycosyle par ouverture du pont 1,6-anhydro de sucres par TMSCN avec des rendements allant de 55 à 93% et une stéréosélectivité bonne voire élevée dans les séries *D-gluco* et *D-galacto*. Le niveau de stéréocontrôle s'est avéré dépendre fortement du solvant utilisé et de la stéréochimie des substrats. Une stéréosélectivité beaucoup plus faible a en effet été observée dans la série *D-manno* ou lorsque l'acétonitrile est utilisé comme solvant à la place du toluène. L'exploration d'autres substrats pour cette réaction ainsi que de ses applications potentielles dans le domaine de la glycochimie représentent les prochaines perspectives de ce travail.

Bibliography

-
- [1] R. J. Nash, A. Kato, C.-Y. Yu, G. W. Fleet, *Future Med. Chem.* **2011**, *3*, 1513–1521.
- [2] A. Lohse, K. B. Jensen, K. Lundgren, M. Bols, *Bioorg. Med. Chem.* **1999**, *7*, 1965–1971.
- [3] J. Diot, M. I. García-Moreno, S. G. Gouin, C. O. Mellet, K. Haupt, J. Kovensky, *Org. Biomol. Chem.* **2008**, *7*, 357–363.
- [4] P. Compain, C. Decroocq, J. Iehl, M. Holler, D. Hazelard, T. Mena Barragán, C. Ortiz Mellet, J.-F. Nierengarten, *Angew. Chem. Int. Ed.* **2010**, *49*, 5753–5756.
- [5] M. L. Lepage, J. P. Schneider, A. Bodlenner, A. Meli, F. De Riccardis, M. Schmitt, C. Tarnus, N.-T. Nguyen-Huynh, Y.-N. Francois, E. Leize-Wagner, C. Birck, A. Cousido-Siah, A. Podjarny, I. Izzo, P. Compain, *Chem. - Eur. J.* **2016**, *22*, 5151–5155.
- [6] É. Bokor, S. Kun, D. Goyard, M. Tóth, J.-P. Praly, S. Vidal, L. Somsák, *Chem. Rev.* **2017**, *117*, 1687–1764.
- [7] A. S. Bhat, J. Gervay-Hague, *Org. Lett.* **2001**, *3*, 2081–2084.
- [8] C. Fischer, F. Lipata, J. Rohr, *J. Am. Chem. Soc.* **2003**, *125*, 7818–7819.
- [9] F. Stauffert, A. Bodlenner, T. M. Nguyet Trinh, M. I. García-Moreno, C. Ortiz Mellet, J.-F. Nierengarten, P. Compain, *New J. Chem.* **2016**, *40*, 7421–7430.
- [10] J. P. Kamerling, in *Compr. Glycosci.* (Ed.: H. Kamerling), Elsevier, Oxford, **2007**, pp. 1–38.
- [11] V. Lombard, H. Golaconda Ramulu, E. Drula, P. M. Coutinho, B. Henrissat, *Nucleic Acids Res.* **2014**, *42*, D490–D495.
- [12] G. J. Davies, T. M. Gloster, B. Henrissat, *Curr. Opin. Struct. Biol.* **2005**, *15*, 637–645.
- [13] R. Wolfenden, X. Lu, G. Young, *J. Am. Chem. Soc.* **1998**, *120*, 6814–6815.
- [14] B. Henrissat, *Biochem. J.* **1991**, *280*, 309–316.
- [15] B. Henrissat, A. Bairoch, *Biochem. J.* **1993**, *293*, 781–788.
- [16] “‘Glycoside hydrolase family classification’ in CAZypedia, available at URL <http://www.cazy.org/Glycoside-Hydrolases.html>, accessed 21 February 2021.,” **n.d.**
- [17] D. E. Koshland, *Biol. Rev.* **1953**, *28*, 416–436.
- [18] D. L. Zechel, S. G. Withers, *Acc. Chem. Res.* **2000**, *33*, 11–18.
- [19] J. D. McCarter, G. Stephen Withers, *Curr. Opin. Struct. Biol.* **1994**, *4*, 885–892.
- [20] W. W. Kallemeijn, M. D. Witte, T. Wennekes, J. M. F. G. Aerts, in *Adv. Carbohydr. Chem. Biochem.* (Ed.: D. Horton), Academic Press, **2014**, pp. 297–338.
- [21] S. W. Steve Withers, “‘Glycoside hydrolases’, in CAZypedia, available at URL https://www.cazypedia.org/index.php/Glycoside_hydrolases#bibkey_Terwisscha1995, accessed 21 February 2021,” **n.d.**
- [22] C. S. Rye, S. G. Withers, *Curr. Opin. Chem. Biol.* **2000**, *4*, 573–580.
- [23] B. L. Mark, D. J. Voadlo, S. Knapp, B. L. Triggs-Raine, S. G. Withers, M. N. G. James, *J. Biol. Chem.* **2001**, *276*, 10330–10337.
- [24] D. Piszkiwicz, T. C. Bruice, *J. Am. Chem. Soc.* **1968**, *90*, 2156–2163.
- [25] V. L. Yip, S. G. Withers, *Curr. Opin. Chem. Biol.* **2006**, *10*, 147–155.
- [26] N. F. Brás, N. M. Cerqueira, M. J. Ramos, P. A. Fernandes, *Expert Opin. Ther. Pat.* **2014**, *24*, 857–874.
- [27] Y. Suzuki, S. Ichinomiya, M. Kurosawa, M. Ohkubo, H. Watanabe, H. Iwasaki, J. Matsuda, Y. Noguchi, K. Takimoto, M. Itoh, M. Tabe, M. Iida, T. Kubo, S. Ogawa, E. Nanba, K. Higaki, K. Ohno, R. O. Brady, *Ann. Neurol.* **2007**, *62*, 671–675.
- [28] A. R. Sawkar, W.-C. Cheng, E. Beutler, C.-H. Wong, W. E. Balch, J. W. Kelly, *Proc. Natl. Acad. Sci.* **2002**, *99*, 15428–15433.
- [29] G. H.-F. Yam, N. Bosshard, C. Zuber, B. Steinmann, J. Roth, *Am. J. Physiol.-Cell Physiol.* **2006**, *290*, C1076–C1082.

- [30] A. J. Krentz, C. J. Bailey, *Drugs* **2005**, *65*, 385–411.
- [31] A. Mehta, N. Zitzmann, P. M. Rudd, T. M. Block, R. A. Dwek, *FEBS Lett.* **1998**, *430*, 17–22.
- [32] R. Hevey, *Pharmaceuticals* **2019**, *12*, 55.
- [33] R. Hevey, *Biomimetics* **2019**, *4*, 53.
- [34] N. Asano, *Cell. Mol. Life Sci.* **2009**, *66*, 1479–1492.
- [35] A. Tamburrini, C. Colombo, A. Bernardi, *Med. Res. Rev.* **2020**, *40*, 495–531.
- [36] R. Lahiri, A. A. Ansari, Y. D. Vankar, *Chem. Soc. Rev.* **2013**, *42*, 5102.
- [37] G. Horne, F. X. Wilson, J. Tinsley, D. H. Williams, R. Storer, *Drug Discov. Today* **2011**, *16*, 107–118.
- [38] R. a Dwek, N. Nichita-Branza, S. Petrescu, S. Pollock, P. Rudd, C. Scanlan, N. Zitzmann, *Liposome Treatment of Viral Infections*, **2008**, US2008138351A1.
- [39] A. Casas-Sanchez, A. Romero-Ramirez, E. Hargreaves, C. C. Ellis, B. I. Grajeda, I. Esteveao, E. I. Patterson, G. L. Hughes, I. C. Almeida, T. Zech, Á. Acosta-Serrano, *bioRxiv* **2021**.
- [40] S. Inouye, T. Tsuruoka, T. Nida, *J. Antibiot. (Tokyo)* **1966**, *19*, 288–292.
- [41] H. Paulsen, I. Sangster, K. Heyns, *Chem. Ber.* **1967**, *100*, 802–815.
- [42] M Yagi, T Kouno, Y. Aoyagi, H. Murai, *Nippon Nogei Kagaku Kaishi* **1976**, *50*, 571–572.
- [43] D. D. Schmidt, W. Frommer, L. Müller, E. Truscheit, *Naturwissenschaften* **1979**, *66*, 584–585.
- [44] S. Murao, S. Miyata, *Agric. Biol. Chem.* **1980**, *44*, 219–221.
- [45] Y. Ezure, S. Maruo, K. Miyazaki, M. Kawamata, *Agric. Biol. Chem.* **1985**, *49*, 1119–1125.
- [46] M. Koyama, S. Sakamura, *Agric. Biol. Chem.* **1974**, *38*, 1111–1112.
- [47] N. Asano, K. Oseki, H. Kizu, K. Matsui, *J. Med. Chem.* **1994**, *37*, 3701–3706.
- [48] T. M. Gloster, G. J. Davies, *Org. Biomol. Chem.* **2009**, *8*, 305–320.
- [49] Z. A. E. D., *Philos. Trans. R. Soc. Lond. B. Biol. Sci.* **2003**, *358*, 961–966.
- [50] R. J. Nash, L. E. Fellows, J. V. Dring, G. W. J. Fleet, A. E. Derome, T. A. Hamor, A. M. Scofield, D. J. Watkin, *Tetrahedron Lett.* **1988**, *29*, 2487–2490.
- [51] S. V. Evans, L. E. Fellows, T. K. M. Shing, G. W. J. Fleet, *Phytochemistry* **1985**, *24*, 1953–1955.
- [52] R. J. Molyneux, M. Benson, R. Y. Wong, J. E. Tropea, A. D. Elbein, *J. Nat. Prod.* **1988**, *51*, 1198–1206.
- [53] A. A. Watson, G. W. J. Fleet, N. Asano, R. J. Molyneux, R. J. Nash, *Phytochemistry* **2001**, *56*, 265–295.
- [54] A. D. Elbein, R. Solf, P. R. Dorling, K. Vosbeck, *Proc. Natl. Acad. Sci.* **1981**, *78*, 7393–7397.
- [55] D. Durantel, *Curr. Opin. Investig. Drugs Lond. Engl.* **2009**, *10*, 860–870.
- [56] A. Choukhi, S. Ung, C. Wychowski, J. Dubuisson, *J. Virol.* **1998**, *72*, 3851–3858.
- [57] P. S. Sunkara, D. L. Taylor, M. S. Kang, T. L. Bowlin, P. S. Liu, A. S. Tyms, A. Sjoerdsma, *The Lancet* **1989**, *333*, 1206.
- [58] S. Rajasekharan, R. Milan Bonotto, L. Nascimento Alves, Y. Kazungu, M. Poggianella, P. Martinez-Orellana, N. Skoko, S. Polez, A. Marcello, *Viruses* **2021**, *13*, 808.
- [59] F. Wong-Staal, G. Liu, J. McKelvy, in *Antivir. Drugs* (Ed.: W.M. Kazmierski), John Wiley & Sons, Inc., Hoboken, NJ, USA, **2011**, pp. 329–337.
- [60] A. L. Thompson, A. Michalik, R. J. Nash, F. X. Wilson, R. van Well, P. Johnson, G. W. J. Fleet, C.-Y. Yu, X.-G. Hu, R. I. Cooper, D. J. Watkin, *Acta Crystallogr. Sect. E Struct. Rep. Online* **2009**, *65*, o2904–o2905.
- [61] X.-G. Hu, B. Bartholomew, R. J. Nash, F. X. Wilson, G. W. J. Fleet, S. Nakagawa, A. Kato, Y.-M. Jia, R. van Well, C.-Y. Yu, *Org. Lett.* **2010**, *12*, 2562–2565.
- [62] A. Goldmann, B. Message, D. Tepfer, R. J. Molyneux, O. Duclos, F. D. Boyer, Y. T. Pan, A.

- D. Elbein, *J. Nat. Prod.* **1996**, *59*, 1137–1142.
- [63] Z. J. Witczak, R. Chhabra, H. Chen, X.-Q. Xie, *Carbohydr. Res.* **1997**, *301*, 167–175.
- [64] R. J. Capon, J. K. MacLeod, *J. Chem. Soc. Chem. Commun.* **1987**, 1200–1201.
- [65] M. Yoshikawa, T. Morikawa, H. Matsuda, G. Tanabe, O. Muraoka, *Bioorg. Med. Chem.* **2002**, *10*, 1547–1554.
- [66] M. Yoshikawa, T. Murakami, K. Yashiro, H. Matsuda, *Chem. Pharm. Bull. (Tokyo)* **1998**, *46*, 1339–1340.
- [67] Y. Ding, O. Hindsgaul, *Bioorg. Med. Chem. Lett.* **1998**, *8*, 1215–1220.
- [68] D. Tardieu, M. Céspedes Dávila, D. Hazelard, P. Compain, *Synthesis* **2018**, *50*, 3927–3930.
- [69] G. E. McCasland, S. Furuta, L. J. Durham, *J. Org. Chem.* **1966**, *31*, 1516–1521.
- [70] A. Wadood, M. Ghufran, A. Khan, S. S. Azam, M. Jelani, R. Uddin, *Int. J. Biol. Macromol.* **2018**, *111*, 82–91.
- [71] L. S. Jeong, J. A. Lee, *Antivir. Chem. Chemother.* **2004**, *15*, 235–250.
- [72] Y.-U. Kwon, S.-K. Chung, *Org. Lett.* **2001**, *3*, 3013–3016.
- [73] O. Seiichiro, K. Miki, *Curr. Top. Med. Chem.* **2008**, *9*, 58–75.
- [74] T. Mahmud, S. Lee, H. G. Floss, *Chem. Rec.* **2001**, *1*, 300–310.
- [75] T. Iwasa, H. Yamamoto, M. Shibata, *J. Antibiot. (Tokyo)* **1970**, *23*, 595–602.
- [76] W.-L. Ng, T. K. M. Shing, *J. Synth. Org. Chem. Jpn.* **2018**, *76*, 1215–1222.
- [77] M. von Itzstein, *Nat. Rev. Drug Discov.* **2007**, *6*, 967–974.
- [78] A. Sato, K. Aso, *Nature* **1957**, *180*, 984–985.
- [79] M. L. Wolfrom, A. Thompson, *J. Am. Chem. Soc.* **1955**, *77*, 6403–6403.
- [80] R. A. Ugalde, R. J. Staneloni, L. F. Leloir, *Eur. J. Biochem.* **2005**, *113*, 97–103.
- [81] M. H. D. Postema, J. L. Piper, L. Liu, J. Shen, M. Faust, P. Andreana, *J. Org. Chem.* **2003**, *68*, 4748–4754.
- [82] Z. Liu, S. Ma, *ChemMedChem* **2017**, *12*, 819–829.
- [83] K. Takada, T. Uehara, Y. Nakao, S. Matsunaga, R. W. M. van Soest, N. Fusetani, *J. Am. Chem. Soc.* **2004**, *126*, 187–193.
- [84] H. GAO, T. NISHIOKA, J. Kawabata, T. KASAI, *Biosci. Biotechnol. Biochem.* **2004**, *68*, 369–375.
- [85] C. Braun, G. D. Brayer, S. G. Withers, *J. Biol. Chem.* **1995**, *270*, 26778–26781.
- [86] R. A. Dwek, T. D. Butters, F. M. Platt, N. Zitzmann, *Nat. Rev. Drug Discov.* **2002**, *1*, 65–75.
- [87] C. Fasting, C. A. Schalley, M. Weber, O. Seitz, S. Hecht, B. Kocsch, J. Dervedde, C. Graf, E.-W. Knapp, R. Haag, *Angew. Chem. Int. Ed.* **2012**, *51*, 10472–10498.
- [88] M. Mammen, S.-K. Choi, G. M. Whitesides, *Angew. Chem. Int. Ed.* **1998**, *37*, 2754–2794.
- [89] S. H. Liyanage, M. Yan, *Chem. Commun.* **2020**, *56*, 13491–13505.
- [90] K. C. Tjandra, P. Thordarson, *Bioconjug. Chem.* **2019**, *30*, 503–514.
- [91] V. G. Cheung, M. Morley, F. Aguilar, A. Massimi, R. Kucherlapati, G. Childs, *Nat. Genet.* **1999**, *21*, 15–19.
- [92] X. Wang, E. Matei, L. Deng, L. Koharudin, A. M. Gronenborn, O. Ramström, M. Yan, *Biosens. Bioelectron.* **2013**, *47*, 258–264.
- [93] C. Kößlinger, E. Uttenthaler, S. Drost, F. Aberl, H. Wolf, G. Brink, A. Stanglmaier, E. Sackmann, *Sens. Actuators B Chem.* **1995**, *24*, 107–112.
- [94] J. Homola, *Chem. Rev.* **2008**, *108*, 462–493.
- [95] F. Markey, in *Real-Time Anal. Biomol. Interact.* (Eds.: K. Nagata, H. Handa), Springer Japan, Tokyo, **2000**, pp. 13–22.
- [96] F. P. Schmidtchen, in *Anal. Methods Supramol. Chem.* (Ed.: C. Schalley), Wiley-VCH Verlag GmbH & Co. KGaA, Weinheim, Germany, **2006**, pp. 55–78.

- [97] N. Markova, D. Hallén, *Anal. Biochem.* **2004**, *331*, 77–88.
- [98] N. Hao, K. Neranon, O. Ramström, M. Yan, *Biosens. Bioelectron.* **2016**, *76*, 113–130.
- [99] X. Wang, E. Matei, A. M. Gronenborn, O. Ramström, M. Yan, *Anal. Chem.* **2012**, *84*, 4248–4252.
- [100] A. A. Keller, H. Wang, D. Zhou, H. S. Lenihan, G. Cherr, B. J. Cardinale, R. Miller, Z. Ji, *Environ. Sci. Technol.* **2010**, *44*, 1962–1967.
- [101] T. Phenrat, N. Saleh, K. Sirk, R. D. Tilton, G. V. Lowry, *Environ. Sci. Technol.* **2007**, *41*, 284–290.
- [102] H. Handa, S. Gurczynski, M. P. Jackson, G. Mao, *Langmuir* **2010**, *26*, 12095–12103.
- [103] M. R. Wormald, A. J. Petrescu, Y.-L. Pao, A. Glithero, T. Elliott, R. A. Dwek, *Chem. Rev.* **2002**, *102*, 371–386.
- [104] E. Howard, A. Cousido-Siah, M. L. Lepage, J. P. Schneider, A. Bodlenner, A. Mitschler, A. Meli, I. Izzo, H. A. Alvarez, A. Podjarny, P. Compain, *Angew. Chem.* **2018**, *130*, 8134–8138.
- [105] C. Decroocq, A. Joosten, R. Sergent, T. M. Barragán, C. O. Mellet, P. Compain, *ChemBioChem* **2013**, *14*, 2038–2049.
- [106] Y. Brissonnet, C. Ortiz Mellet, S. Morandat, M. I. Garcia Moreno, D. Deniaud, S. E. Matthews, S. Vidal, S. Šesták, K. El Kirat, S. G. Gouin, *J. Am. Chem. Soc.* **2013**, *135*, 18427–18435.
- [107] J. J. Lundquist, E. J. Toone, *Chem. Rev.* **2002**, *102*, 555–578.
- [108] P. Compain, *Chem. Rec.* **2020**, *20*, 10–22.
- [109] P. Compain, A. Bodlenner, *ChemBioChem* **2014**, *15*, 1239–1251.
- [110] P. I. Kitov, J. M. Sadowska, G. Mulvey, G. D. Armstrong, H. Ling, N. S. Pannu, R. J. Read, D. R. Bundle, *Nature* **2000**, *403*, 669–672.
- [111] M. Pichon, Conception et synthèse d'iminosucre multivalents bioactifs à motif glycoimidazole – Développement d'une méthode de déshydroxylation sélective, Docteur de l'université de Strasbourg, Université de Strasbourg, **2018**.
- [112] B. A. Johns, C. R. Johnson, *Tetrahedron Lett.* **1998**, *39*, 749–752.
- [113] Y.-P. Pang, P. Quiram, T. Jelacic, F. Hong, S. Brimijoin, *J. Biol. Chem.* **1996**, *271*, 23646–23649.
- [114] T. R. Hoye, Z. Ye, L. J. Yao, J. T. North, *J. Am. Chem. Soc.* **1996**, *118*, 12074–12081.
- [115] M. Bols, R. G. Hazell, I. B. Thomsen, *Chem. – Eur. J.* **1997**, *3*, 940–947.
- [116] I. Thomsen, B. V. Ernholz, M. Bols, *Tetrahedron* **1997**, *53*, 9357–9364.
- [117] R. Zelli, J.-F. Longevial, P. Dumy, A. Marra, *New J. Chem.* **2015**, *39*, 5050–5074.
- [118] I. McCort, M. Sanière, Y. Le Merrer, *Tetrahedron* **2003**, *59*, 2693–2700.
- [119] K. L. Prime, G. M. Whitesides, *J. Am. Chem. Soc.* **1993**, *115*, 10714–10721.
- [120] F. Giacalone, N. Martín, *Chem. Rev.* **2006**, *106*, 5136–5190.
- [121] A. W. Jensen, S. R. Wilson, D. I. Schuster, *Bioorg. Med. Chem.* **1996**, *4*, 767–779.
- [122] T. D. Ros, M. Prato, *Chem. Commun.* **1999**, 663–669.
- [123] A. Hirsch, O. Vostrowsky, *Eur. J. Org. Chem.* **2001**, *2001*, 829–848.
- [124] J. Iehl, J.-F. Nierengarten, *Chem. – Eur. J.* **2009**, *15*, 7306–7309.
- [125] R. Rísquez-Cuadro, J. M. García Fernández, J.-F. Nierengarten, C. Ortiz Mellet, *Chem. – Eur. J.* **2013**, *19*, 16791–16803.
- [126] E. M. Sánchez-Fernández, R. Rísquez-Cuadro, M. Aguilar-Moncayo, M. I. García-Moreno, C. O. Mellet, J. M. García Fernández, *Org. Lett.* **2009**, *11*, 3306–3309.
- [127] E. M. Sánchez-Fernández, R. Rísquez-Cuadro, M. Chasseraud, A. Ahidouch, C. O. Mellet, H. Ouadid-Ahidouch, J. M. G. Fernández, *Chem. Commun.* **2010**, *46*, 5328–5330.

- [128] E. M. Sánchez-Fernández, R. Rísquez-Cuadro, C. O. Mellet, J. M. G. Fernández, P. M. Nieto, J. Angulo, *Chem. – Eur. J.* **2012**, *18*, 8527–8539.
- [129] M. Abellán Flos, M. I. García Moreno, C. Ortiz Mellet, J. M. García Fernández, J.-F. Nierengarten, S. P. Vincent, *Chem. – Eur. J.* **2016**, *22*, 11450–11460.
- [130] J.-F. Nierengarten, J. P. Schneider, T. M. N. Trinh, A. Joosten, M. Holler, M. L. Lepage, A. Bodlenner, M. I. García-Moreno, C. Ortiz Mellet, P. Compain, *Chem. – Eur. J.* **2018**, *24*, 2483–2492.
- [131] T. M. N. Trinh, M. Holler, J. P. Schneider, M. I. García-Moreno, J. M. García Fernández, A. Bodlenner, P. Compain, C. Ortiz Mellet, J.-F. Nierengarten, *J. Mater. Chem. B* **2017**, *5*, 6546–6556.
- [132] J.-F. Nierengarten, *Chem. Commun.* **2017**, *53*, 11855–11868.
- [133] E. Bilensoy, Ed. , *Cyclodextrins in Pharmaceuticals, Cosmetics, and Biomedicine: Current and Future Industrial Applications*, John Wiley & Sons, Inc., Hoboken, NJ, USA, **2011**.
- [134] G. Crini, *Chem. Rev.* **2014**, *114*, 10940–10975.
- [135] Á. Martínez, C. Ortiz Mellet, J. M. García Fernández, *Chem. Soc. Rev.* **2013**, *42*, 4746.
- [136] A. Joosten, J. P. Schneider, M. L. Lepage, C. Tarnus, A. Bodlenner, P. Compain, *Eur. J. Org. Chem.* **2014**, *2014*, 1866–1872.
- [137] M. I. García-Moreno, F. Ortega-Caballero, R. Rísquez-Cuadro, C. Ortiz Mellet, J. M. García Fernández, *Chem. – Eur. J.* **2017**, *23*, 6295–6304.
- [138] M. M. Pichon, F. Stauffert, A. Bodlenner, P. Compain, *Org. Biomol. Chem.* **2019**, *17*, 5801–5817.
- [139] Y. Brissonnet, C. Ortiz Mellet, S. Morandat, M. I. Garcia Moreno, D. Deniaud, S. E. Matthews, S. Vidal, S. Šesták, K. El Kirat, S. G. Gouin, *J. Am. Chem. Soc.* **2014**, *136*, 6773–6773.
- [140] A. S. Culf, R. J. Ouellette, *Molecules* **2010**, *15*, 5282–5335.
- [141] B. Yoo, S. B. Y. Shin, M. L. Huang, K. Kirshenbaum, *Chem. – Eur. J.* **2010**, *16*, 5528–5537.
- [142] M. L. Lepage, A. Meli, A. Bodlenner, C. Tarnus, F. De Riccardis, I. Izzo, P. Compain, *Beilstein J. Org. Chem.* **2014**, *10*, 1406–1412.
- [143] A. Kumar, S. M. Gaikwad, *Int. J. Biol. Macromol.* **2011**, *49*, 1066–1071.
- [144] C. S. Ho, C. W. K. Lam, M. H. M. Chan, R. C. K. Cheung, L. K. Law, L. C. W. Lit, K. F. Ng, M. W. M. Suen, H. L. Tai, *Clin. Biochem. Rev.* **2003**, *24*, 3–12.
- [145] C. D. Gutsche, *Calixarenes: An Introduction: Edition 2*, Royal Society of Chemistry, **2008**.
- [146] A. Dondoni, A. Marra, *Chem. Rev.* **2010**, *110*, 4949–4977.
- [147] F. Sansone, L. Baldini, A. Casnati, R. Ungaro, *New J. Chem.* **2010**, *34*, 2715.
- [148] M. Marradi, S. Cicchi, F. Sansone, A. Casnati, A. Goti, *Beilstein J. Org. Chem.* **2012**, *8*, 951–957.
- [149] F. Cardona, G. Isoldi, F. Sansone, A. Casnati, A. Goti, *J. Org. Chem.* **2012**, *77*, 6980–6988.
- [150] A. Marra, R. Zelli, G. D'Orazio, B. La Ferla, A. Dondoni, *Tetrahedron* **2014**, *70*, 9387–9393.
- [151] R. Zelli, S. Tommasone, P. Dumy, A. Marra, A. Dondoni, *Eur. J. Org. Chem.* **2016**, *2016*, 5102–5116.
- [152] R. Zelli, P. Dumy, A. Marra, *Org. Biomol. Chem.* **2020**, *18*, 2392–2397.
- [153] J. P. Schneider, S. Tommasone, P. Della Sala, C. Gaeta, C. Talotta, C. Tarnus, P. Neri,

- A. Bodlenner, P. Compain, *Pharmaceuticals* **2020**, *13*, 366.
- [154] M. Martínez-Bailén, E. Jiménez-Ortega, A. T. Carmona, I. Robina, J. Sanz-Aparicio, D. Talens-Perales, J. Polaina, C. Matassini, F. Cardona, A. J. Moreno-Vargas, *Bioorganic Chem.* **2019**, *89*, 103026.
- [155] M. Martínez-Bailén, A. T. Carmona, F. Cardona, C. Matassini, A. Goti, M. Kubo, A. Kato, I. Robina, A. J. Moreno-Vargas, *Eur. J. Med. Chem.* **2020**, *192*, 112173.
- [156] C. Bonduelle, J. Huang, T. Mena-Barragán, C. Ortiz Mellet, C. Decroocq, E. Etamé, A. Heise, P. Compain, S. Lecommandoux, *Chem. Commun.* **2014**, *50*, 3350–3352.
- [157] Y. Brissonnet, S. Ladevèze, D. Tezé, E. Fabre, D. Deniaud, F. Daligault, C. Tellier, S. Šesták, M. Remaud-Simeon, G. Potocki-Veronese, S. G. Gouin, *Bioconjug. Chem.* **2015**, *26*, 766–772.
- [158] S. Mirabella, G. D'Adamio, C. Matassini, A. Goti, S. Delgado, A. Gimeno, I. Robina, A. J. Moreno-Vargas, S. Šesták, J. Jiménez-Barbero, F. Cardona, *Chem. - Eur. J.* **2017**, *23*, 14585–14596.
- [159] E. Moreno-Clavijo, A. T. Carmona, A. J. Moreno-Vargas, L. Molina, D. W. Wright, G. J. Davies, I. Robina, *Eur. J. Org. Chem.* **2013**, *2013*, 7328–7336.
- [160] H. C. Kolb, M. G. Finn, K. B. Sharpless, *Angew. Chem. Int. Ed.* **2001**, *40*, 2004–2021.
- [161] C. W. Tornøe, C. Christensen, M. Meldal, *J. Org. Chem.* **2002**, *67*, 3057–3064.
- [162] V. V. Rostovtsev, L. G. Green, V. V. Fokin, K. B. Sharpless, *Angew. Chem. Int. Ed.* **2002**, *41*, 2596–2599.
- [163] R. Huisgen, *Angew. Chem. Int. Ed. Engl.* **1963**, *2*, 565–598.
- [164] S. Díez-González, A. Correa, L. Cavallo, S. P. Nolan, *Chem. – Eur. J.* **2006**, *12*, 7558–7564.
- [165] M. Ahlquist, V. V. Fokin, *Organometallics* **2007**, *26*, 4389–4391.
- [166] C. Shao, G. Cheng, D. Su, J. Xu, X. Wang, Y. Hu, *Adv. Synth. Catal.* **2010**, *352*, 1587–1592.
- [167] B. T. Worrell, J. A. Malik, V. V. Fokin, *Science* **2013**, *340*, 457–460.
- [168] F. Himo, T. Lovell, R. Hilgraf, V. V. Rostovtsev, L. Noodleman, K. B. Sharpless, V. V. Fokin, *J. Am. Chem. Soc.* **2005**, *127*, 210–216.
- [169] L. Jin, D. R. Tolentino, M. Melaimi, G. Bertrand, *Sci. Adv.* **2015**, *1*, e1500304.
- [170] C. Iacobucci, S. Reale, J.-F. Gal, F. De Angelis, *Angew. Chem. Int. Ed.* **2015**, *54*, 3065–3068.
- [171] C. Nolte, P. Mayer, B. F. Straub, *Angew. Chem. Int. Ed.* **2007**, *46*, 2101–2103.
- [172] For a review on the mechanism of CuAAC reaction see : L. Zhu, C. J. Brassard, X. Zhang, P. M. Guha, R. J. Clark, *Chem. Rec.* **2016**, *16*, 1501–1517.
- [173] G.-C. Kuang, P. M. Guha, W. S. Brotherton, J. T. Simmons, L. A. Stanke, B. T. Nguyen, R. J. Clark, L. Zhu, *J. Am. Chem. Soc.* **2011**, *133*, 13984–14001.
- [174] M. Konwar, R. Hazarika, A. A. Ali, M. Chetia, N. D. Khupse, P. J. Saikia, D. Sarma, *Appl. Organomet. Chem.* **2018**, *32*, e4425.
- [175] M. B. Davies, *Polyhedron* **1992**, *11*, 285–321.
- [176] Carol. Creutz, *Inorg. Chem.* **1981**, *20*, 4449–4452.
- [177] E. Haldón, M. C. Nicasio, P. J. Pérez, *Org. Biomol. Chem.* **2015**, *13*, 9528–9550.
- [178] S. Neumann, M. Biewend, S. Rana, W. H. Binder, *Macromol. Rapid Commun.* **2020**, *41*, 1900359.
- [179] C. Wang, D. Ikhlef, S. Kahlal, J.-Y. Saillard, D. Astruc, *Coord. Chem. Rev.* **2016**, *316*, 1–20.
- [180] V. V. Fokin, K. Matyjaszewski, in *Org. Chem. – Breakthr. Perspect.*, John Wiley & Sons,

- Ltd, **2012**, pp. 247–277.
- [181] L. Zhang, X. Chen, P. Xue, H. H. Y. Sun, I. D. Williams, K. B. Sharpless, V. V. Fokin, G. Jia, *J. Am. Chem. Soc.* **2005**, *127*, 15998–15999.
- [182] P. L. Golas, N. V. Tsarevsky, B. S. Sumerlin, K. Matyjaszewski, *Macromolecules* **2006**, *39*, 6451–6457.
- [183] M. Meldal, C. W. Tornøe, *Chem. Rev.* **2008**, *108*, 2952–3015.
- [184] J. E. Hein, V. V. Fokin, *Chem. Soc. Rev.* **2010**, *39*, 1302–1315.
- [185] K. Mashayekh, P. Shiri, *ChemistrySelect* **2019**, *4*, 13459–13478.
- [186] M. S. Shad, P. V. Santhini, W. Dehaen, *Beilstein J. Org. Chem.* **2019**, *15*, 2142–2155.
- [187] N. Moini, M. J. Zohuriaan-Mehr, K. Kabiri, H. A. Khonakdar, *Appl. Surf. Sci.* **2019**, *487*, 1131–1144.
- [188] D. Kushwaha, P. Dwivedi, S. K. Kuanar, V. K. Tiwari, *Curr. Org. Synth.* **2013**, *10*, 90–135.
- [189] C. Decroocq, D. Rodríguez-Lucena, V. Russo, T. Mena Barragán, C. Ortiz Mellet, P. Compain, *Chem. - Eur. J.* **2011**, *17*, 13825–13831.
- [190] Hazelard, D., Lepage, M. L., Schneider, J. P., Pichon, M. M., Massicot, F., Compain, P., in *Carbohydr. Chem. Proven Synth. Methods*, CRC Press, **2017**, pp. 303–314.
- [191] M. Ortega-Muñoz, F. Perez-Balderas, J. Morales-Sanfrutos, F. Hernandez-Mateo, J. Isac-García, F. Santoyo-Gonzalez, *Eur. J. Org. Chem.* **2009**, *2009*, 2454–2473.
- [192] A. Mollard, I. Zharov, *Inorg. Chem.* **2006**, *45*, 10172–10179.
- [193] Fabien Stauffert, Conception et Synthèse d'Iminosucre Di- à Tétravalents Comme Sondes Mécanistiques et Agents Thérapeutiques Potentiels, Docteur de l'université de Strasbourg, Université de Strasbourg, **2015**.
- [194] B. C. Sanders, F. Friscourt, P. A. Ledin, N. E. Mbua, S. Arumugam, J. Guo, T. J. Boltje, V. V. Popik, G.-J. Boons, *J. Am. Chem. Soc.* **2011**, *133*, 949–957.
- [195] Mathieu LEPAGE, Conception et Synthèse de Nouvelles Classes d'Iminosucre d'Intérêt Biologique : Ingénierie Click Pour Des Systèmes Multivalents, Docteur de l'université de Strasbourg, Université de Strasbourg, **2014**.
- [196] A. Theil, J. Hitce, P. Retailleau, A. Marinetti, *Eur. J. Org. Chem.* **2006**, *2006*, 154–161.
- [197] D. A. Goff, G. A. Koolpe, A. B. Kelson, H. M. Vu, D. L. Taylor, C. D. Bedford, R. N. Harris, H. A. Mussalam, I. Koplovitz, *J. Med. Chem.* **1991**, *34*, 1363–1368.
- [198] S. Kim, B. Kim, J. In, *Synthesis* **2009**, *2009*, 1963–1968.
- [199] Z. L. Palchak, P. T. Nguyen, C. H. Larsen, *Beilstein J. Org. Chem.* **2015**, *11*, 1425–1433.
- [200] V. P. Pathak, *Synth. Commun.* **1993**, *23*, 83–85.
- [201] H. F. Gilbert, *Basic Concepts in Biochemistry: A Student's Survival Guide*, **1999**.
- [202] A. Goldstein, *J. Gen. Physiol.* **1944**, *27*, 529–580.
- [203] M. Dixon, E. C. Webb, C. J. R. Thorne, *Enzymes*, London, **1979**.
- [204] Robert A. Copeland, in *Enzym. Pract. Introd. Struct. Mech. Data Anal.*, Wiley-VCH, Inc., **2000**.
- [205] P. M. Turner, K. M. Lerea, F. J. Kull, *Biochem. Biophys. Res. Commun.* **1983**, *114*, 1154–1160.
- [206] J. F. Morrison, *Biochim. Biophys. Acta BBA - Enzymol.* **1969**, *185*, 269–286.
- [207] S. Cha, *Biochem. Pharmacol.* **1975**, *24*, 2177–2185.
- [208] W. R. Greco, M. T. Hakala, *J. Biol. Chem.* **1979**, *254*, 12104–12109.
- [209] P. Kuzmic, *BioKin Tech. Note* **2015**, *TN-2015-01*.
- [210] J. E. Gestwicki, C. W. Cairo, L. E. Strong, K. A. Oetjen, L. L. Kiessling, *J. Am. Chem. Soc.* **2002**, *124*, 14922–14933.

- [211] S. E. Harding, D. Scott, A. Rowe, *Analytical Ultracentrifugation: Techniques and Methods*, Royal Society of Chemistry, **2007**.
- [212] P. Schuck, *Biophys. J.* **2010**, *98*, 2005–2013.
- [213] D. Hazelard, P. Compain, *Eur. J. Org. Chem.* **2021**, *2021*, 3501–3515.
- [214] P. Anbarasan, T. Schareina, M. Beller, *Chem. Soc. Rev.* **2011**, *40*, 5049.
- [215] S. Pimparkar, A. Koodan, S. Maiti, N. S. Ahmed, M. M. M. Mostafa, D. Maiti, *Chem. Commun.* **2021**, *57*, 2210–2232.
- [216] S. Sipos, I. Jablonkai, *Carbohydr. Res.* **2011**, *346*, 1503–1510.
- [217] K. N. Drew, P. H. Gross, *J. Org. Chem.* **1991**, *56*, 509–513.
- [218] Bruce. Coxon, H. G. Fletcher, *J. Am. Chem. Soc.* **1964**, *86*, 922–926.
- [219] J. Gervay, M. J. Hadd, *J. Org. Chem.* **1997**, *62*, 6961–6967.
- [220] Bruce. Coxon, H. G. Fletcher, *J. Am. Chem. Soc.* **1963**, *85*, 2637–2642.
- [221] Y. Igarashi, T. Shiozawa, Y. Ichikawa, *Bioorg. Med. Chem. Lett.* **1997**, *7*, 613–616.
- [222] G. Gryniewicz, J. N. BeMiller, *Carbohydr. Res.* **1983**, *112*, 324–327.
- [223] M. Chmielewski, J. N. BeMiller, D. P. Cerretti, *Carbohydr. Res.* **1981**, *97*, C1–C4.
- [224] A. Rosenthal, M. Ratcliffe, *Can. J. Chem.* **1976**, *54*, 91–96.
- [225] A. Benksim, D. Beaupère, A. Wadouachi, *Org. Lett.* **2004**, *6*, 3913–3915.
- [226] P. Köll, A. Förtsch, *Carbohydr. Res.* **1987**, *171*, 301–315.
- [227] J. Martin, L. M. Jaramillo G, P. G. Wang, *Tetrahedron Lett.* **1998**, *39*, 5927–5930.
- [228] S. Kulkarni, J.-C. Lee, S.-C. Hung, *Curr. Org. Chem.* **2004**, *8*, 475–509.
- [229] K. Furuhashi, H. Ogura, K. Iwaki, *Nucleic Acid Chem.* **1991**, *Volume4*, 109–112.
- [230] B. Sarkar, N. Jayaraman, *Front. Chem.* **2020**, *8*, 570185.
- [231] R. Sangwan, A. Khanam, P. K. Mandal, *Eur. J. Org. Chem.* **2020**, *2020*, 5949–5977.
- [232] M. L. Lepage, A. Bodlenner, P. Compain, *Eur. J. Org. Chem.* **2013**, *2013*, 1963–1972.
- [233] T. Cui, R. Smith, X. Zhu, *Carbohydr. Res.* **2015**, *416*, 14–20.
- [234] S. M. Berberich, R. J. Cherney, J. Colucci, C. Courillon, L. S. Geraci, T. A. Kirkland, M. A. Marx, M. F. Schneider, S. F. Martin, *Tetrahedron* **2003**, *59*, 6819–6832.
- [235] N. Ibrahim, M. Alami, S. Messaoudi, *Asian J. Org. Chem.* **2018**, *7*, 2026–2038.
- [236] G. Lian, X. Zhang, B. Yu, *Carbohydr. Res.* **2015**, *403*, 13–22.
- [237] P. Fügedi, P. J. Garegg, H. Lönn, T. Norberg, *Glycoconj. J.* **1987**, *4*, 97–108.
- [238] R. T. Dere, Y. Wang, X. Zhu, *Org. Biomol. Chem.* **2008**, *6*, 2061.
- [239] X. Zhu, R. T. Dere, J. Jiang, L. Zhang, X. Wang, *J. Org. Chem.* **2011**, *76*, 10187–10197.
- [240] C. Tanret, *Compt. Rend* **1894**, *119*, 158–161.
- [241] R. B. Ward, *Methods Carbohydr. Chem.* **1962**, *2*, 394–396.
- [242] A. E. Knauf, R. M. Harn, C. S. Hudson, *J. Am. Chem. Soc.* **1941**, *63*, 1447–1451.
- [243] M. Vaman Rao, M. Nagarajan, *Carbohydr. Res.* **1987**, *162*, 141–143.
- [244] S. J. Sondheimer, R. Eby, C. Schuerch, *Carbohydr. Res.* **1978**, *60*, 187–192.
- [245] M. Georges, B. Fraser-Reid, *Carbohydr. Res.* **1984**, *127*, 162–164.
- [246] M. A. Zottola, R. Alonso, G. D. Vite, B. Fraser-Reid, *J. Org. Chem.* **1989**, *54*, 6123–6125.
- [247] G. Lauer, F. Oberdorfer, *Angew. Chem. Int. Ed. Engl.* **1993**, *32*, 272–273.
- [248] E. R. Ruckel, C. Schuerch, *J. Org. Chem.* **1966**, *31*, 2233–2239.
- [249] J. P. McDevitt, P. T. Lansbury, *J. Am. Chem. Soc.* **1996**, *118*, 3818–3828.
- [250] M. L. Lepage, J. P. Schneider, A. Bodlenner, P. Compain, *J. Org. Chem.* **2015**, *80*, 10719–10733.
- [251] S. K. Mulani, W.-C. Hung, A. B. Ingle, K.-S. Shiau, K.-K. T. Mong, *Org. Biomol. Chem.* **2014**, *12*, 1184–1197.

- [252] H. Hori, Y. Nishida, H. Ohrui, H. Meguro, *J. Org. Chem.* **1989**, *54*, 1346–1353.
- [253] H. Paulsen, B. Helpap, *Carbohydr. Res.* **1989**, *186*, 189–205.
- [254] T. Tanaka, W. C. Huang, M. Noguchi, A. Kobayashi, S. Shoda, *Tetrahedron Lett.* **2009**, *50*, 2154–2157.
- [255] E. Pretsch, P. Bühlmann, C. Affolter, *Structure Determination of Organic Compounds: Tables of Spectral Data*, Springer, Berlin, Heidelberg, Germany, **2000**.
- [256] J. A. C. Romero, S. A. Tabacco, K. A. Woerpel, *J. Am. Chem. Soc.* **2000**, *122*, 168–169.
- [257] C. G. Lucero, K. A. Woerpel, *J. Org. Chem.* **2006**, *71*, 2641–2647.
- [258] I. Cumpstey, *Org. Biomol. Chem.* **2012**, *10*, 2503.
- [259] T. J. Dudley, I. P. Smoliakova, M. R. Hoffmann, *J. Org. Chem.* **1999**, *64*, 1247–1253.
- [260] L. Ayala, C. G. Lucero, J. A. C. Romero, S. A. Tabacco, K. A. Woerpel, *J. Am. Chem. Soc.* **2003**, *125*, 15521–15528.
- [261] M. T. Yang, K. A. Woerpel, *J. Org. Chem.* **2009**, *74*, 545–553.
- [262] N. Yoneda, Y. Fujii, A. Matsumoto, K. Asano, S. Matsubara, *Nat. Commun.* **2017**, *8*, 1397.
- [263] A. K. Kayastha, S. Hotha, *Tetrahedron Lett.* **2010**, *51*, 5269–5272.
- [264] S. G. Gouin, *Chem. Eur. J.* **2014**, *20*, 11616–11628.
- [265] C. Matassini, C. Parmeggiani, F. Cardona, A. Goti, *Tetrahedron Letters* **2016**, *57*, 5407–5415.

Experiment part

General Methods

Reaction and purification

Commercially available starting materials were purchased from commercial suppliers as SigmaAldrich Co., Merck Co., Alfa Aesar GmbH & Co., Acros Organics, Fluorochem, Carbosynth Limited or VWR and were used without further purification. When specified, anhydrous solvents were required. Tetrahydrofuran (THF) was distilled over sodium/benzophenone under argon. Dichloromethane (DCM) was distilled over CaH₂ under argon. Toluene was dried over molecular sieves. Dimethylformamide (DMF) and acetonitrile were purchased anhydrous over molecular sieves. Triethylamine and pyridine were distilled over KOH under reduced pressure and were stored over KOH under argon.

All the reactions were carried out in standard glassware or in vials adapted to a Biotage Initiator[®] microwave reactor. The reactions were monitored by Thin Layer Chromatography (TLC) on aluminium sheets coated with silica gel 60 F254 purchased from Merck KGaA. Visualization was accomplished with UV light (at 254 nm) and exposure to TLC stains, phosphomolybdic acid (PMA) or potassium permanganate (KMnO₄), followed by heating. Phosphomolybdic acid stain was prepared by dissolving 12MoO₃·H₃PO₄ ·xH₂O (9.6 g) in absolute EtOH (200 mL). Potassium permanganate stain was prepared by dissolving KMnO₄ (2 g), Na₂CO₃ (13.3 g) in water (200 mL) and a 5% NaOH aqueous solution (33 mL). For reaction work-up, “sat. NaHCO₃” means a saturated aqueous solution of sodium hydrogen carbonate, “brine” means a saturated aqueous solution of sodium chloride. Crude mixtures were purified by flash column chromatography on silica gel 60 (230-400 mesh, 0.040-0.063 mm) purchased from Merck KGaA. Automatic flash chromatographies were carried out in a Grace Reveleris[®] flash system equipped with UV/Vis and ELSD detectors.

Characterization

Proton (¹H) and carbon (¹³C) nuclear Magnetic Resonance (NMR) spectra were recorded at 298K on either Bruker Avance 300 MHz, Bruker Avance III HD 400 MHz with BBFO probe or Bruker 500 MHz Avance III HD with Prodigy BBO probe spectrometers. The chemical shifts are reported as δ values in parts per million (ppm) relative to residual solvent signals used as an internal reference. Data are presented as followed : chemical shift, multiplicity (s = singlet, br s = broad singlet, d = doublet, dd = doublet of doublets, ddd = doublet of doublets of doublets, dt = doublet of triplets, ddt = doublet of doublet of triplets, t = triplet, td = triplet of doublets, q = quadruplet, m = multiplet), coupling constants (*J*) are expressed in Hz, integration value and assignment. The indexes “a” or “b” will be used for diastereotopic protons, “a” being assigned to the proton with highest chemical shift and “b” to the proton with the lowest chemical shift. Carbon multiplicities were assigned by Distortionless Enhancement by Polarization Transfer (DEPT) experiments. ¹H and ¹³C signals were assigned by correlation spectroscopy (COSY), Heteronuclear Single Quantum Correlation (HSQC), and Heteronuclear Multiple-Bond Correlation spectroscopy (HMBC). Infrared (IR) spectra (cm⁻¹) were recorded neat on a Perkin-Elmer Spectrum One Spectrophotometer. ESI-TOF high resolution mass spectra (HRMS) were carried out on a Bruker MicroTOF spectrometer. MALDI mass spectra were carried out on a Bruker MALDI-TOF-TOF spectrometer. Optical rotations were measured at 589 nm (sodium lamp) and 20 °C on Anton Paar MCP 200 polarimeter with a path length of 1 dm. The concentration (c) is indicated in gram per deciliter.

General Remarks

In the following sections, solvents will be abbreviated as follows: DCM = dichloromethane; DMF = *N,N*-dimethylformamide; DMSO = Dimethyl sulfoxide; EtOAc = ethyl acetate; MeCN = acetonitrile; THF = tetrahydrofuran.

Synthesis and Analytical Data (Chapter II&III)

➤ General procedure for halide displacement with NaN₃

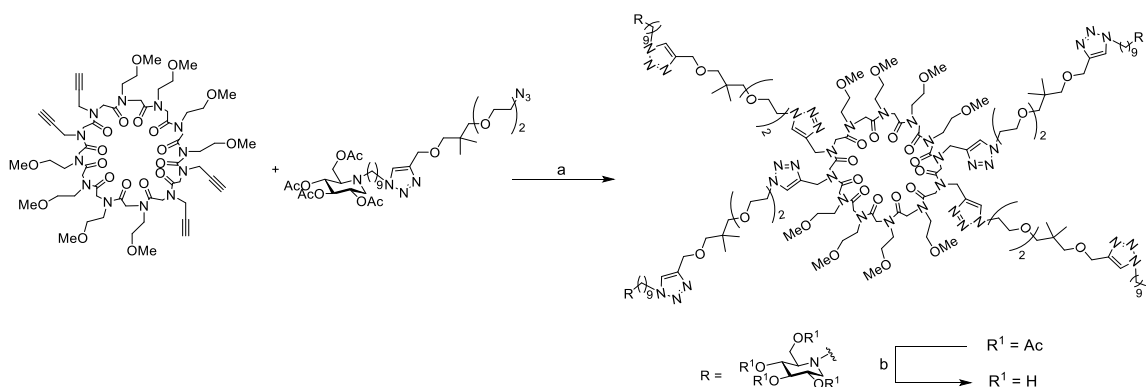
To a solution of halide in DMF was added NaN₃ (10.8 eq.) and Bu₄NI. The resulting mixture was heated 80 °C for 20 h. Then H₂O (50 mL) was poured into the reaction and extracted with EtOAc (3 x 50 mL). The organics layers were combined, washed with brine (50 mL), dried with MgSO₄ and evaporated. The crude was purified by flash chromatography (SiO₂; CH₂Cl₂/MeOH, 99:1 to 95:5) to give the desired product.

➤ General procedure for the CuAAC reaction

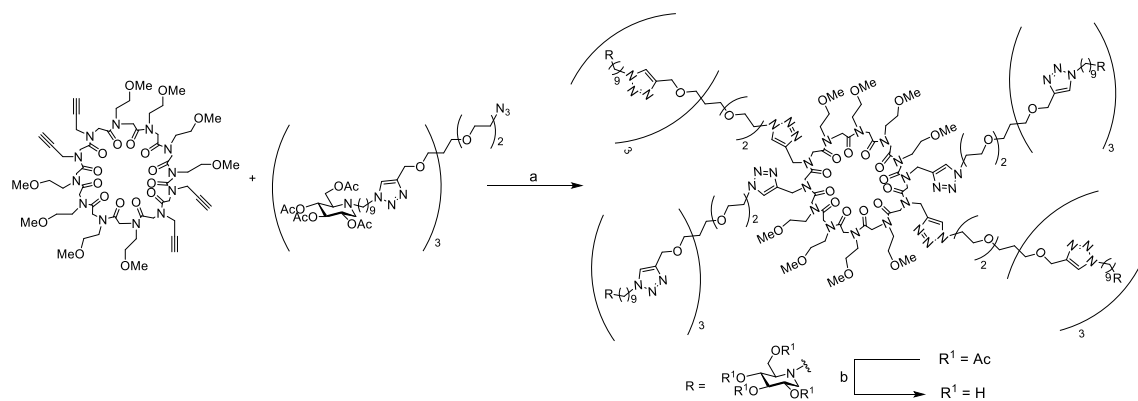
To a 5 mL microwave vial containing the alkyne and azide (1.1 eq./alkyne moiety) in DMF (1 to 3 mL) was added a bright yellow suspension of CuSO₄•5H₂O (0.1 eq./alkyne moiety) and sodium ascorbate (0.2 eq./alkyne moiety) in water (0.2 to 1 mL). The mixture was stirred and heated under microwave irradiation at 80 °C for 1 h. The mixture was concentrated under reduced pressure, diluted in a mixture of MeCN/H₂O/30 wt % -NH₄OH (9:1:1) and filtered with the same eluent (25 mL) on a small pad of SiO₂ (typically 1 to 3 cm thick). Blue copper salts remained on the top of the silica gel pad. The filtrate was evaporated under reduced pressure and then purified by flash chromatography (SiO₂, CH₂Cl₂/MeOH, 100:0 to 90:10) to afford iminosugar click clusters as pale-yellow sticky oils.

➤ General procedure for the deacetylation reaction

To a solution of acetylated iminosugar click cluster in a 1:1 mixture of H₂O/MeOH (1 mL/μmol) was added Amberlite IRA400 (OH⁻) (2.5n to 6n g/mmol of substrate; n = number of acetate groups). The suspension was gently rotated overnight at 25 to 40 °C. The mixture was filtered, washed with methanol and water and the filtrate was concentrated under reduced pressure to afford deprotected iminosugar click cluster as slightly yellow oil.



(a) CuSO₄•5H₂O cat., sodium ascorbate, DMF/H₂O (4:1), MW, 80 °C; 82%; (b) Amberlite IRA 400 (OH⁻), MeOH/H₂O (1:1), 25 °C; quant.

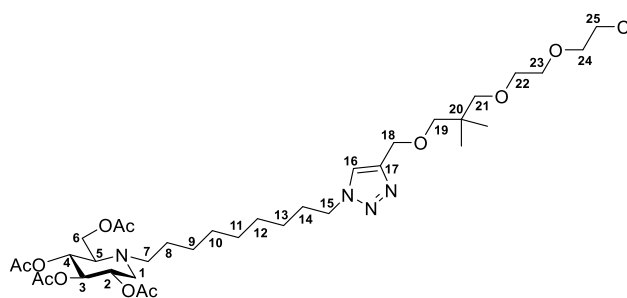


(b) $\text{CuSO}_4 \cdot 5\text{H}_2\text{O}$ cat., sodium ascorbate, DMF/ H_2O (4:1), MW, 80 °C; 79%; (b) Amberlite IRA 400 (OH^-), MeOH/ H_2O (1:1), 25 °C; quant.

➤ General procedure for inhibition assay

The *p*-nitrophenyl- α -D-mannopyranoside and α -mannosidase (EC 3.2.1.24, from Jack Bean, $K_m = 2.0$ mM pH 5.5) were purchased from Sigma Aldrich. The release of *p*-nitrophenol was measured at 405 nm to determine initial velocities after basic quench with 1 M Na_2CO_3 . All kinetics were performed between 23-25 °C and started by enzyme addition in a 100 μL assay medium (acetate buffer, 0.2 M, pH = 5) containing α -mannosidase (72 or 144 mU per mL), substrate (varying concentration from $K_m/8$ to $2K_m$ value) in presence or absence of various concentrations of inhibitor. K_i values were determined in triplicate, using the LB graphical method or non linear regression. The inhibitors were dissolved in DMSO for concentrated mother solutions and DMSO/buffer for diluted solutions with a final DMSO concentration under 2.5 % in all vials. Previously, the stability of the enzyme in presence of various concentrations of DMSO was controlled and the enzyme activity was unaffected.

Compound (153 precursor)



Chemical Formula: $\text{C}_{35}\text{H}_{59}\text{ClN}_4\text{O}_{11}$
Exact Mass: 746.39

Compound **153 precursor** (199.3 mg, 0.27 mmol, 98%) was obtained as a pale-yellow oil according to the general procedure for CuAAC reaction, starting from clickable arm **165** (68 mg, 0.27 mmol) and the iminosugar **155** (150 mg, 0.3 mmol, 1.1 eq.)

$R_f = 0.41$ (DCM/MeOH 95:3).

Specific rotation $[\alpha]_D^{20} = +6.0$ ($c = 1.2$, CHCl_3).

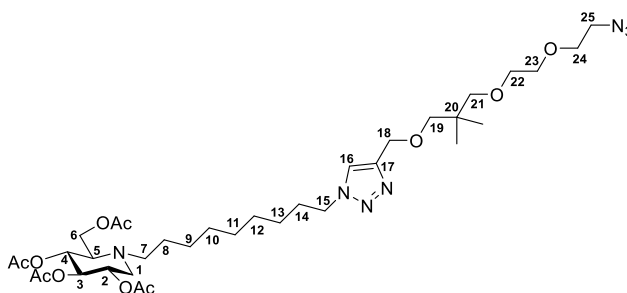
¹H-NMR (CDCl₃, 500 MHz): δ 7.48 (s, 1H, H-16), 5.07-4.99 (m, 2H, H-3, H-4), 4.96-4.91 (m, 1H, H-2), 4.60 (s, 2H, H-18), 4.32 (t, *J* = 7.25 Hz, 2H, H-15), 4.16-4.13 (m, 2H, H-6), 3.73 (t, *J* = 5.8 Hz, 2H, H-24), 3.63-3.58 (m, 4H, H-23 and H-25), 3.56-3.54 (m, 2H, H-22), 3.26 (s, 2H, H-19), 3.20 (s, 2H, H-21), 3.17 (dd, *J* = 11.0, 5.0 Hz, 1H, H-1a), 2.72-2.67 (m, 1H, H-7a), 2.61 (d, *J* = 9.0 Hz, H-5), 2.55-2.51 (m, 1H, H-7b), 2.30 (t, *J* = 10.8 Hz, 1H, H-1b), 2.05 (s, 3H, C(O)CH₃), 2.00 (s, 6H, C(O)CH₃), 1.98 (s, 3H, C(O)CH₃), 1.90-1.85 (m, 2H, H-14), 1.43-1.15 (m, 12H, H-8 to H-13), 0.87 (s, 6H, CH₃) ppm.

¹³C-NMR (CDCl₃, 125 MHz): δ 170.99, 170.43, 170.11, 169.81, 145.86, 122.04, 77.37, 76.69, 74.77, 71.46, 71.15, 70.64, 69.60, 69.51, 65.24, 61.54, 59.59, 52.99, 51.84, 50.38, 43.02, 36.38, 30.40, 29.42, 29.01, 27.21, 26.57, 24.75, 22.25, 20.96, 20.92, 20.83, 20.77 ppm.

IR (neat) 1746 cm⁻¹ (strong, C=O acetate).

MS (ESI) *m/z* calcd for C₃₅H₅₉N₇O₁₁ [M + H]⁺ 747.3942; found 747.3940.

Compound **153**



Chemical Formula: C₃₅H₅₉N₇O₁₁
Exact Mass: 753.43

Compound **153** (131.3 mg, 0.17 mmol, 95%) was obtained as a pale-yellow oil according to the general procedure for halide displacement with NaN₃, starting from **153 precursor** (137 mg, 0.18 mmol).

R_f = 0.79 (DCM/MeOH 95:5).

Specific rotation [α]_D²⁰ = + 5.0 (*c* = 1.8, CHCl₃).

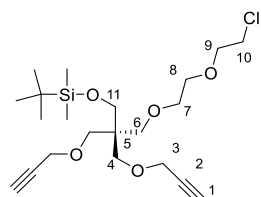
¹H-NMR (500 MHz, CDCl₃): δ 7.47 (s, 1H, H-16), 5.07-4.99 (m, 2H, H-3, H-4), 4.96-4.91 (m, 1H, H-2), 4.59 (s, 2H, H-18), 4.31 (t, *J* = 7.3 Hz, 2H, H-15), 4.13 (s, 2H, H-6), 3.65 (t, *J* = 5.0 Hz, 2H, H-24), 3.62-3.60 (m, 2H, H-23), 3.56-3.54 (m, 2H, H-22), 3.34 (t, *J* = 5.3 Hz, 2H, H-25), 3.26 (s, 2H, H-19), 3.21 (s, 2H, H-21), 3.17 (dd, *J* = 11.0, 5.5 Hz, 1H, H-1a), 2.73-2.67 (m, 1H, H-7a), 2.61 (d, *J* = 8.5 Hz, 1H, H-5), 2.55-2.50 (m, 1H, H-7b), 2.30 (t, *J* = 10.8 Hz, 1H, H-1b), 2.04 (s, 3H, C(O)CH₃), 1.99 (s, 6H, C(O)CH₃), 1.98 (s, 3H, C(O)CH₃), 1.89-1.82 (m, 2H, H-14), 1.40-1.20 (m, 12H, H-8 to H-13), 0.86 (s, 6H, CH₃) ppm.

¹³C-NMR (CDCl₃, 125 MHz): δ 171.03, 170.47, 170.14, 169.85, 145.91, 122.05, 77.41, 76.74, 74.80, 71.22, 70.72, 70.20, 69.62, 69.53, 65.27, 61.56, 59.61, 53.01, 51.86, 50.91, 50.40, 36.42, 30.43, 29.45, 29.04, 27.23, 26.59, 24.77, 22.25, 20.98, 20.95, 20.85, 20.79 ppm.

IR (neat) 2107 cm⁻¹ (N₃), 1744 cm⁻¹ (strong, C=O acetate).

MS (ESI) m/z calcd for $C_{35}H_{60}N_7O_{11}$ $[M + H]^+$ 754.4345; found 754.4360.

13-Chloro-2,2,3,3-tetramethyl-6,6-bis((prop-2-yn-1-yloxy)methyl)-4,8,11-trioxa-3-silatridecane (175)



Chemical Formula: $C_{21}H_{37}ClO_5Si$
Exact Mass: 432.21

Sodium hydride (60w% in oil, 49.1 mg, 1.23 mmol) was added portionwise to a solution of alcohol **174** (211 mg, 0.65 mmol) in THF (2.5 mL) at 0°C. The mixture was stirred at rt. for 2 h. A solution of compound **177** (239.4 mg, 0.90 mmol) in THF (2.5 mL) was added dropwise to it at 0°C. After 1.5 h, the reaction temperature was allowed to increase to rt. and kept for 24 h. The reaction was quenched by adding 3 mL methanol, and then the solution was concentrated in vacuo to give a residue, which was dissolved with DCM. The suspension was filtered through a small pad of SiO_2 and the filtrate was concentrated to give a residue which was purified by column chromatography (pentane/EtOAc, 5:1) to afford the desired compound **175** (218 mg, 78%) as an oil.

R_f = 0.81 (Pentane/EtOAc 5:1).

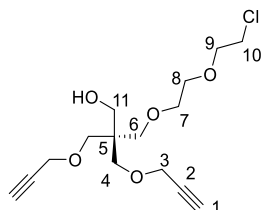
1H -NMR ($CDCl_3$, 500 MHz): δ 4.11 (d, J = 2.5 Hz, 4H, H-3), 3.76 (t, J = 5.75 Hz, 2H, H-10), 3.66-3.58 (m, 6H, H-7 to H-9), 3.57 (s, 2H, H-11), 3.49 (s, 4H, H-4), 3.43 (s, 2H, H-6), 2.39 (t, J = 2.5 Hz, 2H, H-1), 0.88 (s, 9H, CCH_3), 0.03 (s, 6H, $SiCH_3$) ppm.

^{13}C -NMR ($CDCl_3$, 125 MHz): δ 80.32, 74.08, 71.50, 71.26, 70.63, 69.83, 69.07, 61.56, 58.84, 45.91, 42.98, 26.03, 18.39, -5.46 ppm.

IR (neat) 3297 cm^{-1} (strong broad, alkyne CH), 1092 cm^{-1} (strong, C-O-C).

MS (ESI) m/z calcd for $C_{21}H_{37}ClNaO_5Si$ $[M + Na]^+$ 455.1991; found 455.1991.

3-(2-(2-Chloroethoxy)ethoxy)-2,2-bis((prop-2-yn-1-yloxy)methyl)propan-1-ol (178)



Chemical Formula: $C_{15}H_{23}ClO_5$
Exact Mass: 318.12

To a solution of compound **175** (200 mg, 0.46 mmol) in dry THF (10 mL) at 0°C was added dropwise a solution of TBAF (1.85 mL, 1.85 mmol) in THF over 15 min. The reaction mixture was allowed to warm to rt. and stirred for 3.5 h under argon atmosphere. The solvent was evaporated under reduced pressure. The residue was diluted with EtOAc and washed with

water (×2 times) then brine. The organic layers were dried over Na₂SO₄, and concentrated in vacuo to give a residue which was purified by column chromatography (pentane/EtOAc, 4:1) to afford the compound **178** (143 mg, 0.45 mmol) as a pale-yellow sticky oil in 97% yield.

R_f = 0.13 (Pentane/EtOAc 4:1).

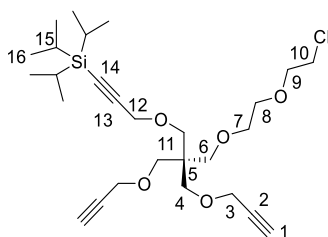
¹H-NMR (CDCl₃, 400 MHz): δ 4.13 (d, *J* = 2.4 Hz, 4H, H-3), 3.75 (t, *J* = 6.0 Hz, 2H, H-10), 3.70 (s, 2H, H-11), 3.67-3.60 (m, 6H, H-7 to H-9), 3.56 (s, 4H, H-4), 3.54 (s, 2H, H-6), 2.42 (t, *J* = 2.4 Hz, H-1) ppm.

¹³C-NMR (CDCl₃, 100 MHz): δ 79.89, 74.54, 71.90, 71.46, 71.09, 70.49, 70.31, 65.46, 58.94, 44.94, 42.92 ppm.

IR (neat) 3484 cm⁻¹ (broad, OH), 3293 cm⁻¹ (strong broad, alkyne CH), 1090 cm⁻¹ (strong, C-O-C) cm⁻¹.

MS (ESI) *m/z* calcd for C₁₅H₂₃ClNaO₅ [M + Na]⁺ 341.1126; found 341.1113.

1-Chloro-14,14-diisopropyl-15-methyl-8,8-bis((prop-2-yn-1-yloxy)methyl)-3,6,10-trioxa-14-silahexadec-12-yne (**179**)



Chemical Formula: C₂₇H₄₅ClO₅Si
Exact Mass: 512.27

To a solution of compound **178** (140 mg, 0.44 mmol) and TIPS protected propargyl bromide (181.4 mg, 0.66 mmol) in dry THF was added sodium hydride (60w% in oil, 26.4 mg, 0.66 mmol) at 0°C, then the mixture was allowed to warm to rt. and was stirred for 24 h. After quenching the reaction with MeOH, the solvent was evaporated under reduced pressure. The residue was diluted with NH₄Cl and extracted with EtOAc (×3 times). The combined organic layers were washed with brine, dried over Na₂SO₄, and concentrated under reduced pressure. The crude residue was purified by column chromatography (pentane/EtOAc, 4:1) to afford the compound **179** (152 mg, 0.30 mmol, 67%) as an oil.

R_f = 0.87 (Pentane/EtOAc 4:1).

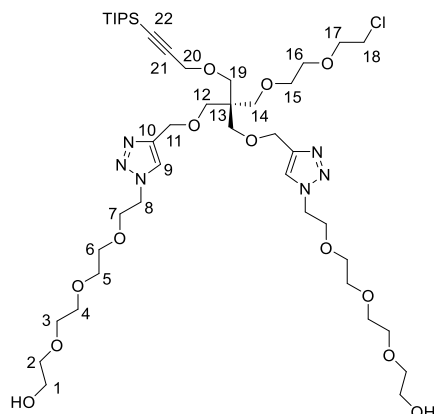
¹H-NMR (CDCl₃, 400 MHz): δ 4.15 (s, 2H, H-12), 4.11 (d, *J* = 2.4 Hz, 4H, H-3), 3.76 (t, *J* = 6.0 Hz, 2H, H-10), 3.66-3.57 (m, 6H, H-7 to H-9), 3.55 (s, 2H, H-11), 3.53 (s, 4H, H-4), 3.47 (s, 2H, H-6), 2.38 (t, *J* = 2.4 Hz, 2H, H-1), 1.08-1.07 (m, 21H, CH(CH₃)₂) ppm.

¹³C-NMR (CDCl₃, 100 MHz): δ 103.91, 87.34, 80.27, 74.10, 71.49, 71.27, 70.57, 70.26, 69.45, 69.01, 59.57, 58.85, 45.05, 42.99, 18.75, 11.33 ppm.

IR (neat) 3302 cm⁻¹ (strong broad, alkyne CH), 1095 cm⁻¹ (strong, C-O-C).

MS (ESI) m/z calcd for $C_{27}H_{45}ClNaO_5Si$ $[M + Na]^+$ 535.2617; found 535.2615.

Compound **180**



Chemical Formula: $C_{43}H_{79}ClN_6O_{13}Si$
Exact Mass: 950.52

Compound **180** (270.9 mg, 0.28 mmol, 97%) was obtained as a colorless oil according to the general procedure for CuAAC reaction, starting from compound **179** (150 mg, 0.29 mmol) and the oligoethylene azide **173** (141 mg, 0.64 mmol, 2.2 eq.).

R_f = 0.5 (DCM/MeOH 9:1).

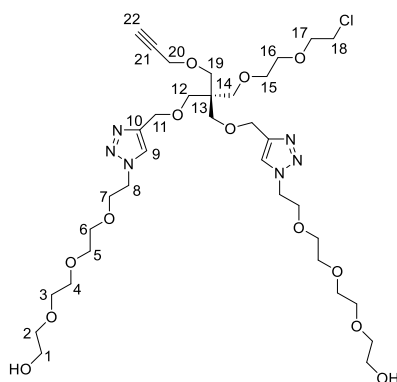
1H -NMR (CDCl₃, 400 MHz): δ 7.72 (s, 2H, H-9), 4.58 (s, 4H, H-11), 4.53 (t, J = 5.2 Hz, 4H, H-8), 4.12 (s, 2H, H-20), 3.87 (t, J = 5.0 Hz, 4H, H-7), 3.74-3.70 (m, 6H, H-1 and H-18), 3.66-3.53 (m, 28H, H-15, H-16, from H-2 to H-6, H-17 and H-19), 3.49 (s, 4H, H-12), 3.44 (s, 2H, H-14), 1.05 (s, 21H, $CH(CH_3)_2$) ppm.

^{13}C -NMR (CDCl₃, 100 MHz): δ 145.41, 123.79, 103.93, 87.31, 72.66, 71.43, 71.16, 70.70, 70.64, 70.57, 70.52, 70.40, 70.22, 69.67, 69.63, 69.09, 65.19, 61.76, 59.56, 50.30, 45.35, 43.07, 18.72, 11.28 ppm.

IR (neat) 3433 cm^{-1} (broad, OH), 1092 cm^{-1} (strong, C-O-C).

MS (ESI) m/z calcd for $C_{43}H_{79}ClN_6NaO_{13}Si$ $[M + Na]^+$ 973.5055; found 973.5064.

Compound **181**



Chemical Formula: C₃₄H₅₉ClN₆O₁₃
Exact Mass: 794.38

To a solution of compound **180** (256.7 mg, 0.27 mmol) in anhydrous MeCN (2.9 mL) was added AgF (51.3 mg, 0.40 mmol) under argon and in the dark. The mixture was stirred for 6 h in the dark at rt. and then 1M HCl (2.7 mL, 2.7 mmol) was added. The mixture was stirred for 5 min, diluted with water then extracted with DCM (×5 times). The combined organic layers were dried over Na₂SO₄, and concentrated under reduced pressure. The crude residue was purified by column chromatography (DCM/MeOH, 9:1) to give compound **181** (182 mg, 0.23 mmol, 85%) as a colorless oil.

R_f = 0.48 (DCM/MeOH 9:1).

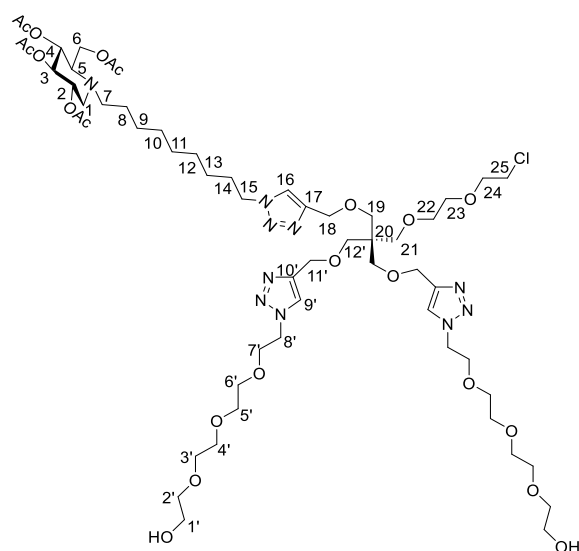
¹H-NMR (CDCl₃, 400 MHz): δ 7.76 (s, 2H, H-9), 4.60 (s, 4H, H-11), 4.54 (t, *J* = 5.2 Hz, 4H, H-8), 4.08 (d, *J* = 2.4 Hz, 2H, H-20), 3.88 (t, *J* = 5.0 Hz, 4H, H-7), 3.75-3.71 (m, 6H, H-1 and H-18), 3.66-3.54 (m, 28H, H-15, H-16, from H-2 to H-6, H-17 and H-19), 3.50 (br s, 4H, H-12), 3.44 (s, 2H, H-14), 2.44 (t, *J* = 2.2 Hz, H-22) ppm.

¹³C-NMR (CDCl₃, 100 MHz): δ 145.35, 123.94, 80.33, 74.43, 72.67, 71.45, 71.18, 70.71, 70.65, 70.57, 70.55, 70.41, 69.96, 69.68, 69.39, 69.20, 65.16, 61.78, 58.80, 50.37, 45.40, 43.11 ppm.

IR (neat) 3435 cm⁻¹ (broad, OH), 3259 cm⁻¹ (broad, alkyne CH), 1092 cm⁻¹ (strong, C-O-C).

MS (ESI) *m/z* calcd for C₃₄H₅₉ClN₆NaO₁₃ [M + Na]⁺ 817.3721; found 817.3700.

Compound **182**



Chemical Formula: C₅₇H₉₇ClN₁₀O₂₁
Exact Mass: 1292.65

Compound **182** (197 mg, 0.15 mmol, 96%) was obtained as an oil according to the general procedure for CuAAC reaction, starting from compound **181** (126 mg, 0.16 mmol) and the iminosugar **155** (86.9 mg, 0.17 mmol, 1.1 eq.).

R_f = 0.72 (DCM/MeOH 9:1).

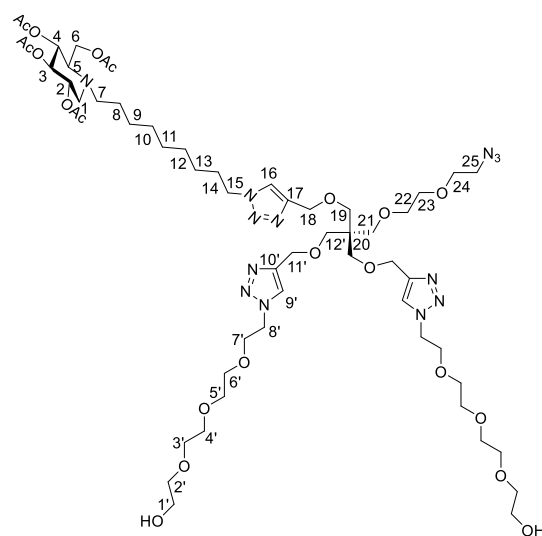
¹H-NMR (CDCl₃, 400 MHz): δ 7.74 (s, 2H, H-9'), 7.55 (s, 1H, H-16), 5.10-4.93 (m, 3H, H-2 to H-4), 4.56 (s, 6H, H-11' and H-18), 4.53 (t, J = 5.2 Hz, 4H, H-8'), 4.32 (t, J = 7.4 Hz, 2H, H-15), 4.15 (s, 2H, H-6), 3.87 (t, J = 5.2 Hz, 4H, H-7'), 3.73-3.70 (m, 6H, H-1' and H-25), 3.65-3.51 (m, 28H, H-22, H-23, from H-2' to H-6', H-24 and H-19), 3.48-3.47 (m, 4H, H-12'), 3.43 (s, 2H, H-21), 3.19 (dd, J = 11.6, 5.2 Hz, 1H, H-1a), 2.75-2.68 (m, 1H, H-7a), 2.63 (d, J = 8.4 Hz, 1H, H-5), 2.58-2.52 (m, 1H, H-7b), 2.32 (t, J = 10.6 Hz, 1H, H-1b), 2.07-2.00 (m, 12H, COCH₃), 1.91-1.87 (m, 2H, H-14), 1.42-1.26 (m, 12H, H-8 to H-13) ppm.

¹³C-NMR (CDCl₃, 100 MHz): δ 171.05, 170.49, 170.16, 169.86, 145.51, 145.28, 123.93, 122.44, 74.81, 72.67, 71.42, 71.14, 70.70, 70.63, 70.56, 70.52, 70.40, 69.98, 69.64, 69.61, 69.55, 69.52, 69.46, 69.35, 65.30, 65.08, 61.74, 61.56, 59.61, 53.04, 51.92, 50.43, 50.28, 45.51, 43.14, 30.50, 29.52, 29.11, 27.29, 26.66, 24.76, 21.01, 20.98, 20.88, 20.82 ppm.

IR (neat) 3471 cm⁻¹ (broad, OH), 1745 cm⁻¹ (strong, C=O acetate), 1096 cm⁻¹ (strong, C-O-C).

MS (ESI) m/z calcd for C₅₇H₉₈ClN₁₀O₂₁ [M + H]⁺1293.6591; found 1293.6559.

Compound **183**



Chemical Formula: $C_{57}H_{97}N_{13}O_{21}$
Exact Mass: 1299.69

Compound **183** (182.6 mg, 0.14 mmol, 92%) was obtained as a yellow oil according to the general procedure for halide displacement with NaN_3 , starting from **182** (197 mg, 0.15 mmol).

R_f = 0.69 (DCM/MeOH 9:1).

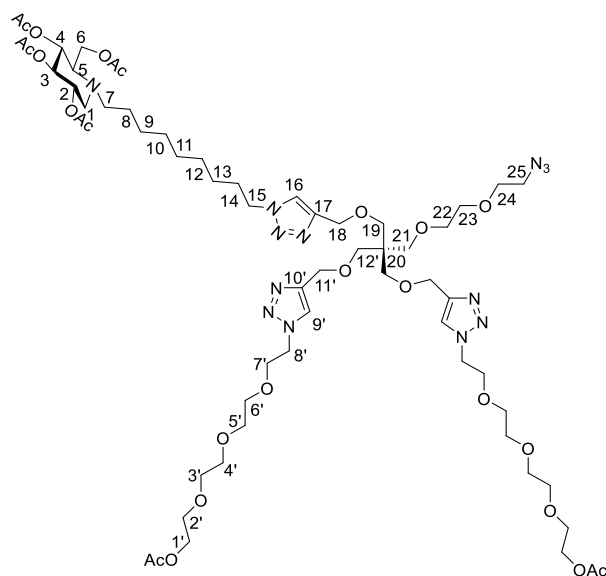
1H -NMR (CDCl₃, 500 MHz): δ 7.74 (s, 2H, H-9'), 7.55 (s, 1H, H-16), 5.09-4.93 (m, 3H, H-2 to H-4), 4.56 (s, 6H, H-11' and H-18), 4.53 (t, J = 5.3 Hz, 4H, H-8'), 4.32 (t, J = 7.3 Hz, 2H, H-15), 4.14 (s, 2H, H-6), 3.87 (t, J = 5.3 Hz, 4H, H-7'), 3.71 (t, J = 4.5 Hz, 4H, H-1'), 3.65-3.48 (m, 32H, H-22, H-23, from H-2' to H-6', H-24, H-19 and H-12'), 3.44 (s, 2H, H-21), 3.34 (t, J = 5.0 Hz, 2H, H-25), 3.18 (dd, J = 11.5, 5.0 Hz, 1H, H-1a), 2.74-2.68 (m, 1H, H-7a), 2.63 (d, J = 9.0 Hz, 1H, H-5), 2.57-2.52 (m, 1H, H-7b), 2.32 (t, J = 10.8 Hz, 1H, H-1b), 2.06-2.00 (m, 12H, COCH₃), 1.90-1.88 (m, 2H, H-14), 1.43-1.26 (m, 12H, H-8 to H-13) ppm.

^{13}C -NMR (CDCl₃, 125 MHz): δ 171.05, 170.49, 170.16, 169.86, 145.52, 145.29, 123.92, 122.42, 74.82, 72.66, 71.15, 70.69, 70.62, 70.55, 70.40, 70.15, 70.01, 69.64, 69.56, 69.55, 69.52, 69.47, 69.35, 65.29, 65.07, 61.73, 61.55, 59.62, 53.05, 51.92, 50.90, 50.42, 50.27, 45.51, 30.49, 29.52, 29.11, 27.29, 26.65, 24.76, 21.00, 20.97, 20.88, 20.81 ppm.

IR (neat) 3457 cm⁻¹ (broad, OH), 2106 cm⁻¹ (N₃), 1744 cm⁻¹ (strong, C=O acetate), 1093 cm⁻¹ (strong, C-O-C).

MS (ESI) m/z calcd for $C_{57}H_{97}N_{13}NaO_{21}$ [$M + Na$]⁺ 1322.6814; found 1322.6808.

Compound **154**



Chemical Formula: C₆₁H₁₀₁N₁₃O₂₃
Exact Mass: 1383.71

To a solution of compound **183** (100 mg, 0.077 mmol) in pyridine (1 mL) under argon was added DMAP (2.44 mg, 0.02 mmol). Then acetic anhydride (0.22 mL) was added dropwise to the mixture. The reaction mixture was stirred at rt. for 26 h and then was added ice water. The solution was stirred for 30 min, then poured into water, extracted with DCM (×3 times). The combined organic layers were washed with 1M HCl (×2 times), then with NaHCO₃, dried over Na₂SO₄, and concentrated under reduced pressure. The crude residue was purified by column chromatography (DCM/MeOH, 9:1) to obtain compound **154** (104.3 mg, 0.075 mmol, 98%) as a pale-yellow oil.

$R_f = 0.81$ (DCM/MeOH 9:1).

Specific rotation $[\alpha]_D^{20} = +1.5$ ($c = 0.4$, CHCl₃).

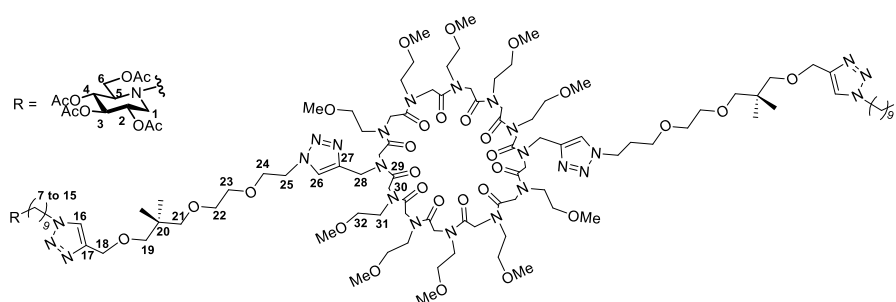
¹H-NMR (CDCl₃, 400 MHz): δ 7.69 (s, 2H, H-9'), 7.54 (s, 1H, H-16), 5.09-4.93 (m, 3H, H-2 to H-4), 4.55 (s, 6H, H-11' and H-18), 4.52 (t, $J = 5.4$ Hz, 4H, H-8'), 4.32 (t, $J = 7.4$ Hz, 2H, H-15), 4.20 (t, $J = 4.8$ Hz, 4H, H-1'), 4.15 (s, 2H, H-6), 3.87 (t, $J = 5.4$ Hz, 4H, H-7'), 3.69-3.48 (m, 32H, H-22, H-23, from H-2' to H-6', H-24, H-19 and H-12'), 3.43 (s, 2H, H-21), 3.34 (t, $J = 5.0$ Hz, 2H, H-25), 3.19 (dd, $J = 11.4, 5.0$ Hz, 1H, H-1a), 2.75-2.68 (m, 1H, H-7a), 2.63 (d, $J = 8.0$ Hz, 1H, H-5), 2.58-2.52 (m, 1H, H-7b), 2.32 (t, $J = 10.8$ Hz, 1H, H-1b), 2.06-2.00 (m, 18H, COCH₃), 1.91-1.87 (m, 2H, H-14), 1.42-1.24 (m, 12H, H-8 to H-13) ppm.

¹³C-NMR (CDCl₃, 100 MHz): δ 171.12, 171.04, 170.49, 170.15, 169.86, 145.54, 145.34, 123.69, 122.38, 74.82, 71.16, 70.68, 70.57, 70.16, 70.02, 69.63, 69.57, 69.55, 69.53, 69.48, 69.38, 69.27, 65.33, 65.10, 63.67, 61.57, 59.62, 53.04, 51.92, 50.90, 50.40, 45.52, 30.50, 29.53, 29.12, 27.30, 26.66, 24.78, 21.10, 21.01, 20.98, 20.88, 20.82 ppm.

IR (neat) 2107 cm⁻¹ (N₃), 1741 cm⁻¹ (strong, C=O acetate).

MS (ESI) average m/z calcd for C₆₁H₁₀₁N₁₃NaO₂₃ [M + Na]⁺ 1406.7025; found 1406.6991.

Compound **184**



Chemical Formula: C₁₃₀H₂₁₈N₂₆O₄₄
Exact Mass: 2847.56

Acetylated compound **184** (27 mg, 9.5 μ mol, 64%) was prepared as a colorless oil according to the general procedure, starting from cyclopeptoid **V** (20 mg, 14.9 μ mol) and ligand **153** (33.7 mg, 44.7 μ mol).

R_f = 0.33 (DCM/MeOH 9:1).

Specific rotation $[\alpha]_D^{20}$ = + 0.5 (c = 0.8, CHCl₃).

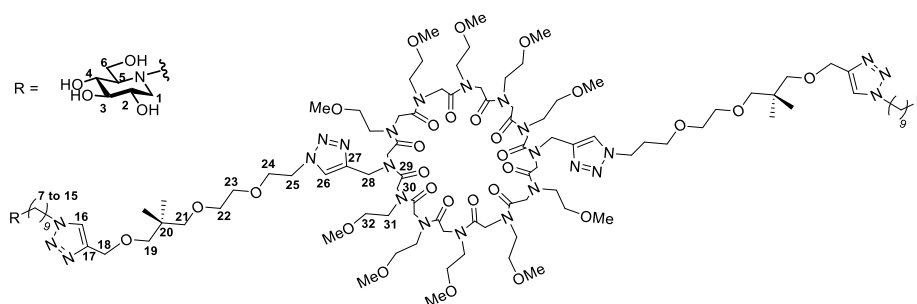
¹H-NMR (CDCl₃, 400 MHz): δ 8.03-7.61 (br s, 2H, H-26), 7.49 (s, 2H, H-16), 5.09-5.00 (m, 4H, H-3 and H-4), 4.98-4.92 (m, 2H, H-2), 4.79-3.75 (m, 48H, H-18, H-28, H-15, H-25, H-30, H-6 and H-24), 3.72-2.95 (m, 88H, H-19, H-21 to H-23, H-31 to H-32, H-1a and OCH₃), 2.75-2.68 (m, 2H, H-7a), 2.62 (d, J = 8.0 Hz, 2H, H-5), 2.57-2.50 (m, 2H, H-7b), 2.31 (t, J = 10.8 Hz, 2H, H-1b), 2.06 (s, 6H, C(O)CH₃), 2.01 (s, 12H, C(O)CH₃), 2.00 (s, 6H, C(O)CH₃), 1.91-1.85 (m, 4H, H-14), 1.45-1.19 (m, 24H, H-8 to H-13), 0.86 (s, 12H, CH₃) ppm.

¹³C-NMR (CDCl₃, 125 MHz): δ 171.04, 170.48, 170.15, 169.86, 169.11, 145.81, 143.64, 124.27, 122.15, 74.82, 71.49, 71.10, 70.61, 70.19, 69.64, 69.56, 65.21, 61.56, 59.63, 59.13, 58.84, 53.04, 51.88, 50.42, 48.16, 42.62, 36.41, 30.45, 29.48, 29.07, 27.26, 26.62, 24.79, 22.26, 21.00, 20.96, 20.87, 20.81 ppm.

IR (neat) 1747 cm⁻¹ (strong, C=O acetate), 1673 cm⁻¹ (strong, C=O amide).

MS (ESI) average m/z calcd for C₁₃₀H₂₁₈KN₂₆NaO₄₄ [M + K + Na]²⁺ 1454.7572; found 1454.7581.

Compound **194**



Chemical Formula: C₁₁₄H₂₀₂N₂₆O₃₆
Exact Mass: 2511.48

Compound **194** was obtained as a colorless oil in quantitative yield (23 mg, 9.1 μmol) from its acetylated precursor **184** (26 mg, 9.1 μmol) according to the general procedure.

Specific rotation $[\alpha]_D^{20} = -5.0$ ($c = 0.8$, CH_3OH).

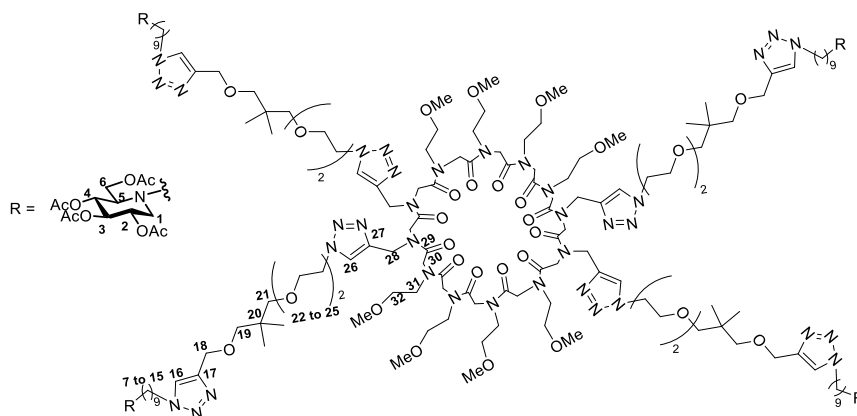
$^1\text{H-NMR}$ (MeOD, 500 MHz): δ 8.17-7.96 (br s, 2H, H-26), 7.95 (s, 2H, H-16), 4.75-3.62 (m, 48H, H-18, H-15, H-25, H-28, H-30, H-6 and H-24), 3.59-3.16 (m, 90H, H-2, H-4, H-19, H-21 to H-23, H-31, H-32 and OCH_3), 3.13 (t, $J = 9.0$ Hz, 2H, H-3), 2.97 (dd, $J = 11.0, 5.0$ Hz, 2H, H-1a), 2.81-2.75 (m, 2H, H-7a), 2.58-2.53 (m, 2H, H-7b), 2.16 (t, $J = 11.0$ Hz, 2H, H-1b), 2.10 (dt, $J = 9.5, 2.5$ Hz, 2H, H-5), 1.92-1.86 (m, 4H, H-14), 1.51-1.45 (m, 4H, H-8), 1.32-1.29 (m, 20H, H-9 to H-13), 0.86 (s, 12H, CH_3) ppm.

$^{13}\text{C-NMR}$ (MeOD, 125 MHz): δ 170.98, 161.46, 146.26, 144.48, 125.64, 124.88, 80.61, 78.18, 77.34, 72.11, 72.03, 71.42, 70.79, 70.42, 67.39, 65.25, 59.56, 59.40, 59.08, 57.75, 53.77, 51.52, 51.31, 43.46, 37.19, 31.30, 30.51, 30.49, 29.99, 28.57, 27.44, 25.22, 22.62 ppm.

IR (neat) 3422 cm^{-1} (strong broad, OH), 1667 cm^{-1} (strong, C=O urea).

MS (ESI) average m/z calcd for $\text{C}_{114}\text{H}_{204}\text{N}_{26}\text{O}_{36}$ $[\text{M} + 2\text{H}]^{2+}$ 1256.7460; found 1256.7464.

Compound **185**



Chemical Formula: $\text{C}_{200}\text{H}_{328}\text{N}_{40}\text{O}_{64}$
Exact Mass: 4314.36

Acetylated compound **185** (68 mg, 16 μmol , 82%) was prepared as a colorless oil according to the general procedure, starting from cycloheptoid **1** (25 mg, 19 μmol) and ligand **153** (63.7 mg, 85 μmol).

$R_f = 0.54$ (DCM/MeOH 90:8).

Specific rotation $[\alpha]_D^{20} = +3.0$ ($c = 2.1$, CHCl_3).

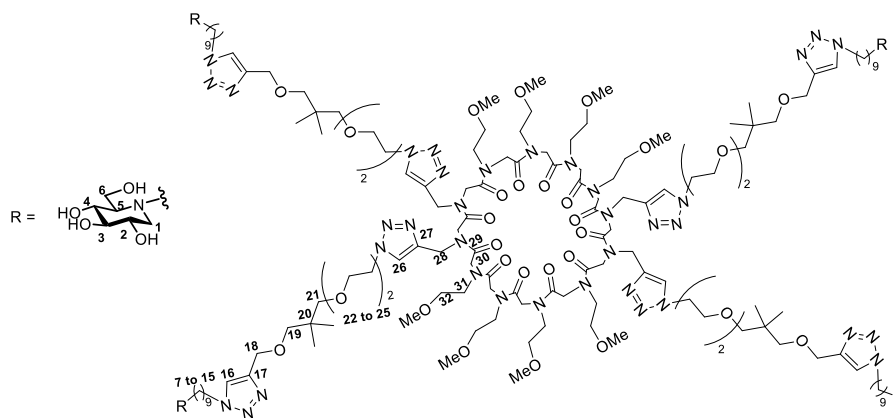
$^1\text{H-NMR}$ (CDCl_3 , 400 MHz): δ 8.02-7.56 (br s, 4H, H-26), 7.48 (s, 4H, H-16), 5.07-4.98 (m, 8H, H-3 and H-4), 4.96-4.90 (m, 4H, H-2), 4.78-3.64 (m, 72H, H-18, H-28, H-25, H-15, H-30, H-6 and H-24), 3.62-3.00 (m, 92H, H-19, H-21 to H-23, H-31 to H-32, H-1a and OCH_3), 2.73-2.66 (m, 4H, H-7a), 2.61 (d, $J = 8.4$ Hz, 4H, H-5), 2.56-2.49 (m, 4H, H-7b), 2.29 (t, $J = 10.6$ Hz, 4H, H-1b), 2.04 (s, 12H, C(O)CH_3), 1.99 (s, 24H, C(O)CH_3), 1.98 (s, 12H, C(O)CH_3), 1.87 (br s, 8H, H-14), 1.44-1.16 (m, 48H, H-8 to H-13), 0.84 (s, 24H, CH_3) ppm.

¹³C-NMR (CDCl₃, 100 MHz): δ 170.98, 170.42, 170.10, 169.81, 168.92, 145.73, 142.30, 124.20, 122.12, 77.38, 76.72, 74.79, 71.08, 70.55, 69.62, 69.52, 65.19, 61.54, 59.61, 59.09, 58.83, 53.01, 51.84, 50.38, 48.31, 48.01, 42.51, 36.39, 30.42, 29.45, 29.04, 27.23, 26.59, 24.77, 22.23, 20.96, 20.93, 20.84, 20.78 ppm.

IR (neat) 1746 cm⁻¹ (strong, C=O acetate), 1673 cm⁻¹ (strong, C=O amide).

MS (ESI) average m/z calcd for C₂₀₀H₃₃₄N₄₀O₆₄ [M + 6H]⁶⁺ 720.0680; found 720.0701.

Compound **195**



Chemical Formula: C₁₆₈H₂₉₆N₄₀O₄₈
Exact Mass: 3642.20

Compound **195** was obtained as a colorless oil in quantitative yield (46 mg, 13 μmol) from its acetylated precursor **185** (58 mg, 13 μmol) according to the general procedure.

Specific rotation $[\alpha]_D^{20} = -4.5$ ($c = 2.2$, CH₃OH).

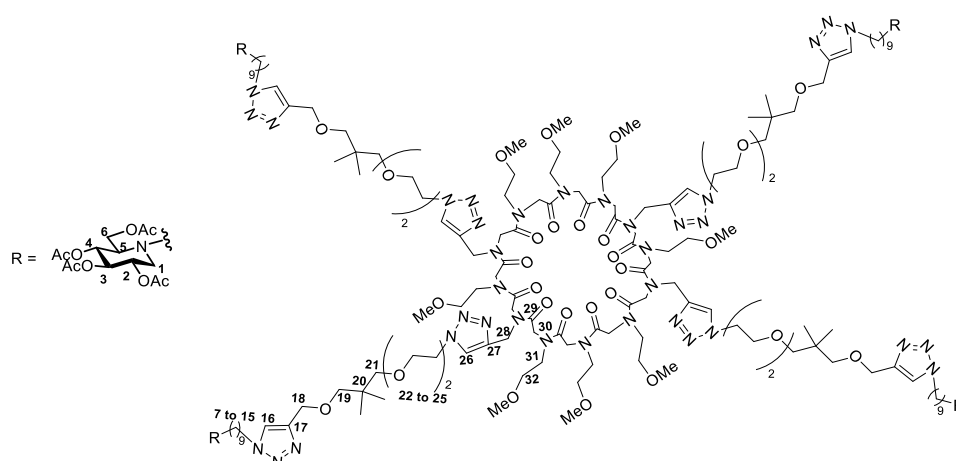
¹H-NMR (MeOD, 500 MHz): δ 8.17-7.96 (br s, 4H, H-26), 7.95 (s, 4H, H-16), 4.78-3.93 (m, 56H, H-18, H-15, H-25, H-28 and H-30), 3.90-3.76 (m, 16H, H-6 and H-24), 3.65-3.16 (m, 96H, H-2, H-4, H-19, H-21 to H-23, H-31, H-32 and OCH₃), 3.13 (t, $J = 9.0$ Hz, 4H, H-3), 2.98 (dd, $J = 11.0, 4.5$ Hz, 4H, H-1a), 2.81-2.75 (m, 4H, H-7a), 2.58-2.53 (m, 4H, H-7b), 2.16 (t, $J = 10.8$ Hz, 4H, H-1b), 2.10 (d, $J = 9.5$ Hz, 4H, H-5), 1.93-1.85 (br m, 8H, H-14), 1.49-1.46 (m, 8H, H-8), 1.31 (br s, 40H, H-9 to H-13), 0.85 (s, 24H, CH₃) ppm.

¹³C-NMR (MeOD, 125 MHz): δ 171.61, 146.24, 144.26, 125.86, 124.87, 80.60, 78.17, 77.33, 72.07, 72.02, 71.41, 70.77, 70.42, 67.37, 65.27, 59.54, 59.43, 59.11, 57.74, 53.76, 51.49, 51.30, 43.56, 37.19, 31.29, 30.49, 29.98, 28.56, 27.43, 25.21, 22.64 ppm.

IR (neat) 3400 cm⁻¹ (strong broad, OH), 1667 cm⁻¹ (strong, C=O urea).

MS (ESI) average m/z calcd for C₁₆₈H₂₉₆N₄₀Na₂O₄₈ [M + 2Na]²⁺ 1844.0868; found 1844.0865.

Compound **186**



Chemical Formula: $C_{200}H_{328}N_{40}O_{64}$
Exact Mass: 4314.36

Acetylated compound **186** (54 mg, 13 μ mol, 68%) was prepared as a colorless oil according to the general procedure, starting from cyclopeptoid **II** (24 mg, 18 μ mol) and ligand **153** (63.7 mg, 85 μ mol).

$R_f = 0.43$ (DCM/MeOH 9:1).

Specific rotation $[\alpha]_D^{20} = +4.0$ ($c = 0.7$, $CHCl_3$).

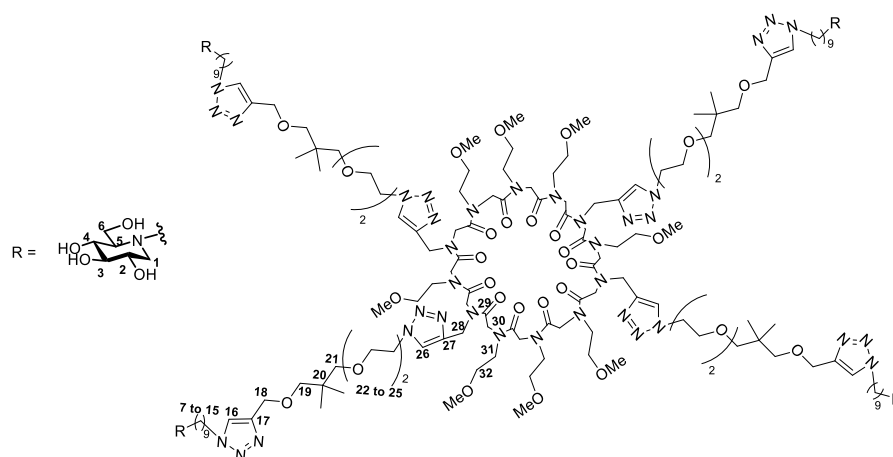
1H -NMR ($CDCl_3$, 500 MHz): δ 8.06-7.59 (br s, 4H, H-26), 7.48 (s, 4H, H-16), 5.07-4.99 (m, 8H, H-3 and H-4), 4.96-4.91 (m, 4H, H-2), 4.85-3.57 (m, 72H, H-18, H-28, H-25, H-15, H-30, H-6 and H-24), 3.54-2.96 (m, 92H, H-19, H-21 to H-23, H-31 to H-32, H-1a and OCH_3), 2.73-2.67 (m, 4H, H-7a), 2.61 (d, $J = 9.0$ Hz, 4H, H-5), 2.54-2.51 (m, 4H, H-7b), 2.30 (t, $J = 11.0$ Hz, 4H, H-1b), 2.05 (s, 12H, $C(O)CH_3$), 2.00 (s, 24H, $C(O)CH_3$), 1.98 (s, 12H, $C(O)CH_3$), 1.88 (br s, 8H, H-14), 1.43-1.17 (m, 48H, H-8 to H-13), 0.84 (s, 24H, CH_3) ppm.

^{13}C -NMR ($CDCl_3$, 100 MHz): δ 170.99, 170.43, 170.11, 169.82, 169.00, 145.71, 143.21, 124.08, 122.13, 77.37, 76.71, 74.79, 71.08, 70.53, 69.61, 69.52, 65.18, 61.53, 59.60, 59.11, 58.84, 53.01, 51.85, 50.39, 48.48, 48.02, 42.44, 36.39, 30.43, 29.46, 29.05, 27.23, 26.59, 24.76, 22.24, 20.97, 20.94, 20.85, 20.78 ppm.

IR (neat) 1746 (strong, C=O acetate), 1673 cm^{-1} (strong, C=O amide).

MS (ESI) average m/z calcd for $C_{200}H_{331}N_{40}O_{64}$ $[M + 3H]^{3+}$ 1439.1287; found 1439.1327.

Compound **196**



Chemical Formula: C₁₆₈H₂₉₆N₄₀O₄₈
Exact Mass: 3642.20

Compound **196** was obtained as a colorless oil in 92% yield (35 mg, 9.6 μ mol) from its acetylated precursor **186** (45 mg, 10.4 μ mol) according to the general procedure.

Specific rotation $[\alpha]_D^{20} = -4.0$ ($c = 1.7$, CH₃OH).

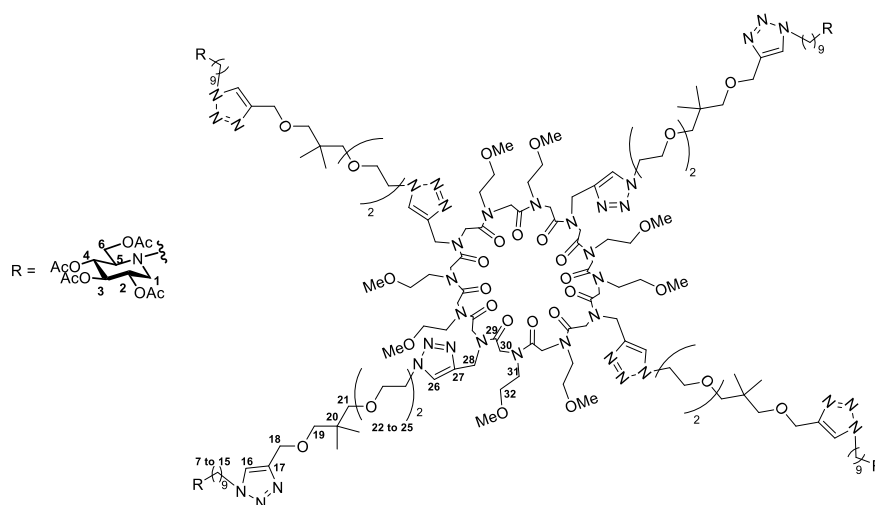
¹H-NMR (MeOD, 400 MHz): δ 8.20-7.96 (br s, 4H, H-26), 7.95 (s, 4H, H-16), 4.80-3.93 (m, 56H, H-18, H-15, H-25, H-28 and H-30), 3.89-3.76 (m, 16H, H-6 and H-24), 3.67-3.16 (m, 96H, H-2, H-4, H-19, H-21 to H-23, H-31, H-32 and OCH₃), 3.13 (t, $J = 9.2$ Hz, 4H, H-3), 2.98 (dd, $J = 11.2, 4.8$ Hz, 4H, H-1a), 2.82-2.74 (m, 4H, H-7a), 2.59-2.52 (m, 4H, H-7b), 2.16 (t, $J = 10.8$ Hz, 4H, H-1b), 2.10 (dt, $J = 9.6, 2.4$ Hz, 4H, H-5), 1.93-1.85 (m, 8H, H-14), 1.51-1.44 (m, 8H, H-8), 1.31 (s, 40H, H-9 to H-13), 0.85 (s, 24H, CH₃) ppm.

¹³C-NMR (MeOD, 100 MHz): δ 171.13, 146.22, 144.21, 125.73, 124.86, 80.59, 78.17, 77.33, 72.07, 72.03, 71.40, 70.77, 70.44, 67.37, 65.27, 59.54, 59.43, 59.09, 57.75, 53.76, 51.50, 51.31, 43.60, 37.19, 31.30, 30.50, 29.99, 28.57, 27.44, 25.21, 22.65 ppm.

IR (neat) 3414 cm⁻¹ (strong broad, OH), 1669 cm⁻¹ (strong, C=O urea).

MS (ESI) average m/z calcd for C₁₆₈H₃₀₁N₄₀O₄₈ [M + 5H]⁵⁺ 729.4463; found 729.4475.

Compound **187**



Chemical Formula: C₂₀₀H₃₂₈N₄₀O₆₄
Exact Mass: 4314.36

Acetylated compound **187** (60 mg, 14 μ mol, 72%) was prepared as a colorless oil according to the general procedure, starting from cyclopeptoid **III** (25 mg, 19 μ mol) and ligand **153** (63.7 mg, 85 μ mol).

R_f = 0.58 (DCM/MeOH 9:1).

Specific rotation $[\alpha]_D^{20} = + 3.0$ ($c = 2.4$, CHCl₃).

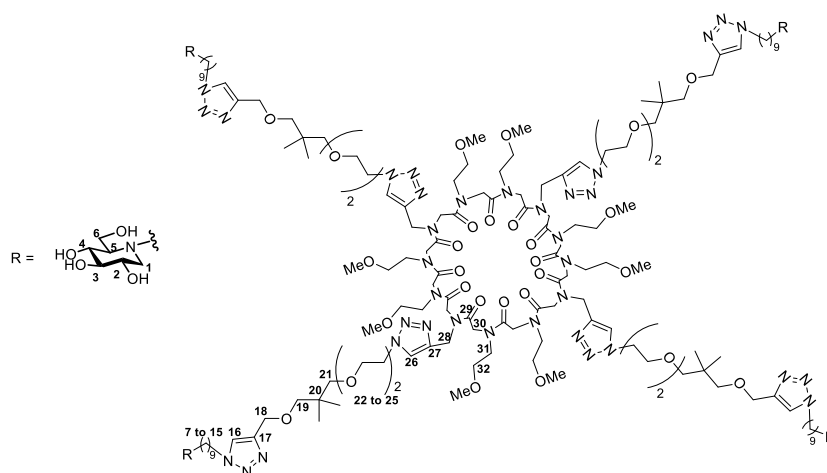
¹H-NMR (CDCl₃, 400 MHz): δ 8.06-7.55 (br s, 4H, H-26), 7.48 (s, 4H, H-16), 5.06-4.98 (m, 8H, H-3 and H-4), 4.95-4.90 (m, 4H, H-2), 4.69-3.63 (m, 72H, H-18, H-28, H-25, H-15, H-30, H-6 and H-24), 3.61-3.05 (m, 92H, H-19, H-21 to H-23, H-31 to H-32, H-1a and OCH₃), 2.72-2.65 (m, 4H, H-7a), 2.60 (d, $J = 8.4$ Hz, 4H, H-5), 2.55-2.48 (m, 4H, H-7b), 2.29 (t, $J = 10.8$ Hz, 4H, H-1b), 2.04 (s, 12H, C(O)CH₃), 1.99 (s, 24H, C(O)CH₃), 1.98 (s, 12H, C(O)CH₃), 1.87 (br s, 8H, H-14), 1.42-1.15 (m, 48H, H-8 to H-13), 0.83 (s, 24H, CH₃) ppm.

¹³C-NMR (CDCl₃, 100 MHz): δ 170.97, 170.41, 170.09, 169.80, 168.86, 145.70, 143.25, 124.14, 122.11, 77.36, 76.69, 74.77, 71.06, 70.54, 69.60, 69.51, 65.16, 61.53, 59.59, 59.07, 58.82, 52.99, 51.83, 50.36, 48.36, 48.05, 42.24, 36.37, 30.41, 29.43, 29.02, 27.21, 26.56, 24.76, 22.21, 20.95, 20.91, 20.82, 20.76 ppm.

IR (neat) 1746 cm⁻¹ (strong, C=O acetate), 1673 cm⁻¹ (strong, C=O amide).

MS (ESI) average m/z calcd for C₂₀₀H₃₃₃N₄₀O₆₄ [M + 5H]⁵⁺ 863.8801; found 863.8805.

Compound **197**



Chemical Formula: C₁₆₈H₂₉₆N₄₀O₄₈
Exact Mass: 3642.20

Compound **197** was obtained as a colorless oil in quantitative yield (42 mg, 12 μ mol) from its acetylated precursor **187** (52 mg, 12 μ mol) according to the general procedure.

Specific rotation $[\alpha]_D^{20} = -5.0$ ($c = 1.8$, CH₃OH).

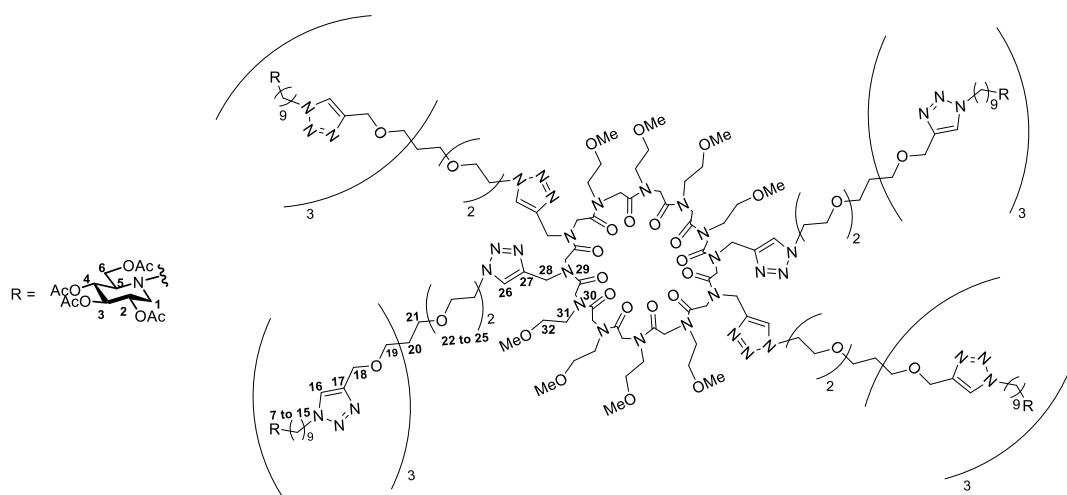
¹H-NMR (MeOD, 500 MHz): δ 8.18-7.96 (br s, 4H, H-26), 7.95 (s, 4H, H-16), 4.77-3.93 (m, 56H, H-18, H-15, H-25, H-28 and H-30), 3.90-3.81 (m, 16H, H-6 and H-24), 3.73-3.17 (m, 96H, H-2, H-4, H-19, H-21 to H-23, H-31, H-32 and OCH₃), 3.13 (t, $J = 9.3$ Hz, 4H, H-3), 2.98 (dd, $J = 11.0$, 4.5 Hz, 4H, H-1a), 2.81-2.75 (m, 4H, H-7a), 2.58-2.53 (m, 4H, H-7b), 2.16 (t, $J = 11.0$ Hz, 4H, H-1b), 2.10 (dt, $J = 9.5$, 2.6 Hz, 4H, H-5), 1.93-1.87 (m, 8H, H-14), 1.50-1.44 (m, 8H, H-8), 1.31 (s, 40H, H-9 to H-13), 0.85 (s, 24H, CH₃) ppm.

¹³C-NMR (MeOD, 125 MHz): δ 171.50, 146.24, 144.55, 125.50, 124.87, 80.60, 78.17, 77.33, 72.08, 72.02, 71.40, 70.78, 70.43, 67.37, 65.27, 59.55, 59.46, 59.41, 59.11, 57.75, 53.76, 51.50, 51.30, 43.35, 37.19, 31.29, 30.49, 29.98, 28.56, 27.43, 25.21, 22.64 ppm.

IR (neat) 3400 cm⁻¹ (strong broad, OH), 1668 cm⁻¹ (strong, C=O urea).

MS (ESI) average m/z calcd for C₁₆₈H₃₀₀N₄₀O₄₈ [M + 4H]⁴⁺ 911.5560; found 911.5587.

Compound **188**



Chemical Formula: $C_{408}H_{648}N_{72}O_{136}$
 Exact Mass: 8732.60

Acetylated compound **188** (56 mg, 6.4 μ mol, 79%) was prepared as a colorless oil according to the general procedure, starting from cyclopeptoid **1** (10.5 mg, 8.1 μ mol) and ligand **152** (69 mg, 37.1 μ mol).

$R_f = 0.40$ (DCM/MeOH 95:5).

Specific rotation $[\alpha]_D^{20} = +4.0$ ($c = 2.1$, $CHCl_3$).

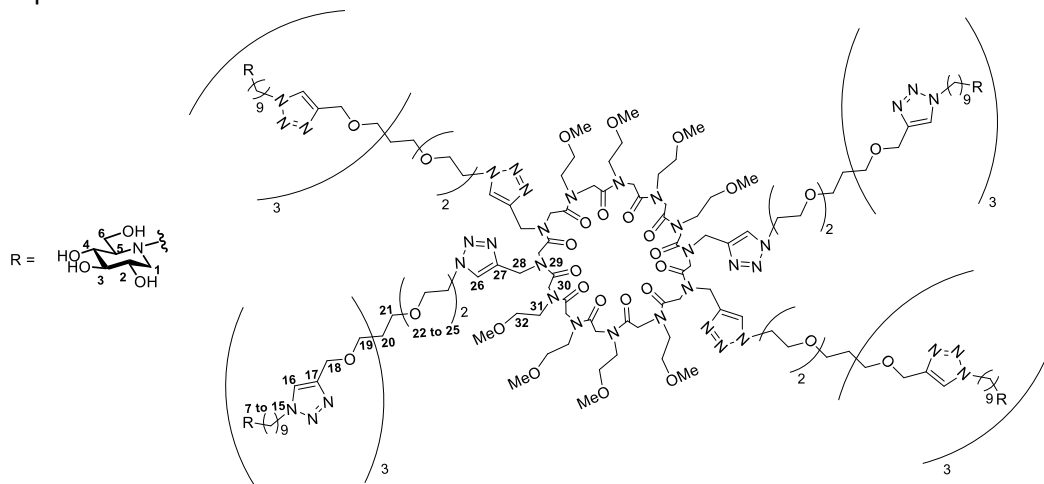
1H -NMR ($CDCl_3$, 500 MHz): δ 8.12-7.64 (br s, 4H, H-26), 7.53 (s, 12H, H-16), 5.06-4.98 (m, 24H, H-3 and H-4), 4.95-4.91 (m, 12H, H-2), 4.65-3.72 (m, 120H, H-18, H-28, H-25, H-15, H-30, H-6 and H-24), 3.63-3.10 (m, 116H, H-19, H-21 to H-23, H-31 to H-32, H-1a and OCH_3), 2.72-2.66 (m, 12H, H-7a), 2.61 (d, $J = 8.0$ Hz, 12H, H-5), 2.52 (br s, 12H, H-7b), 2.30 (t, $J = 10.8$ Hz, 12H, H-1b), 2.04 (s, 36H, $C(O)CH_3$), 1.99 (s, 72H, $C(O)CH_3$), 1.97 (s, 36H, $C(O)CH_3$), 1.86 (br s, 24H, H-14), 1.45-1.17 (m, 144H, H-8 to H-13) ppm.

^{13}C -NMR ($CDCl_3$, 125 MHz): δ 170.94, 170.39, 170.06, 169.78, 168.96, 145.29, 143.41, 124.31, 122.47, 74.73, 71.04, 70.33, 69.86, 69.54, 69.44, 69.29, 65.10, 61.48, 59.54, 59.09, 58.77, 52.95, 51.83, 50.34, 48.03, 45.39, 42.51, 30.42, 29.45, 29.04, 27.21, 26.58, 24.71, 20.92, 20.90, 20.80, 20.74 ppm.

IR (neat) 1746 cm^{-1} (strong, C=O acetate), 1672 cm^{-1} (strong, C=O amide).

MS (ESI) average m/z calcd for $C_{408}H_{657}N_{72}O_{136}$ $[M + 9H]^{9+}$ 971.2962; found 971.2932.

Compound **198**



Chemical Formula: $C_{312}H_{552}N_{72}O_{88}$
Exact Mass: 6716.09

Compound **198** was obtained as a colorless oil in quantitative yield (38.5 mg, 5.7 μ mol) from its acetylated precursor **188** (50 mg, 5.7 μ mol) according to the general procedure.

Specific rotation $[\alpha]_D^{20} = -7.5$ ($c = 1.8$, CH_3OH).

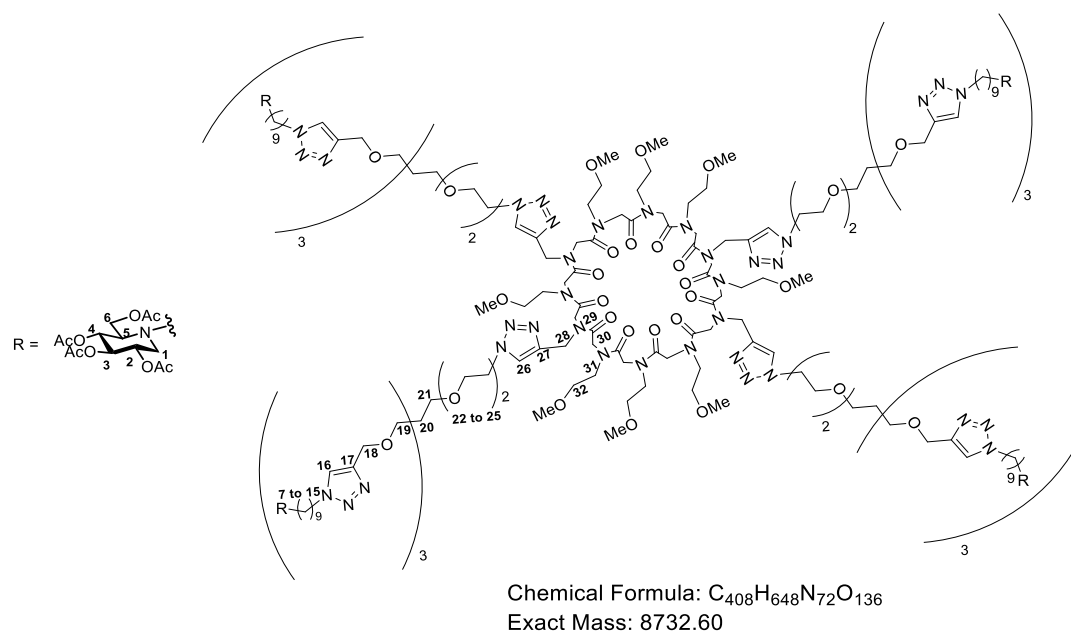
1H -NMR (MeOD, 500 MHz): δ 8.18-7.95 (br s, 4H, H-26), 7.94 (s, 12H, H-16), 4.79-3.88 (m, 88H, H-18, H-15, H-25, H-28 and H-30), 3.87-3.79 (m, 32H, H-6 and H-24), 3.56-3.27 (m, 128H, H-2, H-4, H-19, H-21 to H-23, H-31 to H-32 and OCH_3), 3.13 (t, $J = 9.0$ Hz, 12H, H-3), 2.98 (dd, $J = 11.0, 4.5$ Hz, 12H, H-1a), 2.80-2.75 (m, 12H, H-7a), 2.58-2.53 (m, 12H, H-7b), 2.16 (t, $J = 10.8$ Hz, 12H, H-1b), 2.10 (d, $J = 9.5$ Hz, 12H, H-5), 1.89 (s, 24H, H-14), 1.48-1.46 (m, 24H, H-8), 1.31 (s, 120H, H-9 to H-13) ppm.

^{13}C -NMR (MeOD, 125 MHz): δ 171.63, 146.14, 144.54, 125.82, 124.93, 80.61, 72.09, 71.32, 70.79, 70.45, 70.04, 67.38, 65.43, 59.57, 59.17, 57.78, 53.79, 51.51, 51.34, 49.86, 46.51, 43.48, 31.35, 30.54, 30.05, 28.60, 27.50, 25.24 ppm.

IR (neat) 3380 cm^{-1} (strong broad, OH), 1668 cm^{-1} (strong, C=O urea).

MS (ESI) average m/z calcd for $C_{312}H_{559}N_{72}O_{88}$ $[M + 7H]^{7+}$ 960.4492; found 960.4471.

Compound **189**



Acetylated compound **189** (60 mg, 6.9 μ mol, 63%) was prepared as a colorless oil according to the general procedure, starting from cyclopeptoid **II** (14.2 mg, 10.9 μ mol) and ligand **152** (89.3 mg, 48 μ mol).

R_f = 0.55 (DCM/MeOH 9:1).

Specific rotation $[\alpha]_D^{20}$ = + 4.0 (c = 2.2, CHCl₃).

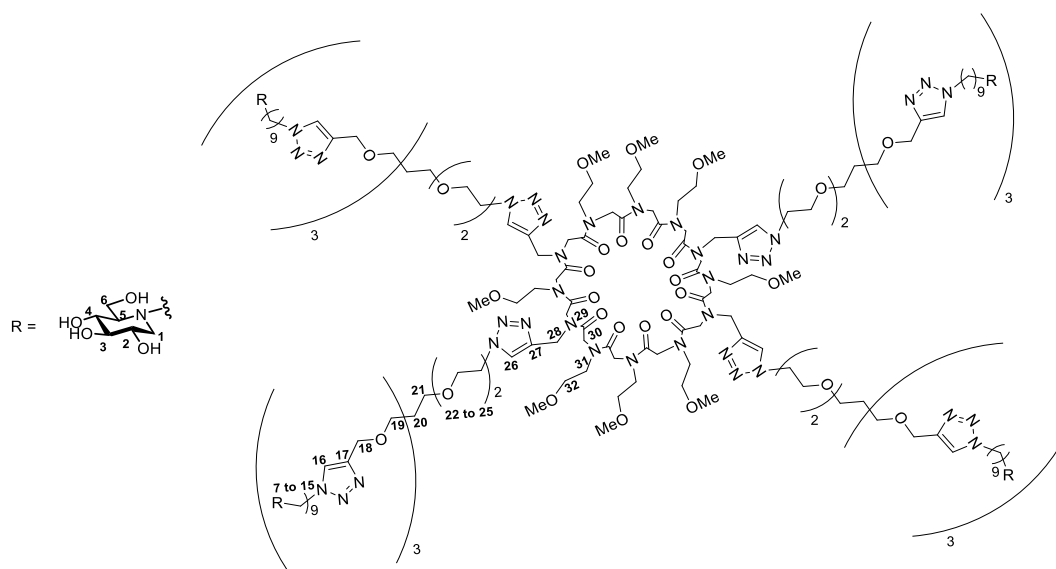
¹H-NMR (CDCl₃, 500 MHz): δ 7.97-7.62 (br s, 4H, H-26), 7.53 (s, 12H, H-16), 5.06-4.98 (m, 24H, H-3 and H-4), 4.95-4.91 (m, 12H, H-2), 4.82-3.69 (m, 120H, H-18, H-28, H-25, H-15, H-30, H-6 and H-24), 3.66-2.87 (m, 116H, H-19, H-21 to H-23, H-31 to H-32, H-1a and OCH₃), 2.71-2.66 (m, 12H, H-7a), 2.60 (d, J = 9.0 Hz, 12H, H-5), 2.54-2.50 (m, 12H, H-7b), 2.29 (t, J = 10.8 Hz, 12H, H-1b), 2.04 (s, 36H, C(O)CH₃), 1.99 (s, 72H, C(O)CH₃), 1.98 (s, 36H, C(O)CH₃), 1.86 (s, 24H, H-14), 1.45-1.14 (m, 144H, H-8 to H-13) ppm.

¹³C-NMR (CDCl₃, 125 MHz): δ 170.96, 170.41, 170.09, 169.80, 168.86, 145.31, 143.41, 124.13, 122.46, 74.78, 71.10, 70.32, 69.90, 69.60, 69.51, 69.31, 65.14, 61.51, 59.58, 59.08, 58.75, 53.00, 51.85, 50.36, 48.09, 45.42, 42.54, 30.44, 29.48, 29.07, 27.25, 26.61, 24.74, 20.95, 20.92, 20.82, 20.76 ppm.

IR (neat) 1745 cm⁻¹ (strong, C=O acetate), 1673 cm⁻¹ (strong, C=O amide).

MS (ESI) average m/z calcd for C₄₀₈H₆₅₄N₇₂O₁₃₆ [M + 6H]⁶⁺ 1456.4407; found 1456.4427.

Compound **199**



Chemical Formula: $C_{312}H_{552}N_{72}O_{88}$
Exact Mass: 6716.09

Compound **199** was obtained as a colorless oil in quantitative yield (32 mg, 4.8 μ mol) from its acetylated precursor **189** (42 mg, 4.8 μ mol) according to the general procedure.

Specific rotation $[\alpha]_D^{20} = -5.0$ ($c = 1.5$, CH_3OH).

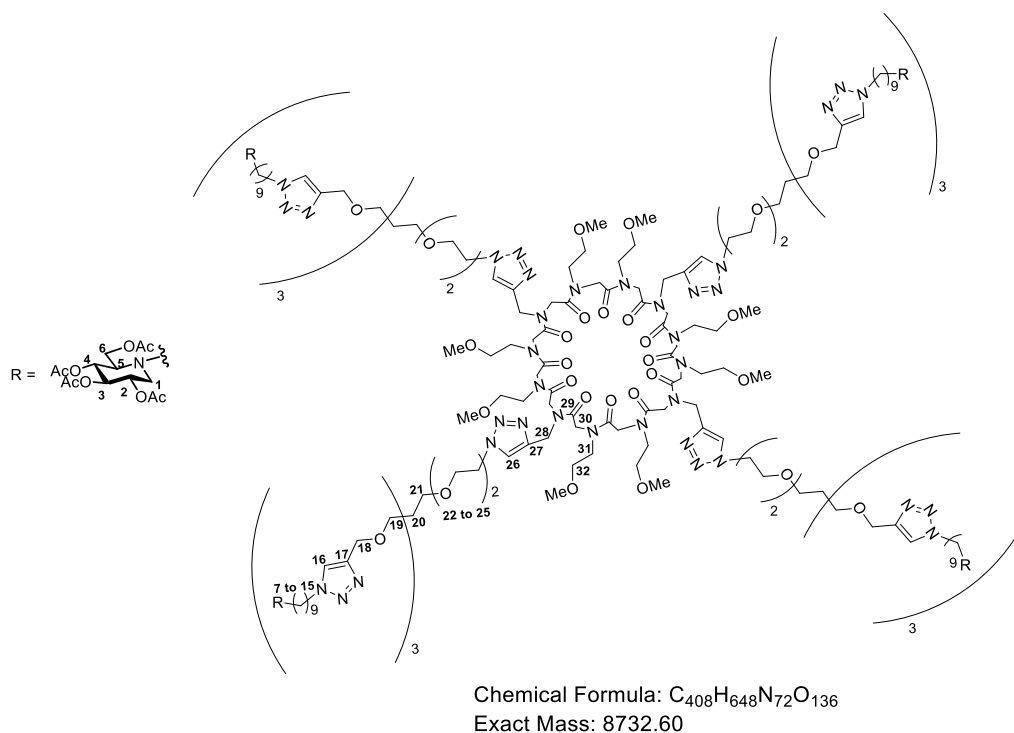
1H -NMR (MeOD, 500 MHz): δ 8.18-7.92 (br s, 4H, H-26), 7.90 (s, 12H, H-16), 4.63-3.65 (m, 120H, H-18, H-15, H-25, H-28, H-30, H-6 and H-24), 3.59-3.17 (m, 128H, H-2, H-4, H-19, H-21 to H-23, H-31, H-32 and OCH_3), 3.12-3.08 (m, 12H, H-3), 2.95-2.92 (m, 12H, H-1a), 2.76-2.71 (m, 12H, H-7a), 2.54-2.49 (m, 12H, H-7b), 2.12 (t, $J = 10.8$ Hz, 12H, H-1b), 2.06 (d, $J = 9.0$ Hz, 12H, H-5), 1.85 (s, 24H, H-14), 1.43 (m, 24H, H-8), 1.27 (s, 120H, H-9 to H-13) ppm.

^{13}C -NMR (MeOD, 125 MHz): δ 171.45, 146.13, 144.61, 125.65, 124.92, 80.60, 72.08, 71.33, 70.78, 70.45, 70.02, 67.37, 65.43, 59.56, 59.15, 57.77, 53.78, 51.50, 51.34, 49.86, 46.50, 43.66, 31.35, 30.54, 30.05, 28.60, 27.50, 25.23 ppm.

IR (neat) 3366 cm^{-1} (strong broad, OH), 1668 (strong, C=O urea) cm^{-1} .

MS (ESI) average m/z calcd for $C_{312}H_{559}N_{72}O_{88}$ $[M + 7H]^{7+}$ 960.4492; found 960.4510.

Compound **190**



Acetylated compound **190** (39 mg, 4.5 μ mol, 55%) was prepared as a colorless oil according to the general procedure, starting from cyclopeptoid **III** (10.5 mg, 8.1 μ mol) and ligand **152** (66 mg, 36 μ mol).

R_f = 0.35 (DCM/MeOH 92:8).

Specific rotation $[\alpha]_D^{20}$ = + 3.5 (c = 1.4, CHCl₃).

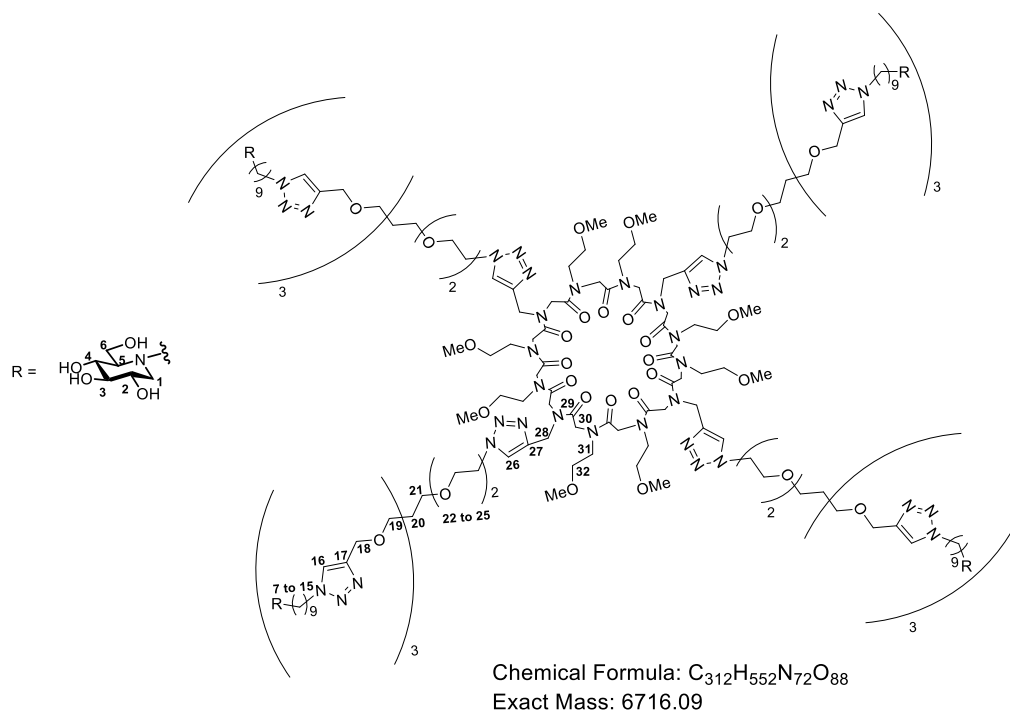
¹H-NMR (CDCl₃, 500 MHz): δ 8.02-7.63 (br s, 4H, H-26), 7.54 (s, 12H, H-16), 5.07-5.00 (m, 24H, H-3 and H-4), 4.97-4.92 (m, 12H, H-2), 4.74-3.65 (m, 120H, H-18, H-28, H-25, H-15, H-30, H-6 and H-24), 3.63-3.10 (m, 116H, H-19, H-21 to H-23, H-31 to H-32, H-1a and OCH₃), 2.73-2.67 (m, 12H, H-7a), 2.62 (d, J = 9.0 Hz, 12H, H-5), 2.56-2.51 (m, 12H, H-7b), 2.30 (t, J = 10.8 Hz, 12H, H-1b), 2.05 (s, 36H, C(O)CH₃), 2.00 (s, 72H, C(O)CH₃), 1.99 (s, 36H, C(O)CH₃), 1.88 (br s, 24H, H-14), 1.42-1.15 (m, 144H, H-8 to H-13) ppm.

¹³C-NMR (CDCl₃, 125 MHz): δ 171.02, 170.46, 170.13, 169.85, 168.96, 145.34, 143.53, 124.11, 122.49, 74.81, 71.14, 70.38, 69.94, 69.63, 69.54, 69.35, 65.17, 61.54, 59.61, 59.14, 58.81, 53.04, 51.89, 50.40, 48.13, 45.45, 42.50, 30.48, 29.52, 29.10, 27.28, 26.65, 24.78, 20.98, 20.96, 20.86, 20.80 ppm.

IR (neat) 1745 cm⁻¹ (strong, C=O acetate), 1673 cm⁻¹ (strong, C=O amide).

MS (ESI) average m/z calcd for C₄₀₈H₆₅₄N₇₂O₁₃₆ [M + 6H]⁶⁺ 1456.4407; found 1456.4396.

Compound **200**



Compound **200** was obtained as a colorless oil in 90% (18 mg, 2.7 μ mol) from its acetylated precursor **190** (26 mg, 3 μ mol) according to the general procedure.

Specific rotation $[\alpha]_D^{20} = -7.5$ ($c = 0.9$, CH_3OH).

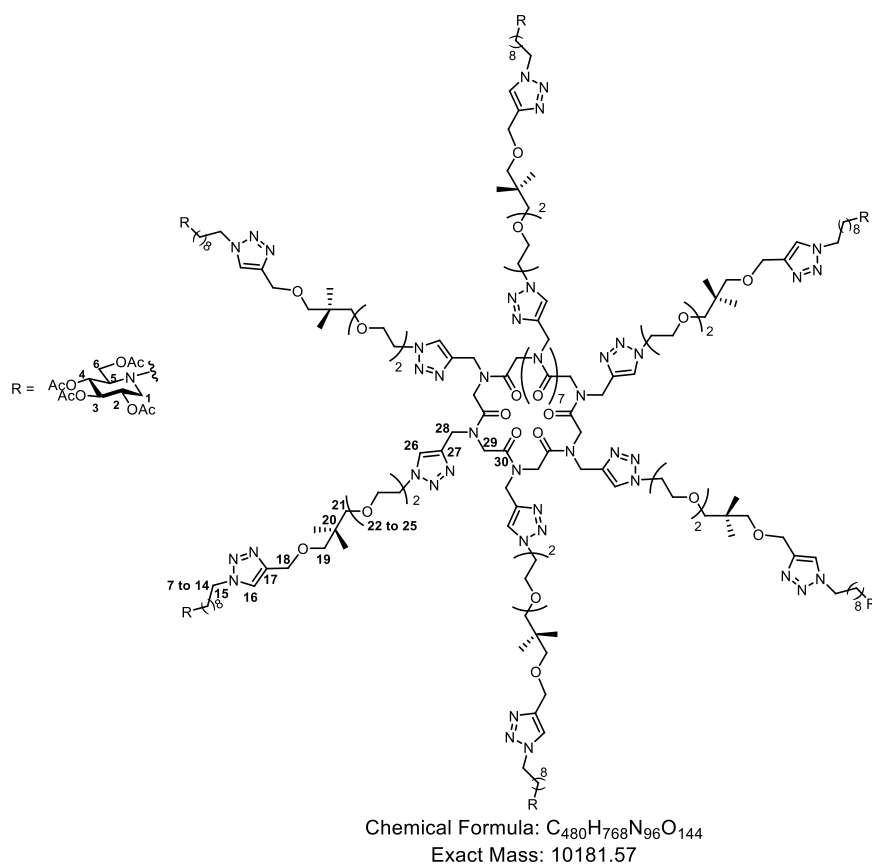
1H -NMR (MeOD, 500 MHz): δ 8.16-7.95 (br s, 4H, H-26), 7.94 (s, 12H, H-16), 4.69-3.93 (m, 88H, H-18, H-15, H-25, H-28 and H-30), 3.89-3.78 (m, 32H, H-6 and H-24), 3.60-3.21 (m, 128H, H-2, H-4, H-19, H-21 to H-23, H-31, H-32 and OCH_3), 3.13 (t, $J = 9.0$ Hz, 12H, H-3), 2.98 (dd, $J = 11.0$, 4.5 Hz, 12H, H-1a), 2.80-2.75 (m, 12H, H-7a), 2.58-2.53 (m, 12H, H-7b), 2.16 (t, $J = 11.0$ Hz, 12H, H-1b), 2.10 (d, $J = 9.5$ Hz, 12H, H-5), 1.89 (m, 24H, H-14), 1.48-1.46 (m, 24H, H-8), 1.31 (s, 120H, H-9 to H-13) ppm.

^{13}C -NMR (MeOD, 125 MHz): δ 171.49, 146.15, 144.55, 125.69, 124.93, 80.62, 72.09, 71.33, 70.80, 70.46, 70.03, 67.39, 65.42, 59.57, 59.16, 57.78, 53.79, 51.53, 51.35, 49.62, 46.48, 43.76, 31.36, 30.55, 30.05, 28.60, 27.50, 25.24 ppm.

IR (neat) 3370 cm^{-1} (strong broad, OH), 1670 cm^{-1} (strong, C=O urea).

MS (ESI) average m/z calcd for $C_{312}H_{560}N_{72}O_{88}$ $[M + 8H]^{8+}$ 840.5189; found 840.5206.

Compound **191**



Acetylated compound **191** (30.3 mg, 3.0 μ mol, 68%) was prepared as a pale-yellow oil according to the general procedure, starting from cyclopeptoid **IV** (5 mg, 4.4 μ mol) and ligand **153** (59 mg, 78.3 μ mol).

$R_f = 0.29$ (DCM/MeOH 100:8).

Specific rotation $[\alpha]_D^{20} = +0.35$ ($c = 0.4$, CHCl₃).

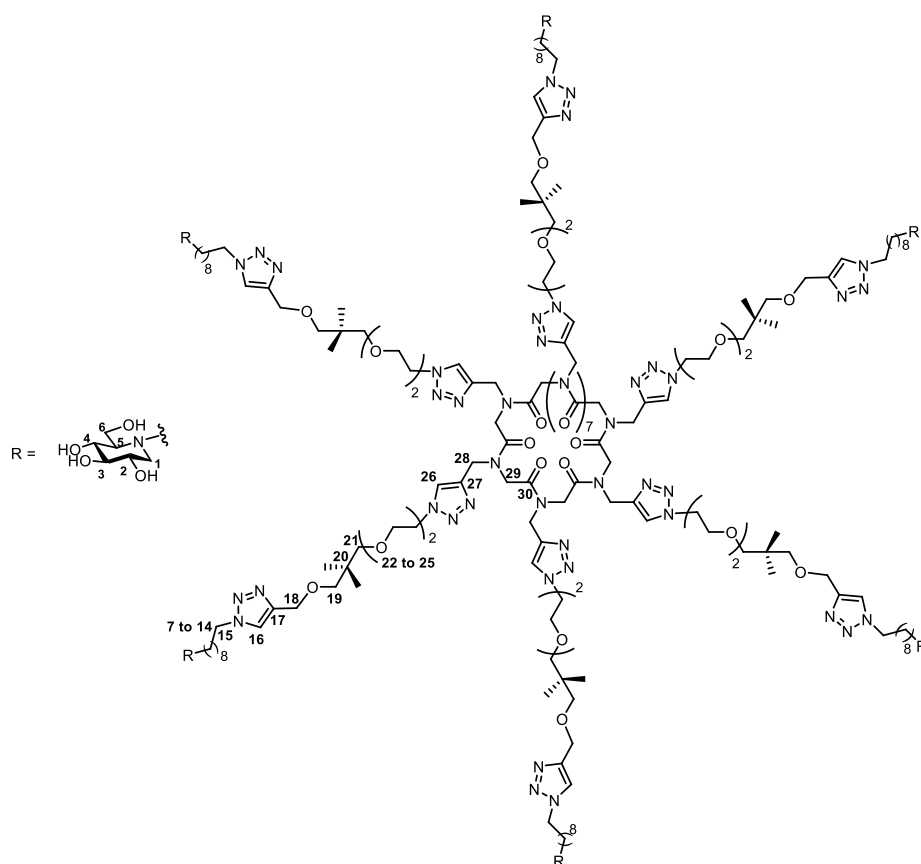
¹H-NMR (CDCl₃, 500 MHz): δ 8.11-7.57 (m, 12H, H-26), 7.51 (s, 12H, H-16), 5.08-4.93 (m, 36H, H-3, H-4, and H-2), 4.70-2.98 (m, 276H, H-18, H-28, H-25, H-15, H-30, H-6, H-24, H-19, H-21 to H-23, H-1a), 2.74-2.68 (m, 12H, H-7a), 2.64 (d, $J = 8.8$ Hz, 12H, H-5), 2.58-2.49 (m, 12H, H-7b), 2.32 (t, $J = 10.8$ Hz, 12H, H-1b), 2.06 (s, 36H, C(O)CH₃), 2.01 (s, 72H, C(O)CH₃), 1.99 (s, 36H, C(O)CH₃), 1.92-1.83 (br s, 24H, H-14), 1.46-1.16 (m, 144H, H-8 to H-13), 0.84 (s, 72H, CH₃) ppm.

¹³C-NMR (CDCl₃, 125 MHz): δ 171.02, 170.47, 170.14, 169.85, 145.72, 142.41, 124.50, 122.26, 74.79, 71.14, 70.48, 69.60, 69.50, 65.19, 61.56, 59.60, 53.00, 51.90, 50.42, 48.41, 42.49, 36.44, 30.47, 29.50, 29.09, 27.27, 26.63, 24.76, 22.28, 21.00, 20.97, 20.87, 20.81 ppm.

IR (neat) 1746 (strong, C=O acetate) cm⁻¹.

MS (ESI) average m/z calcd for C₄₈₀H₇₇₄N₉₆O₁₄₄ [M + 6H]⁶⁺ 1697.9360; found 1697.9332.

Compound **201**



Chemical Formula: C₃₈₄H₆₇₂N₉₆O₉₆
Exact Mass: 8165,07

Compound **201** was obtained as a pale-yellow oil in quantitative yield (24 mg, 3.0 μ mol) from its acetylated precursor **191** (30.3 mg, 3.0 μ mol) according to the general procedure.

Specific rotation $[\alpha]_D^{20} = -6.0$ ($c = 1.0$, CH₃OH).

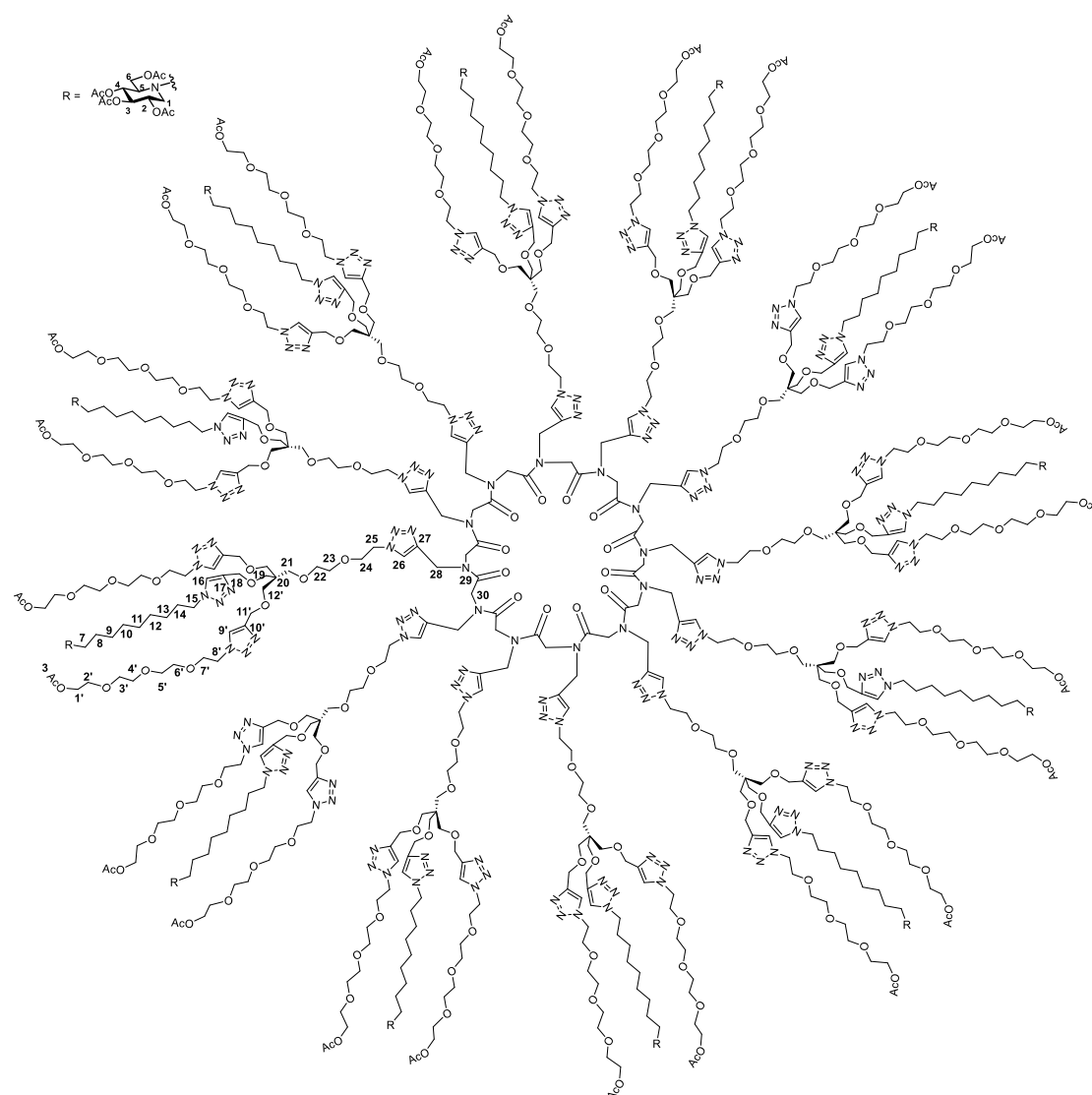
¹H-NMR (MeOD, 500 MHz): δ 8.15-7.90 (br s, 24H, H-26 and H-16), 4.65-3.07 (m, 348H, H-2 to H-4, H-6, H-15, H-18, H-19, H-21 to H-25, H-28, H-30 and OH), 2.97 (dd, $J = 11.1, 4.8$ Hz, 12H, H-1a), 2.80-2.74 (m, 12H, H-7a), 2.58-2.52 (m, 12H, H-7b), 2.16 (t, $J = 10.9$ Hz, 12H, H-1b), 2.10 (d, $J = 9.5$ Hz, 12H, H-5), 1.92-1.85 (br s, 24H, H-14), 1.48-1.44 (m, 24H, H-8), 1.36-1.22 (br s, 120H, H-9 to H-13), 0.83 (s, 72H, CH₃) ppm.

¹³C-NMR (MeOD, 125 MHz): δ 170.30, 146.26, 144.10, 125.91, 124.91, 80.61, 78.22, 77.40, 72.11, 71.41, 70.81, 70.48, 67.38, 65.37, 59.57, 57.79, 53.79, 51.53, 51.35, 43.36, 37.25, 31.34, 30.54, 30.04, 28.61, 27.48, 25.25, 22.75 ppm.

IR (neat) 3367 cm⁻¹ (broad, OH), 1671 cm⁻¹ (strong, C=O urea).

MS (MALDI) 8171.18 (C₃₈₄H₆₇₃N₉₆O₉₆) [M + H]⁺, found : 8171.51; 8193.17 (C₃₈₄H₆₇₂N₉₆NaO₉₆) [M + Na]⁺, found : 8194.71.

Compound **193**



Chemical Formula: $C_{792}H_{1272}N_{168}O_{288}$
Exact Mass: 17745.01

Acetylated compound **193** (45 mg, 2.5 μ mol, 53%) was prepared as a colorless oil according to the general procedure, starting from cyclopeptoid **IV** (5.5 mg, 4.8 μ mol) and ligand **154** (100 mg, 72.3 μ mol).

$R_f = 0.56$ (DCM/MeOH 9:1).

Specific rotation $[\alpha]_D^{20} = +1.0$ ($c = 1.0$, $CHCl_3$).

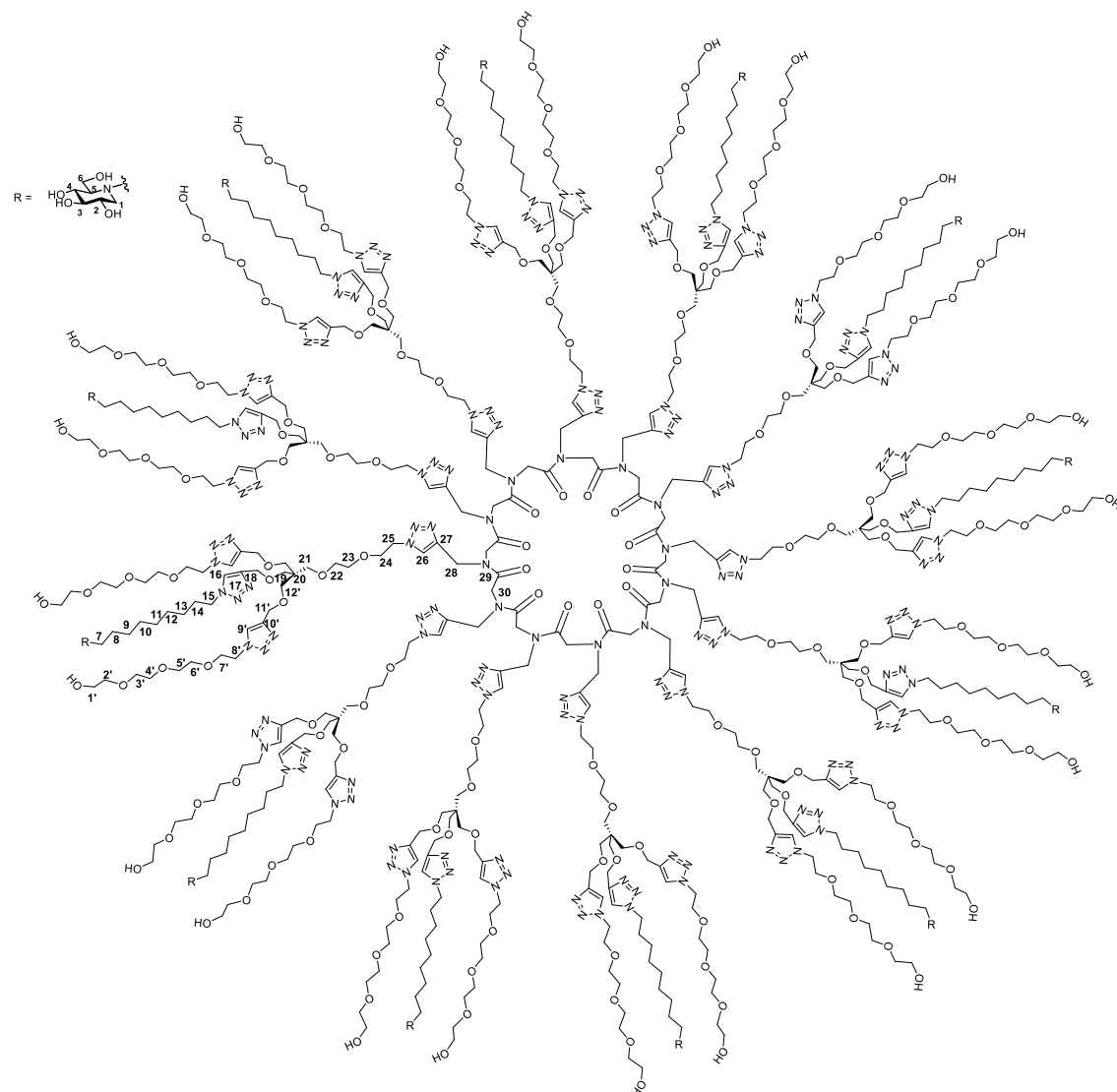
1H -NMR ($CDCl_3$, 500 MHz): δ 8.40-7.75 (br s, 12H, H-26), 7.71 (s, 24H, H-9'), 7.59 (s, 12H, H-16), 5.07-4.99 (m, 24H, H-3 and H-4), 4.96-4.91 (m, 12H, H-2), 4.50-3.44 (m, 744H, H-6, H-15, H-18, H-19, H-21 to H-25, H-1' to H-8', H-11', H-12', H-28 and H-30), 3.17 (dd, $J = 11.3, 4.8$ Hz, 12H, H-1a), 2.73-2.67 (m, 12H, H-7a), 2.62 (d, $J = 9.0$ Hz, 12H, H-5), 2.57-2.51 (m, 12H, H-7b), 2.31 (t, $J = 10.8$ Hz, 12H, H-1b), 2.05-1.99 (m, 216H, $COCH_3$), 1.87 (br s, 24H, H-14), 1.40-1.21 (m, 144H, H-8 to H-13) ppm.

$^{13}\text{C-NMR}$ (CDCl_3 , 125 MHz): δ 171.05, 170.99, 170.44, 170.11, 169.84, 145.31, 145.14, 142.80, 124.54, 123.80, 122.63, 74.81, 71.13, 70.95, 70.59, 70.23, 69.92, 69.62, 69.53, 69.37, 69.24, 69.18, 65.19, 64.98, 63.64, 61.50, 59.59, 53.04, 51.92, 50.35, 50.18, 45.46, 42.55, 30.51, 29.57, 29.14, 27.32, 26.68, 24.74, 21.06, 20.97, 20.94, 20.85, 20.78 ppm.

IR (neat) 1741 cm^{-1} (strong, C=O acetate).

MS (ESI) average m/z calcd for $\text{C}_{792}\text{H}_{1282}\text{N}_{168}\text{O}_{288}$ $[\text{M} + 10\text{H}]^{10+}$ 1776.5164; found 1776.5293.

Compound 202



Chemical Formula: $\text{C}_{648}\text{H}_{1128}\text{N}_{168}\text{O}_{216}$
Exact Mass: 14720.24

Compound **202** was obtained as a colorless oil in quantitative yield (31 mg, 2.1 μmol) from its acetylated precursor **193** (37 mg, 2.1 μmol) according to the general procedure.

Specific rotation $[\alpha]_D^{20} = -3.0$ ($c = 1.6$, CH_3OH).

¹H-NMR (MeOD, 500 MHz): δ 8.23-8.00 (br s, 12H, H-26), 7.99 (s, 24H, H-9'), 7.59 (s, 12H, H-16), 4.55-3.30 (m, 840H, H-2, H-4, H-6, H-15, H-18, H-19, H-21 to H-25, H-1' to H-8', H-11', H-12', H-28, H-30 and OH), 3.14 (t, $J = 9.0$ Hz, 12H, H-3), 2.97 (dd, $J = 11.0, 5.0$ Hz, 12H, H-1a), 2.80-2.74 (m, 12H, H-7a), 2.57-2.52 (m, 12H, H-7b), 2.16 (t, $J = 11.0$ Hz, 12H, H-1b), 2.10 (d, $J = 9.5$ Hz, 12H, H-5), 1.87 (s, 24H, H-14), 1.48-1.45 (m, 24H, H-8), 1.34-1.27 (m, 120H, H-9 to H-13) ppm.

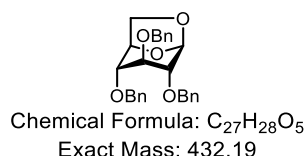
¹³C-NMR (MeOD, 125 MHz): δ 170.27, 146.16, 146.01, 144.41, 143.64, 125.88, 125.77, 124.95, 80.63, 73.70, 72.20, 72.12, 71.55, 71.47, 71.40, 71.23, 70.81, 70.50, 70.41, 70.14, 67.39, 65.54, 65.49, 62.21, 59.60, 57.80, 53.78, 51.45, 51.36, 46.58, 43.70, 31.36, 30.54, 30.05, 28.60, 27.52, 25.26 ppm.

IR (neat) 3381 cm⁻¹ (broad, OH), 1669 cm⁻¹ (strong, C=O urea).

MS (ESI) average m/z calcd for C₆₄₈H₁₁₃₈N₁₆₈O₂₁₆ [M + 10H]¹⁰⁺ 1473.8649; found 1473.8874.

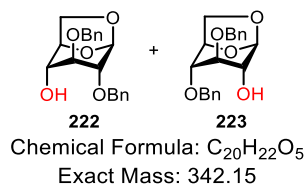
Synthesis and Analytical Data (Chapter IV)

Synthesis of 1,6-anhydro-2,3,4-tri-*O*-benzyl- β -D-glucopyranose **220**



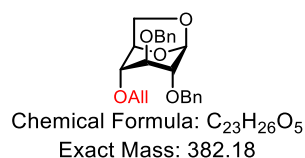
To a solution of 1,6- β -D-anhydroglucose (1.5 g, 9.25 mmol) in DMF (90 mL) at 0 °C was added benzyl bromide (3.65 mL, 30.53 mmol). Sodium hydride (60w% in oil, 1.97 g, 49.03 mmol) was added portionwise. The ice bath was removed, and the reaction was stirred over 2 days at rt. The reaction was quenched by addition of isopropanol (3.7 mL), and 15 min later DMF was removed under high vacuum. The crude mixture was diluted with DCM, filtered and the filtrate was evaporated. The resulting residue was purified by flash chromatography (cyclohexane/EtOAc, 10:1 to 3:1) to afford **220** (3.2 g, 80%) as a white solid. Analytical data of **220** match those from the literature.^[249]

Synthesis of 1,6-anhydro-2,3-di-*O*-benzyl- β -D-glucopyranose **222** and 1,6-anhydro-3,4-di-*O*-benzyl- β -D-glucopyranose **223**



To a solution of **220** (750 mg, 1.73 mmol) in dry DCM (37 mL), SnCl₄ (1.9 mL, 1.91 mmol) was added at room temperature. After 5.5 h at rt., the solution was diluted with DCM and washed with ice-cold sat. NaHCO₃ (2 times), then the organic layer was washed with brine. After separation, the organic solution was dried over Na₂SO₄ and concentrated to a syrup, which was purified with an automatic flash chromatography device (Grace Reveleris) on a 40 g silica gel column (cyclohexane/EtOAc, 9:1 to 2:1) to give pure **222** (312 mg, 53%) and **223** (219 mg, 37%). Analytical data of **222** and **223** match those from the literature.^[252]

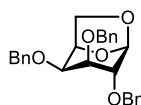
Synthesis of 4-*O*-allyl-1,6-anhydro-2,3-di-*O*-benzyl- β -D-glucopyranose **224**



To a solution of **222** (120 mg, 0.35 mmol) in dry DMF (3.3 mL) was added sodium hydride (60w% in oil, 16.82 mg, 0.42 mmol) portion wise over 5 min at 0 °C. Then allyl bromide (0.04 mL, 0.47 mmol) was added slowly to the suspension. After stirring 2 h at rt., the reaction was quenched by adding 0.15 mL isopropanol at 0 °C. The solution was kept stirring at 0 °C for 1 h, then concentrated under high vacuum to give a residue, which was purified by silica gel column chromatography (cyclohexane/EtOAc, 5:1 to 2:1) to give **224** (111.3 mg) in 83% yield.

Analytical data of **224** match those from the literature.^[253]

Synthesis of 1,6-anhydro-2,3,4-tri-*O*-benzyl- β -D-galactopyranose **226**



Chemical Formula: C₂₇H₂₈O₅

Exact Mass: 432.19

A mixture of D-galactose (200 mg, 1.11 mmol), 2-chloro-1-methylpyridinium iodide (877.2 mg, 3.33 mmol), and triethylamine (4.6 mL, 33.3 mmol) in aqueous solution (20 mL) was stirred for 4 h at 0 °C. The aqueous solution was extracted with DCM (5 times), and the organic layer was separated. The aqueous phases were concentrated under high vacuum. The residue was purified by column chromatography (DCM/MeOH, 6:1 to 3:1) to give D-galactosan mixed with triethylamine.^[254]

To the mixture of D-galactosan and triethylamine was added successively pyridine (12 mL) and acetic anhydride (6 mL) at rt. The solution was stirred for 47 h, then concentrated to a solid, which was dissolved in EtOAc. The suspension was filtered and the filtrate was concentrated in vacuo to give a residue which was purified by column chromatography (cyclohexane/EtOAc, 3:1 to 2:3) to afford the fully *O*-acetylated 1,6-anhydro sugar (in 21% yield over two steps).

To a solution of the fully *O*-acetylated 1,6-anhydro sugar (75 mg, 0.26 mmol) in a mixture of MeOH (30 mL) and H₂O (30 mL) were added Amberlite IRA 400 OH⁻ (3.1 g) (2.5n to 6n g/mmol of substrate; n = number of acetate groups). The suspension was gently rotated overnight at rt. The mixture was filtered, washed with methanol and water and the filtrate was concentrated under reduced pressure to afford the D-galactosan in quant. yield.

To a solution of D-galactosan (62 mg, 0.38 mmol) in DMF (4 mL) at 0 °C was added benzyl bromide (0.23 mL, 1.91 mmol). Sodium hydride (60w% in oil, 137.6 mg, 3.44 mmol) was added portion wise. The reaction mixture was stirred at rt. for 46 h. Isopropanol (0.5 mL) was added to quench the reaction. Then the solution was concentrated to a solid, which was dissolved with DCM. The suspension was filtered and the filtrate was concentrated in vacuo to give a residue which was purified by column chromatography (cyclohexane/EtOAc, 4:1 to 1:1) to afford the desired compound **226** (132 mg) in 80%. Analytical data of **226** match those from the literature.^[263]

➤ **General procedure for the synthesis of glycosyl cyanides **221, 233-236****

To a stirred solution of anhydro sugar (0.23 mmol) in toluene (1.2 mL) were added successively TMSOTf (0.12 mmol) and TMSCN (1.16 mmol) at 0 °C. The reaction mixture was warmed to rt. and kept for 10 min, then stirred at 40 °C until TLC indicated complete consumption of the starting material. The solution was diluted with DCM (4 mL), quenched with ice-cold sat. NaHCO₃ (20 mL), and extracted with DCM (3×25 mL). The combined organic layer was washed with brine (35 mL), dried over Na₂SO₄, and concentrated in vacuo. The crude residue was purified with an automatic flash chromatography device (Grace Reveleris) on a 4 g silica gel column (cyclohexane/EtOAc, 95:5, then 85:15 to 50:50) to afford the desired glycosyl cyanides.

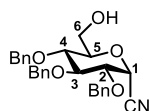
➤ **General procedure for the synthesis of glycosyl cyanides **230-232****

To a stirred solution of anhydro sugar (0.23 mmol) in toluene (1.2 mL) were added successively TMSCN (1.16 mmol) and TMSOTf (0.12 mmol) at 0 °C. The reaction mixture was warmed to rt. and kept for 10 min, then stirred at 40 °C until TLC indicated complete consumption of the

starting material. The solution was diluted with DCM (4 mL), then added ice-cold sat. NaHCO₃ (20 mL), and extracted with DCM (3×25 mL). The combined organic layer was washed with brine (35 mL), dried over Na₂SO₄, and concentrated in vacuo. The crude residue was purified with an automatic flash chromatography device (Grace Reveleris) on a 4 g silica gel column (cyclohexane/EtOAc, 95:5, then 85:15 to 50:50) to afford the desired glycosyl cyanides.

2,3,4-Tri-O-benzyl-D-glucopyranosyl cyanides (221): Compound **220** was treated as described in the general procedure and the reaction mixture was stirred for 47 h at 40 °C. The crude product was purified to provide **221α** (88.3 mg, 83%) as a colorless oil, and **221β** (1 mg, 1%) as a white solid.

221α :



Chemical Formula: C₂₈H₂₉NO₅
Exact Mass: 459.20

R_f = 0.49 (cyclohexane/EtOAc 3:2).

Specific rotation $[\alpha]_D^{20} = +12.0$ (*c* = 1.9, CHCl₃).

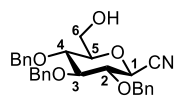
¹H-NMR (CDCl₃, 500 MHz): δ 7.37-7.26 (m, 15H, ArH), 4.99-4.63 (m, 6H, CH₂Ph), 4.57 (d, *J* = 6.0 Hz, 1H, H-1), 3.92 (t, *J* = 9.3 Hz, 1H, H-3), 3.81 (d, *J* = 12.5 Hz, 1H, H-6a), 3.74-3.72 (m, 2H, H-5 and H-6b), 3.63 (dd, *J* = 9.4, 6.0 Hz, 1H, H-2), 3.56 (t, *J* = 9.5 Hz, 1H, H-4), 1.45 (br s, 1H, CH₂-OH) ppm.

¹³C-NMR (CDCl₃, 125 MHz): δ 138.29, 137.89, 137.25, 128.91, 128.71, 128.63, 128.59, 128.25, 128.21, 128.18, 128.13, 128.00, 115.43, 83.15, 77.36, 77.03, 76.14, 75.81, 75.29, 74.14, 66.96, 61.36 ppm.

IR (neat) 3471 cm⁻¹ (broad, O-H).

MS (ESI) *m/z* calcd for C₂₈H₂₉NNaO₅ [*M* + Na]¹⁺ 482.1938; found 482.1936.

221β :



Chemical Formula: C₂₈H₂₉NO₅
Exact Mass: 459.20

R_f = 0.68 (cyclohexane/EtOAc 3:2).

Melting point 84.5-86.2 °C.

Specific rotation $[\alpha]_D^{20} = -34.0$ (*c* = 0.9, CHCl₃).

¹H-NMR (CDCl₃, 400 MHz): δ 7.37-7.26 (m, 15H, ArH), 4.95-4.85 (m, 5H, CH₂Ph), 4.67 (d, *J* = 10.8 Hz, 1H, CH₂Ph), 4.11 (d, *J* = 10.0 Hz, 1H, H-1), 3.88 (ddd, *J* = 12.4, 5.6, 2.4 Hz, 1H, H-6a), 3.79-3.59 (m, 4H, H-2 to H-5), 3.38-3.34 (m, 1H, H-6b), 1.83-1.79 (m, 1H, CH₂-OH) ppm.

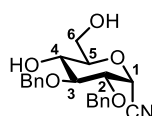
¹³C-NMR (CDCl₃, 100 MHz): δ 138.05, 137.65, 136.89, 128.72, 128.68, 128.64, 128.48, 128.26, 128.19, 128.06, 127.87, 116.86, 85.52, 80.46, 79.88, 76.66, 76.02, 75.98, 75.45, 67.63, 61.56 ppm.

IR (neat) 3468 cm⁻¹ (broad, O-H).

MS (ESI) m/z calcd for C₂₈H₂₉NNaO₅ [M + Na]¹⁺ 482.1938; found 482.1933.

2,3-Di-O-benzyl-D-glucopyranosyl cyanides (230): Compound **222** was treated as described in the general procedure and the reaction mixture was stirred for 49 h at 40 °C. The crude product was purified to provide a 25:1 α/β-mixture of **230** (57.8 mg, 75%) as a colorless oil.

230α :



Chemical Formula: C₂₁H₂₃NO₅
Exact Mass: 369.16

R_f = 0.16 (cyclohexane/EtOAc 3:2).

¹H-NMR (CDCl₃, 400 MHz): δ 7.40-7.26 (m, 10H, ArH), 5.01 (d, *J* = 11.6 Hz, 1H, CH₂Ph), 4.81-4.75 (m, 2H, CH₂Ph), 4.65 (d, *J* = 12.0 Hz, 1H, CH₂Ph), 4.60 (d, *J* = 5.6 Hz, 1H, H-1 α), 3.87-3.77 (m, 2H, H-6), 3.74-3.69 (m, 2H, H-5 and H-3), 3.62 (dd, *J* = 9.4, 5.8 Hz, 1H, H-2), 3.56 (td, *J* = 9.2, 2.8 Hz, 1H, H-4), 2.42 (br s, 1H, CH-OH), 1.81 (br s, 1H, CH₂-OH) ppm.

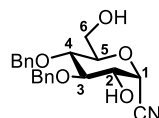
¹³C-NMR (CDCl₃, 100 MHz): δ 138.21, 137.09, 128.95, 128.89, 128.68, 128.32, 128.26, 128.15, 115.38, 82.29, 77.21, 76.99, 75.78, 73.97, 69.17, 66.96, 61.94 ppm.

IR (neat) 3403 cm⁻¹ (broad, O-H).

MS (ESI) m/z calcd for C₂₁H₂₃NNaO₅ [M + Na]¹⁺ 392.1468; found 392.1469.

3,4-Di-O-benzyl-D-glucopyranosyl cyanides (231): Compound **223** was treated as described in the general procedure and the reaction mixture was stirred for 63 h at 40 °C. The crude product was purified to provide **231α** (40 mg, 55%) as a colorless syrup, **231β** (4.5 mg, 6%) as a colorless syrup, and **231'α** (30.7 mg, 35%) as a colorless oil.

231α :



Chemical Formula: C₂₁H₂₃NO₅
Exact Mass: 369.16

R_f = 0.22 (cyclohexane/EtOAc 3:2).

Melting point 86.4-88.1 °C.

Specific rotation $[\alpha]_D^{20} = + 58.0$ ($c = 1.3$, CHCl_3).

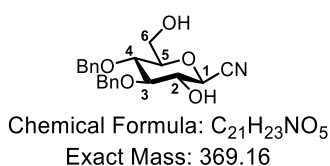
$^1\text{H-NMR}$ (CDCl_3 , 500 MHz): δ 7.40-7.32 (m, 10H, ArH), 4.99 (d, $J = 11.5$ Hz, 1H, CH_2Ph), 4.88 (d, $J = 11.0$ Hz, 1H, CH_2Ph), 4.84 (d, $J = 2.5$ Hz, 1H, H-1), 4.78 (d, $J = 11.0$ Hz, 1H, CH_2Ph), 4.72 (d, $J = 11.0$ Hz, 1H, CH_2Ph), 3.89-3.86 (m, 1H, H-6a), 3.81-3.77 (m, 4H, H-6b, H-3, H-5 and H-2), 3.63 (t, $J = 8.8$ Hz, 1H, H-4), 2.45-2.43 (m, 1H, CH-OH), 1.61-1.57 (m, 1H, $\text{CH}_2\text{-OH}$) ppm.

$^{13}\text{C-NMR}$ (CDCl_3 , 125 MHz): δ 137.98, 137.65, 128.98, 128.77, 128.45, 128.31, 128.12, 128.10, 115.30, 83.41, 77.41, 76.29, 75.84, 75.16, 69.66, 67.93, 61.23 ppm.

IR (neat) 3436 cm^{-1} (broad, O-H), 2091 cm^{-1} (very weak, $\text{C}\equiv\text{N}$).

MS (ESI) m/z calcd for $\text{C}_{21}\text{H}_{23}\text{KNO}_5$ $[\text{M} + \text{K}]^{1+}$ 408.1208; found 408.1220.

231 β :



$R_f = 0.39$ (cyclohexane/EtOAc 3:2).

Specific rotation $[\alpha]_D^{20} = - 159.0$ ($c = 0.3$, CHCl_3).

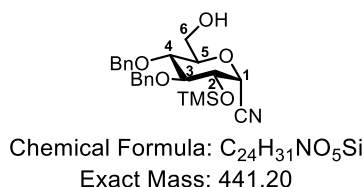
$^1\text{H-NMR}$ (CDCl_3 , 500 MHz): δ 7.37-7.30 (m, 10H, ArH), 4.94 (d, $J = 11.5$ Hz, 1H, CH_2Ph), 4.86 (d, $J = 11.0$ Hz, 1H, CH_2Ph), 4.80 (d, $J = 11.5$ Hz, 1H, CH_2Ph), 4.69 (d, $J = 11.0$ Hz, 1H, CH_2Ph), 4.05 (d, $J = 10.0$ Hz, 1H, H-1), 3.88 (d, $J = 11.5$ Hz, 1H, H-6a), 3.79 (td, $J = 9.9, 9.4, 3.7$ Hz, 1H, H-2), 3.73-3.70 (m, 1H, H-6b), 3.61 (t, $J = 9.3$ Hz, 1H, H-4), 3.50 (t, $J = 8.8$ Hz, 1H, H-3), 3.37 (ddd, $J = 9.7, 4.2, 2.4$ Hz, 1H, H-5), 2.54 (d, $J = 4.0$ Hz, 1H, CH-OH), 1.78-1.76 (m, 1H, $\text{CH}_2\text{-OH}$) ppm.

$^{13}\text{C-NMR}$ (CDCl_3 , 125 MHz): δ 138.10, 137.60, 128.94, 128.76, 128.39, 128.33, 128.22, 128.08, 116.26, 85.23, 80.60, 76.51, 75.78, 75.40, 72.28, 68.82, 61.54 ppm.

IR (neat) 3431 cm^{-1} (broad, O-H), 2082 cm^{-1} (very weak, $\text{C}\equiv\text{N}$).

MS (ESI) m/z calcd for $\text{C}_{21}\text{H}_{23}\text{NNaO}_5$ $[\text{M} + \text{Na}]^{1+}$ 392.1468; found 392.1460.

3,4-Di-O-benzyl-2-O-trimethylsilyl- α -D-glucopyranosyl cyanide (231' α):



$R_f = 0.57$ (cyclohexane/EtOAc 3:2).

Specific rotation $[\alpha]_D^{20} = + 24.0$ ($c = 1.5$, CHCl_3).

¹H-NMR (CDCl₃, 500 MHz): δ 7.35-7.26 (m, 10H, ArH), 4.95 (d, *J* = 11.5 Hz, 1H, CH₂Ph), 4.85 (dd, *J* = 11.2, 1.8 Hz, 2H, CH₂Ph), 4.68-4.64 (m, 2H, H-1 and CH₂Ph), 3.85-3.75 (m, 5H, H-6a, H-2, H-3, H-4, and H-6b), 3.59-3.55 (m, 1H, H-5), 1.58-1.54 (m, 1H, CH₂-OH), 0.19 (s, 9H, TMS) ppm.

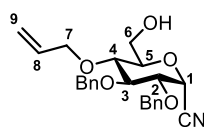
¹³C-NMR (CDCl₃, 125 MHz): δ 138.37, 137.90, 128.66, 128.53, 128.16, 127.83, 115.50, 83.95, 77.16, 76.02, 75.71, 75.26, 71.11, 69.17, 61.37, 0.26 ppm.

IR (neat) 3471 cm⁻¹ (broad, O-H).

MS (ESI) *m/z* calcd for C₂₄H₃₁NNaO₅Si [M + Na]¹⁺ 464.1864; found 464.1850.

4-O-Allyl-2,3-di-O-benzyl-D-glucopyranosyl cyanides (232): Compound **224** was treated as described in the general procedure and the reaction mixture was stirred for 31 h at 40 °C. The crude product was purified to provide **232α** (95.7 mg, 89%) as a colorless oil, and 1:1 mixture of **232α** and **232β** (4 mg, 4%) as a colorless oil.

232α :



Chemical Formula: C₂₄H₂₇NO₅

Exact Mass: 409.19

R_f = 0.60 (cyclohexane/EtOAc 1:1).

Specific rotation [α]_D²⁰ = + 66.0 (*c* = 1.8, CHCl₃).

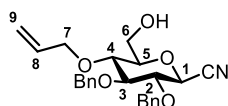
¹H-NMR (CDCl₃, 500 MHz): δ 7.36-7.31 (m, 10H, ArH), 5.94-5.86 (m, 1H, H-8), 5.27 (dq, *J* = 17.5, 1.5 Hz, 1H, H-9a), 5.18 (dq, *J* = 10.5, 1.0 Hz, 1H, H-9b), 4.94-4.81 (m, 3H, CH₂Ph), 4.64 (d, *J* = 12.0 Hz, 1H, CH₂Ph), 4.57 (d, *J* = 6.0 Hz, 1H, H-1), 4.34 (ddt, *J* = 12.4, 5.5, 1.4 Hz, 1H, H-7a), 4.16 (ddt, *J* = 12.4, 5.9, 1.3 Hz, 1H, H-7b), 3.87-3.83 (m, 2H, H-3 and H-6a), 3.79-3.74 (m, 1H, H-6b), 3.73-3.70 (m, 1H, H-5), 3.58 (dd, *J* = 9.3, 6.3 Hz, 1H, H-2), 3.43 (t, *J* = 9.5 Hz, 1H, H-4), 1.72 (br s, 1H, CH₂-OH) ppm.

¹³C-NMR (CDCl₃, 125 MHz): δ 138.30, 137.28, 134.50, 128.87, 128.59, 128.54, 128.19, 128.13, 127.98, 117.51, 115.42, 82.96, 77.16, 77.04, 76.10, 76.02, 74.12, 66.95, 61.34 ppm.

IR (neat) 3468 cm⁻¹ (broad, O-H), 2094 cm⁻¹ (very weak, C≡N).

MS (ESI) *m/z* calcd for C₂₄H₂₇NNaO₅ [M + Na]¹⁺ 432.1781; found 432.1791.

232β :



Chemical Formula: C₂₄H₂₇NO₅

Exact Mass: 409.19

$R_f = 0.74$ (cyclohexane/EtOAc 1:1).

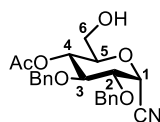
$^1\text{H-NMR}$ (CDCl_3 , 400 MHz): δ 7.35–7.26 (m, 10H, ArH), 5.93–5.83 (m, 1H, H-8), 5.27–5.17 (m, 2H, H-9), 4.94–4.80 (m, 3H, CH_2Ph), 4.63 (d, $J = 12.0$ Hz, 1H, CH_2Ph), 4.30–4.28 (m, 1H, H-7a), 4.18–4.09 (m, 1H, H-7b), 4.10 (d, $J = 10.0$ Hz, 1H, H-1 β), 3.92–3.30 (m, 6H, H-2 to H-6), 1.86–1.83 (m, 1H, $\text{CH}_2\text{-OH}$ α or β), 1.65 (br s, 1H, $\text{CH}_2\text{-OH}$ α or β) ppm.

IR (neat) 3462 cm^{-1} (broad, O-H), 2101 cm^{-1} (very weak, $\text{C}\equiv\text{N}$).

MS (ESI) m/z calcd for $\text{C}_{24}\text{H}_{27}\text{NNaO}_5$ [$\text{M} + \text{Na}$] $^{1+}$ 432.1781; found 432.1776.

4-*O*-Acetyl-2,3-di-*O*-benzyl-D-glucopyranosyl cyanide (233): Compound **225** was treated as described in the general procedure and the reaction mixture was stirred for 16 d at 40 °C. The crude product was purified to provide **233 α** (3 mg, 4%) as a colorless oil.

233 α :



Chemical Formula: $\text{C}_{23}\text{H}_{25}\text{NO}_6$
Exact Mass: 411.17

$R_f = 0.4$ (cyclohexane/EtOAc 3:2).

Specific rotation $[\alpha]_D^{20} = +16.0$ ($c = 0.3$, CHCl_3).

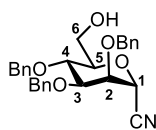
$^1\text{H-NMR}$ (CDCl_3 , 400 MHz): δ 7.38–7.35 (m, 10H, ArH), 4.98 (d, $J = 11.2$ Hz, 1H, CH_2Ph), 4.81 (dd, $J = 11.6$, 4.8 Hz, 2H, CH_2Ph), 4.65 (d, $J = 12.0$ Hz, 1H, CH_2Ph), 4.61 (d, $J = 6.0$ Hz, 1H, H-1), 4.44 (dd, $J = 12.4$, 4.8 Hz, 1H, H-6a), 4.24 (dd, $J = 12.6$, 2.2 Hz, 1H, H-6b), 3.82 (ddd, $J = 9.9$, 4.4, 2.1 Hz, 1H, H-5), 3.73 (t, $J = 9.2$ Hz, 1H, H-3), 3.62 (dd, $J = 9.2$, 6.0 Hz, 1H, H-2), 3.40 (t, $J = 8.4$ Hz, 1H, H-4), 2.59 (br s, 1H, $\text{CH}_2\text{-OH}$), 2.08 (s, 3H, OAc) ppm.

$^{13}\text{C-NMR}$ (CDCl_3 , 125 MHz): δ 171.46, 138.13, 137.11, 128.95, 128.87, 128.68, 128.34, 128.26, 115.28, 82.02, 76.91, 76.00, 75.61, 74.05, 69.02, 67.03, 62.67, 20.92 ppm.

IR (neat) 3478 cm^{-1} (broad, O-H), 2091 cm^{-1} (very weak, $\text{C}\equiv\text{N}$).

MS (ESI) m/z calcd for $\text{C}_{23}\text{H}_{25}\text{NNaO}_6$ [$\text{M} + \text{Na}$] $^{1+}$ 434.1574; found 434.1571.

2,3,4-Tri-*O*-benzyl-D-mannopyranosyl cyanides (234): Compound **226** was treated as described in the general procedure and the reaction mixture was stirred for 72 h at 40 °C. The crude product was purified to provide **234 α** (26.8 mg, 27%) as a colorless syrup, and **234 β** (36.8 mg, 36%) as a colorless syrup.

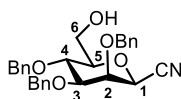
234 α :Chemical Formula: C₂₈H₂₉NO₅

Exact Mass: 459.20

 R_f = 0.55 (cyclohexane/EtOAc 3:2).Specific rotation $[\alpha]_D^{20}$ = +33.5 (c = 1.3, CHCl₃).

¹H-NMR (CDCl₃, 400 MHz): δ 7.35-7.26 (m, 15H, ArH), 4.93 (d, J = 10.8 Hz, 1H, CH₂Ph), 4.74-4.61 (m, 6H, H-1 and CH₂Ph), 4.03-4.00 (m, 1H, H-4), 3.98-3.93 (m, 1H, H-5), 3.88-3.79 (m, 3H, H-2 and H-6), 3.74-3.71 (m, 1H, H-3), 1.82 (br s, 1H, CH₂-OH) ppm.

¹³C-NMR (CDCl₃, 100 MHz): δ 138.08, 137.79, 137.09, 128.81, 128.71, 128.65, 128.43, 128.16, 128.13, 128.08, 128.03, 115.37, 80.07, 77.79, 75.47, 74.98, 73.66, 73.14, 73.08, 65.77, 61.87 ppm.

IR (neat) 3481 cm⁻¹ (broad, O-H).MS (ESI) m/z calcd for C₂₈H₂₉NNaO₅ [M + Na]¹⁺ 482.1938; found 482.1967.**234 β** :Chemical Formula: C₂₈H₂₉NO₅

Exact Mass: 459.20

 R_f = 0.47 (cyclohexane/EtOAc 3:2).Specific rotation $[\alpha]_D^{20}$ = -52.0 (c = 1.3, CHCl₃).

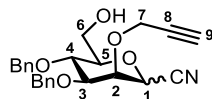
¹H-NMR (CDCl₃, 500 MHz): δ 7.47-7.28 (m, 15H, ArH), 4.99 (d, J = 11.5 Hz, 1H, CH₂Ph), 4.92-4.89 (m, 2H, CH₂Ph), 4.69-4.65 (m, 3H, CH₂Ph), 4.27 (d, J = 1.0 Hz, 1H, H-1), 4.03 (dd, J = 2.8, 1.3 Hz, 1H, H-2), 3.97 (t, J = 9.5 Hz, 1H, H-4), 3.87-3.85 (m, 1H, H-6a), 3.77-3.72 (m, 1H, H-6b), 3.57 (dd, J = 9.3, 2.8 Hz, 1H, H-3), 3.33 (ddd, J = 9.6, 4.9, 2.6 Hz, 1H, H-5), 1.99 (t, J = 6.8 Hz, 1H, CH₂-OH) ppm.

¹³C-NMR (CDCl₃, 125 MHz): δ 137.91, 137.70, 137.41, 128.75, 128.66, 128.60, 128.55, 128.21, 128.19, 128.15, 127.80, 115.90, 82.52, 80.86, 75.66, 75.05, 74.44, 73.84, 72.88, 67.83, 62.01 ppm.

IR (neat) 3468 cm⁻¹ (broad, O-H).MS (ESI) m/z calcd for C₂₈H₂₉KNO₅ [M + K]¹⁺ 498.1677; found 498.1667.

3,4-Di-O-benzyl-2-O-propargyl-D-mannopyranosyl cyanides (235): Compound **227** was treated as described in the general procedure and the reaction mixture was stirred for 163 h at 40 °C. The crude product was purified to provide a 1:2.3 α/β -mixture of **235** (88 mg, 81%) as a pale-yellow oil.

235 (α/β -mixture 1:2.3)



Chemical Formula: C₂₄H₂₅NO₅

Exact Mass: 407.17

R_f = 0.4 (cyclohexane/EtOAc 3:2).

¹H-NMR (CDCl₃, 500 MHz): δ 7.37-7.28 (m, 20H, ArH α and β), 4.94 (d, J = 2.0 Hz, 1H, H-1 α), 4.92-4.63 (m, 10H, CH₂Ph α and β , and H-7 β), 4.39 (d, J = 2.0 Hz, 2H, H-7 α), 4.34-4.33 (m, 1H, H-2 β), 4.31 (d, J = 1.0 Hz, 1H, H-1 β), 4.16 (t, J = 2.5 Hz, 1H, H-2 α), 3.99 (dd, J = 9.5, 3.0 Hz, 1H, H-3 α), 3.94-3.71 (m, 7H, H-4 α and β , H-6 α and β , H-5 α), 3.60 (dd, J = 9.5, 3.0 Hz, 1H, H-3 β), 3.33 (ddd, J = 9.6, 4.7, 2.5 Hz, 1H, H-5 β), 2.56 (t, J = 2.5 Hz, 1H, H-9 β), 2.53 (t, J = 2.5 Hz, 1H, H-9 α), 1.97 (br s, 1H, CH₂-OH β), 1.79 (br s, 1H, CH₂-OH α) ppm.

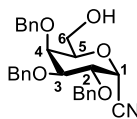
¹³C-NMR (CDCl₃, 125 MHz): δ 138.03, 137.89, 137.53, 137.42, 128.78, 128.66, 128.30, 128.23, 128.20, 128.16, 128.15, 128.11, 128.05, 115.44, 115.16, 82.29, 80.85, 79.96, 78.94, 78.83, 77.76, 76.45, 76.30, 75.70, 75.55, 74.37, 73.73, 73.52, 73.25, 73.06, 72.48, 67.82, 66.08, 61.91, 61.75, 59.72, 58.65 ppm.

IR (neat) 3474 cm⁻¹ (broad, O-H), 3286 cm⁻¹ (alkyne CH), 2122 cm⁻¹ (very weak, C≡N).

MS (ESI) m/z calcd for C₂₄H₂₅KNO₅ [M + K]¹⁺ 446.1364; found 446.1383.

2,3,4-Tri-O-benzyl-D-galactopyranosyl cyanides (236): Compound **228** was treated as described in the general procedure and the reaction mixture was stirred for 196 h at 40 °C. The crude product was purified to provide **236 α** (78.9 mg, 72%) as a colorless syrup, and **236 β** (16.3 mg, 15%) as a colorless syrup.

236 α :



Chemical Formula: C₂₈H₂₉NO₅

Exact Mass: 459.20

R_f = 0.5 (cyclohexane/EtOAc 3:2).

Specific rotation $[\alpha]_D^{20}$ = + 3.0 (c = 1.8, CHCl₃).

¹H-NMR (CDCl₃, 400 MHz): δ 7.40-7.26 (m, 15H, ArH), 4.96 (d, J = 11.6 Hz, 1H, CH₂Ph), 4.88 (dd, J = 12.0, 7.6 Hz, 2H, CH₂Ph), 4.79 (d, J = 11.6 Hz, 1H, CH₂Ph), 4.73-4.62 (m, 3H, H-1 and CH₂Ph), 4.14 (dd, J = 9.8, 6.2 Hz, 1H, H-2), 3.94 (d, J = 2.8 Hz, 1H, H-4), 3.85-3.81 (m, 2H, H-3

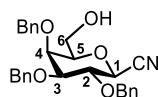
and H-5), 3.73-3.69 (m, 1H, H-6a), 3.53-3.50 (m, 1H, H-6b), 1.62 (br s, 1H, CH₂-OH) ppm.

¹³C-NMR (CDCl₃, 125 MHz): δ 138.15, 137.82, 137.60, 128.79, 128.73, 128.38, 128.14, 128.07, 127.81, 115.82, 80.41, 76.46, 74.89, 74.25, 73.93, 73.89, 73.81, 67.71, 61.84 ppm.

IR (neat) 3469 cm⁻¹ (broad, O-H), 2094 cm⁻¹ (very weak, C≡N).

MS (ESI) m/z calcd for C₂₈H₂₉KNO₅ [M + K]¹⁺ 498.1677; found 498.1709.

236β :



Chemical Formula: C₂₈H₂₉NO₅
Exact Mass: 459.20

R_f = 0.3 (cyclohexane/EtOAc 3:2).

Specific rotation [α]_D²⁰ = -49.5 (c = 0.8, CHCl₃).

¹H-NMR (CDCl₃, 400 MHz): δ 7.37-7.33 (m, 15H, ArH), 4.99-4.92 (m, 3H, CH₂Ph), 4.78 (s, 2H, CH₂Ph), 4.64 (d, J = 11.6 Hz, 1H, CH₂Ph), 4.21 (t, J = 9.8 Hz, 1H, H-2), 4.04 (d, J = 10.0 Hz, 1H, H-1), 3.85 (d, J = 2.0 Hz, 1H, H-4), 3.77 (dd, J = 11.6, 6.8 Hz, 1H, H-6a), 3.53-3.46 (m, 2H, H-3 and H-6b), 3.42-3.39 (m, 1H, H-5), 1.57 (br s, 1H, CH₂-OH) ppm.

¹³C-NMR (CDCl₃, 100 MHz): δ 137.89, 137.77, 137.24, 128.77, 128.74, 128.70, 128.65, 128.58, 128.35, 128.21, 127.80, 116.91, 83.17, 79.88, 76.49, 76.25, 74.71, 73.24, 72.88, 68.17, 61.89 ppm.

IR (neat) 3462 cm⁻¹ (broad, O-H).

MS (ESI) m/z calcd for C₂₈H₂₉NNaO₅ [M + Na]¹⁺ 482.1938; found 482.1945.

**Etude Mécanistique de l'Effet Multivalent sur
l'Inhibition des Glycosidases :
Conception, Synthèse et Evaluation Biologique
d'Iminosucres Multimériques**

Résumé

Depuis la découverte d'un effet multivalent spectaculaire sur l'inhibition des glycosidases en 2010, des résultats impressionnants ont été obtenus, notamment avec un cluster 36-valent montrant la meilleure amélioration d'affinité sur une glycosidase connue à ce jour : un gain d'affinité de 4700 par inhitope par rapport à l'interaction monovalente. Bien que les mécanismes sous-jacents à cet effet aient été étudiés par différentes techniques physiques, le rôle exact et l'impact des différents mécanismes individuels interconnectés restaient non entièrement résolus. Le projet principal a été d'améliorer la compréhension de cet effet multivalent et de chercher le nombre minimum de ligands nécessaires pour atteindre un effet élevé. La synthèse d'une nouvelle bibliothèque d'iminosucres multimériques portés par des cyclopeptoïdes, avec la suppression progressive de différentes sous-parties du meilleur cluster 36-valent, a permis de mieux comprendre l'impact de l'effet de glissement sur la mise en place du complexe reliant deux enzymes. Le deuxième projet portait sur le développement d'une nouvelle méthode pour la synthèse stéréosélective de cyanures de glycosyle en tant que précurseurs de C-glycosides en utilisant l'ouverture d'1,6-anhydrosucres. Cette méthode peut être utile pour la synthèse d'inhibiteurs multimériques basés sur des C-glycosides ciblant des enzymes dont les substrats sont des sucres.

Mots-clés : Iminosucres, inhibiteurs de glycosidase, effet multivalent, relation structure-activité, cyclopeptoïde, CuAAC, cyanures de glycosyles, 1,6-anhydrosucres, réactions d'ouverture de cycle.

Abstract

Since the discovery of a dramatic multivalent effect on glycosidase inhibition in 2010, impressive results have been obtained, especially with a 36-valent cluster showing the best binding enhancement reported on a glycosidase so far: a 4700-fold gain on a valency-corrected basis compared to monovalent interaction. Although the mechanisms underlying this effect had been investigated by different physical techniques, the exact role and impact of different individual interconnected mechanisms was still unsolved. The main project was to push the understanding of the multivalent inhibitory effect and probe the minimum number of ligands needed to reach a high effect. The synthesis of a new library of cyclopeptoid-based iminosugar clusters based on a progressive removal of different sub-sections of the best 36-valent cluster shed light on the impact of the bind-and-recapture effect on the implementation of the cross-linking between two enzymes. The second project was the development of a new method for the stereoselective synthesis of glycosyl cyanides as versatile C-glycoside precursors ring-opening of 1,6-anhydrosugars. This method may be useful for the synthesis of multimeric carbohydrate-processing enzyme inhibitors based on C-glycoside inhitopes.

Key words: Iminosugars, glycosidase inhibitors, Multivalent effect, Structure-activity relationship studies, Cyclopeptoid, CuAAC, glycosyl cyanides, 1,6-anhydrosugars, ring-opening reactions